Interleukin-11 signaling is a global molecular switch between regeneration and scarring in zebrafish

Dissertation
zur Erlangung des Doktorgrades
der Naturwissenschaften

Vorgelegt beim Fachbereich 15
der Johann Wolfgang Goethe-Universität
in Frankfurt am Main

Von
Srinivas Allanki
aus Eluru, Indien

Frankfurt 2022
(D30)

vom Fachbereich Biowissenschaften (FB15) der Johann Wolfgang Goethe-Universität als Dissertation angenommen.

Dekan: Prof. Dr. Sven Klimpel

Gutachter: Prof. Dr. Didier Y. R. Stainier

Prof. Dr. Virginie Lecaudey

Datum der Disputation:

Supervision

Dr. Sven Reischauer
Medical Clinic I, (Cardiology/Angiology) and Campus Kerckhoff
Justus-Liebig-University Giessen
Giessen, Germany

Reviewers

Prof. Dr. Didier Y. R. Stainier
Department of Developmental Genetics
Max Planck Institute for Heart and Lung Research
Bad Nauheim, Germany

&

Prof. Dr. Virginie Lecaudey
Department of Developmental Biology of Vertebrates
Institute of Cell Biology and Neuroscience
Johann Wolfgang Goethe University
Frankfurt, Germany

Erklärung

Ich erkläre hiermit, dass ich mich bisher keiner Doktorprüfung im Mathematisch-Naturwissenschaftlichen Bereich unterzogen habe.

Frankfurt am Main, den .....

(Unterschrift)

Versicherung

Ich erkläre hiermit, dass ich die vorgelegte Dissertation über **Interleukin-11 signaling as a global molecular switch between regeneration and scarring in zebrafish** selbständig angefertigt und mich anderer Hilfsmittel als der in ihr angegebenen nicht bedient habe, insbesondere, dass alle Entlehnungen aus anderen Schriften mit Angabe der betreffenden Schrift gekennzeichnet sind.

Ich versichere, die Grundsätze der guten wissenschaftlichen Praxis beachtet, und nicht die Hilfe einer kommerziellen Promotionsvermittlung in Anspruch genommen zu haben.

Einen Teil der vorliegende Ergebnisse der Arbeit sind in folgendem Publikationsorgan veröffentlicht:

S. Allanki, B. Strilic, L. Scheinberger, Y. L. Onderwater, A. Marks, S. Gunther, J. Preussner, K. Kikhi, M. Looso, D. Y. R. Stainier, S. Reischauer, Interleukin-11 signaling promotes cellular reprogramming and limits fibrotic scarring during tissue regeneration. *Sci. Adv.* **7**, eabg6497 (2021).

Frankfurt am Main, den .....

(Unterschrift)

“*You should not give up, and we should not allow the problem to defeat us*”

- Dr. A. P. J. Abdul Kalam

Table of contents

Abstract

Fibrotic scarring is an intrinsic part of the wound repair process across species with the exception of animals that are capable of complete regeneration, including zebrafish. The general opinion is that scarring prevents regeneration and hence is a leading cause of morbidity in humans. However, unifying mechanisms that prevent scarring and promote regeneration remain elusive. Here, employing comparative transcriptional profiling coupled with genetic loss-of-function studies, I identify a single pathway, Interleukin-11 (Il-11)/Stat3 signaling, as a global upstream regulator of regeneration and scarring in zebrafish. I show that animals lacking Il-11 signaling display strongly impaired regeneration across diverse tissues and developmental stages, essentially resembling non-regenerative adult mammals. By analyzing regeneration in the adult heart and fin, I show that Il-11 acts to reprogram cells to activate global and tissue-specific regenerative gene programs, and to broadly limit hallmarks of the adult mammalian scarring response. Surprisingly, in contrast to the recently proposed pro-fibrotic role of IL-11 in fibroblasts, I identify its anti-fibrotic effects in endothelial cells. Using lineage tracing and transgenic approaches, as well as human cells in culture, I provide evidence that IL-11 signaling in endothelial cells antagonizes pro-fibrotic transforming growth factor beta (TGF-β) signaling and endothelial-to-mesenchymal transition (EndoMT) limiting scarring, and allowing cardiomyocyte protrusion post cardiac injury. Altogether, my findings place Il-11/Stat3 signaling at the crossroad between regeneration and scarring, and define clear targets to develop regenerative therapies.

Abbreviations

Abbreviation	*Description*
µg	microgram
µl	microliter
µm	micrometer
µM	micromolar
4-OHT	4-Hydroxytamoxifen
AFOG	Acid Fuchsin Orange G
ANOVA	One-way analysis of variance
AP	Alkaline Phosphatase
ATP	Adenosine triphosphate
BFP	Blue fluorescent protein
BMP	Bone morphogenetic protein
BOD	Biochemical oxygen demand
bp	basepair
BSA	Bovine serum albumin
CA	constitutively active
$CaCl_2$	Calcium Chloride
CAD	Coronary artery disease
cDNA	Complementary DNA
CDS	Coding sequence
Clo-Lipo	Clodronate Liposomes
CM	Cardiomyocyte

cm	centimeter
Cre	cyclic recombinase
CRISPR	Clustered Regularly Interspaced Short Palindromic Repeats
CVD	Cardiovascular diseases
cxcl12	C-X-C motif chemokine ligand 12
cxcr4	C-X-C motif Chemokine Receptor 4
cyp26a1	cytochrome p450 26a1
DAPI	4',6-diamidino-2-phenylindole
ddH2O	double distilled water
DEPC	Diethyl pyrocarbonate
DIG	Digoxygenin
DMSO	Dimethyl sulfoxide
DN	Dominant negative
DNA	Deoxyribonucleic acid
DNase	Deoxyribonuclease
dNTP	Nucleoside triphosphate
dpa	Days post amputation
dpc	Days post crush
dpci	Days post cryoinjury
dpf	Days post fertilization
dpMI	days post myocardial infarction
dpp	Days post plucking
DSHB	Developmental Studies Hybridoma Bank

E.coli	Escherichia coli
ECM	Extracellular matrix
EDTA	Ethylenediaminetetraacetic acid
EdU	5-ethynyl-2′-deoxyuridine
EGF	Epidermal growth factor
EGFP	Enhanced Green Fluorescent Protein
EGM	Endothelial growth medium
egr	early growth factor
embCMHC	embryonic Cardiac Myosin Heavy Chain
EMT	Epithelial-to-mesenchymal transition
EndoMT	Endothelial-to-mesenchymal transition
EPDCs	Epicardial derived cells
Et	Enhancer trap
FC	Fold change
FGF	Fibroblast growth factor
g	gram
gata4	GATA binding protein 4
GFP	Green Fluorescent Protein
GO	Gene Ontology
gp130	Glycoprotein 130
H&E	Hematoxyline and eosin
H_2O_2	Hydrogen peroxide
HCl	Hydrochloric acid

hif1	hypoxia inducible factor
hpa	Hours post amputation
hpci	Hours post cryoinjury
HRMA	High Resolution Melt Analysis
hrs	hours
HUVECs	Human umbilical vein endothelial cells
IGF	Insulin-like growth factor
IHC	Immunohistochemistry
il11	interleukin-11
il6	interleukin-6
il6st	interleukin-6 signal transducer
ISH	In situ hybridization
jak	janus kinase
kb	kilobase
KCl	Potassium Chloride
KEGG	Kyoto Encyclopedia of Genes and Genomes
L	Liter
LB	Lysogeny broth
lit	Liter
LOF	Loss of function
lox	Lysyl Oxidase
LoxP	locus of X-over P1
LSM	Laser scanning microscope

LV	left ventricle
m	meter
M	molar
MEF2C	Myocyte Enhancer Factor 2C
Mek-Erk	Mitogen-activated protein kinase kinase – extracellular signal–regulated kinase
$MgCl_2$	Magnesium Chloride
$MgSO_4$	Magnesium sulphate
MHC	Myosin heavy chain
MI	Myocardial infarction
mins	minutes
miRNA	micro RNA
MLCK	Myosin Light Chain Kinase
mm	millimeter
MMP	Matrix metalloproteinase
mRNA	messenger RNA
MSigDB	Molecular Signatures database
mstnb	*myostatin b*
mvp	Major vault protein
myl7	myosin light chain 7
Na_2HPO_4	Disodium phosphate
NaCl	Sodium chloride
NaOH	Sodium hydroxide
NF-κB	Nuclear factor kappa light chain enhancer of activated B cells

ng	nanogram
nm	nanometer
nrg	neuregulin
OCT	Optimal cutting temperature
OE	overexpression
O/N	overnight
PBS	Phosphate buffered saline
PCNA	Proliferating cell nuclear antigen
PCR	Polymerase chain reaction
PFA	Paraformaldehyde
pg	picogram
pH	negative log of hydrogen ion concentration
Pi3k-Akt	Phosphatidylinositol 3-kinase – protein kinase B
postnb	periostin b
PTU	1-phenyl-2-thiourea
RA	Retinoic acid
raldh2	retinaldehyde dehydrogenase 2
RCF	relative centrifugal field
RFP	Red fluorescent protein
rh	recombinant human
rm	recombinant mouse
RNA	Ribonucleic acid
RNase	Ribonuclease

rpl13a	60s ribosomal protein L13a
RPM	rotations per minute
RT	room temperature
RT-qPCR	Real-time quantitative PCR
RV	right ventricle
s	second
S.D.	Standard deviation
S.E.M.	Standard error of mean
siRNA	Small interfering RNA
Smad	Small Mothers Against Decapentaplegic
socs3b	Suppressor of cytokine signaling 3b
sox9	SRY-Box Transcription Factor 9
SSC	Saline sodium citrate
stat3	Signal transducer and activator of transcription 3
tbx18	T-box transcription factor 18
tcf21	transcription factor 21
TEM	Transmission electron microscopy
TGF-β	Transforming growth factor beta
Tricaine	Ethyl-m-aminobenzoate methanesulfonate
tRNA	transfer RNA
U	unit
UV	Ultra violet
V	volt

vegf	Vascular endothelial growth factor
WNT	Wingless-related integration site
WT	Wild type
wt1b	Wilm's tumour 1b
X-gal	5-bromo-4-chloro-3-indolyl-D-galactopyranoside
ZIRC	Zebrafish International Resource Center
αSMA	Alpha-Smooth Muscle Actin

1. Introduction

1.1. Consequences of tissue damage

Tissue damage is a part of our daily life and is prevalent across species – be it the predator-prey relationship or a traumatic accident, or something as simple as breathing polluted air that causes lung damage. Various species and even different organs in the same species, respond to tissue damage in different ways. Most often, the two opposing outcomes after tissue damage are functional regeneration or permanent scarring (**Fig. 1.1**) (Goldman and Poss, 2020; Gurtner et al., 2008).

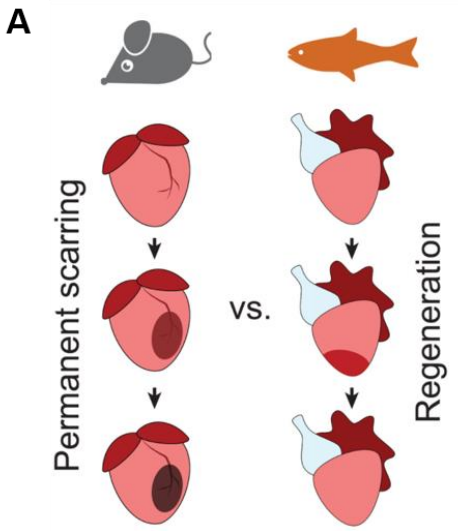

Figure 1.1. Permanent scarring vs. functional regeneration. (**A**) Illustration showing permanent scarring in the adult mammalian heart after myocardial infarction and functional regeneration in the adult zebrafish heart. Adapted from (Allanki et al., 2021), Figure 1A. License: CC BY 4.0.

1.1.1. Permanent scarring

Fibrotic scarring is a process in which excessive amounts of ECM is deposited, which further matures and physically hinders tissue function (Distler et al., 2019). Adult mammals, including humans, predominantly form a functionally inert scar after injuries (Gurtner et al., 2008; Murawala et al., 2012). For example – in the heart, coronary artery occlusion drives the downstream tissue into hypoxia and leads to the death of approximately a billion cardiomyocytes. Such massive loss of tissue activates

fibrogenic gene programs, which then initiate the deposition of excess ECM to form a scar (**Fig. 1.2**) (Davis and Molkentin, 2014). The primary function of scarring is to seal the damaged region from being ruptured and to minimize collateral damage in the adjacent healthy tissue. However, long term, scarring abrogates optimal organ function.

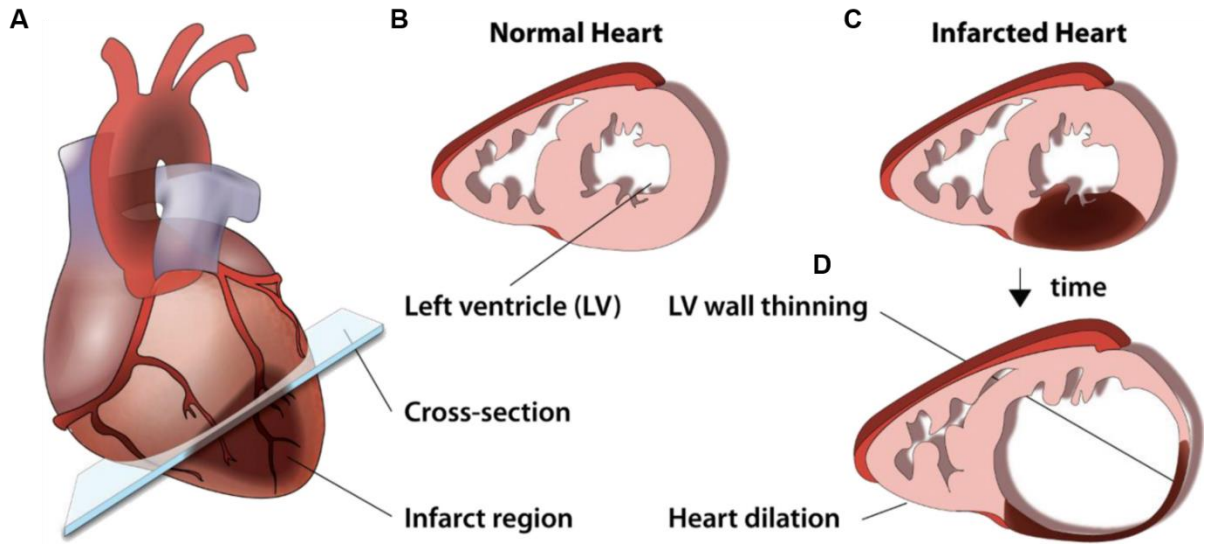

Figure 1.2. Permanent scarring after myocardial infarction in the mammalian heart. (**A**) Illustration showing an infarcted mammalian heart. (**B**) Normal mammalian heart cross section. (**C**) Infarcted mammalian heart cross-section displaying the injury. (**D**) Infarcted mammalian heart cross-section displaying a permanent scar and left ventricular (LV) wall thinning. Adapted from (Awada et al., 2016), Figure 1. License: 5231340204166.

1.1.2. Functional regeneration

Tissue regeneration is a process by which damaged organs and appendages are functionally replaced and the tissue architecture is restored (Gurtner et al., 2008; Murawala et al., 2012). Unlike adult mammals, several species, including teleost fish such as zebrafish, African killifish, urodele amphibians such as the axolotl, and the *Xenopus* tadpole, possess regenerative capabilities (**Fig. 1.3**) (Goldman and Poss, 2020; Joven et al., 2019; Marques et al., 2019; Phipps et al., 2020; Vogg et al., 2019; Wang et al., 2020). The ability to regenerate is highly variable from species to species and even among different organs in the same organism. For example – zebrafish and medaka both belong to teleostei, but display unequal regenerative abilities. Both zebrafish and medaka can regenerate their fins. However, upon heart injury, zebrafish

display robust regeneration while medaka form a permanent scar (Lai et al., 2017; Yoshinari and Kawakami, 2011). The ability to regenerate can also be developmental stage dependent in the same organism. For example – as discussed earlier, adult rodent hearts and spinal cords undergo scarring upon damage while the neonates display robust regeneration (Li et al., 2020; Porrello et al., 2011). These remarkable discoveries aided a plethora of comparative studies in the same organ and organism to unlock the secrets of regeneration.

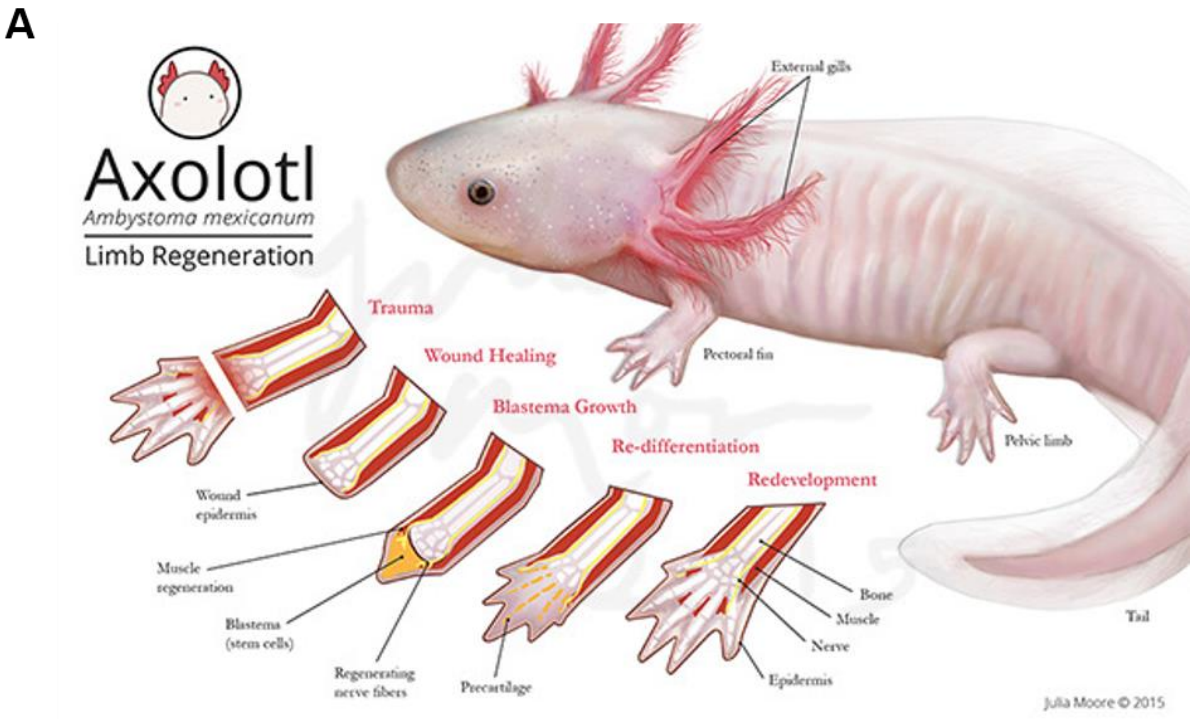

Figure 1.3. Axolotl limb regeneration. (**A**) Illustration showing limb regeneration in axolotl (Ambystoma mexicanum). Adapted from mooreillustrations.tumblr.com. License: Julia Moore © 2015.

1.2. Cellular mechanisms of scarring and regeneration

Typically, any tissue broadly consists of two types of cells: 1. parenchymal cells and, 2. stromal cells (Feeback, 1987). Parenchymal cells are specialized cell types that perform the function of the respective tissue/organ. For example – cardiomyocytes in the heart, neurons in the brain, and nephrons in the kidney (**Fig. 1.4**). On the other hand, the stromal compartment consists of different cell types that surround the tissues and confers them with a structure and framework. Endothelial cells, fibroblasts and

immune cells mainly comprise of the stromal tissue. During homeostasis, these cells help the parenchyma to perform their function efficiently, keeping the day-to-day organ function under check.

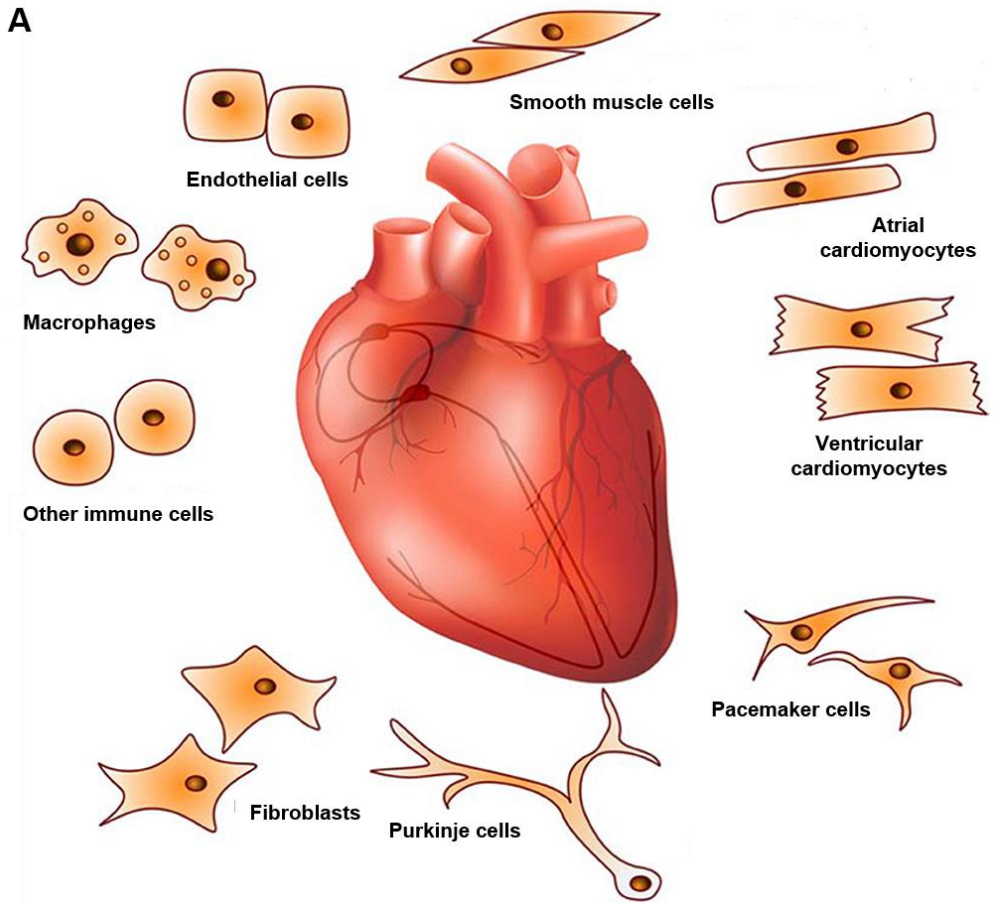

Figure 1.4. Cell types that compose the adult mammalian heart. (**A**) Illustration showing both the parenchymal (cardiomyocytes) and stromal compartments (endothelial cells, fibroblasts, and immune cells) of the adult mammalian heart. Adapted and modified from (Michalak and Agellon, 2018), Figure 1. License: CC BY 4.0.

Upon injury, both the parenchyma and stroma respond to several injury-specific extrinsic and intrinsic cues. Most of the earlier research was focused on the parenchymal response to injury and how one can get them to multiply and replace the damaged tissue functionally – i.e., to regenerate. Hence, the role played by the stroma during homeostasis and in regulating the disease pathology, as well as the tissue response to injury is understudied. However, in the past few years, there is an increasing interest in understanding how the stromal compartment modulates the

parenchymal regeneration and scarring (Sagaradze et al., 2020). Indeed, several studies suggest that the stromal cells can dictate the outcome of tissue damage i.e., to regenerate or to scar (Mascharak et al., 2021; Rinkevich et al., 2015).

1.2.1. Scar formation – the role of myofibroblasts

A specialized cell type called as myofibroblast mainly orchestrates scar formation. One of the primary features of myofibroblasts is to secrete unrestrained amounts of ECM and regulate damaged tissue remodeling (Davis and Molkentin, 2014; Falke et al., 2015). As the term “myo” in their name suggests, these cells express alpha Smooth muscle actin^{+} (αSMA) stress fibers that confer contractility to the injured tissue. These cells are usually not found in the homeostatic tissue. After tissue damage, the scarring species induce a fibrogenic gene program, including several injury- or stress-induced cytokines and other chemokines, changes in the tissue mechanical properties, and other downstream effectors that initiate myofibroblast differentiation. Myofibroblasts have been shown to be derived from varied origins (**Fig. 1.5**) (Falke et al., 2015). In the heart, after myocardial infarction, myofibroblasts are predominantly derived from the resident population of cardiac fibroblasts. However, evidence from lineage tracing experiments suggests that a considerable amount of myofibroblasts are also derived from endothelial cells and circulating blood cells (Kanisicak et al., 2016). Irrespective of their origin, the main role of myofibroblasts is to aid scar formation by secreting excessive ECM, as well as chemokines and cytokines that orchestrate tissue inflammation.

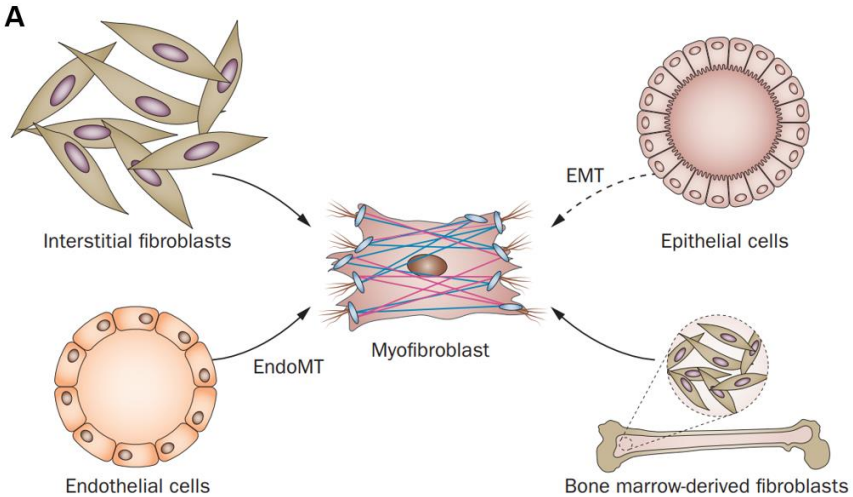

Figure 1.5. Cellular origins of myofibroblasts. (**A**) Illustration showing myofibroblast sources from interstitial fibroblasts, endothelial cells, bone marrow derived cells and epithelial cells. Image from (Falke et al., 2015), Figure 4. License: 5231340947066.

Ablation experiments have suggested that ablating these scar-forming myofibroblasts significantly reduces fibrotic remodeling in the heart and other tissues (Aghajanian et al., 2019; Kaur Harmandeep et al., 2016; Rinkevich et al., 2015; Rurik et al., 2022). These data further confirm the major role of myofibroblasts in scar formation and highlight myofibroblast activation blockers as a potential therapy for fibrotic diseases.

1.2.2. Regeneration – regenerative reprogramming

In contrast to the scarring organisms, the species that are capable of complete regeneration, mount a different response at the transcriptional level (**Fig. 1.6**). After tissue damage, the cells in regenerative species reprogram their homeostatic gene expression landscape. They have been shown to activate several developmental- and regeneration-specific gene programs. These programs orchestrate vital cellular processes like cell proliferation, dedifferentiation and re-differentiation, as well as migration, in order to promote regeneration (Gerber et al., 2018; Hoang et al., 2020; Lin et al., 2021). In the following sections, I will refer to this process as *regenerative reprogramming*.

Axolotls can regenerate a multitude of organs and appendages and are rapidly becoming one of the most studied species in regenerative biology. For the last two decades, the axolotl limb amputation model shed light on various aspects of regeneration, including cell lineage restrictions and plasticity (Joven et al., 2019). Regenerative reprogramming is yet another aspect that is well documented during axolotl limb regeneration, especially in connective tissue cells or fibroblasts, which form one of the major components of the stromal compartment. After limb amputation, the cells close to the amputation plane begin to participate and form a mass of undifferentiated cells called the *blastema*, which then gives rise to a fully regenerated limb (Murawala et al., 2012; Seifert and Muneoka, 2018). However, the cellular mechanisms by which a blastema is formed were elusive. There were two hypotheses for the origin of blastema: 1. pre-existing stem cells and, 2. cell reprogramming and

dedifferentiation. Making use of the Cre-Lox system, Gerber, Murawala and colleagues lineage traced early mesoderm derived connective tissue cells during limb development and regeneration (Gerber et al., 2018). They first found that the limb blastema mainly is comprised of connective tissue derived cells. Using brainbow lineage tracing and single-cell RNA sequencing, they also showed that connective tissue cells dedifferentiate and re-differentiate to regenerate the amputated body part (**Fig. 1.7**). A follow-up study compared the regenerative reprogramming in between the fully regenerative Axolotl limbs and partially regenerative *Xenopus* limbs after amputation (Lin et al., 2021). These data suggest a positive correlation between regenerative outcome and the extent of connective tissue reprogramming. However, further studies are needed to provide functional and mechanistic evidence if regenerative reprogramming is required for tissue regeneration, and if inducing this kind of reprogramming is enough to promote regeneration in non-regenerative species.

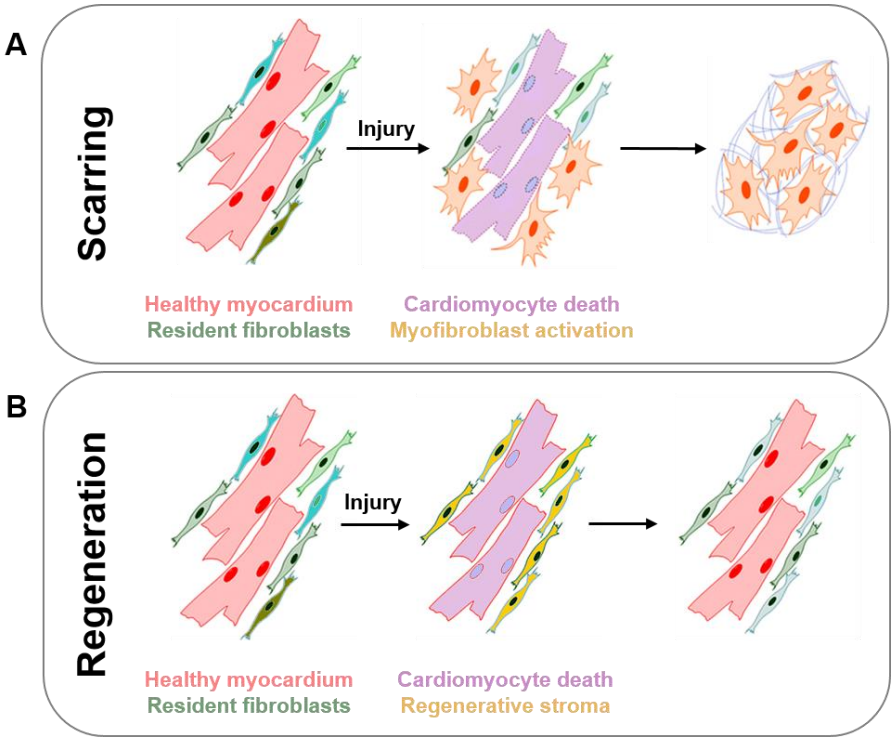

Figure 1.6. Myofibroblast differentiation vs. regenerative reprogramming of the stromal cells. (**A**) Illustration showing myofibroblast differentiation followed by permanent scarring in an adult mammalian heart. (**B**) Illustration showing regenerative reprogramming in the stromal cells during regeneration in a zebrafish heart. Adapted and modified from (Talman and Ruskoaho, 2016), Figure 3. License: CC BY 4.0.

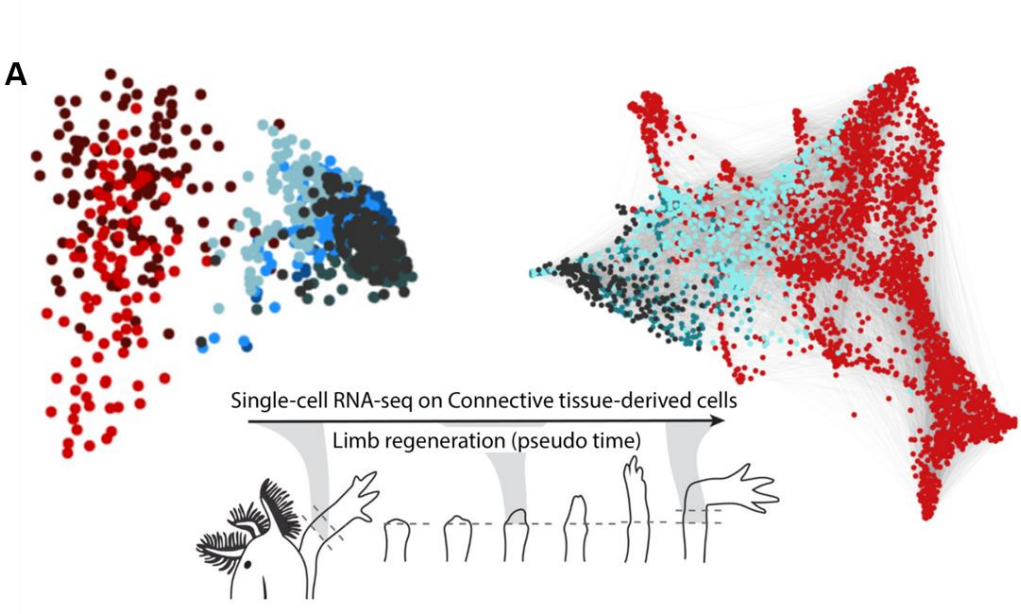

Figure 1.7. Connective tissue reprogramming during axolotl limb regeneration. (**A**) Illustration portraying a single-cell RNA-seq experiment performed on connective tissue-derived cells that shows cell dedifferentiation and redifferentiation during the time course of axolotl limb regeneration. Adapted and modified from (Gerber et al., 2018), Figures 2E and 5D. License: 1178754.

1.3. Tissue regeneration in zebrafish

Model organisms are invaluable tools for understanding how endogenous regeneration happens. Thanks to curiosity-driven research, more than a handful of regenerative model organisms have been discovered and established. To name a few – Arabidopsis (roots), hydra and planarians (full body regeneration), salamanders (various organs and appendages), *Xenopus* tadpole (tail), African spiny mouse (skin and ear pinna), African killifish (heart and appendages), and zebrafish (various organs and appendages) (Mehta and Singh, 2019). Due to their relevance to human biology, powerful genetics, endogenous regenerative capabilities and the relative ease of maintenance, the zebrafish (*Danio rerio*) have rapidly become one of the favorite model systems to study embryonic development and regeneration (Marques et al., 2019). First identified in the river basins in East India, Dr. George Streisinger established the zebrafish as a model organism in his laboratory at the University of Oregon in the 1970's. Since then, zebrafish have aided many crucial discoveries in developmental biology (Gut et al., 2017; Mullins et al., 2021).

Another important aspect of the zebrafish research is their remarkable regenerative capacity in diverse organs and appendages throughout life, including the larval fin fold, spinal cord, heart, adult fins, scales, kidney, liver, retina, hair cells, and brain (**Fig. 1.8**) (Marques et al., 2019). In the next few sections, I will briefly review the current knowledge about a few of these tissues, and some of their regenerative mechanisms.

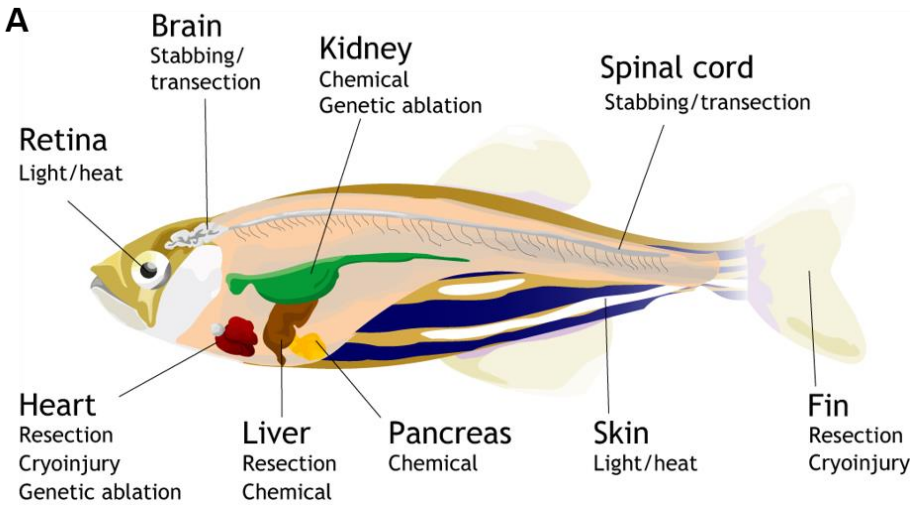

Figure 1.8. Tissue regeneration models in zebrafish. (**A**) Illustration showing various regenerative tissues and their injury models in adult zebrafish. Adapted from (Marques et al., 2019), Figure 2. License: CC BY 4.0.

1.4. Adult zebrafish heart regeneration

The main function of the heart is to pump blood throughout the body via the blood vessels (arteries and veins). Arteries carry oxygenated blood from the heart to various tissues. Veins carry deoxygenated from the tissues back to the heart. Alarmingly, nearly 17 million people die each year due to cardiovascular complications (CVDs, WHO statistics). Approximately half of these deaths result from coronary artery diseases (CAD) leading to myocardial infarction (MI) or heart attacks. Coronary vessels provide oxygen and nutrients to the parenchymal cells via blood, sustaining the cardiac wall function. Acute blockage of these vessels leads to the death of the underlying cardiac tissue. This leads to an irreversible loss of almost a billion cardiomyocytes (Anderson and Morrow, 2017). Unlike other mammalian organs such as the liver, the heart does not possess the innate ability to regenerate. However, several species, including the zebrafish, can regenerate cardiac tissue even after

significant damage (Poss et al., 2002). Hence, it is important to investigate and understand the cellular and molecular mechanisms behind endogenous heart regeneration in regenerative species to develop new therapeutic approaches in regenerative medicine.

1.4.1. Anatomy of the zebrafish heart

In all vertebrates, the heart is one of the first organs to form and function early during embryonic development. Unlike the four-chambered mammalian heart, the simple zebrafish heart consists of only two chambers – one atrium and one ventricle (**Fig. 1.9**). Deoxygenated blood flows into the atrium, then through the ventricle and is pumped out via the outflow tract (also known as *Bulbus arteriosus*) into the gills for oxygenation. Two cardiac valves help maintain unidirectional blood flow – one in between the atrium and the ventricle, called as atrio-ventricular valve and the other in between the ventricle and bulbus, called as bulbo-ventricular valve (Gunawan et al., 2021).

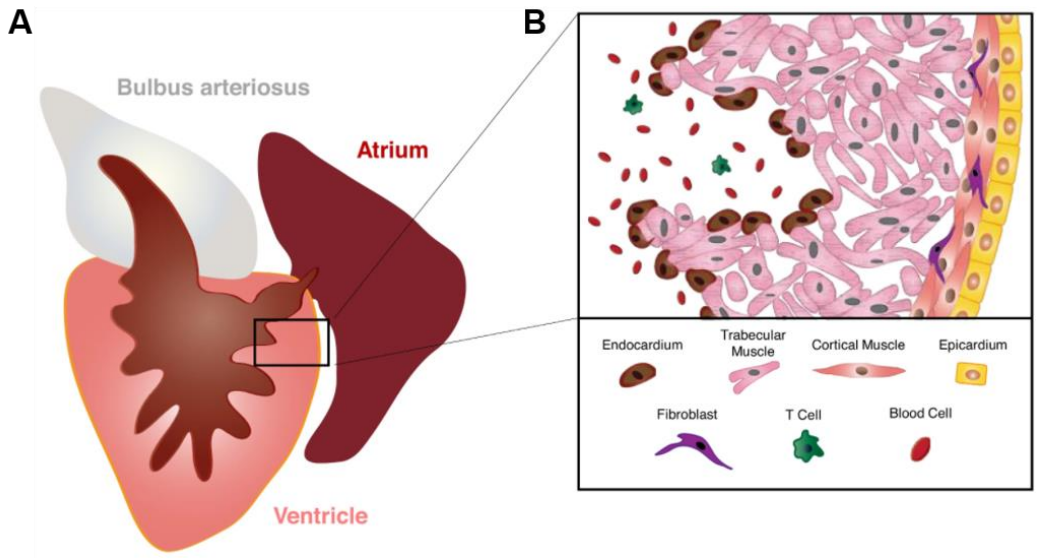

Figure 1.9. Anatomy of the adult zebrafish heart. (**A**) Illustration showing the anatomy of the adult zebrafish heart. (**B**) Illustration showing the various cell types on a longitudinal section of the adult zebrafish heart. Adapted from (Pronobis and Poss, 2020), Figure 1. License: 5231350891896.

1.4.2. Injury models to study heart regeneration

Poss and colleagues first discovered that the zebrafish heart can regenerate after partial ventricular resection (Poss et al., 2002). Meanwhile, a variety of alternative cardiac injury models have been developed, including cryoinjury, genetic cell ablations and cauterization (**Fig. 1.10**) (Choi and Poss, 2012; Dyck et al., 2020). Each of these models has its own advantages and disadvantages depending on the scientific question that is being addressed. However, the cardiac cryoinjury technique is thought to physiologically recapitulate the mammalian myocardial infarction, and is rapidly becoming the most used technique to study cardiac regeneration in zebrafish (Chablais et al., 2011).

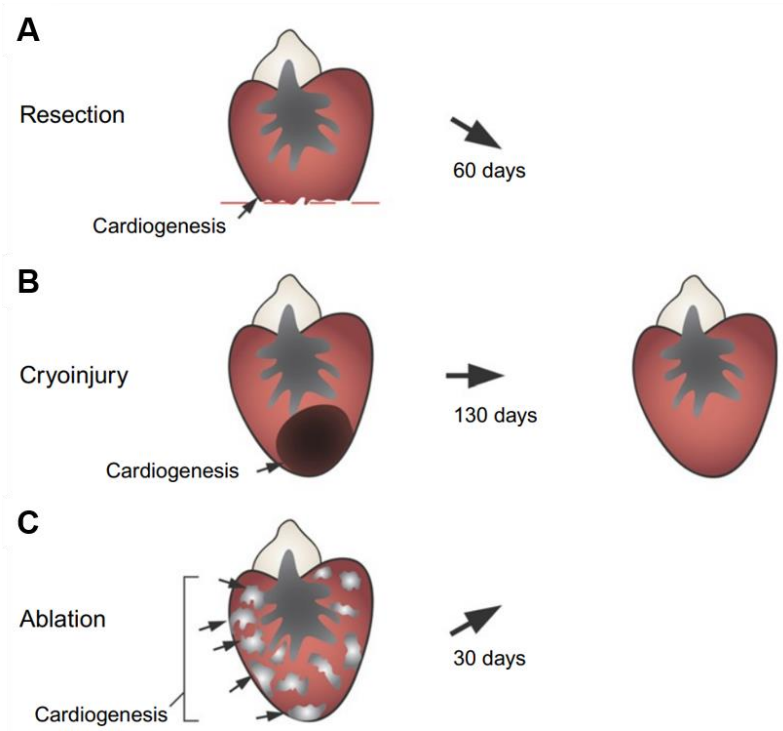

Figure 1.10. Injury models for adult zebrafish heart regeneration. (**A**) Illustration showing ventricular apex resection model. (**B**) Illustration showing ventricular cryoinjury model. (**C**) Illustration showing genetic ablation of cardiomyocytes. Adapted from (Choi and Poss, 2012), Figure 2. License: 5231350994949.

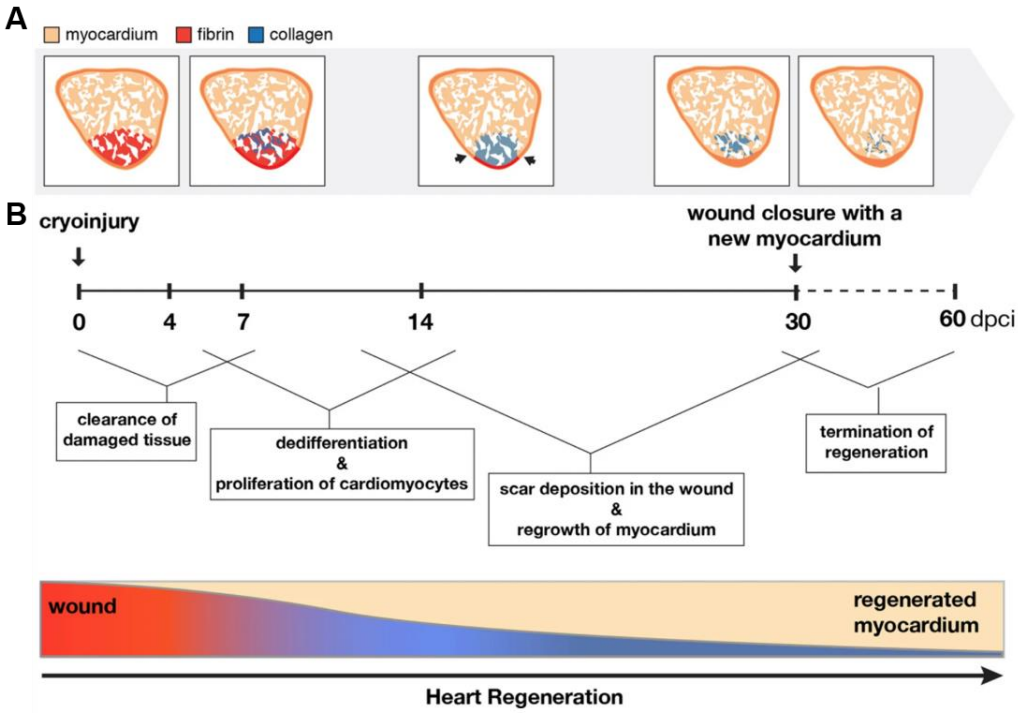

Figure 1.11. Progression of zebrafish cardiac regeneration after cryoinjury. (**A**) Illustrations showing Acid Fuchsin Orange G staining on ventricular sections of adult zebrafish heart. (**B**) Timeline showing major cellular processes during cardiac regeneration after cryoinjury. Adapted from (Bise et al., 2020), Figure 1. License: CC BY 4.0.

1.4.3. Cellular response to cardiac cryoinjury

Like any other organ, the zebrafish heart consists of a parenchymal component and various stromal components. Cardiomyocytes are the parenchyma that confer the heart with its pumping function. The key stromal cell types include the epicardium, fibroblasts, endothelium, resident immune cell populations and the valve cells (**Fig. 1.9B**). The cardiac valves consist of valve interstitial cells that are outlined by valve endothelial cells. After cryoinjury, a series of well-characterized cellular processes take place during heart regeneration (**Fig. 1.11**). In the next few sub-sections, I will review the literature of how each of the cell types responds to cardiac injury and contributes to cardiac regeneration (**Fig. 1.12**).

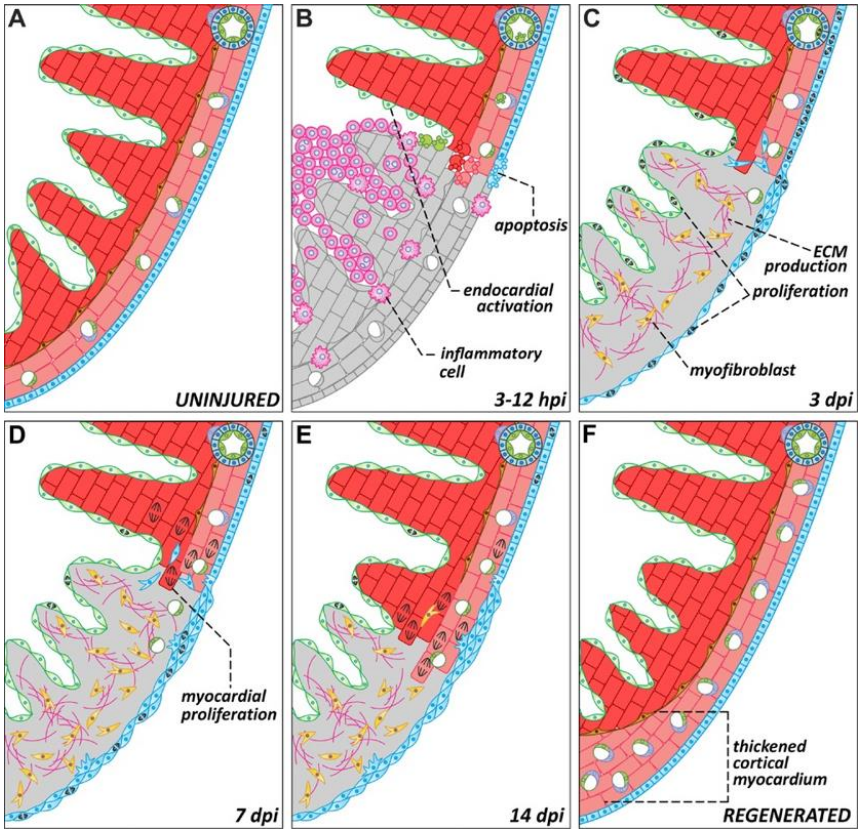

Figure 1.12. Cellular response to cryoinjury in the adult zebrafish heart. (**A**) Longitudinal section of an uninjured heart. (**B**) Illustration showing 3-12 hpci heart with activated endocardium, immune cell infiltration and border zone apoptosis. (**C**) 3 dpci – ECM production by endocardial cells and fibroblasts, proliferation of endocardial cells and fibroblasts, and myofibroblast differentiation. (**D**) 7 dpci – cardiomyocyte proliferation in the border zone. (**E**) 14 dpci – cardiomyocyte migration. (**F**) 60-90 dpci – fully functional and regenerated myocardium. Adapted from (González- Rosa et al., 2017), Figure 4. License: CC BY 4.0.

1.4.3.1. Cardiomyocyte response

The ventricular cardiomyocytes are mainly divided into three main layers – outer cortical, inner trabecular and an intermediate primordial layer (**Fig. 1.9B**) (Gupta and Poss, 2012). The cortical layer of cardiomyocytes form an outer compact wall while the trabecular layer forms a network of cardiomyocytes that are crucial for the heart contraction and conduction. The primordial layer of cardiomyocytes is a single layer of cells that are positioned in between cortical and trabecular layers. In one of our studies, we show that the primordial layer of cardiomyocytes express immature muscle

marker genes and display higher Notch pathway-related gene expression (Tsedeke et al., 2021).

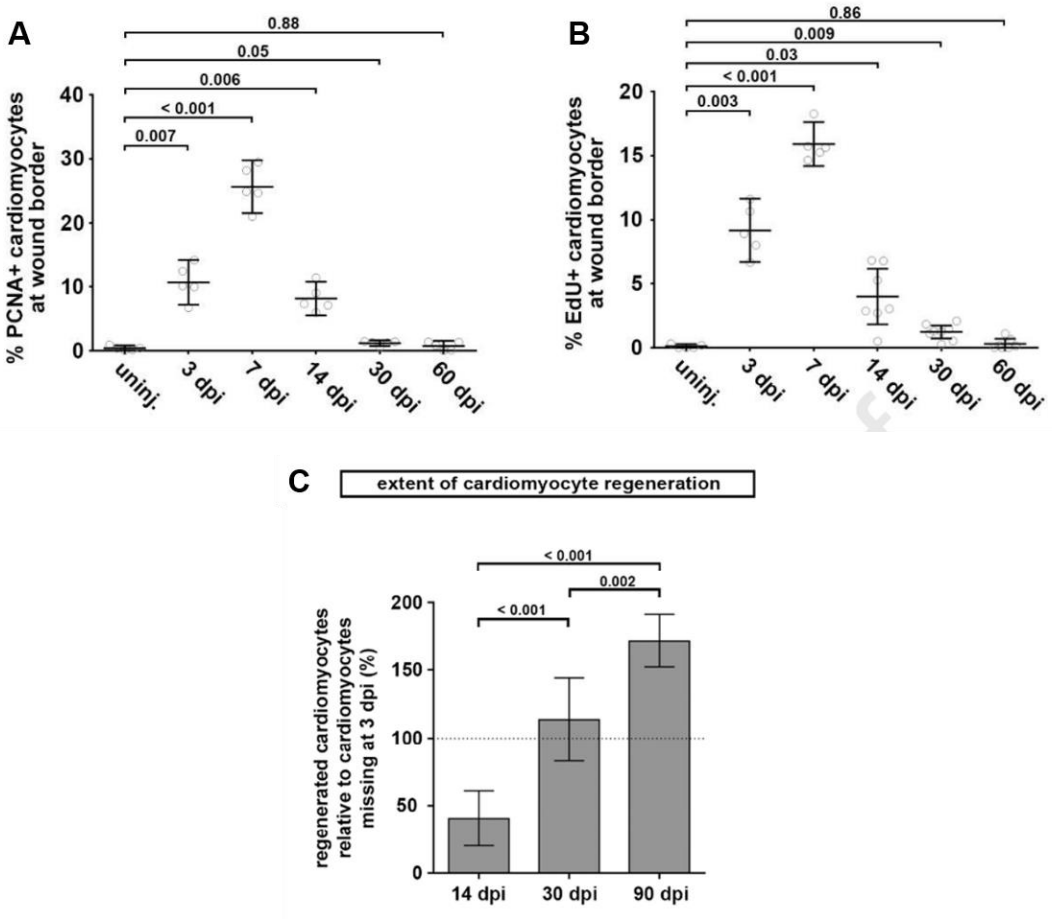

Figure 1.13. Cardiomyocyte proliferation and renewal during zebrafish cardiac regeneration. (**A and B**) Quantification of cardiomyocyte proliferation index using PCNA immunostaining (A) and EdU incorporation (B) at various time points after cardiac cryoinjury. (**C**) Quantification of the absolute number of cardiomyocytes as a percentage of cardiomyocytes lost at 3 dpci, showing that the number of cardiomyocytes lost have been renewed by 30 dpci. Adapted from (Bertozzi et al., 2021), Figures 2A, 2B, and 3F. License: 5231351313151.

Successful cardiomyocyte regeneration involves induction of several fundamental cellular processes, including proliferation, dedifferentiation, and migration (**Fig. 1.12**). As it has been the center of the research interest in mammalian cardiac regeneration, cardiomyocyte proliferation is the most studied aspect of zebrafish cardiac regeneration. In the first few minutes to hours after cardiac cryoinjury, cardiomyocytes

activate protective signals mainly in the border zone, adjacent to the injured area. However, a few of these border zone cells undergo cell death in first 24 hours after injury (**Fig. 1.12B**). It was also shown that cardiomyocytes start to proliferate within the first 3 days after injury, and that the peak of proliferative activity is at 7 dpci (days post cryoinjury). The levels of proliferation start to decline by 14 to 21 dpci, and finally reach the basal uninjured levels by 30 dpci (**Fig. 1.13A and B**). However, zebrafish take around 90 dpci to completely regenerate, including scar resolution (**Fig. 1.13C**) (Bertozzi et al., 2021). These data show that the cardiomyocyte numbers required to replace the lost tissue have already been generated by 30 dpci, and that these cells could be involved in digesting the transient matrix in order to repopulate the injured area. In the same direction, Beisaw and colleagues showed that the border zone cardiomyocytes display protrusive activity, reminiscent of migration, as early as 3 dpci (**Fig. 1.14A**) (Beisaw et al., 2020). In a different study, Itou and colleagues used cardiomyocyte specific photo-convertible fluorescent reporter-based tracing experiment to demonstrate that these cells indeed migrate and repopulate the injured area after partial ventricular resection (**Fig. 1.14B**) (Itou et al., 2012). In addition, it has also been shown that the border zone cardiomyocytes activate embryonic-like muscle markers, including *gata4*, *tnnc2* and embryonic cardiac myosin heavy chain (embCMHC) (**Fig. 1.14C**) (Kikuchi et al., 2010; Sallin et al., 2015; Tsedeke et al., 2021). Furthermore, they have been shown to downregulate mature muscle markers such as *tnni4b.3* after cardiac injury (Tsedeke et al., 2021). These data indicate that zebrafish cardiomyocytes undergo dedifferentiation towards an embryonic fate. Moreover, it has also been shown that the border zone cardiomyocytes switch their metabolic activity from oxidative to glycolytic pathways (Fukuda, 2020; Honkoop et al., 2019).

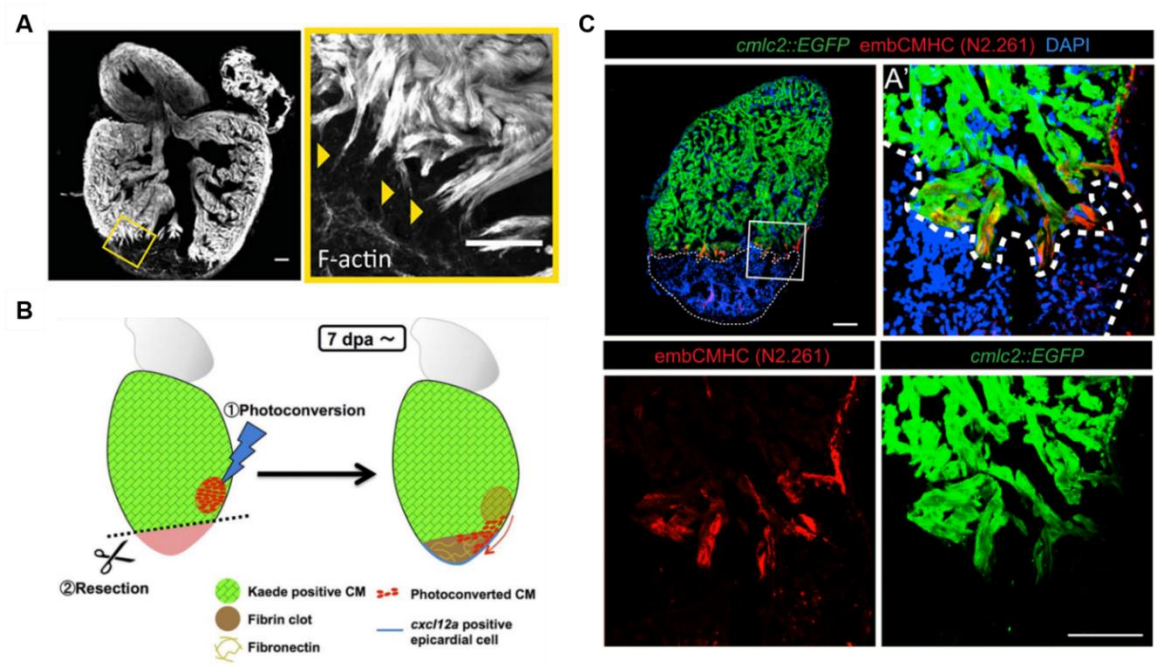

Figure 1.14. Cardiomyocyte protrusion and dedifferentiation during zebrafish cardiac regeneration. (**A**) F-actin staining on wild-type ventricular section at 7 dpci showing cardiomyocyte protrusion. Adapted from (Beisaw et al., 2020), Figure 3C. License: 5231360544437. (**B**) Illustration showing the schematics of a photoconversion experiment to demonstrate cardiomyocyte migration after ventricular resection. Adapted from (Tahara et al., 2016), Figure 3B. License: 5231360700115. (**C**) Immunostaining for GFP and embCMHC on a wild-type ventricular section at 7 dpci showing immature cardiomyocyte marker reactivation (embCMHC) in the border zone. Adapted from (Sallin et al., 2015), Figure 5. License: CC BY-NC-ND 4.0.

1.4.3.2. Endothelial cell response

The zebrafish cardiac ventricle consists of at least 4 types of anatomically different endothelial cells. Endocardium, coronary endothelium, lymphatic endothelium and the valve endothelium (Lowe et al., 2021). Endocardium is the innermost lining of endothelial cells that envelope the cardiomyocytes and faces the lumen (**Fig. 1.9B**). Coronary endothelium lines the coronary vessels that supply the cardiac wall with oxygen and nutrients. The lymphatic endothelium lines the lymphatic vessels that clear the tissue of excessive fluids and maintains fluid balance (Gutierrez-Miranda and Yaniv, 2020). Valve endothelium envelopes the valve interstitial cells and faces the blood flow (Bensimon-Brito et al., 2020).

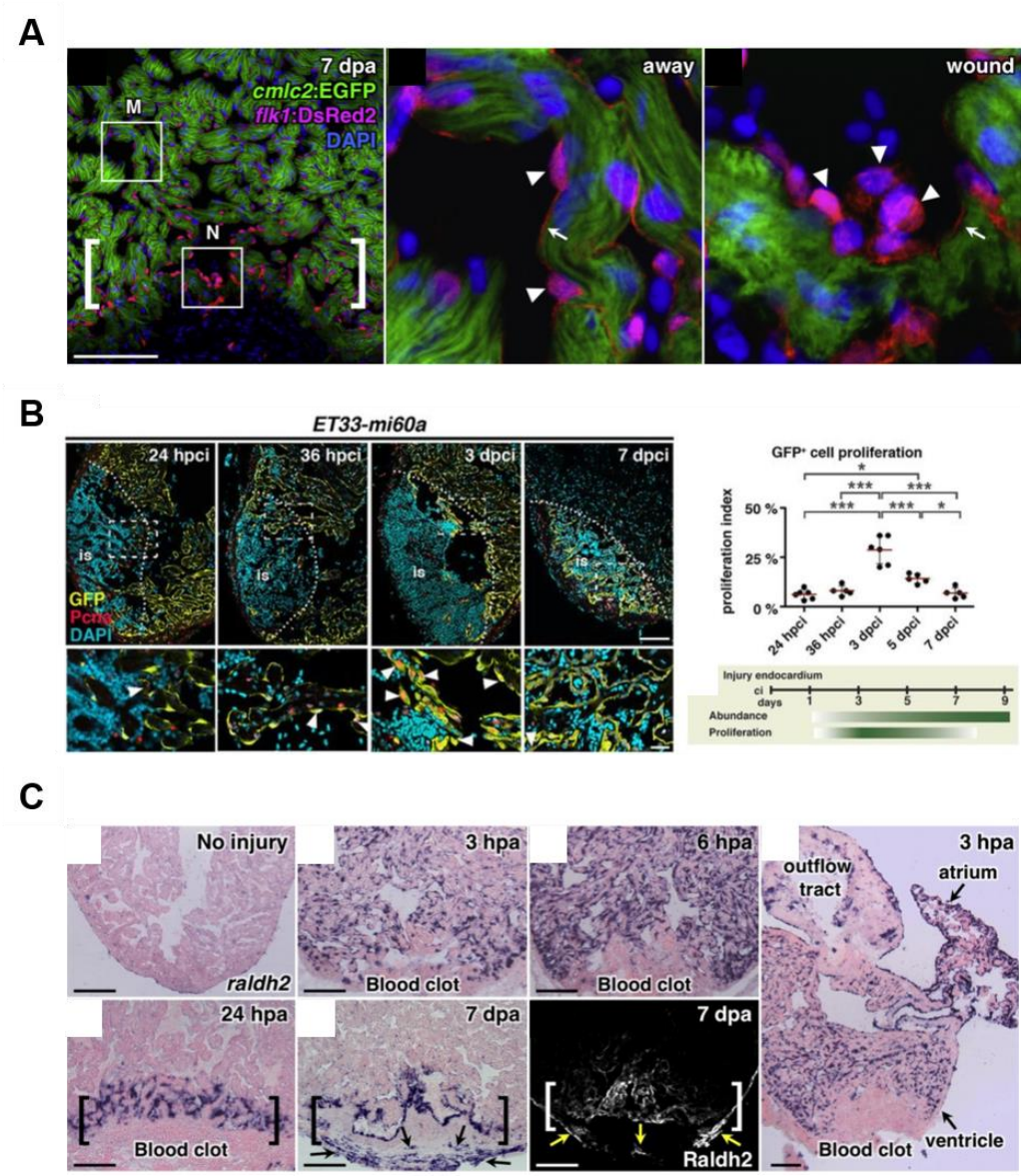

Figure 1.15. Endocardial dynamics during cardiac regeneration. (**A**) Immunostaining for GFP, DsRed2 on *Tg(cmlc2:EGFP); Tg(flk1:DsRed2)* ventricle sections at 7 dpa showing endocardial shape changes after ventricular resection. Adapted from (Kikuchi et al., 2011b), Figure 1. License: 5231361058582. (**B**) Immunostaining for GFP and PCNA on *Et(krt4:GFP)sqet33-mi60a* ventricle sections at various time points showing endocardial migration and proliferation. Adapted from (Münch et al., 2017), Figure 1. License: User License 1.1. (**C**) In situ hybridization for *aldh1a2* mRNA levels and immunostaining for Aldh1a2 expression after ventricular resection at various time points showing the endocardial Retinoic acid activation. Adapted from (Kikuchi et al., 2011b), Figure 1. License: 5231361058582.

The endocardium is activated in response to cardiac injury. Kikuchi and colleagues used transmission electron microscopy (TEM) to study the morphological changes that the endocardium undergoes after partial ventricular resection (Kikuchi et al., 2011b). As early as 1-3 hours post amputation (hpa), the endocardium detaches from the underlying myocardium and attains a round morphology throughout the ventricle. Within 24 hpa, endocardial cells in the remote area resemble the ones in an uninjured ventricle. However, the cells at the injury border and in the injury area remain rounded until 7 days post amputation (dpa) (**Fig. 1.15A**). In another study, Münch and colleagues characterized the endocardial response to cardiac cryoinjury (Münch et al., 2017). An endocardial specific enhancer trap line [*Et(krt4:EGFP)sqet33-mi60A*] was used. After cryoinjury, endocardial cells in the border zone acquire a round morphology, and begin to proliferate and migrate into the injured area. The peak of endocardial proliferation is at 3 dpci, and they form a coherent network that repopulates the injury by 9 dpci (**Fig. 1.15B**). It was also shown that, similar to the migrating cardiomyocytes, the migrating endocardial cells extend philopodia-like protrusions into the injured area (Münch et al., 2017). The endocardial cells that have invaded the injured area also secrete collagens contributing to the transient matrix deposition. Sanchez-Iranzo and colleagues have shown that these collagen-expressing cells are required for cardiomyocyte proliferation and regeneration (Sánchez-Iranzo et al., 2018). In addition, these activated endocardial cells express retinoic acid signaling related genes, including *raldh2*/*aldh1a2* (**Fig. 1.15C**) (Kikuchi et al., 2011b).

Coronary endothelial cells are thought of as mere conduits that supply the cardiac muscle with oxygen and nutrients. However, recent work from Marin-Juez, El-Sammak and colleagues suggests an additional role of the coronary vasculature in forming a scaffold and guiding the regenerating cardiomyocytes (**Fig. 1.16**) (Marín-Juez et al., 2019, 2016). Briefly, coronaries start to sprout into the injury area as early as 15 hpci (Marín-Juez et al., 2016). Their peak of proliferation is at 4 dpci and they have been shown to cover the entire injured area by 7 dpci. Two types of coronary revascularization after cryoinjury were described – superficial and intraventricular coronaries. Superficial coronaries are guided by *cxcl12b* from the epicardial-derived cells that binds to *cxcr4a* that is expressed on regenerating coronaries. On the other

hand, hypoxia and Vegfa signaling axes guide intraventricular coronaries. Together, these vessels form a scaffold that is required for cardiomyocyte repopulation of the injured area (Marín-Juez et al., 2019). More recently, El-Sammak and colleagues have shown that Vegfc-Emilin2a-Cxcl8a axis is required for coronary revascularization. However, coronary specific manipulations will be needed to further strengthen the newly postulated role of coronaries in cardiomyocyte regeneration.

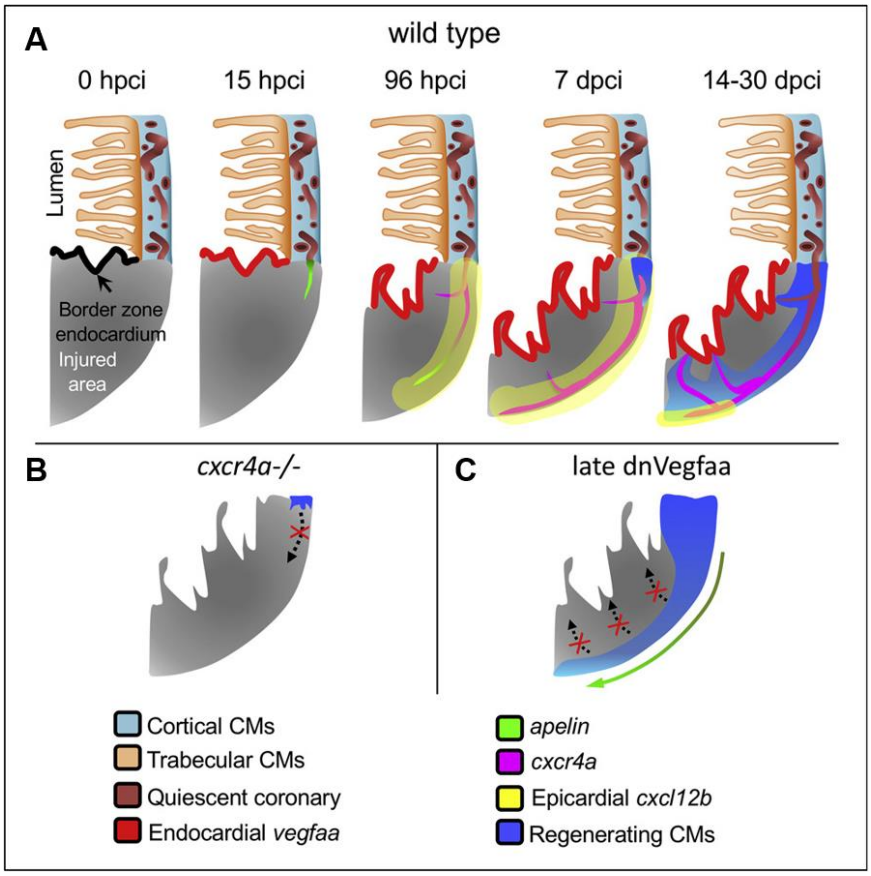

Figure 1.16. Coronary revascularization during cardiac regeneration. (**A**) Illustration showing the different modes of coronary regeneration after cardiac cryoinjury. (**B**) Illustration showing the role of Cxcl12b-Cxcr4a signaling axis in driving superficial coronary regeneration. (**C**) Illustration showing the role of hypoxia and Vegfaa signaling axes in driving intraventricular coronary regeneration. Adapted from (Marín-Juez et al., 2019), graphical abstract. License: 5231361438934.

The role of lymphatic endothelial cells during cardiac regeneration is understudied. However, a couple of recent studies have reported the development and function of lymphatics in the regenerating zebrafish heart (Gancz et al., 2019; Harrison et al.,

2019). Harrison et al. show that lymphatics start to develop in the young adult zebrafish using the already established coronary vasculature as a roadmap. They also show that the injured zebrafish heart undergoes vigorous lymphangiogenesis and that impaired lymphangiogenesis leads to permanent scarring after injury. Furthermore, as suggested in the mouse models of myocardial infarction, it was shown that the zebrafish lymphatics act as conduits for neutrophil and macrophage clearance from the injured area. A recent study in mice identified Reelin as a lymphatic endothelial-specific protein that promotes cardiomyocyte proliferation during development and regeneration (Liu et al., 2020). The valve endothelial response to cardiac cryoinjury has not been studied yet. However, the regenerative response to cardiac valve injury was recently characterized (Bensimon-Brito et al., 2020). Further studies are needed to characterize the roles of these individual endothelial types and how they affect cardiomyocyte regeneration, using endothelial-compartment specific tools.

1.4.3.3. Epicardial and epicardial-derived fibroblast response

Like in the mammals, the zebrafish heart is superficially enveloped by a single-layered epithelium called as the epicardium (**Fig. 1.9B**). In the zebrafish heart, the transcription factor *tcf21* is expressed in epicardial and epicardial derived cells, both during development and regeneration (Cao and Poss, 2018). The developing epicardium gives rise to various types of epicardial-derived cells (EPDCs), including perivascular cells and fibroblasts (Kikuchi et al., 2011a). The perivascular cells, including the pericytes and smooth muscle cells are embedded in the cortical layer of cardiomyocytes enveloping the coronaries (**Fig. 1.17A**). Tissue resident cardiac fibroblasts in the zebrafish cardiac ventricle are located in the interstitial space between cortical layer and trabecular layer, adjacent to the primordial layer of cardiomyocytes (**Fig. 1.17B**) (Sánchez-Iranzo et al., 2018). These 3 populations – the outer layer of epicardium, inner layer of fibroblasts, and the intermediate layer of EPDCs (mostly perivascular cells) – were also identified by Cao and colleagues using single-cell RNA-seq analysis on *tcf21* reporter expressing cells in the uninjured zebrafish ventricle (Cao et al., 2016).

The epicardium is one of the first tissues to respond to cardiac injury. The tightly adhered outer epicardial layer displays reduced cell-cell adhesion within the first few hours after cryoinjury (**Fig. 1.17C**) (González-Rosa et al., 2012). The epicardial cells in the injury border then begin to migrate onto the injury. Using ex-vivo heart slice cultures, Cao and colleagues have shown that the migrating epicardial cells could be divided into two populations: leader cells and follower cells. The leader cells display high mechanical tension and undergo endoreplication (Cao et al., 2017). These data suggest a similar migratory behavior of the regenerating epicardial layer after cryoinjury. Within the first few days, the regenerating epicardial cells activate several embryonic epicardial markers, including the genes expressing Wt1b, Tbx18, and Aldh1a2 (**Fig. 1.17D**) (Lepilina et al., 2006). By 3 dpci, the thin layer of outer epicardial cells, together with the *wt1a*-expressing inner epicardial-derived cells at the injury border expand into a multilayered scaffold that envelopes the whole injury area superficially by 7 dpci (González-Rosa et al., 2012). A subpopulation of these cells activate *postnb* expression, which are termed as activated fibroblasts. Although these cells persist in the injury site for longer duration, it was reported that they are deactivated at around 60 dpci. It was also reported that these collagen-expressing/ECM-depositing cells are important contributors to efficient cardiomyocyte regeneration (Sánchez-Iranzo et al., 2018).

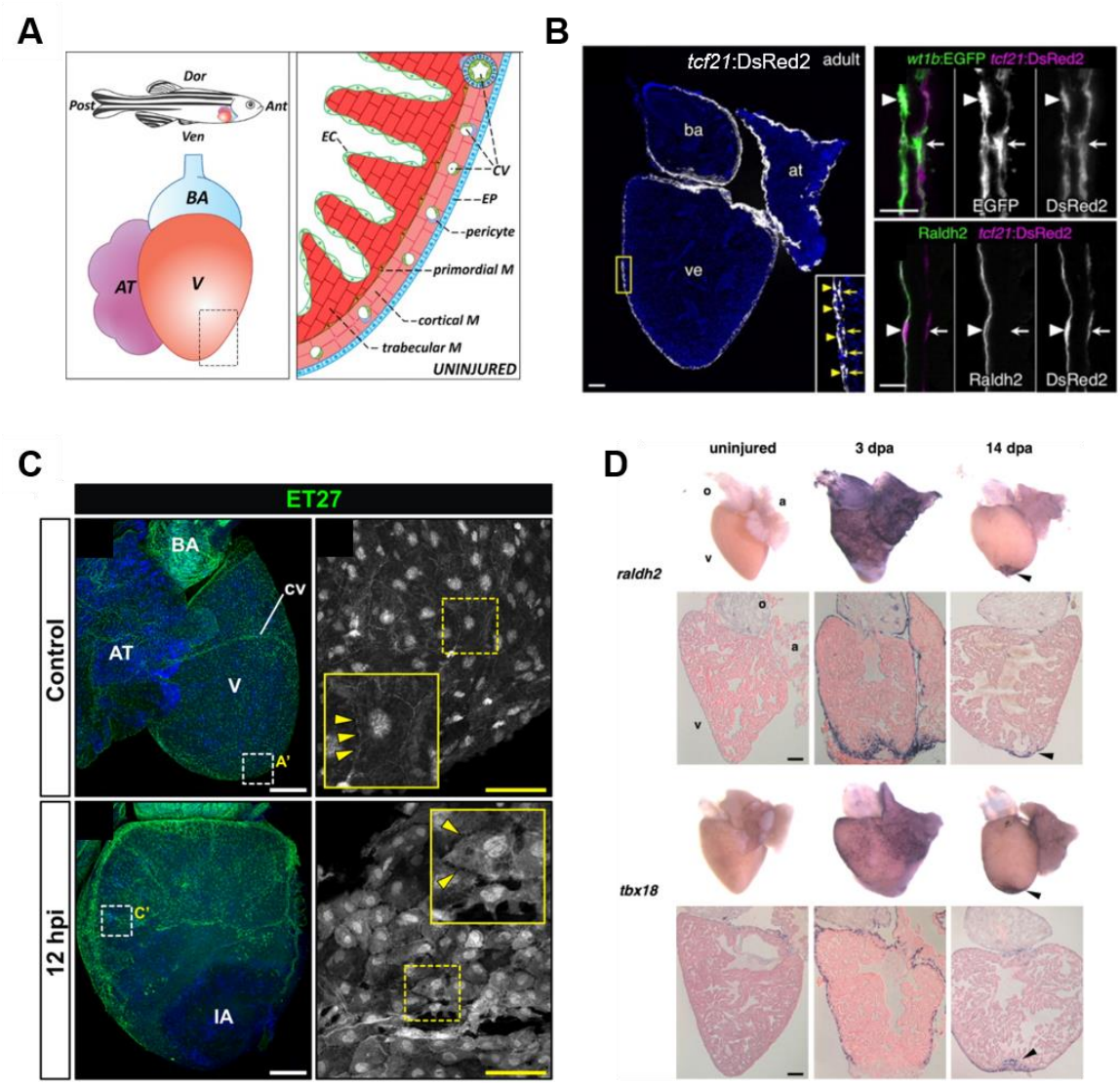

Figure 1.17. Epicardial dynamics during cardiac regeneration. (**A**) Illustration showing the anatomy of the zebrafish heart and its cellular make-up. Adapted from (González-Rosa et al., 2017), Figure 4. License: CC BY 4.0. (**B**) Immunostaining for DsRed2, GFP and Aldh1a2 on *Tg(tcf21:DsRed2); Tg(wt1b:EGFP)* uninjured ventricular sections showing different layers of epicardial and epicardial-derived cells. Adapted from (Kikuchi et al., 2011a), Figure 1. License: 1178770. (**C**) Wholemount images of *Et(krt4:EGFP)sqet27* showing epicardial architecture at uninjured and 12 hpci. Adapted from (González-Rosa et al., 2012), Figure 1. License: 5231370574613. (**D**) In situ hybridization for embryonic epicardial genes that are reactivated after ventricular resection, including *aldh1a2* and *tbx18.* Adapted from (Lepilina et al., 2006), Figure 3. License: 5231370788489.

The epicardium has been shown to be important for cardiac regeneration in adult zebrafish (Cao and Poss, 2018). Ablating *tcf21* expressing cells after ventricular

resection resulted in reduced cardiomyocyte proliferation, indicating the importance of epicardial cells in aiding heart regeneration (Wang et al., 2015). Two possible hypotheses were put forth regarding how epicardial cells could contribute to cardiac regeneration: 1. direct contribution to the regenerating cardiomyocytes by cell reprogramming, and 2. aiding cardiomyocyte regeneration by paracrine signaling. Kikuchi and colleagues have generated a robust CreER driver line under the influence of *tcf21* regulatory elements to lineage trace the epicardial and EPDCs during development and after injury. They have found that the embryonic epicardial layer stays lineage restricted and gives rise to epicardial-derived cells in all the three layers in the adult stages (Kikuchi et al., 2011a). Furthermore, they have concluded that, after ventricular resection, the epicardial cells give rise to several regeneration-specific epicardial-derived cell populations, but do not directly reprogram into the cardiomyocyte lineage. These data strongly indicate a paracrine signaling role for the epicardium during heart regeneration.

Here, I briefly review the relevant literature highlighting a few epicardial-derived paracrine factors. Similar to endocardial cells, the epicardium upregulates the retinoic acid synthesizing enzyme (Aldh1a2) within a few minutes after injury. Blocking retinoic acid (RA) signaling by either a dominant negative receptor (DN-Rar) or overexpressing an enzyme that degrades RA (Cyp26a1) severely reduced cardiomyocyte proliferation after resection (**Fig. 1.18C and D**) (Kikuchi et al., 2011b). However, cell-specific manipulations will give more information about the cell-autonomous and cell non-autonomous roles of RA signaling during heart regeneration. Other pro-regenerative molecules, including Fibronectin-1, Hyaluronan and proteoglycan link protein (hapln1a), Wilm's tumour 1b, Neuropilin, Neuregulin 1a, chemokines (Cxcl12, Cxcl8) and the connective tissue specific transcription factor Prrx1b have been shown to be expressed by the epicardial cells upon injury (Cao and Poss, 2018; de Bakker et al., 2021). As discussed earlier, it was also shown that the EPDCs secrete *cxcl12b* and form a scaffold for coronary regeneration, which then supports cardiomyocyte migration (Marín-Juez et al., 2019). Furthermore, the epicardium also secretes the evolutionarily conserved pro-regenerative ECM molecule Fibronectin-1. Blocking Fibronectin function by either loss-of-function mutations or dominant negative

approaches, surprisingly did not affect cardiomyocyte proliferation, but only CM migration (**Fig. 1.18A and B**) (Wang et al., 2013). The epicardium also contributes to the scar-forming myofibroblasts (González-Rosa et al., 2012). More studies are needed to uncover the signaling mechanisms on how zebrafish limit myofibroblast differentiation.

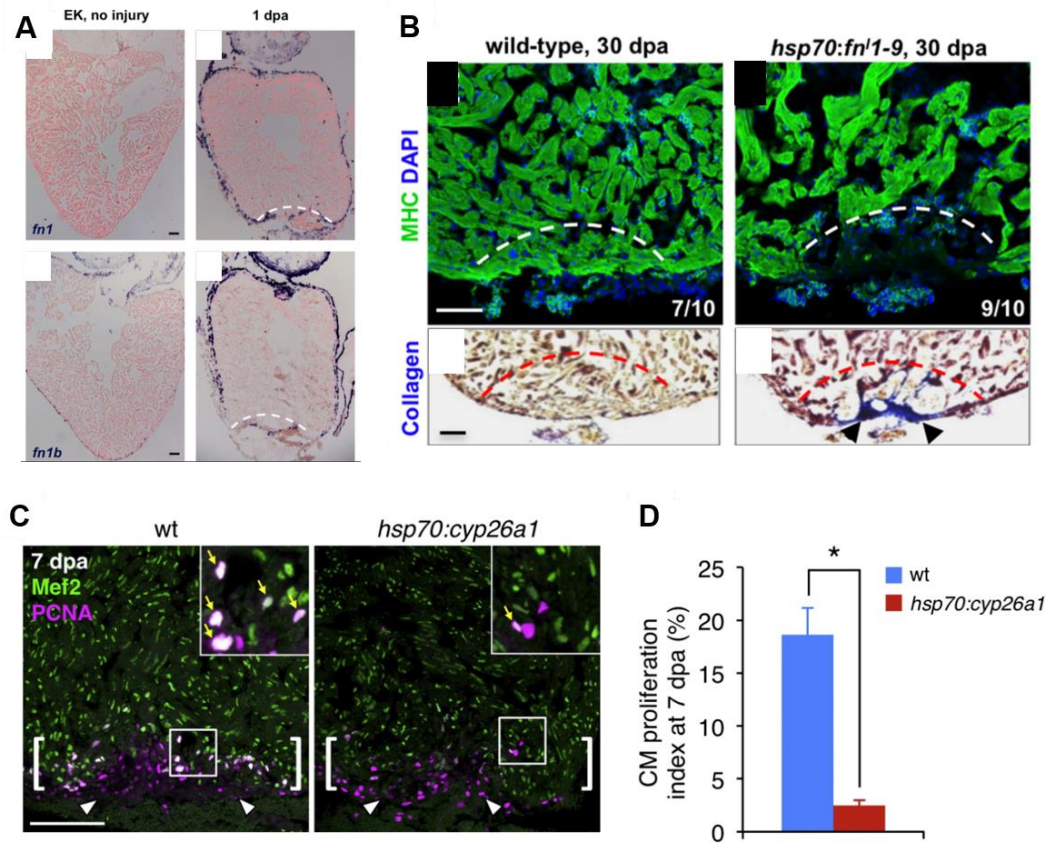

Figure 1.18. Role of epicardial derived molecules in cardiac regeneration. (**A**) In situ hybridization to detect Fibronectin1 mRNA levels (*fn1a, fn1b*) on uninjured and 1 dpa ventricular sections. (**B**) Immunostaining for cardiac muscle (top) and AFOG staining (bottom) on wild-type and dominant negative fibronectin overexpressing ventricles at 30 dpa. Adapted from (Wang et al., 2013), Figures 2 and 5. License: 5231410446514. (**C and D**) Immunostaining (C) for MEF2 and PCNA and quantification (D) to investigate cardiomyocyte proliferation index on wild-type and Cyp26a1 overexpressing ventricles at 7 dpa. Adapted from (Kikuchi et al., 2011b), Figure 3. License: 5231410566382.

1.4.3.4. Immune cell response

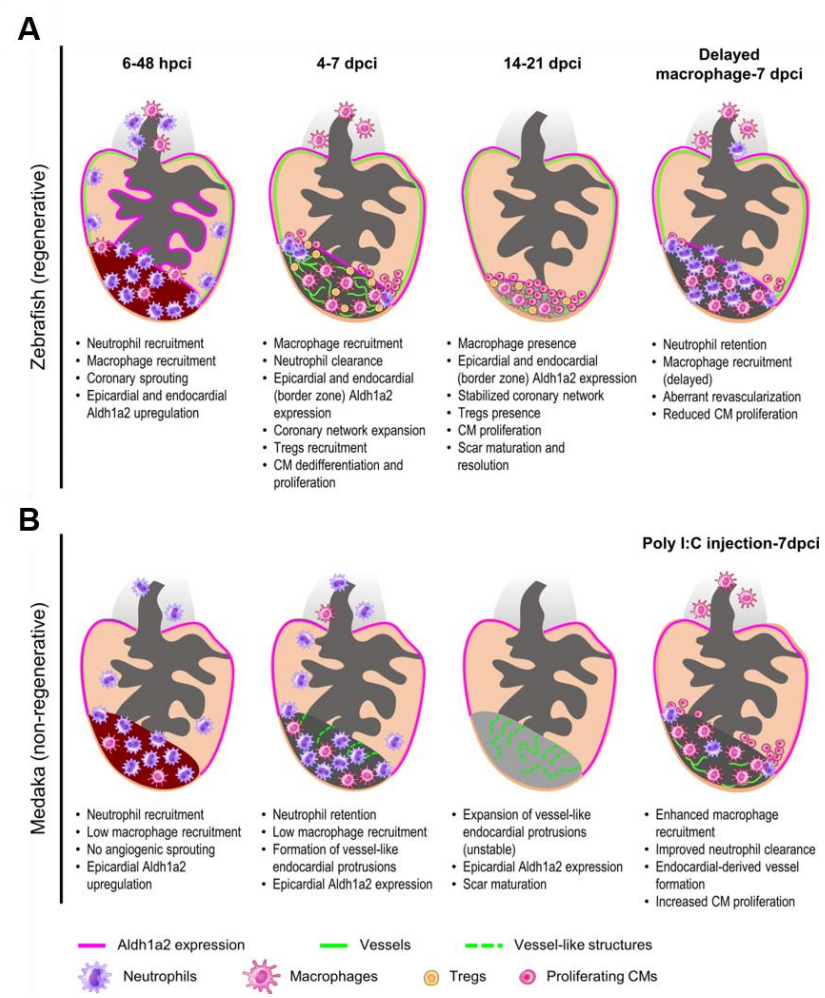

Figure 1.19. Immune response in regenerative and non-regenerative organisms after cardiac injury. (**A and B**) Illustrations showing the immune response and other cellular responses after cardiac injury in the regenerative zebrafish vs. non-regenerative medaka. Adapted from (Lai et al., 2019), Figure 3. Licence: CC BY 4.0.

The immune response to tissue damage can be mainly divided into two types: innate immunity and adaptive immunity (Lai et al., 2019). The innate immune response forms the first line of cellular defense, including neutrophil and macrophage infiltration. Adaptive immunity is a slower and more stable response mainly orchestrated by T-cells and B-cells. The innate immune dynamics are the most studied during tissue regeneration. Within the first few hours after injury, the first innate immune cells to infiltrate the lesion are neutrophils. The stereotypic function of these cells is to phagocytose cell debris and clear them. However, a deeper understanding of the

subtypes and their specific roles is much needed. Around 3 dpci, the neutrophils are followed by macrophages. These cells are mainly divided into two subtypes depending on their phenotype: inflammatory M1-type and anti-inflammatory M2-type. M1 macrophages first infiltrate the tissue and phagocytose the neutrophils – a process termed as efferocytosis (Lai et al., 2019). Following these events, M2 macrophages infiltrate the tissue. M2 macrophages are the pro-regenerative and anti-inflammatory type. It is hypothesized that the macrophages mainly act as paracrine signaling centers, orchestrating tissue fibrosis and regeneration. Furthermore, studies on various regenerative species and tissues show that ablating macrophages (phagocytes) using clodronate liposomes severely impairs tissue regeneration (**Fig. 1.20**) (Godwin et al., 2017, 2013). On the other hand, studies that compared regenerative and non-regenerative model systems (eg. zebrafish vs. medaka) have identified differences in their innate immune responses (Lai et al., 2017). These reports highlight modulation of the immune response as a potential therapeutic strategy for regenerative medicine. This calls for a deeper understanding of the immune-related phenomena during regeneration and scarring.

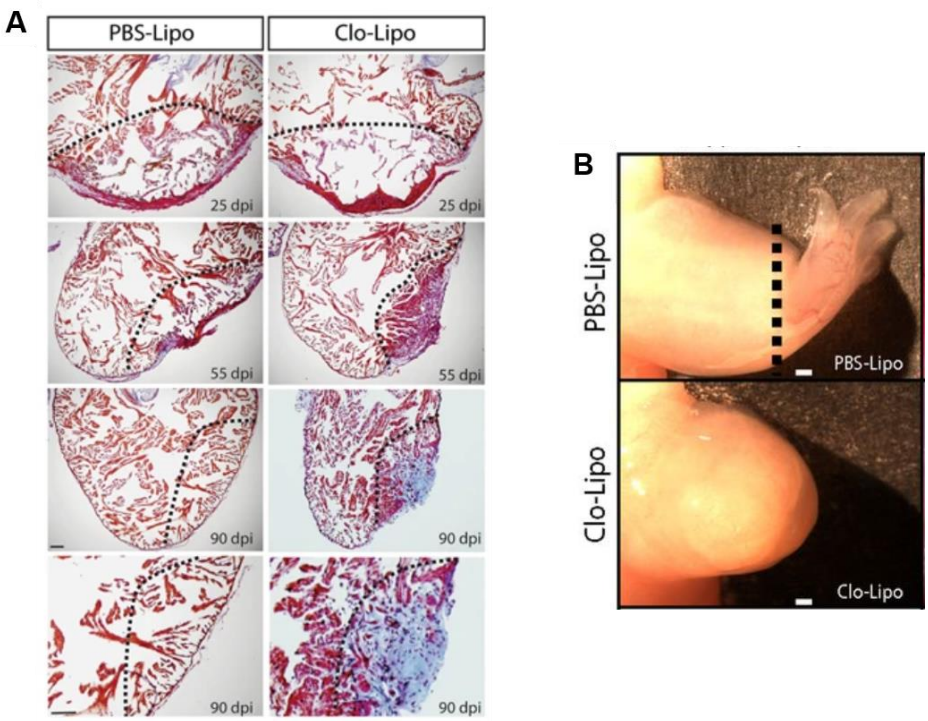

Figure 1.20. Macrophage infiltration is required for regeneration. (**A**) PBS-Liposome vs. Clodronate Liposome injected salamander heart sections stained with Picrosirius Red technique, showing regeneration with PBS, and scarring with Clo-Lipo. Adapted from (Godwin

et al., 2017), Figure 3. License: CC BY 4.0. (**B**) PBS-Liposome vs. Clodronate liposome injected salamanders with limb amputation, showing regeneration with PBS and scarring with Clo-Lipo. Adapted from (Godwin et al., 2013), Figure 4.

1.5. Zebrafish fin regeneration

Zebrafish can regenerate their appendages throughout life, including the fins. As the adult caudal fins are easily accessible for live imaging and genetic manipulations, they are the most used model systems to understand appendage regeneration (Pfefferli and Jaźwińska, 2015). However, during development, it has also been shown that the larvae can regenerate their fin folds within 3 days after amputation (Yoshinari and Kawakami, 2011). Other models, including bone crush injury and cryoinjury have also been established (Chassot et al., 2016; Sousa et al., 2012).

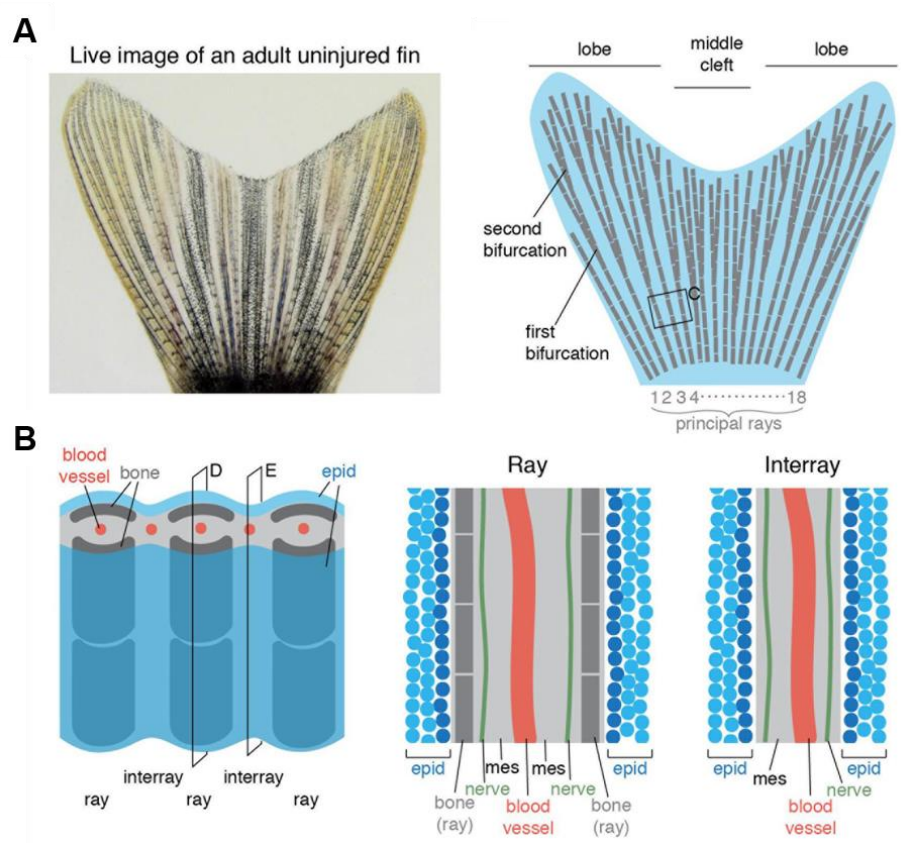

Figure 1.21. Anatomy of the adult zebrafish caudal fin. (**A**) Whole mount brightfield image of adult zebrafish caudal fin (left) and illustration of the same (right). (**B**) Illustrations describing the components of a fin ray and interray space on whole mount (left) and cross-sections (right). Adapted from (König et al., 2019), Figure 1. Licence: CC BY 4.0.

1.5.1. Adult caudal fin regeneration

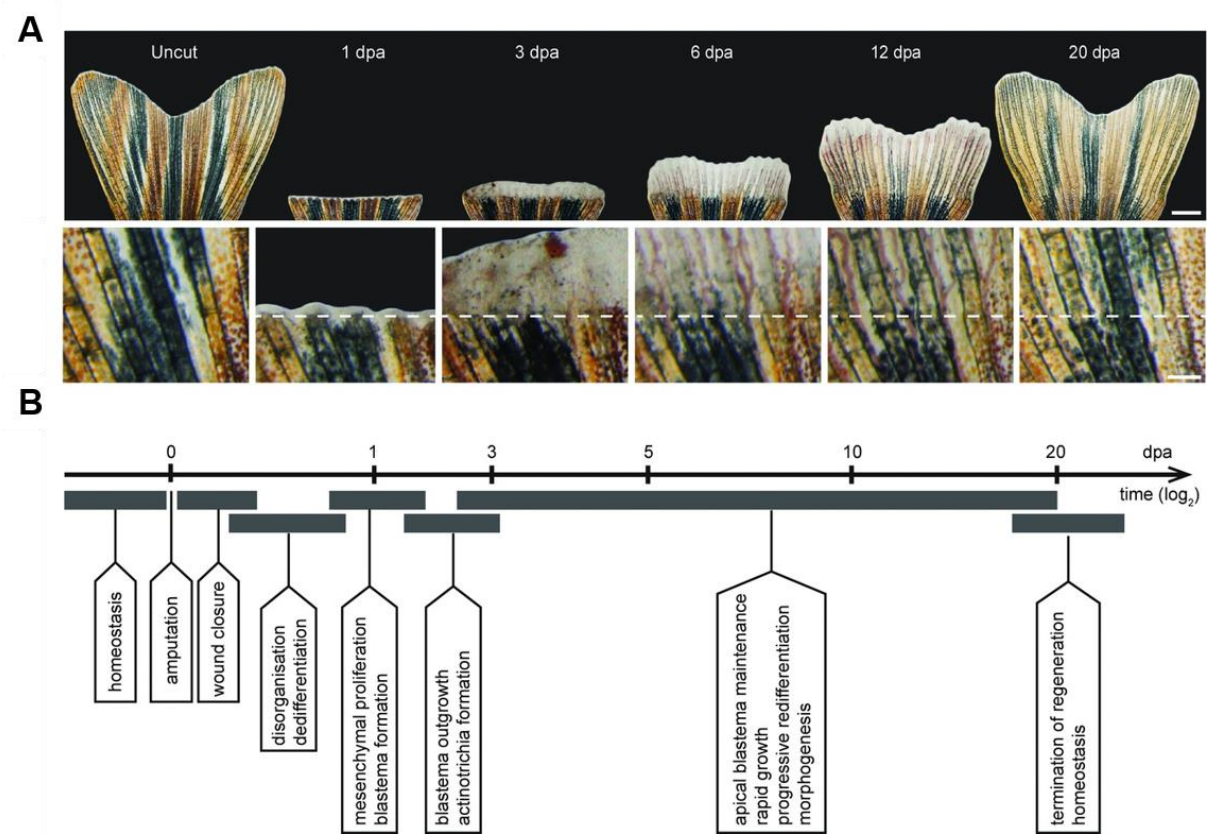

Figure 1.22. Cellular processes during adult caudal fin regeneration. (**A**) Wholemount brightfield images of a time course of regenerating caudal fin. (**B**) Timeline describing the major cellular processes during fin regeneration. Adapted from (Pfefferli and Jaźwińska, 2015), Figure 3. License: CC BY 3.0.

The adult zebrafish caudal fin mainly consists of osteoblasts (bone matrix secreting cells), fin mesenchymal cells, various layers of epithelial cells, blood vessel endothelium, and vessel-associated cells (smooth muscle cells) (**Fig. 1.21**). After amputation, one of the first cellular events is wound re-epithelialization (**Fig. 1.22**). The fin epithelium adjacent to the amputation plane migrates (without proliferating) to envelope the damaged and exposed area (Chen et al., 2016). It was shown that the migrating epithelium acts as a paracrine signaling centre to the underlying mesenchymal cells inducing blastema formation (Pfefferli and Jaźwińska, 2015). Blastema is a mass of undifferentiated cells that arises from pre-existing mesenchymal cells close to the damaged area (more discussed in the Section 1.2.2). Fin mesenchyme proximal to the amputation plane undergoes dedifferentiation, and

migrates to seed the initial blastema (Knopf et al., 2011; Sousa et al., 2011). The blastemal cells proliferate, migrate and ultimately re-differentiate to give rise to a fully regenerated fin. It was also reported that certain signaling gradients are established to pattern the blastema and the regenerating fin. So far, cell dedifferentiation and migration has been extensively characterized in the fin osteoblasts. Osteocalcin (*bglap*) is a mature osteoblast marker. Within 24-48 hpa, the osteoblasts in close proximity to the amputation plane downregulate *bglap* as a proxy for dedifferentiation (Knopf et al., 2011). On the other hand, these osteoblasts also upregulate transcription factors known to promote bone development, including *sp7* (*osterix*) and *runx2* (Sousa et al., 2011). Simultaneously, these cells also extend protrusions past the amputation plane and migrate contributing to blastema formation. Several manipulations to FGF and WNT signaling pathways resulted in no blastema formation and severely hampered regeneration (Owlarn et al., 2017; Wehner et al., 2014; Whitehead et al., 2005). These models displayed impaired osteoblast dedifferentiation showing the requirement for cell dedifferentiation for blastema formation and regeneration.

Certain cellular features during regeneration, including wound re-epithelialization and blastema formation, are conserved among various species throughout evolution (Murawala et al., 2012). To identify the evolutionarily conserved molecular patterns that govern regeneration, Wang and colleagues performed a multi-omics based comparison of zebrafish and African Killifish fins (Wang et al., 2020). Both these fish species are 230 million years apart in evolution; however, they both display a blastema-dependent adult caudal fin regeneration. This comparative study uncovered ~50 regeneration responsive program genes that are evolutionarily conserved during fin regeneration. This gene list includes the well-known pro-regenerative ECM component Fibronectin 1, the Interleukin-6 family cytokine Interleukin-11, and the FGF family ligand Fgf20a. Further studies are needed to delineate the roles of each of these molecules during regeneration, and what that could mean for mammalian appendage regeneration.

1.5.2. Larval fin fold regeneration

Another model to study appendage regeneration in zebrafish is the larval fin fold amputation (Yoshinari and Kawakami, 2011). Live imaging at single-cell resolution, ease of genetic manipulations to understand the cell-specific roles, and the relatively simple tissue architecture are some of the advantages of this model (Hasegawa et al., 2017; Miskolci et al., 2019; Sanz-Morejón et al., 2019). However, since this is an embryonic/larval tissue, drawing parallels to mammalian regeneration is difficult. Similar to adult caudal fin regeneration, the larval amputation results in wound re-epithelialization, blastema formation and expansion (**Fig. 1.23**). Most of the evolutionarily conserved regeneration program is also activated during larval fin fold regeneration, including Fibronectin 1, Interleukin-11, and Jun-Fos signaling (Yoshinari et al., 2009). Together, larval fin fold is a powerful model to screen for and understand molecular mechanisms that facilitate regeneration.

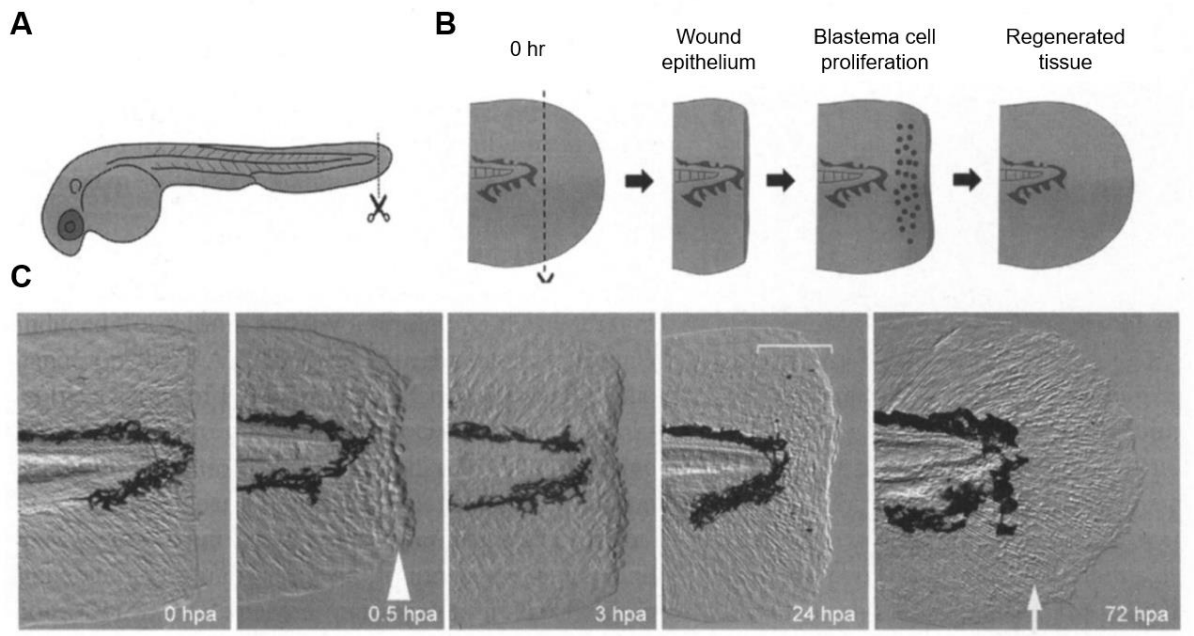

Figure 1.23. Zebrafish larval fin fold regeneration. (**A-C**) Illustrations (A and B), and wholemount brightfield images showing zebrafish larval fin fold regeneration timeline. Adapted from (Yoshinari and Kawakami, 2011), Figure 3. License: 1178828.

1.6. Adult zebrafish scale regeneration

Zebrafish scales for a skeletal envelope that protects the body. Upon losing them or experimental plucking, it has been reported that the scales regenerate within 5-10 days (**Fig. 1.24**) (Cox et al., 2018). The scales possess a characteristic arrangement of osteoblasts, which deposit the scale matrix. Each scale is embedded into a pocket that is enveloped by a layer of epidermis. During regeneration, it has been shown that the new osteoblasts arise by de novo differentiation. These pool of osteoblasts first proliferate and then undergo hypertrophic growth to ultimately regenerate. A train of Erk activity waves, at least in part, mediates this hypertrophic growth of osteoblasts (De Simone et al., 2021). This is an understudied model system compared to other tissue regeneration in zebrafish. However, it offers great opportunities to perform live imaging, genetic manipulations and mathematical modeling (Hayden et al., 2021).

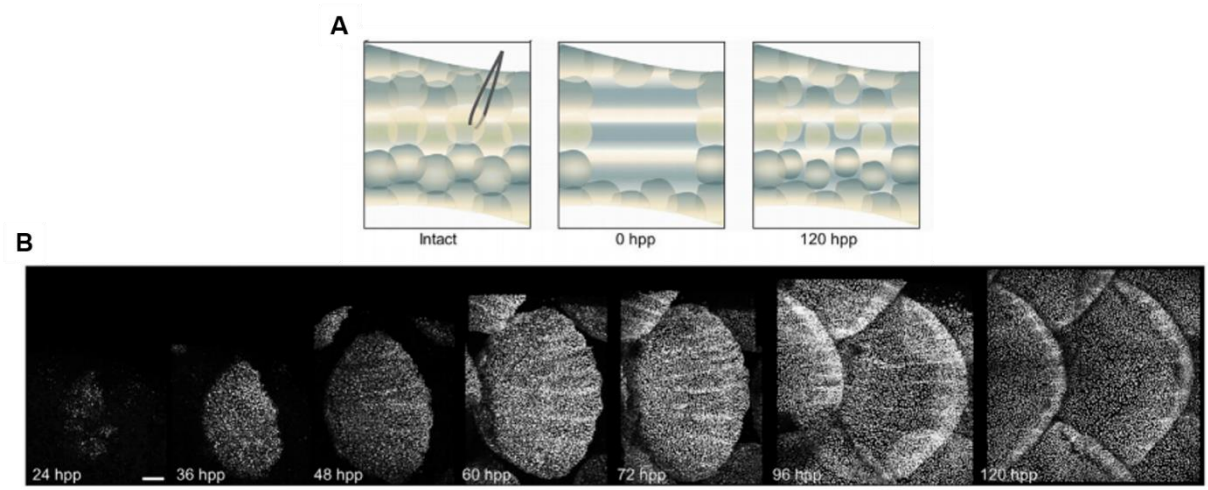

Figure 1.24. Scale regeneration in zebrafish. (A and B) Illustration (A) and confocal imaging (B) of regenerating zebrafish scales. Adapted from (Cox et al., 2018), Figure 1. License: 5231420245632.

1.7. Molecular regulators of regeneration

As discussed in the earlier sections, several pathways and molecules, including TGF-β, FGF, WNT, Retinoic acid, BMP, IL-6 family/Stat3, EGF, IGF, and NF-κB, have been shown to regulate various aspects of tissue regeneration and scarring (González-Rosa et al., 2017). Out of all these pathways, an Interleukin-6 family cytokine – Interleukin-11 – has been shown to induce myofibroblast differentiation in mammals,

thereby portrayed as a pro-fibrotic molecule (Schafer et al., 2017). However, studies on the regenerative *Xenopus* tail suggest that it is a pro-regenerative molecule (Tsujioka et al., 2017). Here, I will review what is known about Interleukin-6 family of cytokines during regeneration and scarring.

1.7.1. Interleukin-6 family of cytokine signaling

The zebrafish Il-6 family consists of seven cytokines – Interleukin-6, Interleukin-11a, Interleukin-11b, Ciliary neurotrophic factor, Leukemia inhibitory factor, Oncostatin M, and Cardiotrophin-like cytokine factor. Each cytokine binds to its specific receptor forming a ligand-receptor complex, which then heterodimerize with a common co-receptor – Interleukin-6 signal transducer (Il6st; also known as Gp130 – glycoprotein 130). The intracellular domain of Il6st has been shown to signal downstream via three major pathways. The most prominent is the canonical Janus Kinase (Jak)- Signal transducer and activator of transcription (Stat3) signaling pathway, whereas mitogen-activated protein kinase kinase (Mek)/extracellular signal–regulated kinase (Erk) and phosphatidylinositol 3-kinase (Pi3k)/protein kinase B (Akt) pathways form the non-canonical wing (**Fig. 1.25**) (Allanki et al., 2021; Rose-John, 2018).

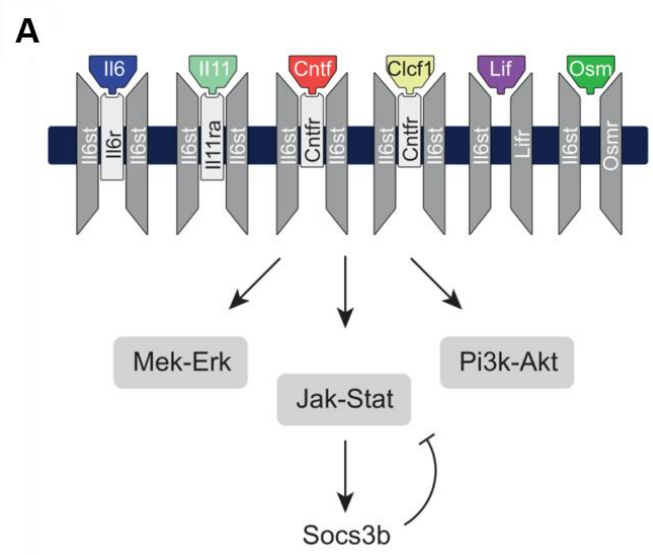

Figure 1.25. Interleukin-6 family of cytokine signaling. (**A**) Illustration showing the zebrafish Il-6 family members and their downstream signaling pathways. Adapted from (Allanki et al., 2021), Figure 2. License: CC BY 4.0.

1.7.2. Interleukin-11 signaling

Due to genome duplication in zebrafish, the gene encoding Interleukin-11 has two paralogues – Interleukin-11a (*il11a*) and Interleukin-11b (*il11b*). These cytokines bind to Interleukin-11 receptor alpha (*il11ra*) and form a ligand-receptor complex. These complexes then heterodimerize with Il6st, which then triggers the downstream activity. Of note, zebrafish and humans have one Il-11 receptor, while the mice have two (Il11ra1 and Il11ra2). In mice, Il11ra1 is more broadly expressed across tissues, while Il11ra2 is restricted to some mouse strains and is expressed in confined to testis, lymph node and thymus (Nandurkar et al., 1997; Schaum et al., 2018). This gene duplication makes a mechanistic understanding of the pathway difficult in mouse. Interleukin-11 has been shown to have an effect in megakaryopoiesis and thrombopoiesis. Indeed, recombinant human Interleukin-11 (rhIL-11) is an Food and Drug Administration (FDA) approved drug under the name of Neumega or Oprelvekin to treat thrombocytopenia (Cook and Schafer, 2020). To study the role of *Il11ra1*, Nandurkar and colleagues generated *Il11ra1* global knockout mice (Nandurkar et al., 1997). These mutants survived to adulthood without any observable defects in hematopoiesis. However, further research picked up a role for Il-11 signaling during tissue regeneration and fibrosis.

1.7.2.1. Role of Interleukin-11 signaling in regeneration

The Fujio lab (Osaka University) published a series of reports implying the cardioprotective role of IL-11/STAT3 signaling after myocardial infarction. First, they showed that Il-11 transcripts and protein are upregulated upon myocardial infarction in adult mice (Obana Masanori et al., 2010). Injecting IL-11 intravenously, activated STAT3 signaling in cardiomyocytes suggesting that IL-11 directly acts on them. Next, they administered IL-11 after MI and observed a reduction in cardiac scarring and a betterment of cardiac function. After MI, IL-11 treatment reduced apoptotic cell death in the border zone cardiomyocytes and increased angiogenic activity in the infarct region (**Fig. 1.26A**). Furthermore, a cardiomyocyte specific deletion of Stat3 abrogated the protective effects of IL-11 treatment, strongly indicating the cardioprotective effects of IL-11/STAT3 signaling. Together with these and other follow up reports in mice, rhIL-11 was injected into human MI patients to screen for any adverse drug reactions.

rhIL-11 treatment did not have any noticeable adverse reactions on the treated 4 MI patients (Nakagawa et al., 2016).

In addition to these reports in mice and humans, studies in the regenerative organisms, including zebrafish and *Xenopus*, also supported the pro-regenerative role of Il-11/Stat3 signaling (Fang et al., 2013; Tsujioka et al., 2017). An evolutionarily conserved induction of Il-11 transcripts during regeneration was reported in the axolotl limb, *Xenopus* tail, zebrafish heart, and Lung fish limb. Using CRISPR-Cas9 based knock down strategies, knocking down *il-11* in the Xenopus tadpoles resulted in impaired regeneration. This study concluded that the injury-induced Il-11 signaling is necessary for maintaining the progenitor state in the blastema (**Fig. 1.26B**) (Tsujioka et al., 2017). Next, a zebrafish study showed that *il-11* cytokine transcripts and Stat3 signaling are induced in cardiomyocytes after cardiac ventricular resection. They then identified *relaxin 3a* as a downstream candidate molecular and observed that inducing *relaxin 3a* specifically in cardiomyocytes promoted cell proliferation (Fang et al., 2013). However, a precise cellular and molecular analysis of the role of Il-11 signaling during regeneration using genetic mutants is lacking until now.

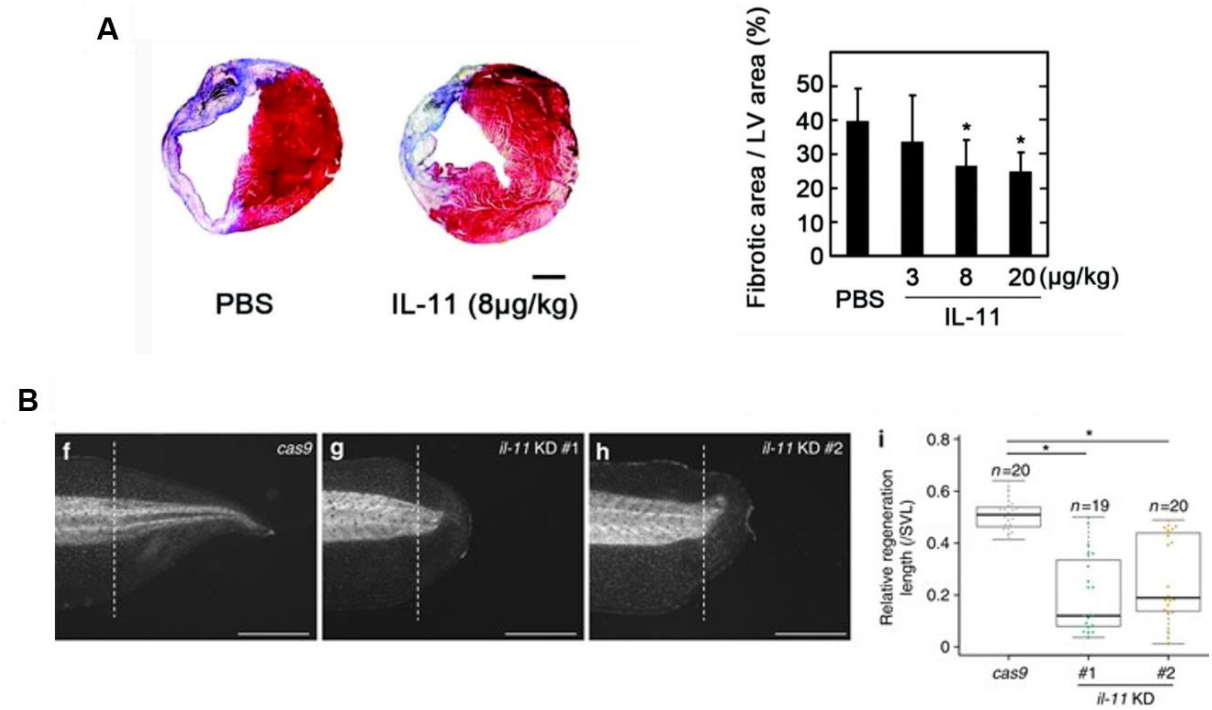

Figure 1.26. Pro-regenerative role of IL-11 signaling in mammals and *Xenopus*. (**A**) Masson's trichrome staining on PBS and IL-11 treated mice after inducing experimental

myocardial infarction, and the quantification of fibrotic area 14 dpMI. Adapted from (Obana Masanori et al., 2010), Figure 2. License: 5231420451212. (**B**) Brightfield images and quantification of regeneration upon CRISPR-mediated knockdown of *il-11* in the *Xenopus* tail regeneration model. Adapted from (Tsujioka et al., 2017), Figure 2. License: CC BY 4.0.

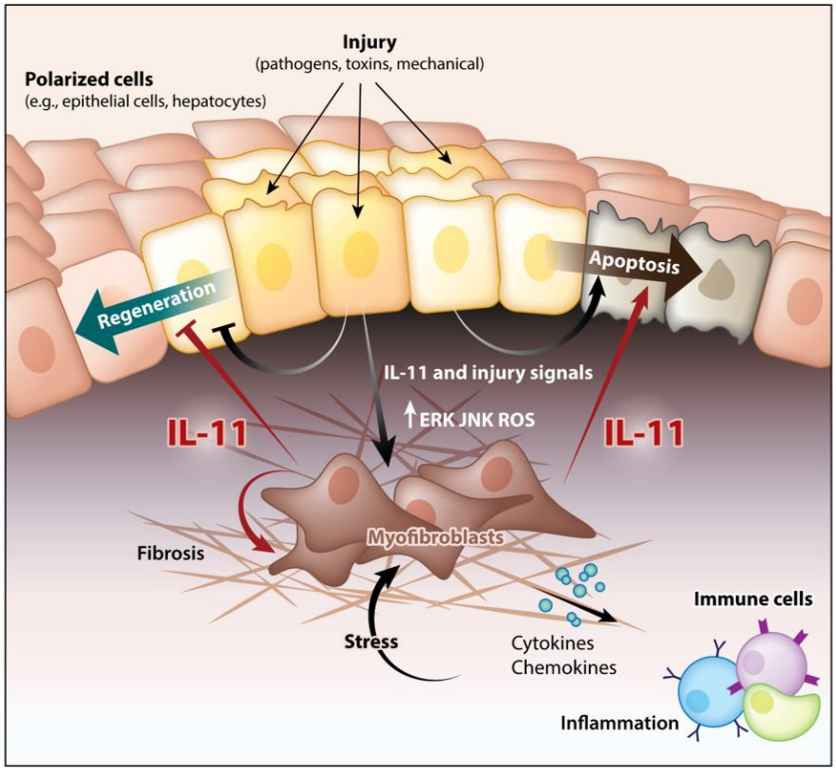

Figure 1.27. Pro-fibrotic role of IL-11/ERK signaling. Illustration showing that IL-11 signaling induces fibrosis via myofibroblast differentiation and limits regeneration. Adapted from (Cook and Schafer, 2020), Figure 1. License: CC BY 4.0.

1.7.2.2. Role of Interleukin-11 signaling in fibrotic scarring

Following these publications that suggest a pro-regenerative and anti-fibrotic role of IL-11/STAT3 signaling, more recently, a group from Singapore performed a detailed analysis on IL-11 signaling and tissue fibrosis. In their first report, Schaefer and colleagues identified that IL-11 is a primary target of TGF-β signaling, a master regulator of tissue fibrosis (Schafer et al., 2017). They also provide evidence in the heart and kidney that TGF-β exerts its pro-fibrotic effects via IL-11. Data from this report and others show that these pro-fibrotic effects of IL-11 go through the non-canonical ERK signaling, but not the canonical STAT3. In brief, treating primary human cardiac fibroblasts with IL-11 induces myofibroblast differentiation. They also show

that the mouse *Il11ra1* mutants are protected from injury-induced fibrosis. Furthermore, they show that antibody-based antagonism of IL-11 signaling protects mice from fibrosis, proposing potential therapies to limit human fibrosis. Recent studies from the same group broaden the scope of IL-11 mediated fibrosis from heart and kidney pathologies to lung, colon and other inflammatory diseases (Cook and Schafer, 2020; Corden et al., 2020; Lim et al., 2020; Ng et al., 2020, 2019).

These contradictory and debated results from regenerative and non-regenerative species demand a deeper investigation of the IL-11/STAT3 and IL-11/ERK signaling in tissue regeneration and fibrotic scarring.

2. Aims of the project

In mammals, injury-induced fibrotic scarring limits regeneration and leads to impaired tissue health. An ideal regenerative mechanism should be able to both promote regeneration and limit scarring. Here, we first compared the scarring response in between the regenerative zebrafish and non-regenerative adult mouse hearts. We have identified that zebrafish display limited scarring in response to injury compared to the adult mammals. These data led us to hypothesize that zebrafish employ mechanisms to limit their scarring response and promote regeneration. Furthermore, given the existence of an evolutionarily conserved regeneration responsive gene program, and the common regenerative molecular patterns that have been uncovered in diverse tissues and organisms, it has become increasingly clear that a global regulator of regeneration exists. However, the identity of such a global regenerative mechanism that limits fibrotic scarring remains elusive. To identify such mechanisms, we performed a comparative transcriptomic profiling on injured vs. exercised adult zebrafish ventricles.

The project thus carried out had the following aims:

Aim 1: Identify a regenerative mechanism that limits fibrotic scarring (myofibroblast differentiation) using the proposed comparative expression profiling.

Aim 2: Investigate the cellular mechanisms downstream of the candidate pathway using gene loss-of-function analyses and deep phenotyping.

Aim 3: Uncover the downstream molecular mechanisms that the candidate pathway employs to promote regeneration and limit fibrotic scarring.

3. Materials and methods

3.1 Materials

3.1.1. Antibiotics

Table 3.1. List of antibiotics used in this thesis with their respective working concentrations.

Antibody	Working concentration
Ampicillin	100 µg/ml

3.1.2. Antibodies

Table 3.2. List of antibodies used in this thesis for immunofluorescence, with their respective sources, references and suppliers.

Antibody	Source	Reference	Supplier
pSTAT3	Rabbit	9131s	Cell Signaling Technology
MEF2	Rabbit	sc-313	Santa Cruz
PCNA	Mouse	sc-56	Santa Cruz
Myosin Heavy Chain	Mouse	MF-20	DSHB
αSMA (Acta2)	Rabbit	GTX124505	GeneTex
GFP	Chicken	GFP-1010	Aves Labs
Elastin1	Rabbit	-	(Miao et al., 2007)
Fibronectin1	Rabbit	F3648	Sigma-Aldrich
Aldh1a2	Rabbit	GTX124302	GeneTex
Aldh1a2	Mouse	sc-393204	Santa Cruz
mCherry	Chicken	CPCA-mCherry	Encor Bio

mCherry	Mouse	632543	Takara Living Colors
mCherry	Rat	M11217	Thermo Fisher Scientific
Myosin Light Chain Kinase	Mouse	M7905	Sigma-Aldrich
zf-Cdh5	Rabbit	AS-55715	Anaspec
pSmad3	Rabbit	ab52903	Abcam
Zns5	Mouse	ZDB-ATB-081002-37	ZIRC
Donkey anti-Mouse Alexa Fluor 488	Donkey	A-21202	Invitrogen
Donkey anti-Mouse Alexa Fluor 568	Donkey	A-10037	Invitrogen
Donkey anti-Mouse Alexa Fluor 647	Donkey	A-31571	Invitrogen
Donkey anti-Rabbit Alexa Fluor 488	Donkey	A-21206	Invitrogen
Donkey anti-Rabbit Alexa Fluor 568	Donkey	A-10042	Invitrogen
Donkey anti-Rabbit Alexa Fluor 647	Donkey	A-31573	Invitrogen
Goat anti-Chicken Alexa Fluor 488	Goat	A-11039	Invitrogen
Goat anti-Chicken Alexa Fluor 568	Goat	A-11041	Invitrogen
Goat anti-Chicken Alexa Fluor 647	Goat	A-21449	Invitrogen
Anti-DIG-AP, Fab fragments	Sheep	11093274910	Roche

3.1.2. Bacterial strains

Table 3.3. Bacterial strain used and its application

Bacterial strain	Application
DH5α	Competent cells for transformation

3.1.3. Buffers and solutions

Table 3.3. List of buffers, solutions used, and their compositions

Buffer/Solution	Composition
Alkaline Tris Buffer	100mM Tris HCl pH 9.5, 100mM NaCl, 50mM MgCl2
DEPC Water	0.01% DEPC dissolved in distilled water and autoclaved
E3 embryo medium	3g Instant Ocean, 0.75g Calcium sulphate dissolved in 10 L of distilled water
PBS	8g NaCl 0.2g KCl 1.44g Na2HPO4 0.24g KH2PO4 dissolved in 900 ml of distilled water, pH was adjusted to 7.4, volume was made up to 1000 ml with distilled water
PBST	0.1% Tween 20 in PBS
PBSTx	0.1% Triton-X in PBS
20x SSC	175.3g NaCl, 88.2g Sodium Citrate dissolved in 800 ml distilled water and pH was adjusted to 7, volume was made up to 1000 ml with distilled water

DEPC-PBS	1 L PBS was filtered and 1 ml DEPC was added, followed by stirring for 1 hour and autoclaving.
1M (10x) Triethanolamine, pH 8.0	66.5 mL Triethanolamine and 20 mL concentrated HCl were added to 413.5ml DEPC-water
Hybridization Solution for Day1 in situ hybridization	50% Formamide 5X SSC 0.3 mg/mL Yeast tRNA 0.1 mg/mL Heparin 0.1% Tween 20 Adjust to pH 6.0 with 1M Citric acid
Hybridization Solution for Day2 in situ hybridization	50% Formamide 5X SSC 0.1% Tween 20 Adjust to pH 6.0 with 1M Citric acid
Blocking buffer (in situ)	2mg/ml BSA 2% Sheep Serum Dissolved in PBT
TBS	50mM Tris-HCl pH 7.4 150mM NaCl
Blocking buffer (IHC)	PBS 1% DMSO 2% Donkey Serum 1% BSA 0.1% Tween 20
Permeabilization buffer (IHC)	PBS 0.3% Triton-X
Sodium Citrate antigen retrieval buffer (IHC)	2.94 g of Tri-sodium citrate (dehydrate) was added to distilled water (made up to 1 L) and

	stirred to dissolve. pH was adjusted to 6.0 and 0.5 ml of Tween 20 was added
Lysis buffer (genotyping)	50mM NaOH
Neutralization buffer (genotyping)	1M Tris-HCl pH 8.0
TBST	TBS with 0.1% Tween-20
PEM fixative	3% Paraformaldehyde, 100 mM PIPES, 1 mM MgSO4, 2 mM EGTA in distilled water and adjusted to pH 7.4

3.1.4. Centrifuges

Table 3.4. List of centrifuges used in this thesis with their respective suppliers

Centrifuge	Supplier
Centrifuge (slow speed, 1.5-2ml tubes)	VWR Ministar
Centrifuge (slow speed, 1.5-2ml tubes)	VWR Ministar
Centrifuge 5415 D (1.5-2 ml tubes)	Eppendorf
Centrifuge 5418 (1.5-2 ml tubes)	Eppendorf
Centrifuge 5418 (1.5-2 ml tubes)	Eppendorf
Centrifuge 5417 R (200 µl tubes)	Eppendorf
Centrifuge 5810 R (15-50 ml tubes and 96-well plates)	Eppendorf

3.1.5. Chemicals and reagents

Table 3.5. List of all the chemical and reagents used in this thesis, with their suppliers.

Chemical/reagent	Supplier	Catalogue no.
Mineral oil	Sigma-Aldrich	M8410
LB agar	Roth	X969

DIG RNA labelling mix	Roche	11277073910
Bovine serum albumin (BSA)	Sigma-Aldrich	A2153
Chloroform	Merck	102445
Citric acid	Sigma-Aldrich	27487
DNA ladder (100bp)	Thermo Fisher Scientific	SM0241
DNA ladder (1kbp)	Thermo Fisher Scientific	SM0311
Ethanol (molecular grade)	Roth	5054.4
Ethanol (denatured)	Roth	K928.3
Methanol	Roth	4627.5
16% Paraformaldehyde (PFA)	Alfa Aesar	43368
1X HBSS	Gibco	14175
Gel loading dye	Thermo Fisher Scientific	R0611
Heparin	Sigma-Aldrich	H5515
Isopropanol	Roth	6752.4
20X SSC	Ambion	AM9763
Methylene blue	Sigma-Aldrich	M9140
BM Purple	Roche	11442074001
Tricaine	Pharmaq	NA
Phosphate-buffered saline (PBS) tablets	Sigma-Aldrich	P4417
Dimethylsulfoxide (DMSO)	Sigma-Aldrich	D4540
Sheep serum	Sigma-Aldrich	S3772
Tris	Roth	5429.2
Tween-20	Sigma-Aldrich	P1379

Triton X-100	Sigma-Aldrich	RES3103T-A101X
tRNA	Sigma-Aldrich	R7876
CutSmart buffer	NEB	B7204S
Agarose, low gelling temperature	Sigma-Aldrich	A9414
Agarose	Peqlab	35-1020
LB medium	Roth	X968
Nuclease-free water	Ambion	AM9938
TRIzol	Ambion	15596018
Glycerol	Millipore	356350
Pronase	Roche	10165921001
SYBR safe	Invitrogen	S33102
NaCl	Sigma-Aldrich	S3014
KCl	Sigma-Aldrich	P9541
MgSO4	Sigma-Aldrich	M2643
H_2O_2	Sigma-Aldrich	31642
KOH	Sigma-Aldrich	P1767
Proteinase K	Roche	1092766
Formamide (deionized)	Ambion	AM9342
Sucrose	Sigma-Aldrich	S0389
Phenol red	Sigma-Aldrich	P0290
$MgCl_2$	Sigma-Aldrich	63068
HCl	Sigma-Aldrich	H1758
HEPES	Sigma-Aldrich	H3375

NaHCO3	Roth	965.1
MgSO4.7H2O	VWR	437044K
Alexa Fluor 568 Phalloidin	Thermo Scientific	A12380
DAPI	Thermo Scientific	D1306
O.C.T.	Sakura	4583
Fluorescence Mounting Medium	Dako (Agilent)	s3023

3.1.6. Microscopes

Table 3.6. List of microscopes used in this thesis and their respective suppliers.

Microscope	Supplier
Confocal microscope LSM 700	Zeiss
Confocal microscope LSM 800 Examiner	Zeiss
Confocal microscope LSM 800 Observer	Zeiss
Confocal microscope LSM 880 AxioExaminer	Zeiss
Spinning disk CSU-X1 confocal microscope	Zeiss
SMZ25 stereo microscope	Nikon
SMZ18 stereo microscope	Nikon
Stemi 2000 stereomicroscope	Zeiss
Stemi 305 EDU microscope set	Zeiss

3.1.7. Enzymes

Table 3.7. List of enzymes used in this thesis and their respective suppliers.

Enzymes	Supplier

AgeI-HF, XhoI, NheI, BamHI, NotI and other restriction enzymes	NEB
Pronase	Roche
Proteinase K	Roche
Rnasein	Promega
RQ1 RNase free DNase	Promega
SP6 RNA Polymerase	Promega
T4 DNA ligase	NEB
T3 RNA Polymerase	Promega
T7 RNA Polymerase	Promega
RNase-free DNase set	Qiagen
KAPA 2G fast DNA polymerase	Kapa Biosystems
SYBR green PCR mastermix	Thermo Fisher Scientific
Phusion DNA polymerase	NEB
Primestar Max DNA polymerase	Takara
2x Dynamo Color Flash	Thermo Fisher Scientific

3.1.8. Growth media

Table 3.8. List of all the growth media used in this thesis and their respective suppliers.

Growth media	Supplier
LB medium	Roth
LB agar	Roth
Endothelial growth medium (EGM-2)	Lonza

3.1.9. Cell lines

Table 3.9. List of the cell lines used in this thesis and their respective suppliers.

Cell lines	Supplier
HUVECs (primary cell line)	Lonza

3.1.10. Kits

Table 3.10. List of all the kits used in this thesis and their respective suppliers.

Kits	Supplier
Cold Fusion Cloning Kit	System Biosciences
Gel extraction kit	Thermo Fisher Scientific
Mini Prep Plasmid isolation kit	Thermo Fisher Scientific
Maxima cDNA synthesis kit	Thermo Fisher Scientific
miRNAeasy micro kit	Qiagen
mMessage mMachine kits (SP6, T7)	Ambion
PCR product Cleanup	Jena Bioscience
PCR purification kit	Thermo Fisher Scientific
pGEM-T easy cloning kit	Promega
RNA cleanup and concentrator kit	Zymo research
Superscript III first strand synthesis	Invitrogen
Pierce Cardiomyocyte dissociation kit	Thermo Fisher Scientific
T7 and SP6 in vitro transcription kits	Promega
Lipofectamine RNAiMAX kit	Invitrogen

3.1.11. Lab equipment

Table 3.11. List of the all the lab equipment used in this thesis, and their respective suppliers.

Equipment	Supplier
PCR Mastercycler pro	Eppendorf
PTC-100 thermalcycler	MJ Research
NanoDrop 2000c	Thermo Fisher Scientific
Injection micromanipulator	World precision instruments
Picospritzer III	Parker
CFX connect Real Time PCR	BioRad
Eco Real-time PCR system	Illumina
Gel Doc EZ	BioRad
Electrophoresis power supply	BioRad
Microscale	Novex
Weighing balance	Sartorius
Micropipette puller P-1000	Sutter Instrument
Bacterial shaker	Infors HAT
Bacterial incubator	Heraeus
Bacterial incubator shaker	Infors HAT
Heating block	VWR
Microwave oven	Bosch
Zebrafish breeding tanks	Techniplast
Zebrafish aquaculture system	Techniplast

Zebrafish incubator	Binder
CM1950 cryostat	Leica
Bullet Blender	Next Advance

3.1.12. Lab supplies

Table 3.12. List of all the lab supplies and their respective suppliers.

Supplies	Supplier
Bacterial culture tubes	Sarstedt
Latex gloves	Roth
Nitrile gloves	VWR
Beakers	VWR
Eppendorf tubes	Sarstedt
Falcon tubes	Greiner bio-one
Glass bottom dish	MatTek
Microloader pipette tips	Eppendorf
PCR tubes	Sarstedt
Scalpel	Braun
Pipettes	Gilson
Petri dishes	Greiner bio-one
Forceps	Dumont
Glass bottles	Duran
Laboratory film	Parafilm
Pipetboy	Integra

Pipette tips	Greiner bio-one
Filtered pipette tips	Greiner bio-one
Conical flasks	VWR
Serum pipette	Greiner bio-one
Spring scissors	Dumont
0.5 mm Cryoprobe	Custom-made
DNA and RNA Oligos	Sigma
CELLSTAR cell culture multi-well plates (6 well plates)	Greiner bio-one

3.1.13. Plasmids

Table 3.13. List of the plasmids used in this thesis and their details.

Plasmids	Antibiotic resistance	Source
pGEM-T	Ampicillin	Promega
pCS2+	Ampicillin	Addgene
HOTCre plasmid (modified)	Ampicillin	(Hesselson et al., 2009)
Mosaic expression plasmid	Ampicillin	(Sawamiphak et al., 2017)

3.1.14. Peptides and inhibitors

Table 3.14. List of the peptides, chemical inhibitors, used in this thesis, and their suppliers.

Peptide/Inhibitor	Supplier
rhIL-11 (CYT-214)	Pepnet
rhTGFB2 (100-35B)	Peprotech
SB431542 (TGFB inhibitor)	Calbiochem

3.1.15. Oligonucleotides

Table 3.15. List of all the DNA and RNA oligos used in this thesis.

Oligo name	Sequence	Application
il6st^{sa1462}	GCAGTTATTTCAATACTGGCAT	HRMA
	AGAGGTATTCACTGGAAGTGC	
stat3^{stl27}	ACCTCTTACTCATCCTCCACAGG	HRMA
	AATCATCCTGCAGATTCTCCAA	
il11ra^{bns251}	ACATCACTGAAATCAACCCGC	HRMA
	AAGAGGGTTCATTGACTTACAGA	
il11a^{bns311}	AGACCGGGTGTTTAGTACAGA	HRMA
	CTGCTGATTGCTGGAAGAGA	
il11b^{bns312}	TACTCTGGTCTTAAATCTTTCAAGT	HRMA
	ATCGTTCCCCAATTCGTCAC	
rpl13a	TCTGGAGGACTGTAAGAGGTATGC	RT-qPCR
	AGACGCACAATCTTGAGAGCAG	
socs3b	GACCATCACCACTTCTTCAC	RT-qPCR
	ATGGATGAGTTTGAGGACAC	
il11a	GGACAAATATGAAATTGCTGGGTG	RT-qPCR
	AGCGTCAGAAGGAGTTTGGT	
il11b	TGAACGCAAATGAGTTGACTG	RT-qPCR
	CCCAATTCGTCACTATTCCGT	
il6	CAGAGACGAGCAGTTTGAGAG	RT-qPCR
	CCAGTTGTCTTTATACCATGTCAG	

lif (m17)	CCGTTCAGTTAGTGCAACCA	RT-qPCR
	TGACCGGAGATTGTAGACAC	
cntf	GTCACCTAATATCCATCCCTCC	RT-qPCR
	GTCCAGCTCCTCTTTAACTTCAG	
osm (*si:ch73-47f2.1*)	AAACCCCTCATTTCTAAGACCA	RT-qPCR
	GTTCTTCAAGTCAAGTTCAGGA	
clcf1	GAGACACTTACCTGTCATATCTC	RT-qPCR
	ATGAGCCCAGATATTGAGCC	
aldh1a2	GTACCCAATCCTGAGATCAA	RT-qPCR
	CTCACAGAATCATGCCATTC	
fn1b	CTCTTCCAAATGGTGTCACG	RT-qPCR
	CACACTTGAACTCTCCTTTGC	
acta2	GAAGATCAAGATAATCGCTCCAC	RT-qPCR
	GCAATAGCAGAATTACGGGAC	
mylka	CCTCAAATCCAGCAGTTTCCT	RT-qPCR
	CTTCCTGAATTGGTTTGCGG	
cilp2	TCGAGAAAGAGTCTGCTCAC	RT-qPCR
	CAGTATGAGTGCACTGGTGG	
egr1	GAGATGATCATGCTGAACTCTG	RT-qPCR
	GCCTGTGTAGGATATGGGAG	
egr2b	GCCGATAGCATCTATTCGGT	RT-qPCR
	CGTTAATCAGGCCATCTCCT	
elnb	CGGAACAGGAACTGGCATTAGG	RT-qPCR

	ACCACCAGGCCCAATTCC	
loxa	CACAGAAGAGTAGCAGAGGG	RT-qPCR
	CTGGGATTAACACTAACTTTGAGG	
loxl2b	CAAGGGAGAAGGTCGTATCTG	RT-qPCR
	CTATTGATGTTGTTGGTAAGGGTG	
vcanb	CCAAACCGTCAGATATCCCA	RT-qPCR
	TCATACTTCTCATAGGCGTTCC	
tgfb2	ACAGCGATACATCAACAGCA	RT-qPCR
	GAATCCTTTGTTTCTGTCTCTGTG	
tgfb1a	TTCCAGCAAGCTCAGAATAACAC	RT-qPCR
	GAGACAAAGCGAGTTCCCAG	
tgfb1b	GGGTTGCTGTGTTAGAAGTC	RT-qPCR
	CAACTGTTCCACCTTATGCTG	
fli1a	GGTCCGTCATCTTGAACTCTC	RT-qPCR
	TCCTCAGCCAGATCCTTATCAG	
il11ra	CATACAGAGCCTCATACAGTCAG	RT-qPCR
	TGGTTTCAAGAGTTCACGGA	
snai1b	CAGTGAACTGGAGAGTCAGACTG	RT-qPCR
	CACTGCGGGACGACTGCATA	
col1a1a	GTACTGGATTGACCCTGACC	RT-qPCR
	CATACTCGAACTGGAAGCCA	
col1a1b	CCCTATCACTCCGACATTCC	RT-qPCR
	TACCATACTGGAACTGGAAGC	

tie1	TTTGACCACAGTGGGATTTTC	RT-qPCR
	CATTGAATTTCCAAGCGATG	
tie2 (tek)	TCAACACAGAGCCCTACAGC	RT-qPCR
	TGGGTCAGGTACTGGGTCAT	
mvp	ATCCTTACAGACAAGAAAGCCCT	RT-qPCR
	GTCACAAGCCACTCTTCTCC	
mmp9	CAGTGGAAATGATGTGCTTGG	RT-qPCR
	GAAGTAGAAGAATCCCTTGTAGAG	
junba	TTTGCCTGATGTAATATAACGGAG	RT-qPCR
	ATGACCATAAGCAGAAAGAAACGA	
junbb	GCTTGTGTTTAATTCATTCCAGAG	RT-qPCR
	GTTTGTAGTCGTGTAGAGCC	
edn1	GTTACAGTTTAAAGCAGCGTCAG	RT-qPCR
	GTTCTCACCCTTCTAATCTTTGTC	
sox9a	ACTTTGGAGATTACTGAACGAGG	RT-qPCR
	GTTCTTCACCGACTTCCTCC	
il11a	AGCTATTTAGGTGACACTATAGATGAAATTGCTGGGTGACTC	ISH
	TAATACGACTCACTATAGGGCTATTTCCCCACAATTCGAA	
il11b	AGCTATTTAGGTGACACTATAGATGAAACTGTCGCCTGACTC	ISH
	TAATACGACTCACTATAGGGTTATGATGGTGTATCAGGGT	
GAPDH	ATGGAAATCCCATCACCATCTT	RT-qPCR
	CGCCCCACTTGATTTTGG	
IL11RA	CTATGAGAACTTCTCTTGCACTTGGAG	RT-qPCR

	ACTGTCTTCTTCCTGTAGGAGGTG	
TGFB2	TTGCAGAACCCAAAAGCCAG	RT-qPCR
	TCACAACTTTGCTGTCGATGT	
TGFB1	TTCTTCAACACATCAGAGCTCC	RT-qPCR
	GTATCGCCAGGAATTGTTGC	
SNAI1	TAATCCAGAGTTTACCTTCCAGCA	RT-qPCR
	CAGGACAGAGTCCCAGATGAG	
IL11	CACAGCTGAGGGACAAATTCC	RT-qPCR
	CAGGTAGGACAGTAGGTCCGC	
siIL11RA	Predesigned oligo (SASI_Hs01_00156548)	siRNA
il11ra (exon 6)	ATGGTGGAGTTAGATCCCA**CGG**	CRISPR gRNA
il11a (exon 3)	GTACAGAGATTAATCATCAC**CGG**	CRISPR gRNA
il11b (exon 3)	TCCGTTGGACCCAATCAAGA**TGG**	CRISPR gRNA
SP6 promoter	ATTTAGGTGACACTATAG	Sequencing
T7 promoter	TAATACGACTCACTATAGGG	Sequencing

3.1.16. Software and databases

Table 3.16. List of software and databases used in this thesis and their purposes.

Software	**Purpose**
Adobe Illustrator	Image formatting
Adobe Photoshop	Image formatting
Fiji (ImageJ)	Image processing and data analysis
Zen (Zeiss, Blue and Black)	Image acquisition, processing and data analysis

GraphPad Prism	Data analysis
Microsoft Office (Word, Excel, PowerPoint)	Writing, data analysis, and presentation
R Studio	Data analysis and visualization
Ensembl.org	Genome browsing and analysis
ZFIN	Zebrafish gene expression and nomenclature
IGV	NGS analysis
Primer BLAST	Primer generation
ApE	Plasmid editor
UCSC genome browser	Genome browsing and analysis
CHOPCHOP	gRNA design
Nikon (NIS elements)	Image acquisition, processing and analysis
Gitools	Gene Ontology analysis
PerlPrimer	Primer design
cellxgene	single-cell RNA-seq data browser
zfregeneration.org	Zebrafish regeneration data repository

3.1.17. Zebrafish lines

Table 3.17. List of zebrafish lines used in this thesis and their details.

Line	Description	Source
TgBAC(cryaa:EGFP,tcf21:Cre-ERT2)pd42	Lineage tracing epicardial-derived cells	(Kikuchi et al., 2011a)
Tg(kdrl:Cre)s898	Lineage tracing endothelial-derived cells	(Bertrand et al., 2010)
Tg(fli1:Cre-ERT2)cn9	Lineage tracing endothelial-derived cells	(Sánchez-Iranzo et al., 2018)
Tg(-3.5ubb:LOXP-EGFP-LOXP-mCherry)cz1701	Switch line for lineage tracing	(Mosimann et al., 2011)

Tg(-3.5ubb:LOXP-LacZ-LOXP-egfp)cn2	Switch line for lineage tracing	(Donato et al., 2016)
Tg(-14.8gata4:GFP)ae1	Labels regenerating cardiomyocytes	(Heicklen-Klein and Evans, 2004)
Tg1(Ola.Bglap:EGFP)hu4008	Labels mature osteoblasts	(Vanoevelen et al., 2011)
Tg(fli1:EGFP)y1	Labels endothelial cells	(Lawson and Weinstein, 2002)
ET(krt4:EGFP)sqet33-1A	Labels endocardial cells	(Poon et al., 2010)
Tg(hsp70l:loxp-lox2272-mCherry-loxp-il11ra-V5-p2a-GFP-lox2272)bns546	Mosaic *il11ra* overexpression	This study (Allanki et al., 2021)
Tg(hsp70l:loxP-TagBFP-loxP-il11ra-t2A-mCherry)bns417	HOTCre *il11ra* overexpression	This study (Allanki et al., 2021)
stat3^{stl27}	*stat3* mutant	(Liu et al., 2017)
il6st^{sa1462}	*il6st* mutant	(Kettleborough et al., 2013)
il11ra^{bns251}	*il11ra* mutant	This study (Allanki et al., 2021)
il11a^{bns311}	*il11a* mutant	This study (Allanki et al., 2021)
il11b^{bns312}	*il11b* mutant	This study (Allanki et al., 2021)

3.1.18. Zebrafish food

Table 3.18. List of zebrafish food used and the feeding regime.

Food	Regime
SDS100	5 dpf - 12 dpf
Brine Shrimp	> 1 months
SDS200	1 - 2 months
SDS300	2 - 3 months
SDS400	> 3 months

3.2 Methods

Note: As mentioned in the individual cases throughout the section, some parts are quoted *verbatim* from the following article published in *Science Advances*.
[**S. Allanki**, B. Strilic, L. Scheinberger, Y. L. Onderwater, A. Marks, S. Gunther, J. Preussner, K. Kikhi, M. Looso, D. Y. R. Stainier, S. Reischauer, Interleukin-11 signaling promotes cellular reprogramming and limits fibrotic scarring during tissue regeneration. *Sci. Adv*. 7, eabg6497 (2021)].

3.2.1. Zebrafish maintenance and breeding

All zebrafish (Danio rerio, strain: Tüb/AB) husbandry was performed in accordance with Max-Planck-Gesellschaft, national ethical and animal welfare guidelines. The procedures were approved by Regierungspräsidium Darmstadt, Germany (the ethics committee for animal experiments).

All the strains were maintained in Techniplast fish culture system at 26-28.5°C water temperature. Zebrafish embryos until 5 dpf were kept in egg water in BOD incubator at 28°C, and later moved to the fish culture system. For breeding, male and female zebrafish were placed in a breeding tank with a divider between them the evening before. The dividers were removed the next morning, and the fish would lay eggs within 20-30 mins. The eggs were collected from the bottom of the mating tanks into 10 cm Petri dishes. The fertilized eggs were then sorted into a fresh Petri dish in the evening (~6 hpf).

3.2.2. Microinjections in zebrafish embryos

3.2.2.1. Preparing microinjection plates

The injection plates were prepared using 2% agarose solution made in egg water in 10 cm petri dishes. A plastic mould with lanes is then placed on the agarose solution and let dry at room temperature. After solidification, the mould is removed and the injection plate is stored at 4°C until usage.

3.2.2.2. Preparing microinjection needles

The needles were prepared from the glass capillaries using the needle puller instrument as per the manufacturer's instructions (Sutter instruments).

3.2.2.3. Microinjections

Microinjection needles were loaded with ~5 µl of the injection mix (DNA/RNA) with Phenol red for visual confirmation. The loaded needle was then fixed into the micromanipulator. The injection pressure was calibrated to get a consistent droplet size as measured by the microscale. One-cell stage embryos were aligned in the injection plate lanes and were injected with the mix. Injections were performed into the cell for DNA mixes or into the yolk for RNA mixes.

3.2.3. RNA isolation

RNA was isolated using 3 means. (1) RNA precipitation, (2) Zymo research kit, and (3) Qiagen miRNeasy micro kit. The tissue of interest was collected into 500 µl TRIzol, snap-frozen in liquid nitrogen, and stored in -80°C until further processing. On the day of isolation, the samples were thawed to room temperature and the tissue was homogenized using a bullet blender (Next Advance) following the manufacturer's protocol. 100 µl of Chloroform was added and mixed vigorously. The tubes were then left undisturbed at room temperature for 5 mins. This was followed by centrifugation at >12,000g for 15 mins at 4°C. The upper aqueous phase was collected into a different tube and processed as per the kit manufacturer protocol (in the case of Zymo and Qiagen kits). For precipitation, 1:1 volume of isopropanol was added and gently mixed. This solution was incubated for 1 hr at -20°C and then centrifuged at full speed at 4°C. The supernatant was removed and the pellet was washed with ice-cold 75% ethanol by carefully flicking the tube. This was followed by centrifugation at full speed at 4°C. The supernatant was removed and the pellet was air dried at room temperature for several minutes. The dried pellet was finally resuspended into nuclease-free water and the RNA concentration was measured using Nanodrop. The RNA was stored at -80°C until further usage.

3.2.4. cDNA synthesis

cDNA synthesis was performed by following the manufacturer's protocol from Maxima first strand cDNA synthesis kit for RT-qPCR (Thermo Fisher Scientific). The reaction was set up as follows:

Components	Reaction volume
Template RNA	100 ng – 1 µg
5x reaction mix	4 µl
Maxima enzyme mix	2 µl
Nuclease-free water	Upto 20 µl

Table 3.19. Components of the cDNA synthesis reaction mixture.

The components were mixed gently. Using the thermocycler, the reaction was incubated at 25°C for 10 mins followed by 30 mins at 50°C. The reaction termination was performed at 85°C for 5 mins. The 20 µl of cDNA thus obtained was diluted 2x with nuclease-free water and stored at -20°C for further usage.

For whole ventricles, total RNA was isolated from uninjured and cryoinjured whole ventricles or dissected injured areas using TRIzol-chloroform method. Single whole ventricle or injured area per biological replicate and at least 250 ng of total RNA was reverse transcribed. For sorted cells, total RNA was isolated using TRIzol-chloroform method. At least 80 ng of total RNA was reverse transcribed. For HUVECs, total RNA was isolated using the RNA Clean and Concentrator kit (Zymo Research). At least 500 ng of total RNA was reverse transcribed. For larval fin fold regeneration, total RNA was isolated from a pool of 20 dissected larvae using the RNA Clean and Concentrator kit (Zymo Research). At least 500 ng of total RNA was reverse transcribed.

[*The last paragraph in this subsection is quoted verbatim from Allanki et al., Sci. Adv. 7, eabg6497 (2021)*]

3.2.5. Real-time quantitative PCR (RT-qPCR)

RT-qPCR technique used to test the gene expression levels relative to a housekeeping gene and their respective control conditions. SYBR green reagent-based enzyme mix (DyNAmo color flash, Thermo Fisher Scientific) was used. mRNA levels of the genes of interest were normalized against the mRNA levels of *rpl13a* (zebrafish) and *GAPDH* (HUVECs). All reactions were performed in at least technical duplicates using the SYBR Green PCR Master Mix (Thermo Fisher Scientific) on CFX Connect Real-Time System (Bio-Rad). The following reaction mix and reaction settings were used:

Components	Reaction volume
2x Maxima SYBR mastermix	5 µl
Forward and reverse primer mix	1 µl
cDNA	0.5 – 1 µl
Nuclease-free water	Upto 10 µl

Table 3.20. Components of the RT-qPCR reaction mix.

Step	Temperature	Duration	No. of cycles
Polymerase activation	95°C	2 mins	1
PCR cycling	95°C	5 secs	44
	60°C	30 secs	
HRMA	95°C	5 secs	1
	65°C	5 secs	
	95°C	5 secs	

Table 3.21. Reaction conditions for RT-qPCR.

3.2.6. PCR amplifying genes from cDNA

Gene-specific primers were designed using DNA sequences acquired from Ensembl.org and PerlPrimer software. Primer specificity was verified using NCBI Primer BLAST database. PCR was carried out using the Eppendorf Mastercycler Pro

machines and 2x Takara PrimeSTAR Max polymerase mastermix. The following reaction mix and reaction conditions were used:

Components	Reaction volume
2x PrimeSTAR Max mix	5 µl
Forward and reverse primer mix	1 µl
cDNA template	0.5 – 1 µl (50 pg)
Nuclease-free water	Upto 10 µl

Table 3.22. Components of the PCR reaction mix.

Step	Temperature	Duration	No. of cycles
Polymerase activation	95°C	3 mins	1
PCR cycling	95°C	10 secs	40
	55°C	5 secs	
	72°C	5 sec/kb	
Final extension	72°C	5 mins	1
Storage	4°C	∞	

Table 3.23. Reaction conditions - PCR.

3.2.7. Agarose gel electrophoresis

The samples after PCR were resolved on an agarose gel containing SYBR safe to visualize the DNA bands and to verify the size of the amplicons. Larger DNA fragments (>5 kb) were loaded on 0.8% agarose gels and smaller fragments were resolved on 1-2% agarose gels, using appropriate DNA ladders (1 kb and 100 bp). The time of electrophoresis depended on the size and the concentration of the gels (20-40 mins at 120-150 V). The DNA fragments were visualized under a UV light using a gel doc imager.

3.2.8. PCR product purification

Once the size of the PCR products was confirmed, the gel slice containing the band was excised using a scalpel and processed further using the GeneJet Gel Extraction kit (Thermo Fisher Scientific). The gel slice was transferred to a clean 1.5 ml Eppendorf tube and 1:1 (weight to volume) binding buffer was added. The gel-buffer mixture was incubated at 55°C until the gel slice was completely dissolved. Optimal DNA binding was detected by the color of the solution (yellow). 700 µl of this solution was transferred to a gel purification column and centrifuged for 1 min at 13000 RPM. The flow-through was discarded and the column was washed with 700 µl of wash buffer by centrifugation. After discarding the flow-through, the empty column was centrifuged at full speed for 2 mins to remove any residual solutions on the membrane. A few µl of nuclease-free water was added to the column and centrifuged to elute the DNA. The concentration was then measured and DNA stored at -20°C.

3.2.9. Preparation of competent cells

3.2.9.1. Day 1

3 ml of liquid LB medium was filled in two 15 ml falcons each. E.coli competent cells from the stock were inoculated in one of the falcons. The other falcon stood as a sterile control, and the cells were grown at 37°C overnight.

3.2.9.2. Day 2

After confirming for no contamination in the sterile control tube, 200 ml of liquid medium was filled into 500 ml flasks with 1 ml of the overnight culture. The flasks were incubated at 37°C for 4 hrs. Meanwhile, the centrifuge was pre-cooled to 4°C. After 4 hrs, the 200 ml culture was cooled on ice for a few minutes and was aliquoted into pre-cooled 50 ml falcon tubes. The bacterial culture was then pelleted down using centrifugation at 4000 RPM for 10 mins at 4°C. After discarding the supernatant, the pellet was air dried on clean tissues by inverting the tubes. 5 ml ice-cold 0.1 M CaCl2 was added to the tubes and the pellet was homogenized by pipetting. After cooling the homogenate on ice for a few minutes, it was centrifuged at 4000 RPM for 5 mins at 4°C. All the previous steps were repeated till the pellet was obtained again. Once again the pellet was dried after discarding the supernatant. 1 ml cold 0.1 M CaCl2,

15% glycerol was added to dried pellet and falcons were kept on ice. The pellet was then homogenized and the solution was aliquoted and snap-frozen in liquid nitrogen. The eppendorfs were then stored at -80°C until further use.

3.2.10 Transformation of competent cells

The competent cells were taken out of -80°C and thawed on ice. A 5 µl mix of vector-insert solution was then added to the competent cells and the mixture is incubated for 10 minutes on ice. This is followed by a brief heat shock at 42°C for 45 secs and then the solution was incubated on ice for 5 mins. Next, the transformed cells were plated into LB-agar plates with specific antibiotics.

3.2.11 DNA restriction digestion

NEB enzymes and buffers were used to digest the DNA fragments or plasmids at specific temperatures and incubation timings specified on the NEB manuals.

3.2.12. Molecular cloning

3.2.12.1. TA cloning

pGEM-T Easy Vector system was used to perform TA cloning. TA cloning was mainly used to insert the PCR products into the pGEM-T vector for synthesizing RNA probes for in situ hybridization and other sequencing purposes. The ligation reaction was set and carried out as per the instructions on the manufacturer's guide. The reaction mixture is then incubated for 1 hr or overnight at room temperature. The ligation mix is then transformed into competent cells.

3.2.12.2. Cold Fusion cloning

This strategy was used to clone HOTCre *il11ra* overexpression plasmid and mosaic *il11ra* overexpression plasmids. In general, the vectors were linearized in specific restriction enzymes and the inserts were amplified either from cDNA or from other plasmids. The primers for insert amplification were designed in ApE plasmid editor by visualizing the finished product. The primers contained at least 15 bp overhangs that are homologous to the digested vector. The digested and purified vector and purified insert were then mixed with the 5x Cold Fusion mastermix. The reaction was mixed

via pipetting gently, and placed at room temperature for 5 mins followed by 10 mins on ice. The mix is then transformed into competent cells.

3.2.13. Plasmid DNA isolation

GeneJET Plasmid Miniprep Kit (Thermo Fisher Scientific) was used for plasmid isolation at room temperature. All the centrifugation steps were performed at 13,500 RPM. The bacterial culture tubes were centrifuge at 4°C at 4000 RPM to pellet down the bacteria. The supernatant was discarded. 250 µl of resuspension buffer was added to the pellet, followed by the resuspension. This is followed by addition of 250 µl of lysis buffer and the solution was mixed by inverting the tube. 350µl of neutralization buffer was added and the tube was inverted for 6-8 times. This was followed by centrifugation for 5 minutes. 700 µl of the supernatant was added in the spin column and was centrifuged for 1 minute. After discarding the flow-through, the column was washed with 500 µl of wash buffer, followed by centrifugation for 1 minute. The wash buffer step was repeated. The empty column was centrifuged for 1 min at full speed to remove any residual solution. 35 µl of elution buffer was added to the column and centrifuged at full speed for 1 min. The elute was was collected into 1.5 ml Eppendorf tubes and the plasmid was stored at -20°C.

3.2.14. Genotyping by High Resolution Melt Analysis (HRMA)

Genomic DNA was extracted either from the fin clips or embryos or larvae. PCR was performed using primers adjacent to the mutation using SYBR green reagents similar to RT-qPCR analysis described earlier. The only difference being that a HRMA-specific RT-qPCR machine (Illumina Eco) was used in this case.

3.2.15. CRISPR-Cas9 mutagenesis

3.2.15.1. gRNA design

CHOPCHOP (http://chopchop.cbu.uib.no/) was used to design gRNAs specific to the genes of interest. The gRNAs targeting important domains or the first few exons of the gene were picked, which were predicted to be highly efficient (low non-specificity).

3.2.15.2. Generation of zebrafish mutant lines

CRISPR/Cas9 technology was used to generate *il11ra*^{bns251}, *il11a*^{bns311} and *il11b*^{bns312}. The protocol was followed as previously described (Gagnon et al., 2014). The following guide RNA (gRNA) sequences (5'-3') were used: ATGGTGGAGTTAGATCCCA**CGG** (exon 6 – *il11ra*), GTACAGAGATTAATCATCAC**CGG** (exon 3 – *il11a*) and TCCGTTGGACCCAATCAAGA**TGG** (exon 3 – *il11b*), respectively.

gRNAs were transcribed as follows. A gRNA sequence and T7 promoter containing oligo was designed (with the following sequence: TAATACGACTCACTATAggXXXXXXXXXXXXXXXXXXXXGTTTTAGAGCTAGAAAT AGCAAG, where multiple Xs are the gRNA sequence) and annealed to another constant oligo containing the gRNA scaffold sequence (TAATACGACTCACTATAggagaaggtgaaggacactgGTTTTAGAGCTAGAAATAGCAA G). The annealing and extension protocol is as follows:

Step	**Temperature**	**Duration**
1	95°C	5 mins
2	95°C to 85°C	2°C decrease/sec
3	85°C to 25°C	0.1°C decrease/sec
Halt		
Add the following to the 10 µl-mix for the extension step: 2.5 µl dNTPs (10µM), 2 µl 10X NEB buffer 2.1, 0.2 µl 100x BSA, 0.5 µl T4 DNA polymerase, and 4.8 µl dH2O		
4	12°C	20 mins
5	4°C	∞

Table 3.24. Program conditions for annealing and extension of gRNA oligos.

GeneJET PCR purification kit was used to cleanup the PCR product and eluted into 30 µl dH2O. To confirm the successful annealing and extension, the sample was run

a 3% agarose gel. Following this, 6 µl was used to synthesize gRNA using T7 mMessage mMachine kit.

50 pg of individual gRNAs together with 150 pg of Cas9 mRNA were injected into zebrafish embryos at the one-cell stage and raised to adulthood. To identify F0's (fish carrying germline mutations), fish were outcrossed to wild types and the progeny was tested with HRMA, using primers flanking the potential mutation (gRNA). These F1's are raised and the mutation site was sequenced to identify the type of mutation (in-frame, out-of-frame). The F1 bearing the mutation of interest was further outcrossed to generate F2. An incross of such F2 would give the first generation of global homozygous mutants.

3.2.16. Generating transgenic zebrafish

Transgenic lines were generated by injecting column purified plasmids together with 50 pg of Tol2 mRNA into single-cell staged zebrafish embryos using a microinjector. These injected animals were raised to adulthood and were screened for F0 founders by outcrossing with wild types. For generating the *Tg(hsp70l:loxp-lox2272-mCherry-loxp-il11ra-V5-p2a-GFP-lox2272)bns546* and *Tg(hsp70l:loxP-TagBFP-loxP-il11ra-t2A-mCherry)bns417* lines, the following plasmids were injected: *hsp70l:loxp-lox2272-mCherry-loxp-il11ra-V5-p2a-GFP-lox2272* and *hsp70l:loxP-TagBFP-loxP-il11ra-t2A-mCherry*, respectively. Founders were identified by heatshock treatment to the F1 embryos and screening for mCherry or tagBFP expression, respectively.

3.2.17. Injury models for zebrafish regeneration studies

3.2.17.1. Cardiac cryoinjury

The cryoinjury protocol was followed as described earlier (Chablais et al., 2011). Adult zebrafish (4–8 mpf) were anaesthetized using 0.016% tricaine mixed in system water. They were then tested for reflexes and placed on a wet sponge. An incision was made through the chest on the ventral side to access the heart. A liquid nitrogen precooled cryoprobe was placed on the ventricular apex until the cryoprobe thawed. The fish were then recovered in fresh system water.

3.2.17.2. Adult caudal fin and larval fin fold injuries

Adult fin injuries were performed as described before (Sousa et al., 2011). Adult zebrafish (4-8 mpf) were anaesthetised using 0.016% tricaine mixed in system water and the caudal fins were amputated under a stereomicroscope using a scalpel. In the case of the crush injury model, 5-6 individual fin rays were gently crushed using a pair of forceps. The fish were then recovered in fresh system water. Caudal fin tissue 2 bone segments proximal to the amputation plane was collected for gene expression analyses.

Larval fin injuries were performed as described before (Yoshinari et al., 2009). Zebrafish larvae at 48-72 hpf were anaesthetized in 0.016% tricaine in egg water and their fin folds posterior to the notochord were amputated under a stereomicroscope using a scalpel. The fin folds were allowed to regenerate at 28°C until the indicated time points. For gene expression analysis, tissue posterior to the yolk extension was collected.

[*Certain lines in this subsection are quoted verbatim from Allanki et al., Sci. Adv. 7, eabg6497 (2021)*].

3.2.17.3. Adult scale injury

Adult scale injuries were performed as described before (Cox et al., 2018). Adult zebrafish (4-8 mpf) were anaesthetized in 0.016% tricaine in system water. Subsequently, they were placed on a Petri dish lid under a stereomicroscope. 3-4 scales each from 3 rows on the lateral side of the body posterior to the pectoral fins, were plucked with forceps. The fish were then recovered in fresh system water.

3.2.18. Zebrafish exercise training

Exercise training was performed as described (Boskovic et al., 2018). Adult zebrafish (6-8 mpf) were placed in a 5-liter glass beaker filled with four liters of system water. To simulate exercise, a magnetic stirrer was used to generate a stream, which induced swimming behavior. Fish were trained for two times four hours a day with one hour of rest in between. This procedure was repeated for 5 days in a row. No stir bar condition

was used as a control experiment. The fish were then sacrificed on Day5 for organ organ harvestation.

3.2.19. Tamoxifen treatment

Tamoxifen treatments were performed as described before (Kikuchi et al., 2010). Zebrafish embryos and larvae were treated with 5 µM 4-hydroxytamoxifen (4-OHT; H7904-Sigma) dissolved in pure ethanol (25 mM stock) and diluted in egg water at 28°C for time periods as mentioned in the respective figures. 4-OHT stock was preheated at 60°C for 10 minutes before diluting in egg water. Adult fish were injected intraperitoneally with 10 µl of 1.25 mM 4-OHT or 5% ethanol as a vehicle control, diluted in sterile 1x PBS.

[*Certain lines in this subsection are quoted verbatim from Allanki et al., Sci. Adv. 7, eabg6497 (2021)*].

3.2.20. Histological analysis and imaging

3.2.20.1. Tissue fixation and sectioning

The hearts and fins were fixed using PEM fixative for 1 hour at RT on a nutator. The tissues were cryopreserved overnight (O/N) at 4°C in 30% (w/v) sucrose solution prepared in 1x PBS. The hearts were then embedded in O.C.T. (Tissue-Tek) and stored at -80°C.

The adult caudal fins were pre-embedded in 7.5% (w/v) porcine gelatin (Sigma)/15% (w/v) sucrose in 1x PBS at 37°C for 1 h and embedded with a new solution of gelatin, as described before (Sousa et al., 2011). Fin tissue blocks were gradually frozen in isopentane (Sigma) cooled in liquid nitrogen. 11 and 50 µm thick cryosections were collected on SuperFrost Plus (Thermo Scientific) slides using Leica CM1950 cryostat and stored at -20°C.

[*Certain lines in this subsection are quoted verbatim from Allanki et al., Sci. Adv. 7, eabg6497 (2021)*].

3.2.20.2. AFOG staining

For AFOG staining, Bouin's solution was used to fix the sections for 2 h at 60°C and stained according to the manufacturer's instructions (AFOG staining kit, BioGnost), without hematoxylin solution. Imaging was performed using Nikon SMZ25 or Zeiss widefield (AxioImager) microscopes.

3.2.20.3. Immunohistochemistry on tissue sections

To perform immunofluorescence staining, O.C.T was removed from 11 µm thick cryosections by rinsing the slides with 1x PBS. To remove gelatin from the fin cryosections, slides were rinsed with 1x PBS at 37°C for 10 min. The sections were then permeabilized with 0.5% Triton-X in 1x PBS for 20 min (2 h for 50 µm cryosections) at RT followed by incubation in blocking buffer (1x PBS, 2% (v/v) donkey serum, 0.2% Triton X-100 and 1% DMSO) for 1 h at RT. Later, the sections were incubated with primary antibodies in blocking buffer O/N at 4°C with parafilm coverslips for even distribution. After washing for at least 2 h, the sections were incubated with secondary antibodies in blocking buffer for 3 h at RT. Finally, the immunostained slides, after washing and staining with 4′,6-diamidino-2-phenylindole (DAPI; 1:10,000, 10 mg/ml stock, Sigma), were mounted with fluorescence mounting medium (S3023, Agilent Dako) for imaging. Mef2, PCNA, pSTAT3 immunostaining was performed as described earlier (Marín-Juez et al., 2016). Imaging was performed using Zeiss LSM 800 Observer or inverted Zeiss Cell Observer SD confocal microscopes. Nikon SMZ25 was used for wholemount ventricle (fluorescence and brightfield), adult fin and larval fin fold imaging.

[*Certain lines in this subsection are quoted verbatim from Allanki et al., Sci. Adv. 7, eabg6497 (2021)*].

3.2.20.4. RNA in situ hybridization

For RNA in situ hybridization on paraffin sections, dissected hearts were fixed in sterile 4% PFA at 4°C O/N. Hearts were then washed in 1x DEPC-PBS twice for 5 minutes, followed by 15-30 minutes incubation through a gradient of ethanol in DEPC-water (50%, 70%, 80%, 95% and 100%) at RT. Hearts were then washed in 50% xylene in

ethanol, and in 100% xylene for 30 minutes at RT, followed by 3 washes in 100% paraffin at 50°C for one hour. Hearts were embedded in paraffin and stored at 4°C and sectioned into 8 µm sections and stored at RT. Sections were washed twice in xylene for 10 min each, followed by rehydration in a gradient of ethanol in DEPC-water for 2 min each (100%, 95%, 80%, 70% and 50%). Slides were then washed twice for 5 min with TBST (50mM pH7.4 Tris, 150mM NaCl, 0.05% Tween-20). Slides were then incubated for 20 min in sterile 4% PFA, followed by 2 washes in TBST. Slides were then incubated in 0.5 mg/ml Proteinase K diluted in TBS (50mM pH7.4 Tris, 150mM NaCl, 2mM CaCl2) for 15 min at 37°C, followed by a 5 min wash in ice cold Tris/Glycine (50mM pH7.4 Tris, 50mM Glycine) to stop the reaction. Slides were then washed twice in TBST, re-fixed in sterile 4% PFA for 5 min, and washed with TBST. Slides were then immersed in Triethanolamine (0.1 M, pH 8.0) and acetic anhydride was added to reach 0.25% under agitation for 12 min. This step is followed by 2x TBST washes, followed by pre-hybridization in hybridization buffer (50% Formamide, 5X SSC, 0.1% Tween-20, 50 µg/ml Heparin, 500 µg/ml yeast t-RNA, 460 µl 1M Citric acid) in 60-65°C for at least 1 hr. Probe (1 µg/ml in hybridization buffer) is denatured at 60-65°C for 15 min. Probe is then applied to sections at 60-65°C O/N. Slides were then washed in 50% Formamide in 2x SSC for 30 min at 60-65°C. Slides were then washed at 60-65°C for 15 min once with 2x SSC and twice with 0.1x SSC, followed by TBST at RT. Slides were then washed at 37°C for 15 min once with 2x SSC and twice with 1x SSC, followed by TBST at RT. Slides were then incubated in blocking solution (TBST + 0.5% BSA) for at least 1 hr at RT. Alkaline phosphatase-tagged anti-Digoxigenin antibody (Roche, 1:1000 in blocking solution) was applied to slides at RT for at least 2 hr. Slides were then washed 5x with TBST. Pre-filtered BM-Purple (Roche) was then applied, and the slides were incubated in a dark, humid chamber until the signal was observed. Slides were then washed with TBST, fixed in 4% PFA for 5 min, and mounted for imaging.

In situ hybridization on wholemount adult caudal fins was performed as described (Knopf et al., 2011). Digoxygenin-labelled anti-sense probes were synthesized using T7 polymerase (Roche) and DIG RNA labelling kit (Roche). Stained samples were imaged on a Nikon SMZ25 stereomicroscope.

[*Certain lines in this subsection are quoted verbatim from Allanki et al., Sci. Adv. 7, eabg6497 (2021)*].

3.2.20.5. Alizarin Red S staining

Adult zebrafish were sacrificed and fixed in 4% PFA overnight at 4°C. After washing with 1x PBS, the fish were stained with Alizarin Red S (0.01% final concentration in 1x PBS) for 1 h on a nutator. This is followed by 3 PBS washes. Imaging was performed using inverted Zeiss Cell Observer SD confocal microscope.

3.2.21. Tissue dissociation and cell sorting

Adult zebrafish cardiac endothelial (*Tg(fli1:EGFP)*$^{+}$) and non-endothelial cells (*Tg(fli1:EGFP)*$^{-}$) were isolated from a pool of 2 ventricles per replicate. Tissue dissociation was performed as described before (Marín-Juez et al., 2019), using manufacturer's protocol (Pierce Primary Cardiomyocyte Isolation Kit, Thermo Fisher Scientific) with some changes. The dissociates were incubated at 30°C with gentle shaking for 15 minutes. The cells were then resuspended in 1x HBSS (Gibco) with 0.25% BSA. These cells were immediately sorted using FACSAria III (BD) sorter for EGFP+ and EGFP- cells. DAPI negative cells were considered as live cells and further used for analysis.

3.2.22. Gene expression profiling

3.2.22.1. Microarray

For the microarray, total RNA was isolated from control vs. 96 hpci ventricles, and control vs. exercised ventricles using TRIzol-chloroform method. Dual color cDNA labeling and hybridization was performed by MOgene (commercial service) using the Agilent Zebrafish (V3) 4 × 44 K platform.

3.2.22.2. RNA-seq

For RNA-seq, RNA was isolated from adult zebrafish ventricles and caudal fin tissues using the miRNeasy micro Kit (Qiagen) combined with on-column DNase digestion (DNase-Free DNase Set, Qiagen) to avoid contamination by genomic DNA. RNA and library preparation integrity were verified with LabChip Gx Touch 24 (Perkin Elmer).

200-500ng of total RNA was used as input for Truseq Stranded mRNA Library preparation following the low sample protocol (Illumina). Sequencing was performed on the NextSeq500 instrument (Illumina) using v2 chemistry, resulting in minimum of 15 million reads per library with 1x75bp single end setup. The resulting raw reads were assessed for quality, adapter content and duplication rates with FastQC (Andrews S. 2010, FastQC: a quality control tool for high throughput sequence data. Available online). Trimmomatic version 0.39 was employed to trim reads after a quality drop below a mean of Q20 in a window of 10 nucleotides (Bolger et al., 2014). Only reads between 30 and 150 nucleotides were cleared for further analyses. Trimmed and filtered reads were aligned versus Ensembl zebrafish genome version danRer11 (GRCz11) using STAR 2.7.3a with the parameter "--outFilterMismatchNoverLmax 0.1" to increase the maximum ratio of mismatches to mapped length to 10% (Dobin et al., 2013). The number of reads aligning to genes was counted with featureCounts 1.6.5 tool from the Subread package (Liao et al., 2014). Only reads mapping at least partially inside exons were admitted and aggregated per gene. Reads overlapping multiple genes or aligning to multiple regions were excluded. Differentially expressed genes were identified using DESeq2 version 1.26 (Love et al., 2014). The Ensemble annotation was enriched with UniProt data (release 06.06.2014) based on Ensembl gene identifiers (Activities at the Universal Protein Resource (UniProt)). Cutoffs for identifying differentially expressed genes are as mentioned wherever needed.

[*This subsection is quoted verbatim from Allanki et al., Sci. Adv. 7, eabg6497 (2021) for precise explanation*].

3.2.23. Transcriptomic data re-analysis

3.2.23.1. Bulk RNA-seq reanalysis

We obtained the processed counts per million (CPM) of the bulk RNA-seq experiment from GEO - GSE95755 (Quaife-Ryan Gregory A. et al., 2017) and the microarray raw data from GEO - GSE111059 (Fu et al., 2018) to calculate fold changes and *P*-values.

3.2.23.2. Single-cell RNA-seq reanalysis

We obtained raw count matrices of single-cell RNA sequencing from adult zebrafish hearts - GSE106121 (Spanjaard et al., 2018) and regenerating adult zebrafish caudal fins - GSE137971 (Hou et al., 2020), and reanalysed the data as follows. We calculated the number of expressed genes, total reads and the percentage of counts assigned to mitochondrial transcripts per cell and filtered low quality cells with a mitochondrial content exceeding 30%. Next, we filtered genes that were expressed in less than 100 remaining cells. We normalized read counts to the number of total counts using scanpy (Wolf et al., 2018), transformed gene expression data into log space and applied principal component analysis, retaining the top 50 components. Next, we used BBKNN (Polański et al., 2020) to calculate a batch-balanced k-nearest neighborhood graph using the animal ID as covariate. UMAP (McInnes et al., 2020) was used to embed cells into a two-dimensional space. Further, we used the Leiden algorithm (Traag et al., 2019) to cluster cells using a resolution of 0.3 to 0.4. Finally, the data were visualized using cellxgene platform (*chanzuckerberg/cellxgene*, 2020).

[*This subsection is quoted verbatim from Allanki et al., Sci. Adv. 7, eabg6497 (2021) for precise explanation*].

3.2.24. Gene ontology analysis

Ingenuity pathway analysis (IPA, Qiagen) was run with default settings with 180 co-regulated genes (Appendix I) as a query dataset. R-package fgsea (Korotkevich et al., 2019) was used for all GSE analyses, by converting zebrafish and mouse gene symbols to human symbols. Pre-annotated gene lists from Hallmark, KEGG and Reactome databases were downloaded from Molecular Signatures database (MSigDB) (Subramanian et al., 2005).

3.2.25. Primary human endothelial culture

Human umbilical vein endothelial cells (HUVEC, Lonza) were cultured in endothelial growth medium (EGM-2, Lonza) using collagen I-coated 6-well plates, and only cells of passages P<5 were used. For knockdown experiments, HUVECs were double-transfected at consecutive days each with 29 nM of siRNA (SASI_Hs01_00156548,

Sigma) using Lipofectamine(TM) RNAiMAX (Invitrogen) and/or treated with 10 ng/ml Activin type 1 receptor inhibitor (SB431542, Calbiochem). Alternatively, cells were stimulated with 10 ng/ml rhIL-11 (CYT-214, Pepnet) and/or 10 ng/ml rhTGF-β2 (100-35B, Peprotech) in EGM-2 for 96 h with renewal of culture medium and cytokines every 24 h.

3.2.26. Phylogenetic analysis

Phylograms showing the orthology of *il11a*, *il11b*, and *il11ra* within the IL-6 family of cytokines and receptors across human, mouse and zebrafish, were established based on the respective full-length protein sequences. Phylogeny.fr (Dereeper et al., 2008), was used at default settings. Details of peptides used are as follows:

Protein	Encoding transcript ID	Peptide length
hCNTFR	ENST00000351266.8	372 aa
hIL6R	ENST00000368485.8	486 aa
hIL11RA	ENST00000441545.7	422 aa
hLIFR	ENST00000263409.8	1097 aa
hOSMR	ENST00000274276.8	979 aa
zIl11ra	ENSDART00000030976.7	402 aa
mIL11RA1	ENSMUST00000098132.10	432 aa
mIL11RA2	ENSMUST00000179253.1	432 aa

Table 3.25. IL-6 family receptor peptide details.

Protein	Encoding transcript ID	Peptide length
hCNTF	ENST00000361987.6	200 aa
hIL6	ENST00000404625.5	212 aa
hIL11	ENST00000264563.7	199 aa

hLIF	ENST00000249075.4	202 aa
hOSM	ENST00000215781.3	252 aa
zIl11a	XM_693882.9	219 aa
zIl11b	ENSDART00000081440.4	192 aa
mIL11	ENSMUST00000094892.11	199 aa

Table 3.26. IL-6 family cytokine peptide details.

3.2.27. Quantification

Cardiac scar was assessed using consecutive sections and the quantification was performed on the section with the largest scar area. Trabecular CM protrusion was measured on at least two non-consecutive 50 µm thick cryosections. CM proliferation and cortical CM protrusion were measured on at least two non-consecutive 11 µm thick cryosections. For measuring endothelial invasion on wholemount ventricles, injured area was determined by the corresponding brightfield images. pSmad3+ endothelial cells were quantified using Analyze particles function in Fiji. Zen 3.2 (blue edition) or NIS-Elements BR Analysis 4.30.00 64-bit or Fiji were used for quantifications.

[*This subsection is quoted verbatim from Allanki et al., Sci. Adv. 7, eabg6497 (2021) for precise explanation*].

3.2.28. Statistical analyses

GraphPad Prism 8 was used to determine the *P*-values and perform all statistical analyses. Each sample group was tested for Gaussian distribution using the Shapiro-Wilk normality test. If the data were normally distributed, parametric tests were used: two-tailed Student's t-test for comparing 2 samples. If the data were not normally distributed, non-parametric tests were used: Mann-Whitney U test for comparing 2 samples. For HUVEC experiments, paired two-tailed Student's t-test was used for comparing 2 samples or repeated measures (RM) one-way analysis of variance (ANOVA) with Tukey's multiple corrections test was used for comparing more than 2 samples. The exact *P*-values and the statistical tests performed are indicated in the figures and figure legends, respectively.

[*This subsection is quoted verbatim from Allanki et al., Sci. Adv. 7, eabg6497 (2021) for precise explanation*].

4. Results

Note: Parts of this chapter have been published as an article in the journal *Science Advances*.

[**S. Allanki**, B. Strilic, L. Scheinberger, Y. L. Onderwater, A. Marks, S. Gunther, J. Preussner, K. Kikhi, M. Looso, D. Y. R. Stainier, S. Reischauer, Interleukin-11 signaling promotes cellular reprogramming and limits fibrotic scarring during tissue regeneration. *Sci. Adv*. 7, eabg6497 (2021)].

The authors' contribution was described in the paper as follows:
"Conceptualization: S.A., D.Y.R.S., and S.R. Methodology: S.A., D.Y.R.S., and S.R. Investigation: S.A., B.S., L.S., Y.L.O., A.M., S.G., J.P., and K.K. Resources: M.L. and D.Y.R.S. Writing: S.A., D.Y.R.S., and S.R., with inputs from all authors. Supervision: D.Y.R.S. and S.R. Project administration and funding acquisition: D.Y.R.S. and S.R."

4.1. Zebrafish display limited scarring response to cardiac injury

Fibrotic scarring limits tissue regeneration (Gurtner et al., 2008). Specialized cell types called as Myofibroblasts orchestrate scarring, by secreting excessive extracellular matrix. These cells arise from various cell lineages, including tissue resident fibroblasts and endothelial cells, in response to injury (Davis and Molkentin, 2014; Kanisicak et al., 2016). Myofibroblasts further differentiate into matrifibrocytes to maintain and mature the scar that hinders optimal tissue function (Fu et al., 2018). I hypothesized that the regenerative species display a milder scarring response (myofibroblast differentiation) than the non-regenerative counterparts do (**Fig. 4.1A**). To investigate these differences, using lineage-tracing strategies, I quantified the myofibroblast differentiation from fibroblasts and endothelial cells in the zebrafish heart. I then compared these numbers to those reported in the adult mouse heart after MI. I found that only ~12% of the zebrafish fibroblasts differentiate into myofibroblasts (**Fig. 4.1B and C**), while in the mouse, majority of all the resident fibroblasts (~95%) differentiate into myofibroblasts (Fu et al., 2018). Similarly, the endothelial lineage in zebrafish (~4%) displayed a very limited myofibroblast differentiation than that of the adult mouse (~35%) (**Fig. 4.1B and D**) (Aisagbonhi et al., 2011). These data show

that the zebrafish heart indeed displays a limited scarring response in comparison with the non-regenerative adult mouse. Furthermore, these data led me to hypothesize that the regenerative species employ mechanisms to limit the scarring response, thereby aiding regeneration.

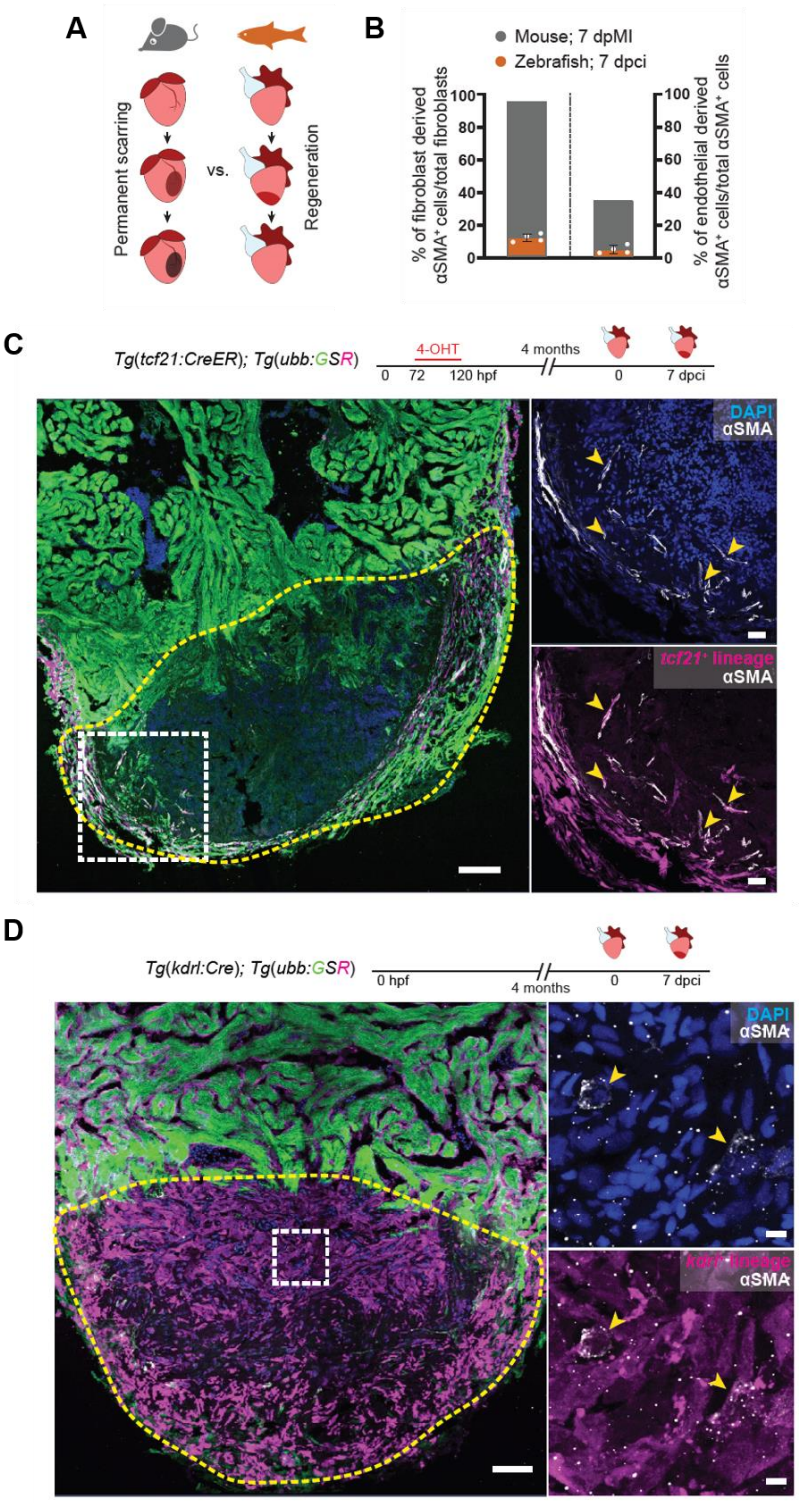

Figure 4.1. Analyzing the zebrafish myofibroblast response to cardiac cryoinjury. (**A**) Illustration of scarring in an adult mammalian heart in contrast to regeneration in an adult zebrafish heart. (**B**) Quantification of epicardial- and endothelial-derived αSMA$^+$ cells after MI in mouse [fibroblasts (Fu et al., 2018); endothelial cells (Aisagbonhi et al., 2011)] and 7 dpci in zebrafish [fibroblasts, *Tg(tcf21:CreER)*, n = 4; endothelial cells, *Tg(kdrl:Cre)*, n = 4]. (**C**) Experimental design and immunostaining (GFP - green, αSMA – white, and mCherry – magenta; n=4; 7 dpci) on cryosections from *Tg(tcf21:CreER); Tg(ubb:GSR)* ventricles. (**D**) Experimental design and immunostaining (GFP - green, αSMA – white, and mCherry – magenta; n=4; 7 dpci) on cryosections from *Tg(kdrl:Cre); Tg(ubb:GSR)* ventricles. n= ventricles (A, B). Yellow dashed lines demarcate the injured area (A, B); arrowheads point to αSMA$^+$ cells derived from *tcf21*$^+$ lineage (A insets) and *kdrl*$^+$ lineage (B insets). Scale bars, 100 μm (A), 50 μm (B), 10 μm (A insets), 5 μm (B insets). Adapted from (Allanki et al., 2021). License: CC BY 4.0.

4.2. Interleukin-6 cytokine family-mediated Stat3 signaling is pro-regenerative

4.2.1. Comparative transcriptional profiling identifies Il-6 cytokine family/Stat3 signaling as pro-regenerative

To identify the mechanisms that limit scarring response in zebrafish, I performed a microarray-based transcriptional profiling of the regenerating ventricles at 96 hpci (**Fig. 4.2A**). However, nearly 16% of the transcriptome is significantly altered after cryoinjury, which made candidate identification difficult. To shortlist the number of genes in a meaningful way, I performed another microarray experiment on exercised zebrafish ventricles (**Fig. 4.2A**). Moderate physical exercise has been shown to be cardioprotective even in human MI patients. Hence, I reasoned that the genes that are co-regulated both after cryoinjury and after moderate exercise would be the ideal pro-regenerative and cardioprotective candidates. I found 180 co-regulated genes (**Appendix I**). Pathway and upstream regulator analyses (**Appendix II**) on these co-regulated genes gave me promising hints that Interleukin-6 cytokine family-mediated Jak-Stat3 signaling is a pro-regenerative pathway (**Fig. 4.2B and C**).

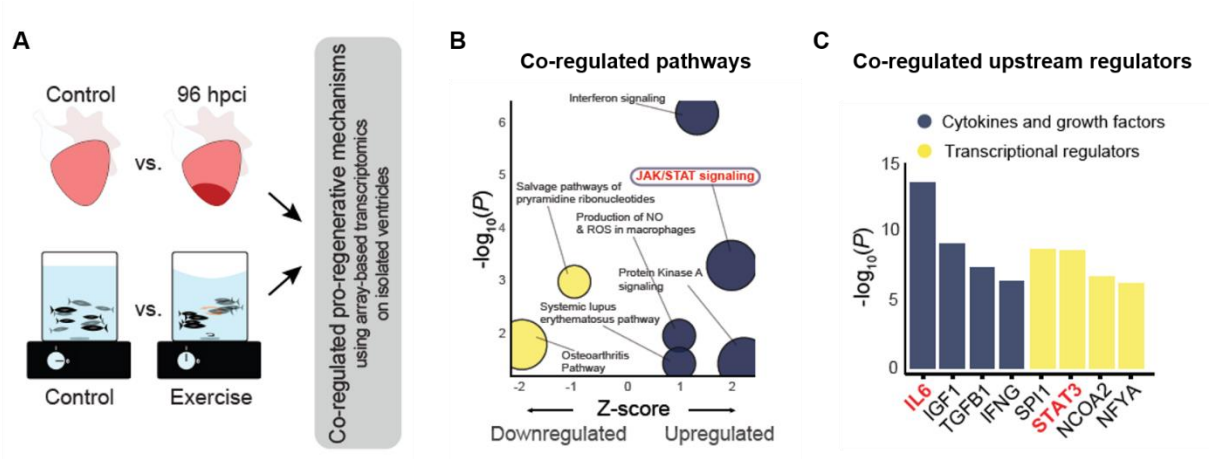

Figure 4.2. Comparative transcriptional profiling of the regenerating and exercised zebrafish ventricles. (**A**) Schematics of the comparative transcriptional profiling. (**B and C**) Results from pathway and upstream regulator analyses using Ingenuity pathway analysis (IPA). Adapted from (Allanki et al., 2021). License: CC BY 4.0.

4.2.2. Zebrafish *il6st* and *stat3* mutants display severely impaired regeneration

To investigate if the Il-6 cytokine family mediated Stat3 signaling is required for regeneration in zebrafish, I challenged the zebrafish *il6st*^{sa1462} and *stat3*^{stl27} mutant alleles with tissue damage. Similar to their mouse mutant counterparts, both the *il6st* and *stat3* (Liu et al., 2017) mutant zebrafish displayed early lethality starting from larval to juvenile stages (**Fig. 4.3A and B**), rendering adult regeneration studies impossible. Both the adult mutant survivors displayed similar gross morphological defects, including bone deformities in the spine and smaller body length (**Fig. 4.3A and B**), indicating that Il6st majorly acts through Stat3 signaling. However, both the mutant larvae displayed indistinguishable gross morphology compared to their wild-type and heterozygous siblings. Hence, I decided to test their regenerative capabilities using larval fin fold amputations. Unlike their wild-type siblings, both the mutants displayed severely impaired regeneration (**Fig. 4.3C and D**). The *stat3* mutant phenotype is in line with the earlier reports (Miskolci et al., 2019). These data strongly indicate that Il6st/Stat3 signaling is essential for regeneration in zebrafish at least at the larval stages.

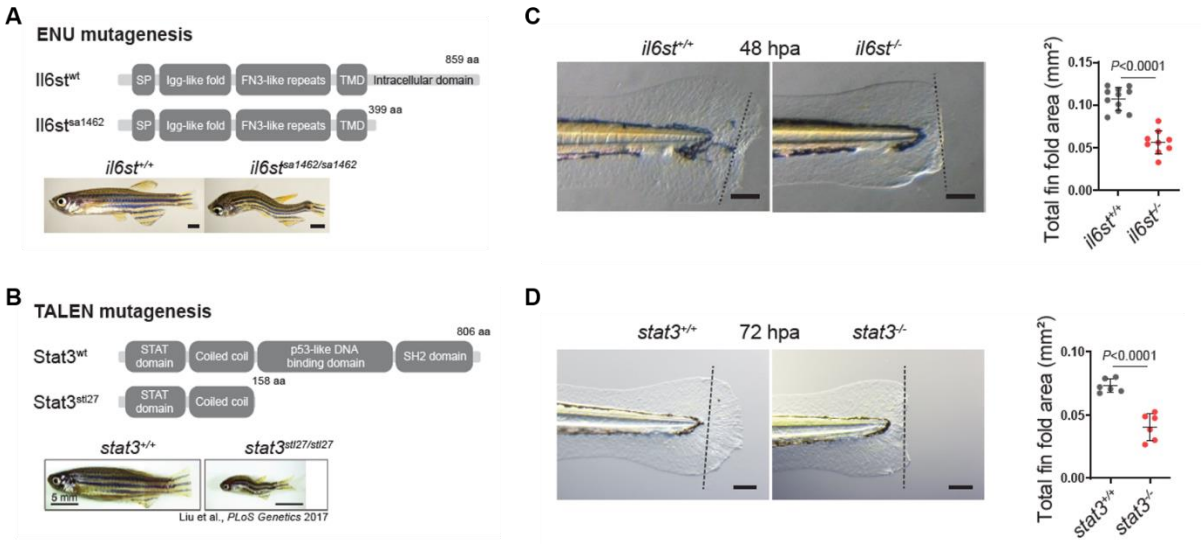

Figure 4.3. Impaired larval fin fold regeneration in *il6st* and *stat3* mutants. (**A and B**) Illustration of wild-type and the predicted mutant proteins, gross morphology of adult zebrafish mutants (A, *il6st*^{sa1462}; B, *stat3*^{stl27}) and their respective wild-type siblings. (**C and D**) Bright-field images of larval fin fold regeneration [amputated at 48 to 60 hpf)] and their corresponding quantification of the fin fold area [*il6st*^{sa1462}; wt siblings, n = 11; mut, n = 9, 48 hpa; *stat3*^{stl27}, wt siblings, n = 6; mut, n = 6, 72 hpa]. Data represent means ± SD (C and D). Student's t tests (C and D). n = larvae (C and D). Black dashed lines demarcate the amputation plane (C and D). Scale bars, 1 mm (A), 5 mm (B), and 100 µm (C and D). Adapted from (Allanki et al., 2021). License: CC BY 4.0.

4.3 Interleukin-11/Stat3 signaling is a global regulator of regeneration in zebrafish

4.3.1. Evolutionarily conserved induction of Il-11 cytokine levels during tissue regeneration

To narrow down my search for pro-regenerative molecules, I profiled through the Interleukin-6 family of cytokine levels, and the downstream target *socs3b* levels, after heart and fin injuries in adult zebrafish (**Fig. 4.4A**). I performed RT-qPCRs to assess the mRNA levels at 1 hpci in the whole ventricle and at 1 hpa in the adult caudal fin. I found that both tissues displayed ~6-fold upregulation of *socs3b*, indicating a robust activation of Jak-Stat3 pathway within minutes after damage (**Fig. 4.4B and C**). In addition, both the paralogues of Interleukin-11 cytokine encoding genes, *il11a* and *il11b*, were the most expressed and the highest induced Il-6 family of cytokines, in both

the heart and the fin. Furthermore, published transcriptomic datasets during regeneration in lungfish limbs, axolotl limbs, African Killifish fins, *Xenopus* tails also show a sharp and evolutionarily conserved upregulation of Il-11 levels (Darnet et al., 2019; Fang et al., 2013; Gerber et al., 2018; Tsujioka et al., 2017; Wang et al., 2020).

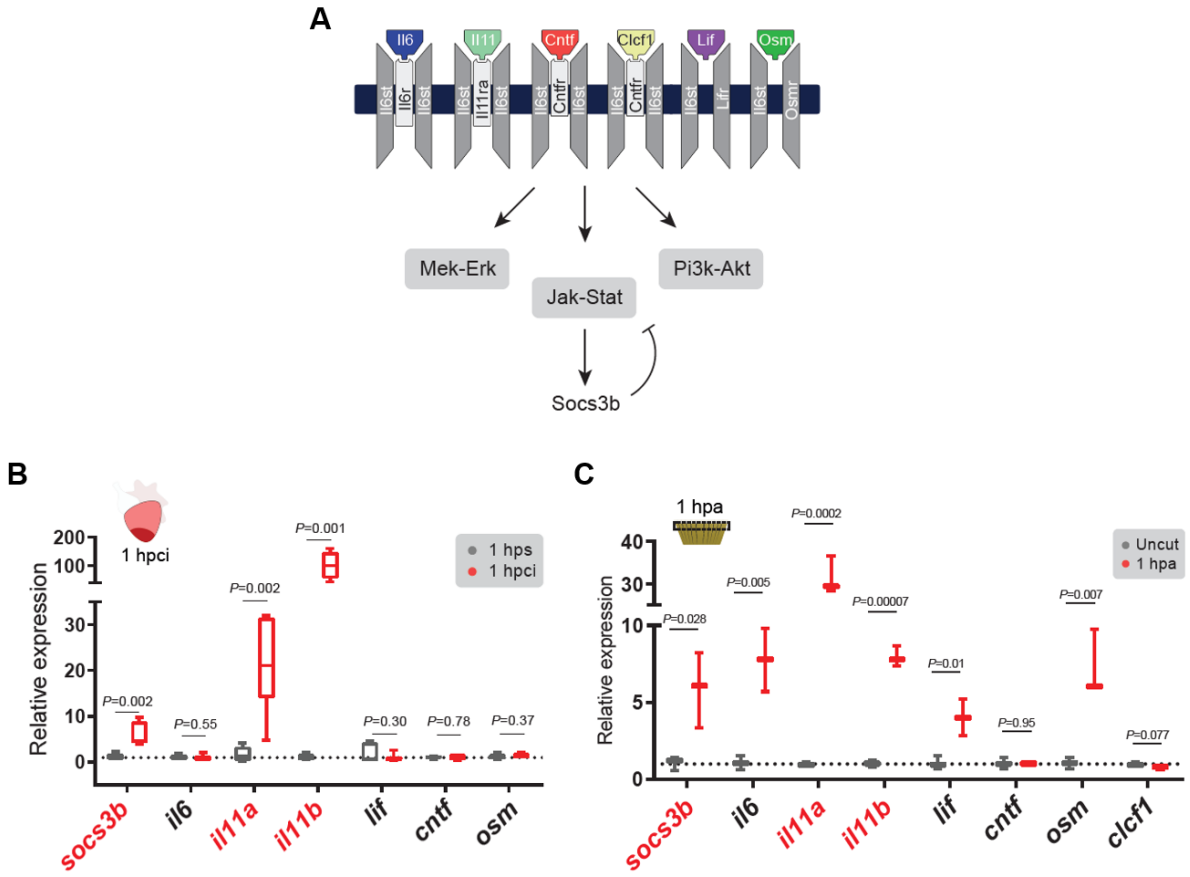

Figure 4.4. Il-11 cytokine gene mRNA levels are upregulated after tissue damage in zebrafish. (**A**) Illustration of zebrafish Il-6 family cytokines and receptors and the downstream signaling pathways. (**B**) RT-qPCR analysis of Il-6 family cytokine mRNA levels (1 hpci, n=6; 1 hps, n=5) on adult cardiac ventricles. (**C**) RT-qPCR analysis of Il-6 family cytokine mRNA levels (1 hpa, n=3; uncut, n=3) on adult caudal fins. Adapted from (Allanki et al., 2021). License: CC BY 4.0.

I also performed spatial expression analysis for *il11a* and *il11b* by using RNA in situ hybridization (ISH) on injured hearts and fins. In both the tissues tested, in line with the RT-qPCR data, I observed a clear induction of mRNA levels of both the cytokine genes (**Fig. 4.5A and C**). Taking a closer look at the expression patterns in the heart, both *il11a* and *il11b* are enriched in the border zone at 24 hpci (**Fig. 4.5A**). Based on

these spatial expression patterns and previous reports after ventricular resection (Fang et al., 2013), I suspected that endothelial cells could be the major source of Il-11 cytokine expression. To test this hypothesis, I performed RT-qPCRs on sorted endothelial vs. non-endothelial cells at 96 hpci from *Tg(fli1:EGFP)* ventricles. In line with the ISH data, both the cytokines were enriched in endothelial cells when compared with non-endothelial cells at 96 hpci (**Fig. 4.5B**). Together, these data suggested that Il-11 signaling could be a global regulator of regeneration. Hence, I chose Il-11 signaling to be the prime candidate pathway for further analysis.

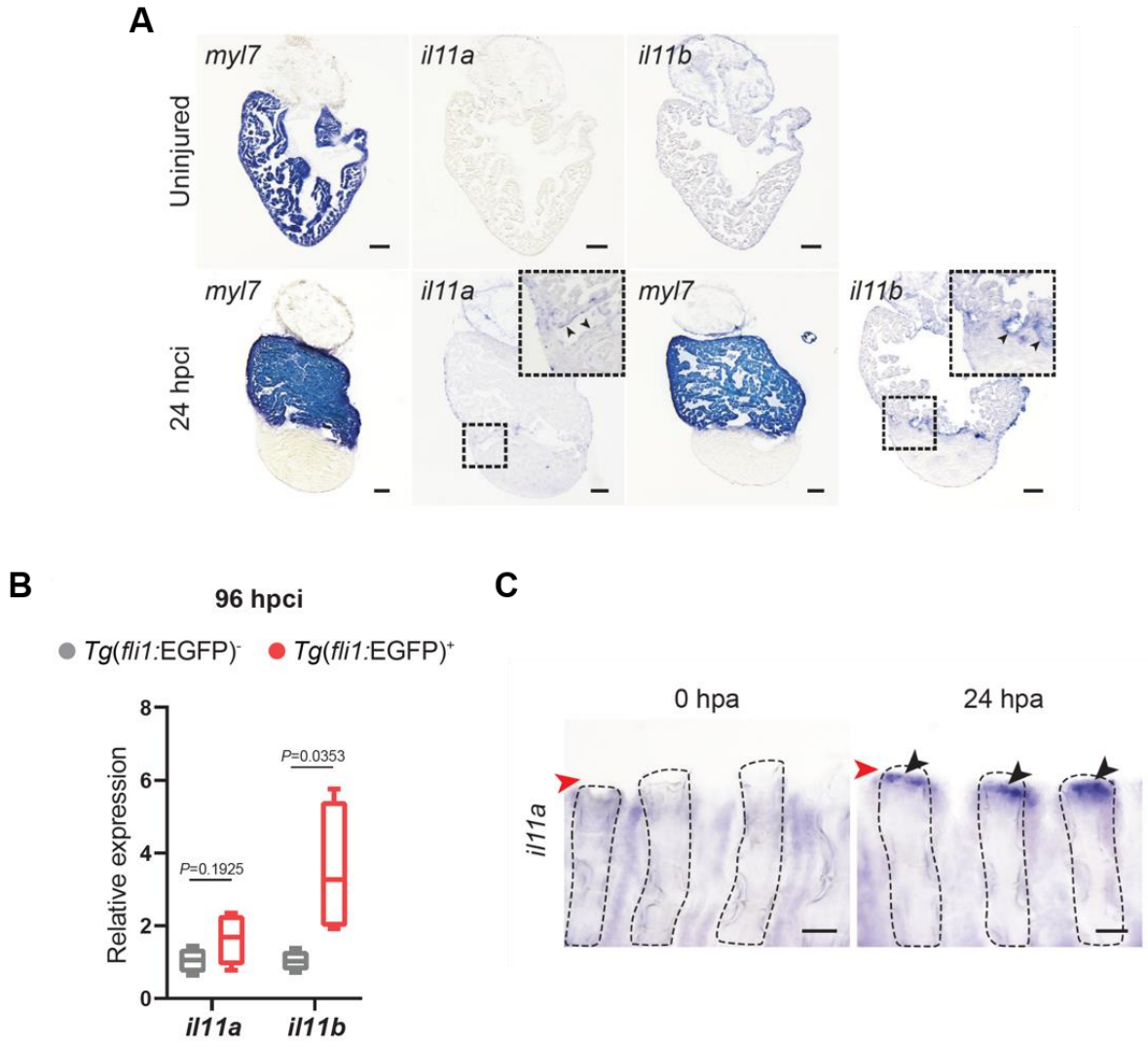

Figure 4.5. Spatial expression analysis of Il-11 cytokine genes after tissue damage. (**A**) Brightfield images of RNA in situ hybridization for *myl7*, *il11a*, *il11b* on 11 µm thick cryosections from uninjured and 24 hpci wild-type ventricles. (**B**) RT-qPCR analysis on sorted

*Tg(fli1:*EGFP)$^{+}$ vs. *Tg(fli1:*EGFP)$^{-}$ cardiac ventricular cells (96 hpci, n=4 each). (**C**) Brightfield images of RNA in situ hybridization for *il11a* on wholemount adult caudal fins, 24 hpa. Box plots (B) show median, interquartile range (IQR, box margins) and 5th and 95th percentiles (whiskers). Student's t-tests (B). n= pools of two ventricles (B). Black arrowheads point to border zone endothelial gene expression (A) and blastemal expression (C); red arrowheads point to the amputation plane (C); black dashed lines outline the fin rays (C). Scale bars, 200 µm (A), 100 µm (C). Adapted from (Allanki et al., 2021). License: CC BY 4.0.

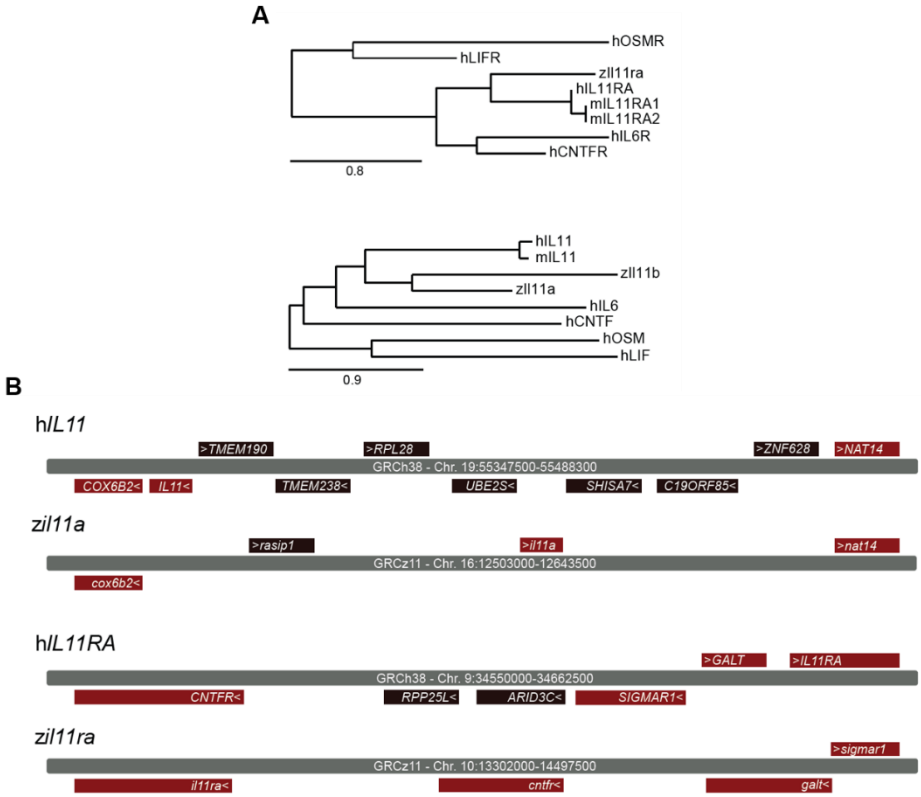

Figure 4.6. Phylogenetic and synteny analyses of Il-11 pathway components. (**A**) Phylogenetic analysis of human, mouse, and zebrafish Il-11 cytokine receptor and ligands. (**B**) Synteny analysis for human and zebrafish genes encoding Il-11 ligands and receptors; gene sizes are not to scale. Adapted from (Allanki et al., 2021). License: CC BY 4.0.

4.3.2. Members of the Il-11 pathway are evolutionarily conserved

Given the seemingly opposite roles reported for Il-11 signaling in regenerative vs. non-regenerative species (Cook and Schafer, 2020), I investigated the phylogeny of the Il-11 signaling components. Using both phylogenetic analysis and synteny, I found that both the zebrafish ligands (*il11a* and *il11b*) and receptor (*il11ra*) are closer in evolution

to their mammalian (mouse and human) orthologues (**Fig. 4.6**). These data confirm that the zebrafish Il-11 components are direct orthologues of their mammalian counterparts.

4.3.3. Analyzing regeneration in the zebrafish *il11a*, *il11b*, *il11ra* loss-of-function alleles

To investigate the specific roles of Il-11 signaling pathway components during regeneration, I have generated genetic loss-of-function alleles for both the Il-11 ligand encoding genes (*il11a* and *il11b*) and the receptor encoding gene (*il11ra*) using CRISPR-Cas9 technology (**Fig. 4.7**). All the mutants were indistinguishable in the embryonic, larval and adult stages when compared to their respective wild-type siblings (data not shown). However, the *il11ra* adult mutants displayed minor bone deformities, as reported in their mammalian counterparts (**Fig. 4.7B**) (Nandurkar et al., 1997).

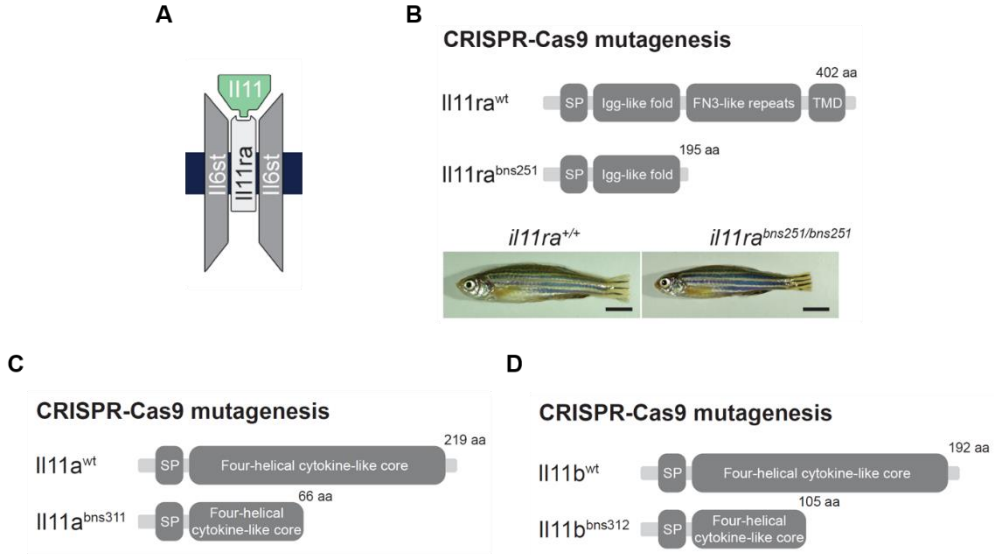

Figure 4.7. Generation of *il11a*, *il11b* and *il11ra* loss-of-function alleles. (**A**) Schematic of the zebrafish Il-11 signaling. (**B**) Illustration of wild-type and predicted mutant proteins and gross morphology of adult zebrafish siblings. (**C and D**) Illustration of wild-type and the predicted mutant proteins (C, Il11a^{bns311}; D, Il11b^{bns312}). Scale bars, 5 mm (B). Adapted from (Allanki et al., 2021). License: CC BY 4.0.

Unlike the *il6st* and *stat3* mutants, *il11ra*, *il11a* and *il11b* mutants survived to adulthood, indicating that Il-11 signaling is dispensable for animal development. Next, using these

mutant alleles, I investigated their regeneration capabilities in various tissues, including larval fin folds, adult caudal fins, adult scales and the adult heart.

4.3.3.1. Il11a/Il11ra signaling is required for larval fin fold regeneration

Similar to what I observed in *il6st* and *stat3* mutants, both *il11ra*, *il11a*, but not *il11b* mutants displayed severe regeneration defects after larval fin fold amputation (**Fig. 4.8**). These data indicate that Il11a-Il11ra-Il6st-Stat3 axis is indispensable for larval fin fold regeneration.

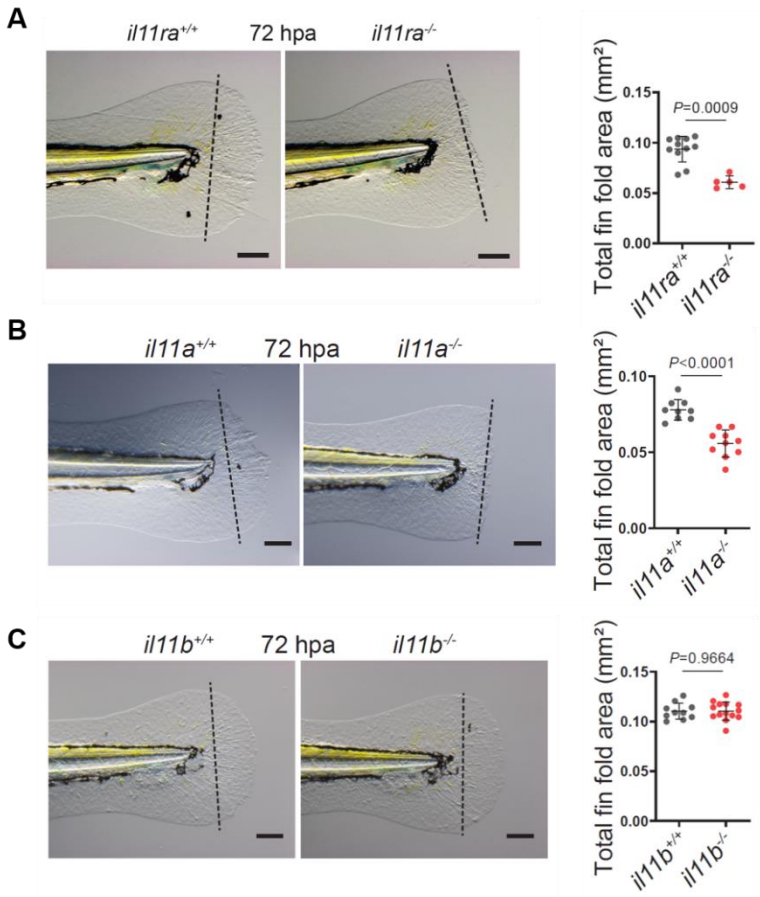

Figure 4.8. Il-11a/Il11ra signaling is required for larval fin fold regeneration. (**A**) Bright-field images of larval fin fold regeneration (wt siblings, n = 11; mut, n = 5; 72 hpa) and their corresponding quantification of the total fin fold area. (**B and C**) Brightfield images of larval fin fold regeneration (amputated at 48-72 hpf), and their corresponding quantification of the fin fold area at 72 hpa (B, *il11a*^{bns311}, wt siblings, n=9; mut, n=10; C, *il11b*^{bns312}, wt siblings, n=10; mut, n=14). Data represent mean ± S.D. Student's t-tests. n= larvae. Black dashed lines

demarcate the amputation plane. Scale bars, 100 μm. Adapted from (Allanki et al., 2021). License: CC BY 4.0.

4.3.3.2. Il11a/Il11ra signaling is required for adult caudal fin regeneration

Next, I tested for adult caudal fin regeneration using two different injury models – amputation and bone crush. Similar to larval fin fold regeneration, upon amputation, unlike the wild-type fins, *il11ra* and *il11a*, but not *il11b* mutants displayed impaired adult caudal fin regeneration (**Fig. 4.9A and C**). The most severe phenotype was observed in *il11ra* mutants. After amputation, wound re-epithelialization response was observed similar to the wild-type levels, but the blastema formation is severely impaired. The *il11ra* mutants, after fin amputation, could not regenerate past the amputation plane throughout the rest of their lives (**Fig. 4.9A**). These mutants are one of the very few genetic mutants (*hspd1*/*nbl* – *no blastema*, and *fgf20a*/*dob* – *devoid of blastema*) that display such a drastic fin regeneration phenotype (Makino et al., 2005; Whitehead et al., 2005). By performing histological analysis, I observed that the non-regenerative *il11ra* mutant fin hemi-rays fuse together and form a calcified cap on each fin ray, sealing the fin growth (**Fig. 4.9B**).

To assess if these regeneration defects require a missing tissue context, I performed bone crush injuries on *il11ra* mutants. While the crushed wild-type fin rays regenerated by 17 days post crush (dpc), the *il11ra* mutants' displayed a non-regenerative callus formation (**Fig. 4.9D**).

To assess if Stat3 signaling downstream of Il11ra is required for adult caudal fin regeneration, I used the compound heterozygous fish (*il11ra*$^{+/-}$;*stat3*$^{+/-}$). While the *stat3*$^{+/-}$ already display a mild phenotype, the compound heterozygous fish displayed severely impaired outgrowth (**Fig. 4.10**). These data strongly indicate that Il11a-Il11ra-Stat3 signaling is required for adult caudal fin regeneration.

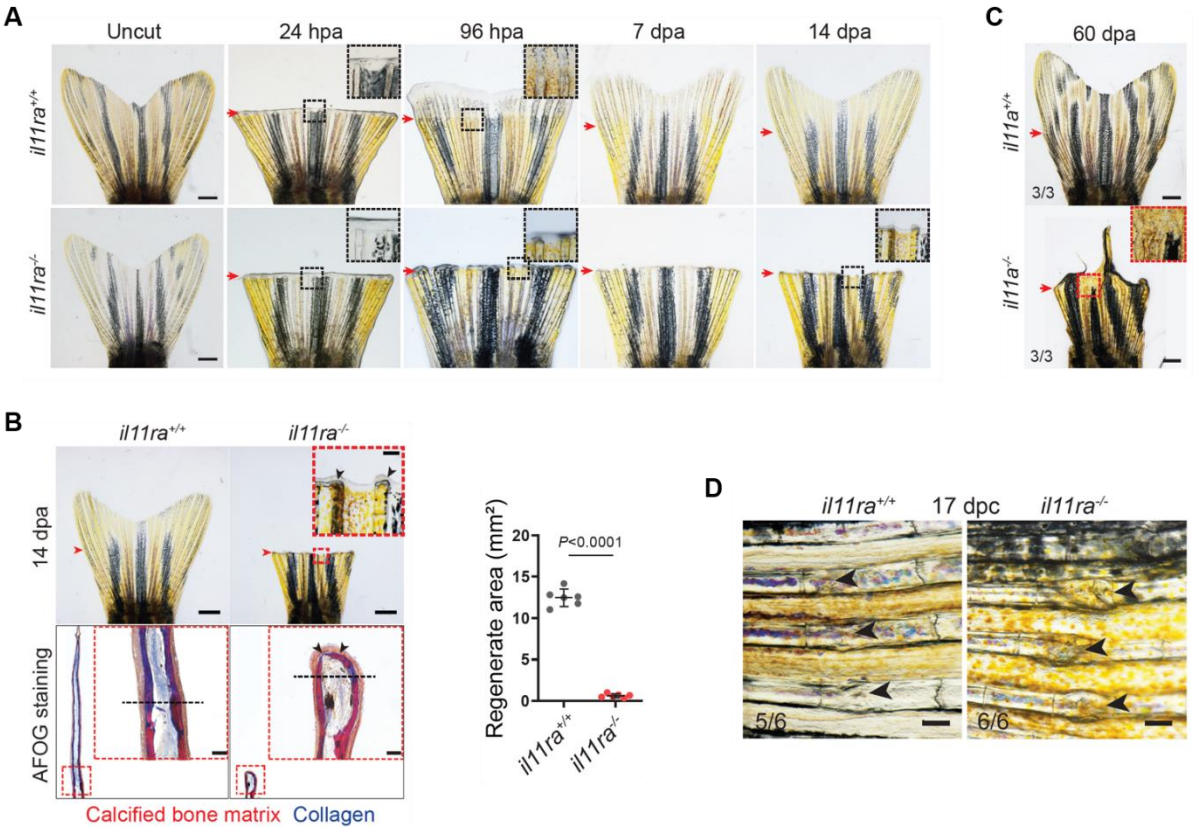

Figure 4.9. Il11a-Il11ra signaling is required for adult caudal fin regeneration. (**A**) Wholemount images of time course of caudal fin regeneration in *il11ra*$^{-/-}$ vs. wild-type siblings. (**B**) Wholemount images of caudal fins [wt, n = 6; mut, n = 6, 14 days post amputation (dpa)], AFOG staining on longitudinal cryosections, and quantification of the regenerate area. (**C**) Wholemount images of caudal fin regeneration in *il11a*$^{-/-}$ (n=3) vs. wild-type siblings (n=3), 60 dpa. (**D**) Wholemount images of bone crush injury in *il11ra*$^{-/-}$ (n= 6) vs. wild-type (n= 6) caudal fins at 17 days post crush (dpc). Data represent means ± SD (B). Student's t tests (B). n, caudal fins (B and C). Black dashed lines demarcate the amputation plane (B); black arrowheads point to fused hemirays (insets in B) and crushed regions (D); red arrowheads point to the amputation plane (A and C). Scale bars, 1 mm (A, B - wholemount, C), 100 µm (D), and 50 µm (B - AFOG). Adapted from (Allanki et al., 2021). License: CC BY 4.0.

4.3.3.3. Il11ra signaling is required for adult scale regeneration

From the previous analyses in the larval fin fold and adult caudal fin, it is evident that *il11ra* mutants display the most severe phenotypes compared to the individual ligand mutants (*il11a* and *il11b*). Hence, we decided to use the *il11ra* mutant allele for further analyses.

Next, we tested for scale regeneration. As it was reported earlier (Cox et al., 2018; De Simone et al., 2021), the wild-type scales regenerated almost completely within 7 days post plucking (dpp), but the *il11ra* mutant scales displayed impaired and delayed regeneration.

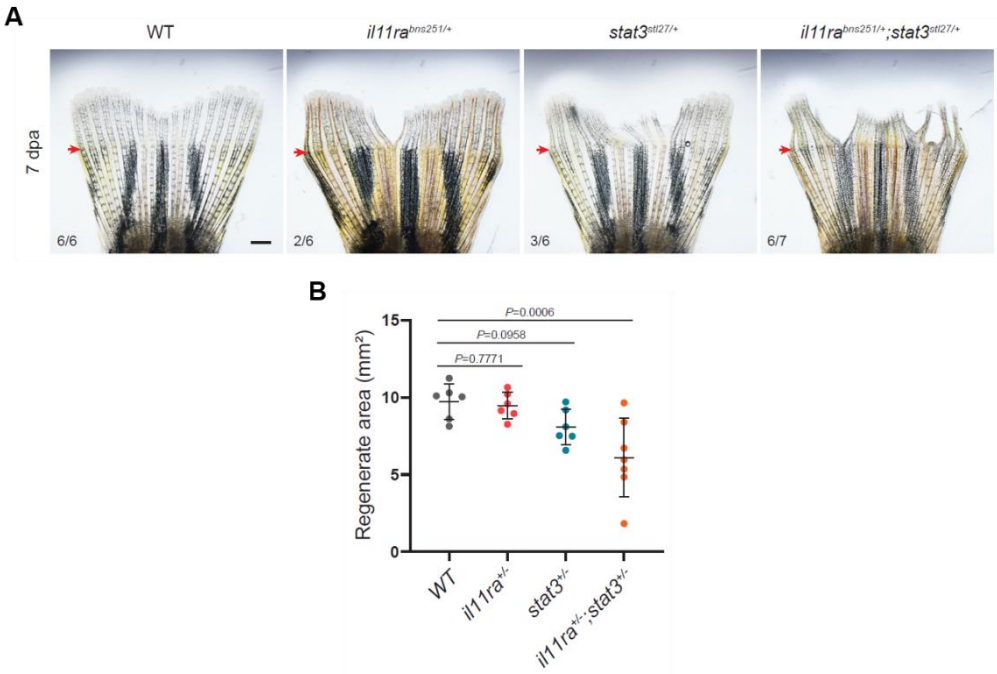

Figure 4.10. Il11ra-Stat3 signaling is required for adult caudal fin regeneration. (**A and B**) Wholemount images of caudal fin regeneration in *il11ra*$^{+/-}$ (n=6), *stat3*$^{+/-}$ (n=6), *il11ra*$^{+/-}$*;stat3*$^{+/-}$ (n=7) vs. wild-type siblings (n=6) (A) and quantification of the regenerate area, 7 dpa (B). n= caudal fins (A). Data represent mean ± S.D. (B). One-way ANOVA (B). Red arrows point to the amputation plane (A). Scale bar: 1 mm (A). Adapted from (Allanki et al., 2021). License: CC BY 4.0.

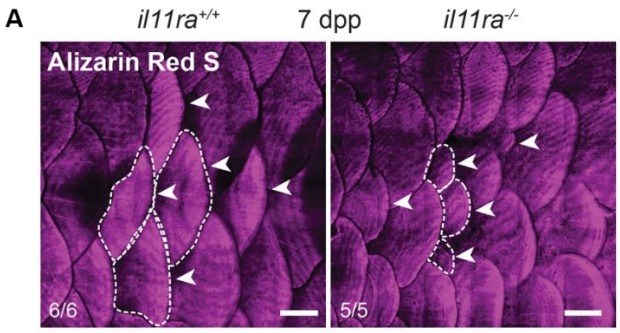

Figure. 4.11. Scale regeneration in *il11ra* mutants. (**A**) Wholemount images of Alizarin Red S stained regenerating adult scales [wt siblings, n = 6; mut, n = 5; 7 days post plucking (dpp)].

n, adult zebrafish. White dashed lines demarcate and white arrowheads point to regenerating scales. Scale bars, 500 µm. Adapted from (Allanki et al., 2021). License: CC BY 4.0.

4.3.3.4. Il11ra signaling is required for adult heart regeneration

Next, I tested for adult heart regeneration in the *il11ra* mutants. I performed cardiac cryoinjuries and harvested the hearts at 90 dpci, at which the wild-type hearts were reported to undergo near-complete regeneration. While the wild-types retained a residual collagenous scar, the mutants displayed a significantly larger scar areas, indicating permanent scarring (**Fig. 4.12A**). These permanent collagenous scars in the mutant ventricles are reminiscent of the adult mammalian cardiac scars. Below are the serial sections for reference from the same ventricles (**Fig. 4.12B**).

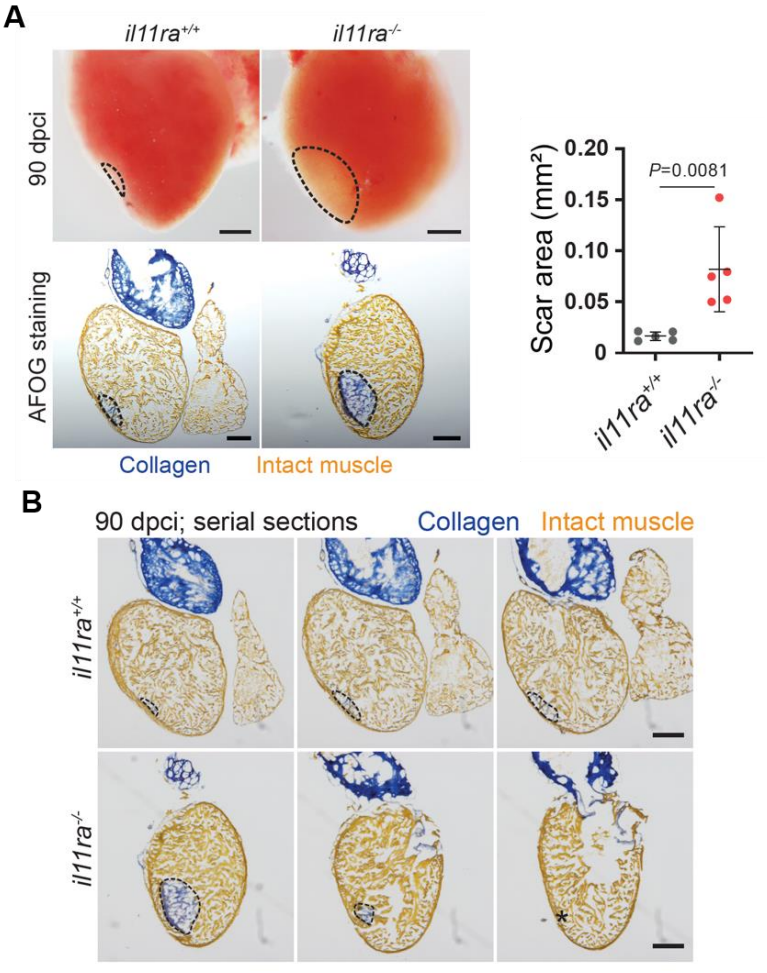

Figure. 4.12. Heart regeneration in *il11ra* mutants. (**A**) Wholemount images of cardiac ventricles (wt siblings, n = 5; mut, n = 5; 90 dpci), Acid Fuchsin Orange G (AFOG) staining on cryosections, and quantification of the scar area. (**B**) AFOG staining on serial sections from

the same ventricles in A. Data represent means ± SD (A). Student's t tests (A). n, ventricles (A). Black dashed lines demarcate the injured area (A and B); black asterisks mark the lack of injury. Scale bars, 200 µm (A and B). Adapted from (Allanki et al., 2021). License: CC BY 4.0.

4.3.4. Injury-specific Il-11 signaling is required for adult caudal fin regeneration

One of the primary concerns of using global mutants for adult regeneration studies is the effect of developmental defects that accumulate throughout life on regeneration. However, making conditional alleles in zebrafish is not as established as it is in the mouse. Hence, I resorted to an alternative approach to answer the same question. I re-expressed *il11ra* in *il11ra* mutants in an injury specific way to observe for any detectable rescue of the fin regeneration phenotype. To this end, I have generated a new transgenic line that re-expresses *il11ra* under a heat shock promoter, in the *il11ra* mutant background (**Fig. 4.13A**).

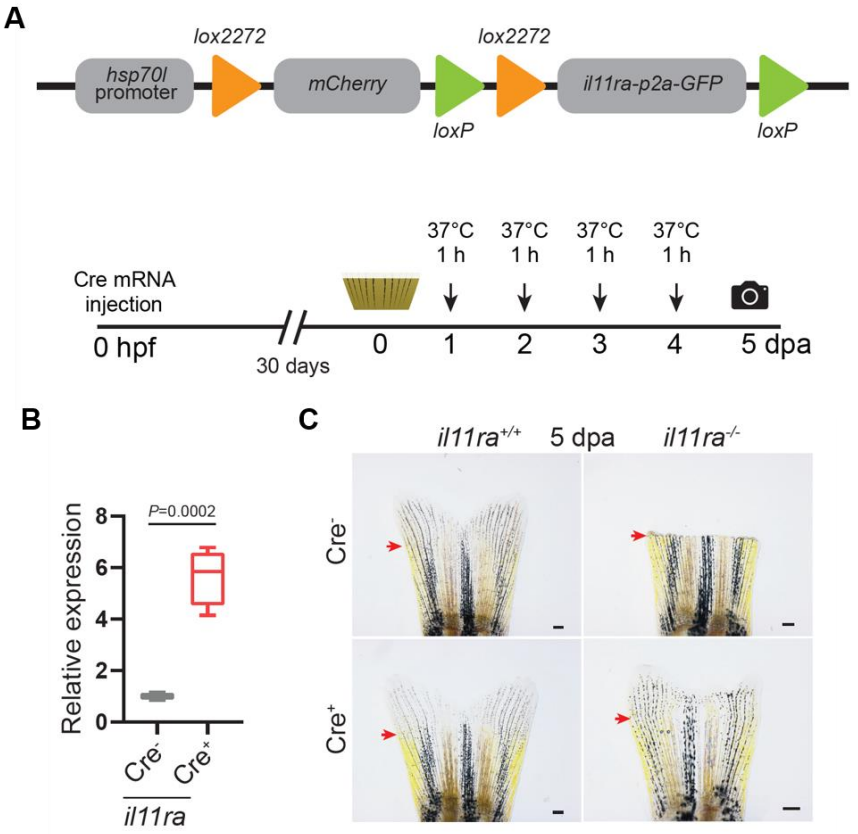

Tg(hsp70l:loxp-lox2272-mCherry-loxp-il11ra-V5-p2a-GFP-lox2272)

Figure. 4.13. Injury-specific requirement of Il-11 signaling for successful regeneration. (**A**) Illustration of *il11ra* re-expression construct and experimental set-up. (**B**) RT-qPCR analysis to test the induction of *il11ra* expression in caudal fins of *Tg(hsp70l:loxp-lox2272-mCherry-loxp-il11ra-V5-p2a-GFPlox2272)* zebrafish (n=4 each; Cre mRNA injected vs. uninjected), 5 dpa. (**C**) Wholemount images of fin regeneration at 5 dpa in *Tg(hsp70l:loxp-lox2272-mCherry-loxp-il11ra-V5-p2a-GFP-lox2272)* zebrafish in *il11ra*$^{-/-}$ vs. wild-type backgrounds, and with or without Cre mRNA injection at the one-cell stage. Box plot (B) shows median, interquartile range (IQR, box margins) and 5th and 95th percentiles (whiskers). Student's t-test (B). n= adult caudal fins (B). Red arrows point to the amputation plane (C). Scale bars, 200 µm (C). Adapted from (Allanki et al., 2021). License: CC BY 4.0.

First, I tested the re-expression by performing RT-qPCR for *il11ra* on heat shocked transgenic fish. Indeed, I observed a ~6-fold upregulation of *il11ra* upon the heat shock regimen in Fig. 4.13A (**Fig. 4.13B**), validating the line. I then used the same regimen on the mutants vs. wild types, with (Cre^{+}) or without (Cre^{-}) re-expression of *il11ra*. The wild types with or without an active re-expression of *il11ra* did not display any detectable phenotypes. However, the mutants re-expressing *il11ra* (Cre^{+}) displayed a clearly visible rescue of the fin regeneration defect while the mutants without re-expression (Cre^{-}) retained the severe phenotype (**Fig. 4.13C**). These data highlight the injury-specific requirement of Il-11 signaling for successful regeneration.

4.4. Il-11 signaling promotes regenerative reprogramming and cell repopulation of the injured area

So far, I have shown that Il-11/Stat3 signaling is a global regulator of regeneration in zebrafish. The next question that I asked is – how does Il-11 signaling regulate regeneration? To identify the global regenerative mechanisms employed by Il-11 signaling, we decided to perform an in-depth analysis of the *il11ra* mutant phenotypes at least in two major tissues – the adult caudal fin and the adult heart.

4.4.1. Il-11 signaling orchestrates regenerative reprogramming

During regeneration, regenerative reprogramming is a phenomenon by which cells change their homeostatic gene expression landscape to a regenerative gene program. This process involves up- and down-regulation of thousands of genes in order to

promote regenerative cellular processes, including dedifferentiation, proliferation, and migration. To investigate the gene expression landscape, I performed RNA-seq on the mutant and wild type hearts and fins, after injury. I then screened for deregulated genes both in a tissue-specific manner and globally across tissues.

4.4.1.1. Regenerative reprogramming during adult fin regeneration

First, to identify cell-type specific gene expression changes, I have reanalysed a published single-cell dataset during adult zebrafish caudal fin regeneration. The two main cellular compartments during fin regeneration are the epithelium and the blastema. I have observed that several genes, including *ptgdsb.2*, *rbp4*, and *bhmt*, were silenced after amputation, while others, including *fn1b*, *vmp1*, *palld*, and *dlx5a* were induced in both cell types (**Fig. 4.14A**). I then cross-referenced these genes to our RNA-seq data from the mutant and wild type fins. The genes that are silenced in the wild types after injury were maintained at higher levels in the mutants when compared with wild types at 24 hpa. On the contrary, the genes that are induced upon injury in the wild types were not induced in the mutants (**Fig. 4.14B**). These data indicate that regenerative reprogramming at the transcriptomic level is impaired in the mutants. However, a thorough single-cell analysis of the mutant fins is needed to investigate this process better.

In addition, I have also observed that *il11ra* mutant fins display an impaired induction of the prominent fin regeneration genes, including *no blastema* (*nbl/hspd1*) and *devoid of blastema* (*dob/fgf20a*) (**Fig. 4.14B**) (Makino et al., 2005; Whitehead et al., 2005). These data led me to investigate whether Il-11 signaling regulates the evolutionarily conserved regeneration gene program. Out of the 49 regeneration program genes, 27 were not induced, while only 2 were upregulated in the mutant fins when compared with wild types at 24 hpa (**Fig. 4.15A and B; Appendix III**). Furthermore, several transcription factor genes that induce osteoblast formation during development (immature osteoblast markers), which are induced after injury, indicating osteoblast dedifferentiation, were not induced in the mutants. These data led me to suspect if osteoblast dedifferentiation is affected in the mutants. *Osteocalcin* (*bglap*) is a well-known mature osteoblast marker that has been reported to get downregulated during regeneration using the *Tg(bglap:GFP)* reporter line (Knopf et al., 2011). I employed

this reporter to study osteoblast dedifferentiation in the mutants. As reported earlier (Knopf et al., 2011), I have observed that the osteoblasts proximal to the amputation plane in wild types downregulated *bglap:*GFP, indicating dedifferentiation (**Fig. 4.15C and D**). In contrast, the mutant osteoblasts failed to downregulate *bglap:*GFP, indicating that Il-11 signaling is required for osteoblast dedifferentiation.

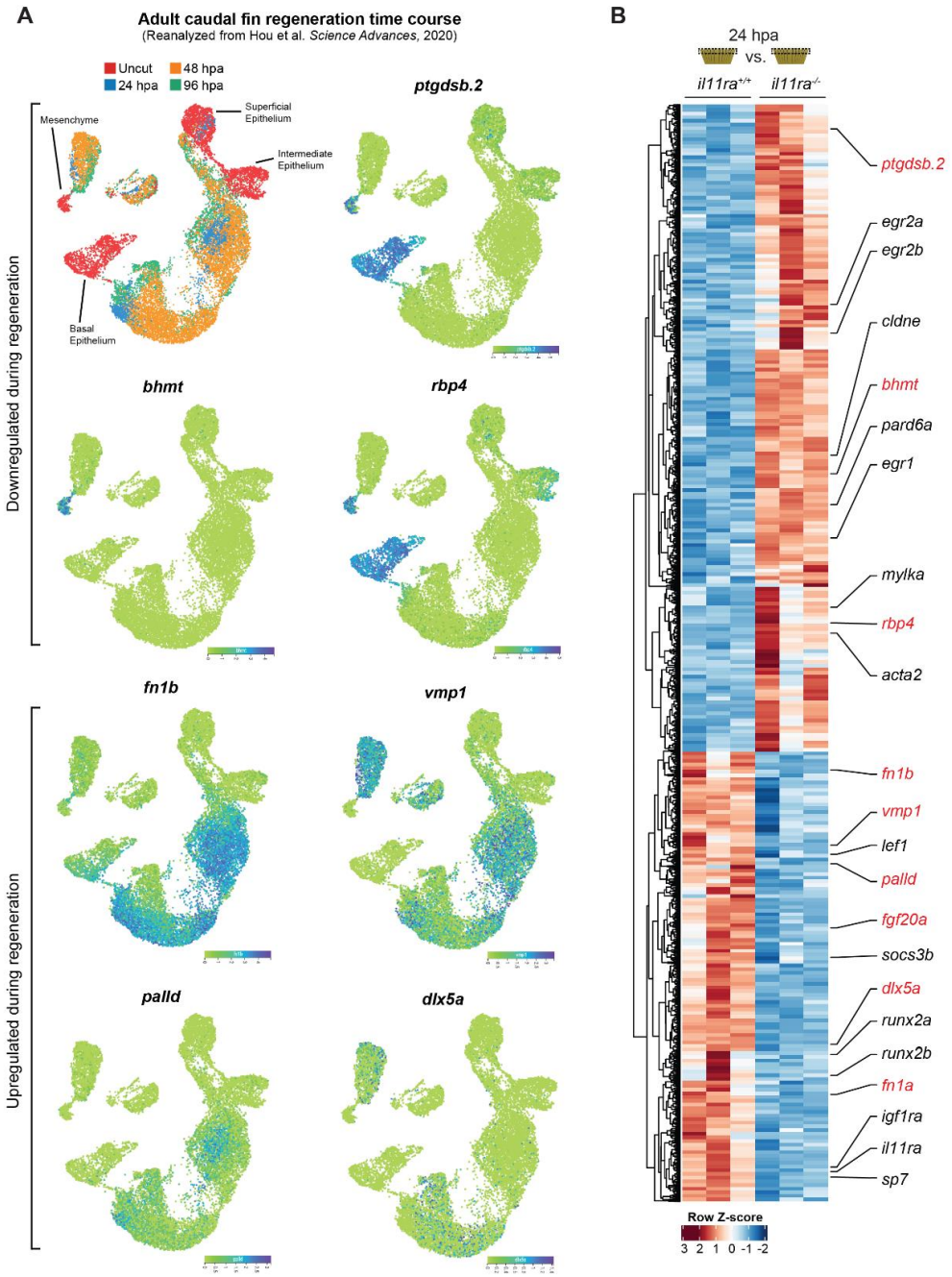

Figure 4.14. Il-11 signaling is required for reprogramming of regeneration gene expression in the adult caudal fin after amputation. (**A**) Expression patterns of selected

genes from single-cell RNA-seq (reanalyzed from (Hou et al., 2020)) that are specifically upregulated (*fn1b, vmp1, palld, dlx5a*) and downregulated (*rbp4, ptgdsb.2, bhmt*) during adult caudal fin regeneration that are dysregulated in *il11ra* mutants at 24 hpa. (**B**) Differential expression of zebrafish adult caudal fin regeneration genes in *il11ra*$^{-/-}$ vs. wild-type sibling adult caudal fin transcriptomic analysis, 24 hpa. Adapted from (Allanki et al., 2021). License: CC BY 4.0.

Furthermore, it was also reported that the osteoblasts proximal to the amputation plane migrate past the amputation to seed the nascent blastema (Sousa et al., 2011). I have observed that the mutant osteoblasts failed to cross the amputation plane, unlike the wild types' (**Fig. 4.15C and E**). Since osteoblast dedifferentiation and migration happen simultaneously, further cell-specific analysis is required to decouple both the processes and understand the primary vs. secondary effects of Il-11 signaling. These data show that Il-11 signaling is required for regenerative reprogramming during adult caudal fin regeneration.

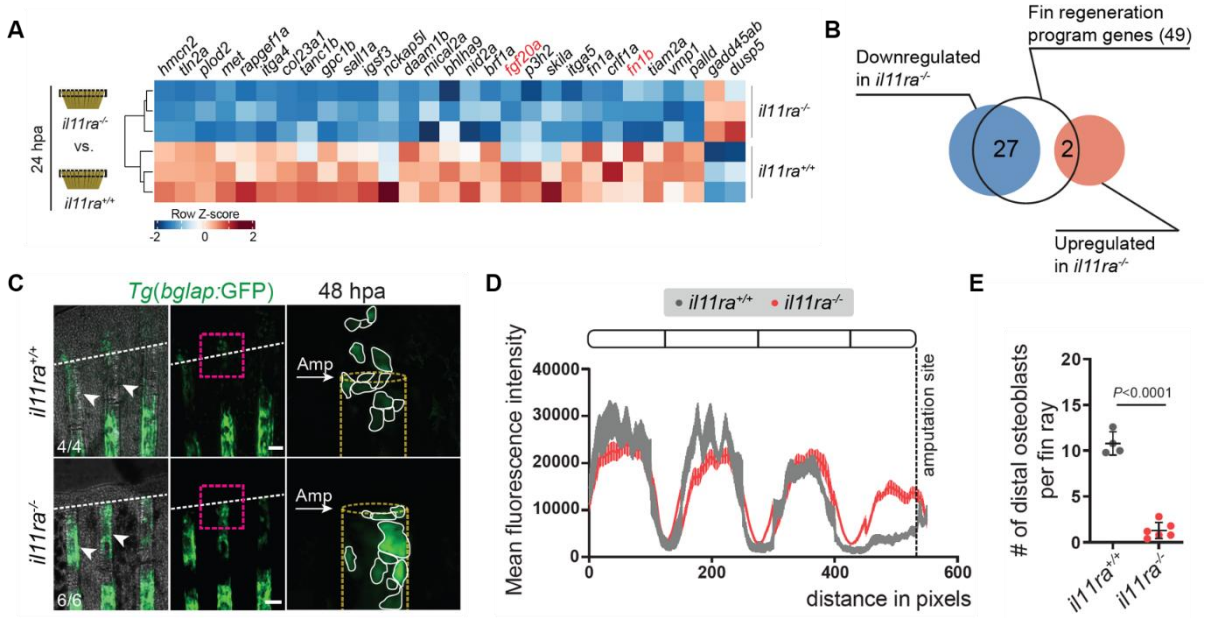

Figure 4.15. Il-11 signaling regulates evolutionarily conserved fin regeneration program, as well as osteoblast dedifferentiation and migration. (**A and B**) Differential expression of fin regeneration genes (Wang et al., 2020) in *il11ra*$^{-/-}$ vs. wild-type sibling caudal fin transcriptomic analysis, 24 hpa. (**C to E**) Confocal images of *Tg(bglap:GFP)* expression in wholemount caudal fins (C) (wt siblings, n = 4; mut, n = 6; 48 hpa), quantification of *Tg(bglap:GFP)* fluorescence intensity (D), and the number of distal osteoblasts (E). Data

represent means ± SD (E); means ± SEM (D). Student's t tests (E). n, caudal fins (C). White arrows point to and white dashed lines demarcate the amputation plane (C); white arrowheads point to *Tg(bglap:GFP)* expression (C); yellow dashed lines demarcate the bone rays (C). Scale bars, 100 μm (C). Adapted from (Allanki et al., 2021). License: CC BY 4.0. Certain legends are quoted *verbatim* from Allanki et al., *Sci. Adv*. 7, eabg6497 (2021) for precise explanation.

4.4.1.2. Regenerative reprogramming during larval fin fold regeneration

During larval fin fold regeneration, several genes have been shown to be induced as a part of the regenerative reprogramming. To investigate if Il11ra/Stat3 signaling regulates these gene expression changes, I have performed RT-qPCR on both the non-regenerative *il11ra* and *stat3* mutants after fin fold amputation. Regeneration genes (Yoshinari et al., 2009), including *fn1b*, *mmp9*, *mvp*, *junba*, and *junbb* are consistently not induced in both the mutants when compared with their respective wild-type siblings (**Fig. 4.16**). These data show that Il11ra/Stat3 signaling regulates regenerative reprogramming during larval fin fold regeneration.

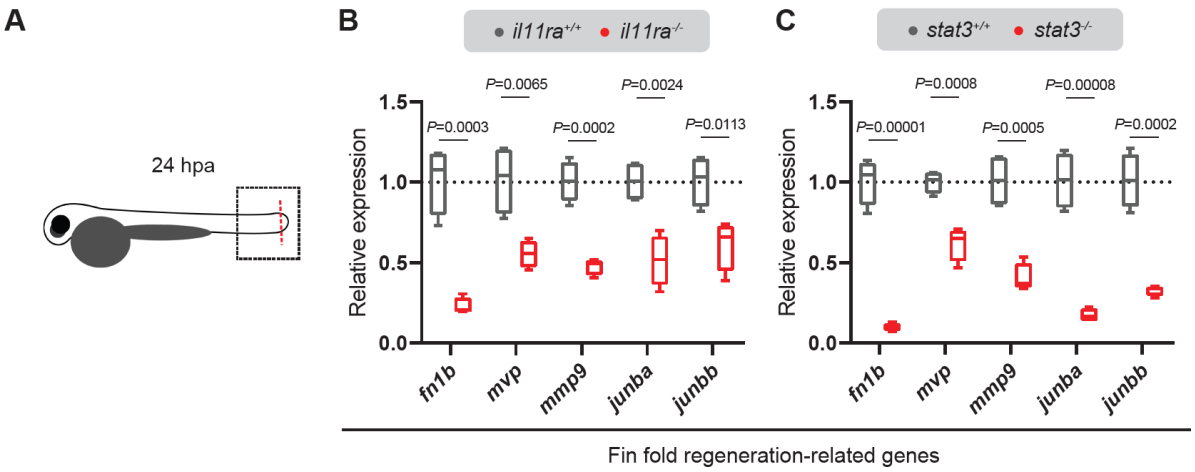

Figure 4.16. Comparable deficiency in regeneration gene activation between *il11ra* and *stat3* mutants during larval fin fold regeneration. (**A to C**) Schematic (A) and RT-qPCR analysis on *il11ra*^{bns251} (B, wt siblings, n=4; mut, n=4; 24 hpa) and *stat*^{stl27} (C, wt siblings, n=4; mut, n=4; 24 hpa) for selected fin fold regeneration genes (Yoshinari et al., 2009). Box plots (B, C) show median, interquartile range (IQR, box margins) and 5th and 95th percentiles (whiskers). Student's t-tests (B, C). n= pools of 20 larval tails (B, C). Black dashed box

demarcates dissected tissue processed for RT-qPCR (A); red dashed line demarcates amputation plane (A). Adapted from (Allanki et al., 2021). License: CC BY 4.0.

4.4.1.3. Regenerative reprogramming during adult heart regeneration

Similar to fin regeneration, several genes have been shown to be modulated in both directions during adult heart regeneration, indicating regenerative reprogramming. I performed literature survey and gathered all the pro-regenerative genes that have been reported until recently (González- Rosa et al., 2017). I then cross-referenced these genes with our RNA-seq data (mutant vs. wild-type adult ventricles at 96 hpci). I have observed that majority of these known regulators of heart regeneration are downregulated in the mutant ventricles, including the genes encoding retinoic acid synthesizing enzyme (*aldh1a2*) (Kikuchi et al., 2011b), Wilm's tumour (*wt1b*) (Sanz-Morejón et al., 2019), components of the complement system (Natarajan et al., 2018), Hedgehog pathway (Choi et al., 2013), and Notch signaling (Münch et al., 2017) (**Fig. 4.17**). On the other hand, genes detrimental for regeneration, including *mstnb*, *cilp*, *meox1*, and *fap* are not downregulated in the mutants when compared with wild types (**Fig. 4.17**) (Aghajanian et al., 2019; Alexanian et al., 2021; Dogra et al., 2017).

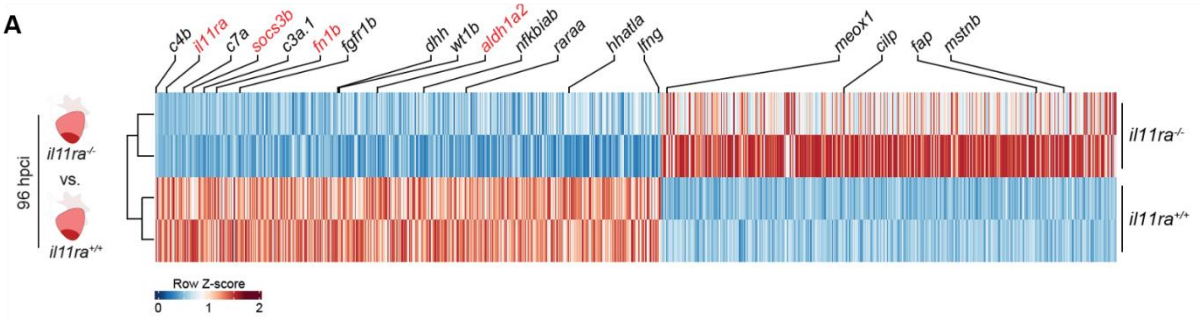

Figure 4.17. Il-11 signaling mediated regenerative reprogramming after cardiac injury. (**A**) Differential expression of known regulators of zebrafish cardiac regeneration (González-Rosa et al., 2017) in *il11ra*$^{-/-}$ vs. wild-type sibling ventricle transcriptomic analysis, 96 hpci. Adapted from (Allanki et al., 2021). License: CC BY 4.0.

Gene ontology analysis on the RNA-seq from the heart indeed revealed that the mutants display severe reduction in retinoic acid signaling (**Fig. 4.18A**). I then performed RT-qPCR and found that *aldh1a2* is not induced in the mutant ventricles as early as 24 hpci (**Fig. 4.18B**). Retinoic acid synthesizing enzyme Aldh1a2 has been

reported to be activated upon various kinds of cardiac injuries, in an evolutionarily conserved manner (Kikuchi et al., 2011b). Blocking RA signaling severely impaired cardiomyocyte proliferation in the zebrafish heart after ventricular resection. It was reported that primarily the injury-activated endocardial cells, as well as epicardial and epicardial-derived cells induce Aldh1a2 expression. Using immunohistological analysis for the expression patterns of Aldh1a2, I have identified that, in the mutants, endocardial-specific Aldh1a2 is significantly silenced, while the epicardial signal was not affected (**Fig. 4.18C**). These data indicate that Il-11 signaling plays an important role in the endocardial cells after cardiac injury to promote cardiomyocyte regeneration (proliferation and migration).

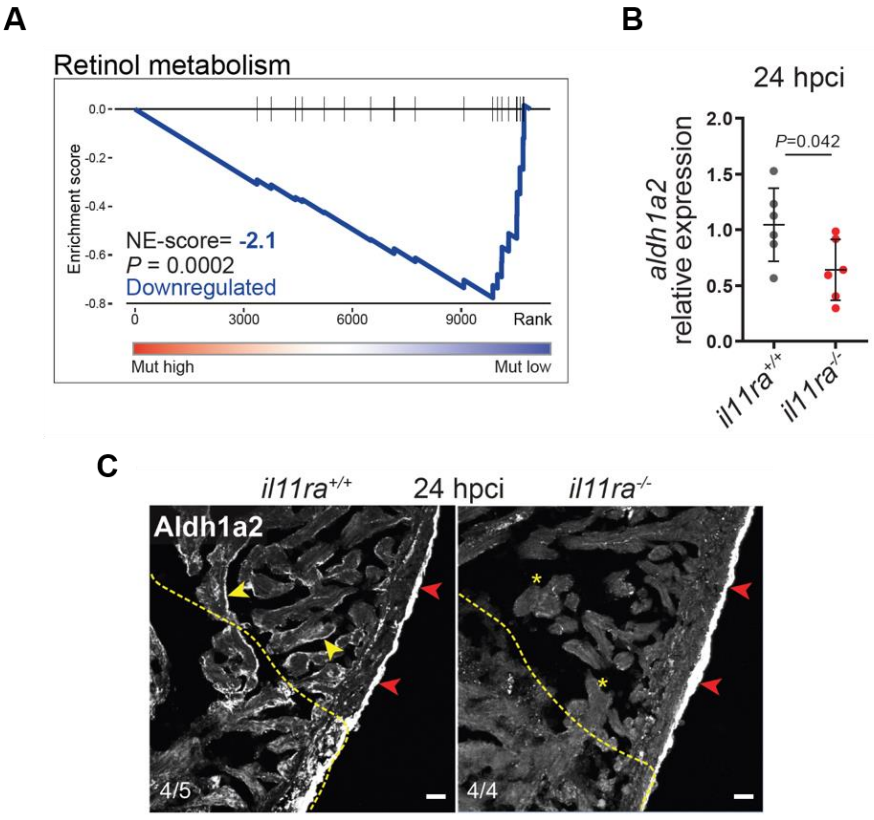

Figure 4.18. Il-11 signaling is required for endocardial RA activation. (**A**) GSE analysis plot of KEGG Retinol metabolism from *il11ra*$^{-/-}$ vs. wild-type sibling ventricle transcriptomic analysis, 96 hpci. NE score, normalized enrichment score. (**B and C**) RT-qPCR analysis of *aldh1a2* mRNA levels (B) (wt siblings, n = 6; mut, n = 6; 24 hpci) and immunostaining for Aldh1a2 expression on cardiac ventricle cryosections (C) (wt siblings, n = 5; mut, n = 4; 24 hpci). Data represent means ± SD (B). Student's t tests (B). n, ventricles (B and C). Yellow dashed lines demarcate the injured area (C); yellow arrowheads and asterisks indicate

endocardial Aldh1a2 expression (C); red arrowheads point to epicardial Aldh1a2 expression (C). Scale bars, 20 μm (C). Adapted from (Allanki et al., 2021). License: CC BY 4.0. Certain legends are quoted *verbatim* from Allanki et al., *Sci. Adv*. 7, eabg6497 (2021) for precise explanation.

During regeneration, Fibronectin is deposited in the injured area in an evolutionarily conserved manner (Calve et al., 2010; Govindan and Iovine, 2015; Li et al., 2020; Wang et al., 2013). Notably, from my analyses in the adult heart, adult fin, and larval fin fold, I have observed a consistent reduction of Fibronectin encoding gene expression (*fn1b*) in the *il11ra* mutants (**Fig. 4.19A, and Fig. 4.16B**). Furthermore, immunostaining for Fn1 confirmed reduced deposition in the mutant cardiac lesions (**Fig. 4.19B**). Blocking Fibronectin function using dominant negative approaches and genetic loss-of-function mutants impaired heart regeneration in zebrafish (Wang et al., 2013). Specifically, blocking Fibronectin function affected cardiomyocyte migration, but not proliferation. These data show a pro-migratory role for Fibronectin in promoting cardiomyocyte regeneration.

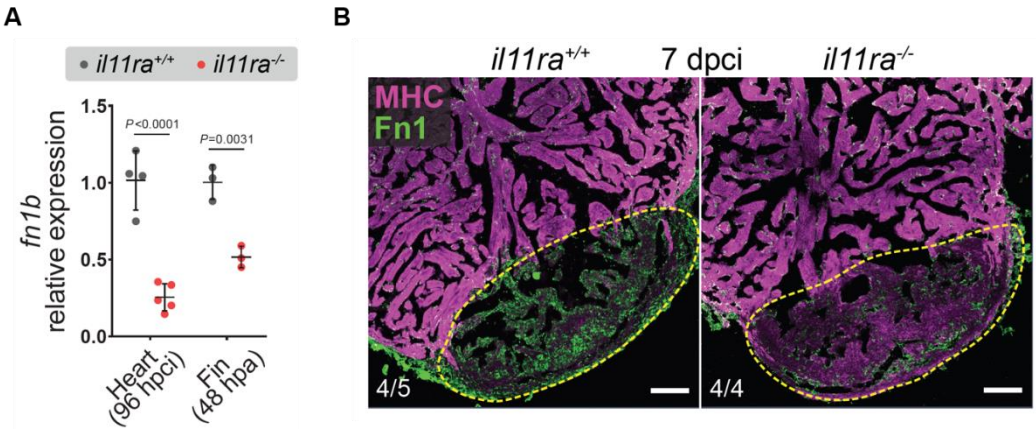

Figure 4.19. Il-11 signaling is required for the formation of a regenerative niche. (**A and B**) RT-qPCR analysis of *fn1b* mRNA levels on dissected injured areas from cardiac ventricles (A) (wt siblings, n = 4; mut, n = 5; 96 hpci) and caudal fins (A) (wt siblings, n = 3; mut, n = 3; 48 hpa) and immunostaining on cryosections (B) (wt siblings, n = 5; mut, n = 4; 7 dpci) for Fibronectin1 (green) and myosin heavy chain (MHC; magenta) expression. Data represent means ± SD (A). Student's t tests (A). n, ventricles [(A) heart, and B]; n, caudal fins [(A) fin]. Yellow dashed lines demarcate the injured area (B). Scale bars, 100 μm (B). Adapted from (Allanki et al., 2021). License: CC BY 4.0. Certain legends are quoted *verbatim* from Allanki et al., *Sci. Adv*. 7, eabg6497 (2021) for precise explanation.

4.4.2. Il-11 signaling promotes cell repopulation during regeneration

Since blocking Fibronectin function or RA signaling affected cardiomyocyte regeneration, and *il11ra* mutants display permanent scarring at 90 dpci, we hypothesized that cardiomyocyte behaviour is affected in *il11ra* mutants. Hence, I investigated cardiomyocyte behaviour in terms of proliferation and protrusion of the injured area.

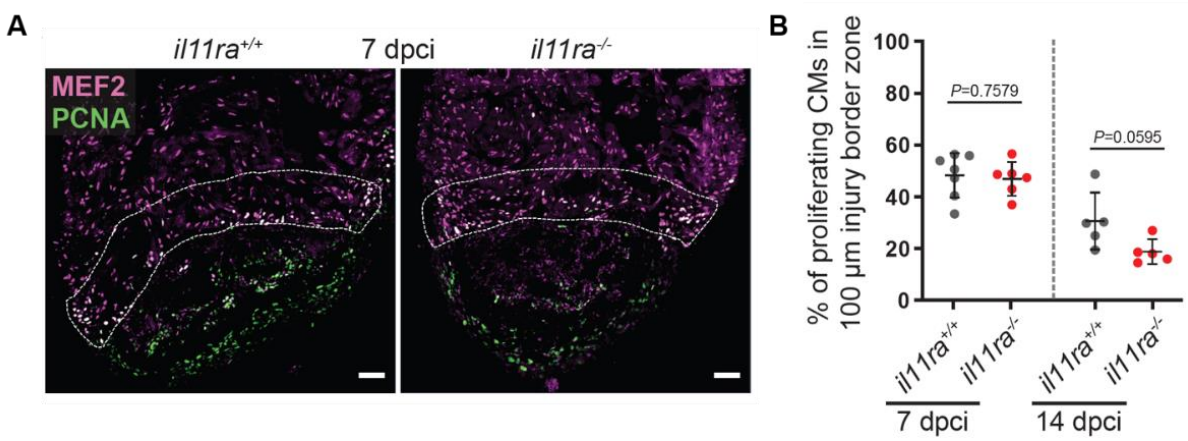

Figure 4.20. Cardiomyocyte proliferation in *il11ra* mutants. (**A and B**) Co-staining for MEF2 (magenta) and PCNA (green) expression to determine CM mitotic index on cryosections from ventricles (A) (wt siblings, n = 7; mut, n = 6; 7 dpci) and quantification within the 100-µm wound border zone for 7 and 14 dpci (B). Data represent means ± SD (B). Student's t tests (B). n, ventricles (A). White dashed lines demarcate 100-µm injury border zone (A). Scale bars, 50 µm (A). Adapted from (Allanki et al., 2021). License: CC BY 4.0. Certain legends are quoted *verbatim* from Allanki et al., *Sci. Adv*. 7, eabg6497 (2021) for precise explanation.

First, I quantified cardiomyocyte proliferation at 7 and 14 dpci, where it reaches a peak during regeneration. Surprisingly, cardiomyocyte proliferation is not affected at 7 dpci, but is only mildly reduced at 14 dpci (**Fig. 4.20**). These data suggest that the reduction in cardiomyocyte proliferation at 14 dpci in the mutants is a secondary phenotype downstream of Il-11 signaling. I then assayed for cardiomyocyte migration in terms of the number and length of protrusions extended by trabecular cardiomyocytes into the injured area. I observed that number of protrusions is reduced from 7 dpci onwards, but the length of protrusions is consistently reduced from 72 hpci to 14 dpci (**Fig. 4.21**).

I then used the *Tg(gata4:EGFP)* line that predominantly marks cortical layer of regenerating cardiomyocytes (Beisaw et al., 2020; Marín-Juez et al., 2019). Although *gata4:*EGFP^{+} cardiomyocyte protrusions were not affected at 7 dpci in the mutants, I observed a drastic reduction at 14 dpci when compared with the wild-type protrusions that envelope the periphery of the injured area (**Fig. 4.22A and B**). In line with these wholemount data, quantifying the cortical cardiomyocyte coverage on tissue sections confirmed a severe reduction in protrusive activity of cardiomyocytes in the mutants at 14 dpci (**Fig. 4.22C and D**).

Altogether, these data show that Il-11 signaling promotes regenerative reprogramming and cell repopulation in a tissue-specific and global manner during regeneration in zebrafish.

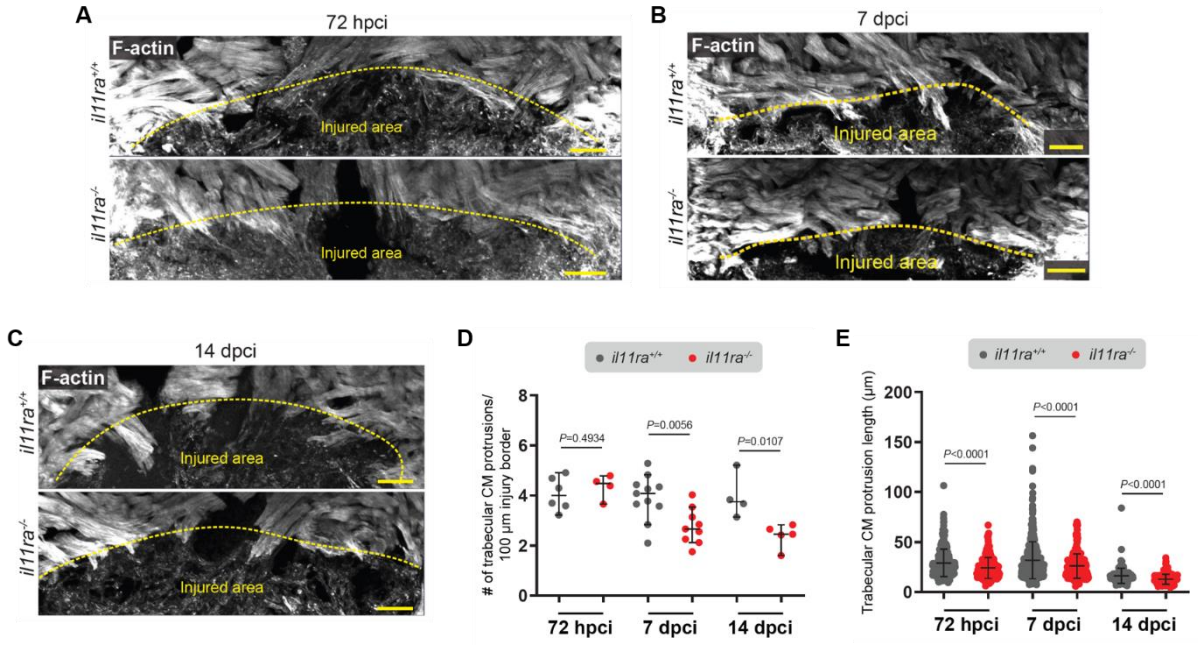

Figure 4.21. Trabecular cardiomyocyte protrusion in *il11ra* mutants after injury. (**A to E**) F-actin staining on 50 µm thick cryosections from *il11ra*$^{-/-}$ vs. wild-type sibling ventricles, 72 hpci (A), 7 dpci (B), 14 dpci (C), and quantification of the number per ventricle (D, 72 hpci, wt, n=6; mut, n=4; 7 dpci, wt siblings, n=11; mut, n=9; 14 dpci, wt siblings, n=4; mut, n=5), and length (E, 72 hpci, wt, n=357; mut, n=239; 7 dpci, wt, n=540; mut, n=281; 14 dpci, wt, n=148; mut, n=141) of CM protrusions. Data represent mean ± S.D. (D) and mean ± S.E.M. (E). Student's t-tests (D); Mann-Whitney U tests (E). n= ventricles (D); n= CM protrusions (E).

Yellow dashed lines demarcate the injured area (A, B, C). Scale bars, 50 µm (A, B, C). Adapted from (Allanki et al., 2021). License: CC BY 4.0.

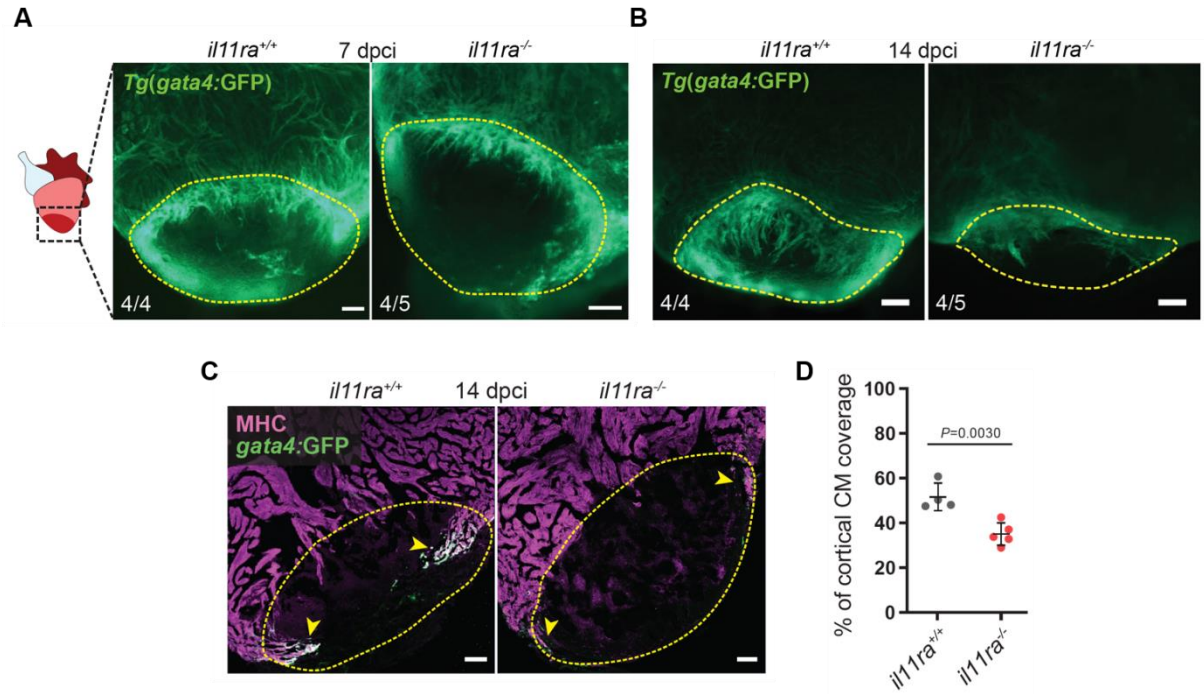

Figure 4.22. Cortical cardiomyocyte protrusion in *il11ra* mutants after injury. (**A and B**) Wholemount fluorescence images of *Tg(gata4:*EGFP*)* expression in ventricles [(A), wt siblings, n=4; mut, n=5, 7 dpci; (B), wt siblings, n=4; mut, n=5, 14 dpci). (**C and D**) Immunostaining (GFP – green, MHC – magenta) on cryosections from *Tg(gata4:EGFP)* ventricles (C) and quantification of cortical cardiomyocyte coverage (D, wt siblings, n=4; mut, n=5; 14 dpci) corresponding to B. Data represent mean ± S.D. (D). Student's t-tests (D). n= ventricles (A, B, C, D). Yellow dashed lines demarcate the injured area (A, B, C); arrowheads point to protruding *Tg(gata4:*GFP*)*$^{+}$ MHC^{+} cortical CMs (C). Scale bars, 50 µm (C), 100 µm (A, B). Adapted from (Allanki et al., 2021). License: CC BY 4.0.

4.5 Il-11/Stat3 signaling limits mammalian-like scarring response during regeneration

Previous mammalian studies proposed a pro-regenerative and anti-fibrotic role for IL-11/STAT3 signaling (Cook and Schafer, 2020). However, many recent studies revisited IL-11 signaling and fibrosis, and provide evidence showing its pro-fibrotic role (Ng et al., 2019; Schafer et al., 2017). In view of these contradicting data, and the non-

regenerative phenotype of the *il11ra* mutants, I were curious to identify the role of Il-11 signaling in the context of zebrafish regeneration.

4.5.1. Il-11 signaling limits myofibroblast and matrifibrocyte differentiation

The recent mammalian studies show that treating human cardiac fibroblasts with IL-11 induces ectopic myofibroblast differentiation (Schafer et al., 2017). To test this effect in the context of regeneration, I quantified myofibroblast differentiation using immunostaining against αSMA at several time points and tissues in *il11ra* mutants and compared with their wild-type siblings. At 7 dpci, I observed a significant increase in myofibroblasts in the mutant ventricles when compared with the wild types (**Fig. 4.23A**). As I have shown earlier, the mammalian hearts display nearly 10-fold increase in myofibroblast differentiation when compared with zebrafish at 7 days post cardiac injury. In addition, in mammals, these myofibroblasts reside in the injured area, differentiate further into matrifibrocytes, and maintain the mature scar. To test if the permanent scarring *il11ra* mutant ventricles also maintain these cells, I performed αSMA staining at 90 dpci. While I rarely observed any myofibroblasts in the regenerating wild-type scars, the mutants displayed a significantly increased myofibroblast density in the injured area (**Fig. 4.23C**).

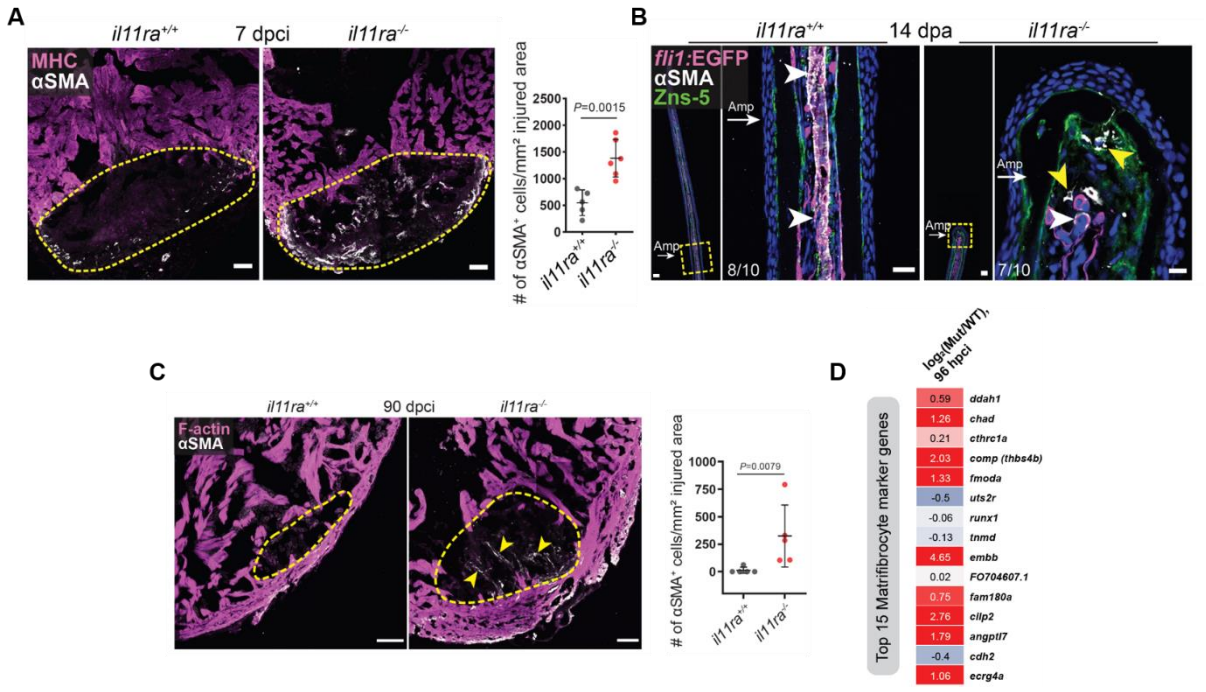

Figure 4.23. Myofibroblast differentiation in *il11ra* mutants after injury. (**A**) Immunostaining for αSMA (white) and MHC (magenta) expression on cryosections from cardiac ventricles (wt siblings, n = 5; mut, n = 6; 7 dpci), and quantification of $αSMA^+$ cell density. (**B**) Immunostaining for αSMA (white), GFP (magenta), and Zns-5 antigen (scleroblasts, green) expression on longitudinal cryosections from *Tg(fli1:EGFP)* caudal fins (wt, n = 10; mut, n = 10; 14 dpa). (**C**) Immunostaining (αSMA – white) and F-actin (magenta) staining on cryosections from ventricles (wt siblings, n=5; mut, n=5; 90 dpci) and quantification of $αSMA^+$ cells in the scar tissue. (**D**) Expression of top 15 matrifibrocyte genes (reanalyzed from (Fu et al., 2018)) in *il11ra*$^{-/-}$ vs. wild-type sibling ventricle transcriptomic profiles, 96 hpci. Data represent means ± SD (A, C). Student's t tests (A, C). n, ventricles (A, C); n, caudal fins (B). Yellow dashed lines demarcate the injured area (A, C); yellow arrowheads point to $αSMA^+$ myofibroblasts in *il11ra* mutant fins (B); white arrowheads point to vessel-associated $αSMA^+$ smooth muscle cells (B). Scale bars, 50 μm (A, B, C). Adapted from (Allanki et al., 2021). License: CC BY 4.0. Certain legends are quoted *verbatim* from Allanki et al., *Sci. Adv*. 7, eabg6497 (2021) for precise explanation.

Furthermore, I cross-referenced the previously established matrifibrocyte marker genes with the mutant RNA-seq data (Fu et al., 2018). I found that most of the top 15 matrifibrocyte markers were enriched in the mutant ventricles when compared to the wild types (**Fig. 4.23D**). Finally, I also tested the fins for myofibroblast differentiation. While the wild-type fin regenerates were devoid of myofibroblasts, the non-regenerative mutant stumps displayed an increased density of myofibroblasts at 14 dpa (**Fig. 4.23B**).

4.5.2. Pro-fibrotic extracellular matrix remodeling

Next, I tested if the mutant hearts and fins display pro-fibrotic tissue remodeling. Gene ontology analysis on the RNA-seq data at 96 hpci showed a clear downregulation of Jak-Stat activation, as a positive control for the dataset (**Fig. 4.24A**). We also observed that GO terms, including ECM organization and elastic fiber formation were upregulated in the mutant ventricles, indicating an increased ECM deposition (**Fig. 4.24A**). In addition, we also observed a significant activation of TGF-β pathway, the master regulator of tissue fibrosis (**Fig. 4.24A**) (Frangogiannis, 2020).

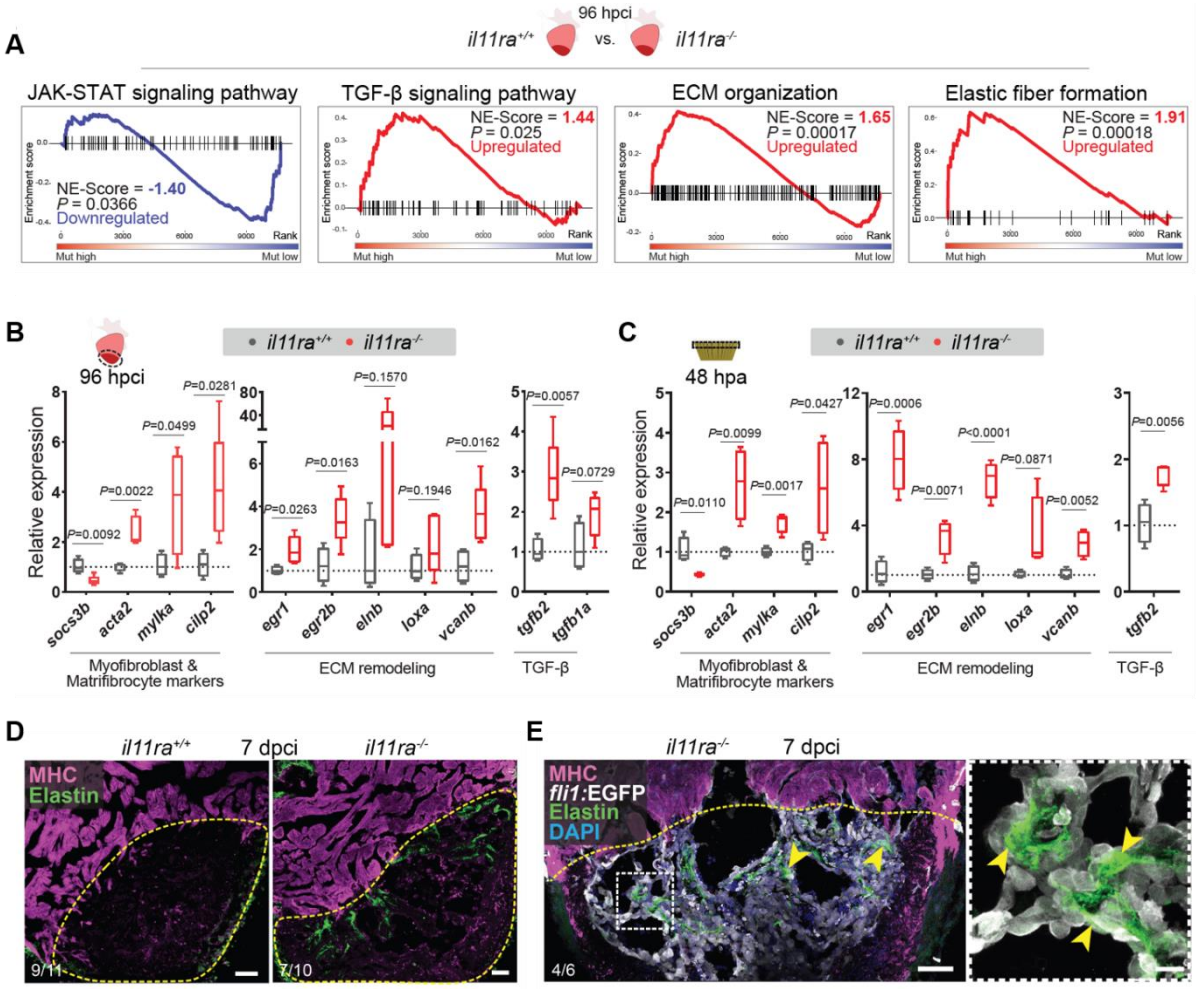

Figure 4.24. Pro-fibrotic ECM remodeling in *il11ra* mutants after injury. (**A**) GSE analysis plots for Reactome and KEGG pathway terms from *il11ra*$^{-/-}$ vs. wild-type sibling adult ventricle transcriptomic analyses, 96 hpci. (**B and C**) RT-qPCR analysis on dissected injured areas from cardiac ventricles (B) (wt siblings, n = 4; mut, n = 5; 96 hpci) and caudal fins (C) (wt siblings, n = 4; mut, n = 4; 48 hpa) for selected profibrotic gene expression levels. (**D and E**) Immunostaining [(D) Elastin, green; MHC, magenta; (E) GFP, white] on cryosections from cardiac ventricles [(D) wt siblings, n = 11; mut, n = 10; (E) *Tg(fli1:EGFP)*; mut, n = 6; 7 dpci]. Box plots (C and D) show median, interquartile range (IQR; box margins), and 5th and 95th percentiles (whiskers). Student's t tests (C and D). n, ventricles (B, D, E); n, pools of two caudal fins (C). Yellow dashed lines demarcate the injured area (D, E); yellow arrowheads point to Elastin1 expression associated with endocardial cells in the injured area [inset in (E)]. Scale bars, 50 μm (D, E), 10 μm (E inset). Adapted from (Allanki et al., 2021). License: CC BY 4.0. Certain legends are quoted *verbatim* from Allanki et al., *Sci. Adv*. 7, eabg6497 (2021) for precise explanation.

RT-qPCR analysis on the hearts and fins showed a consistent increase in several myofibroblast and matrifibrocyte marker genes (*acta2, mylka,* and *cilp2*), ECM remodeling transcription factors (*egr1* and *egr2b*) and molecules (*elnb*, *vcanb*, and *loxa*), as well as TGF-β ligands (*tgfb1a, tgfb2*) (**Fig. 4.24B and C**). Of note, the EGR transcription factors have been shown to directly regulate collagen encoding gene expression downstream of TGF-β signaling, and the LOX enzymes crosslink collagen fibrils during scarring (Fang et al., 2011). Furthermore, together with the *elnb* gene expression, immunostaining for Elastin1 showed an excessive deposition in the mutant lesions when compared to the wild types (**Fig. 4.24D**). Taking a closer look at the mutant ventricles, I have also identified that the excessive Elastin1 is deposited adjacent to the endocardial cells inside the injured region (**Fig. 4.24E**). These data show that Il-11 signaling limits pro-fibrotic ECM remodeling after tissue damage in zebrafish. Furthermore, after injury, I observed that the *stat3* heterozygotes displayed pro-fibrotic remodeling similar to the *il11ra* mutants, suggesting that the anti-fibrotic effects of Il-11 signaling at least in part go through the Stat3 pathway (**Fig. 4.25**).

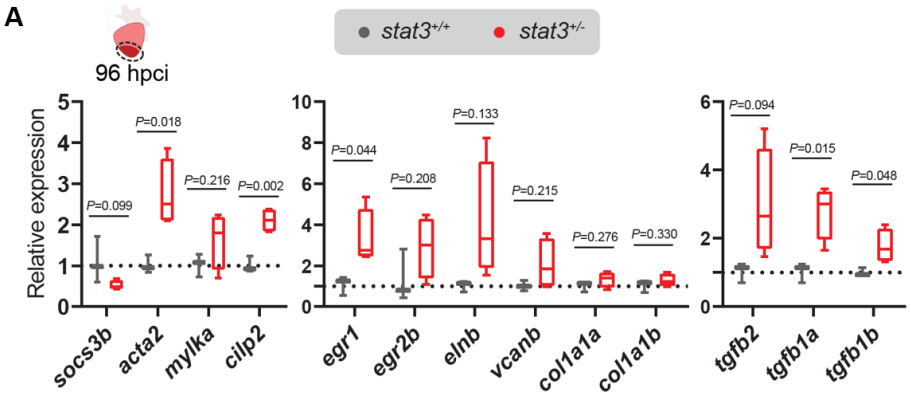

Figure 4.25. Pro-fibrotic remodeling in stat3 heterozygotes after cardiac injury. (**A**) RT-qPCR analysis on dissected injured areas of heterozygous *stat3*^{stl27} (n=4) vs. wild-type sibling (n=3) ventricles for selected fibrosis-associated genes, 96 hpci. Adapted from (Allanki et al., 2021). License: CC BY 4.0.

4.5.3. Unbiased comparison of the *il11ra* mutant fibrosis with mammalian scarring

In light of these data showing mammalian features of scarring response in *il11ra* mutants, I investigated this phenotype on a whole transcriptome level. I compared our

zebrafish RNA-seq data with that of the reanalysed neonatal and adult mouse MI (Quaife-Ryan Gregory A. et al., 2017). Several fibrosis related gene ontology terms, including epithelial-to-mesenchymal transition (EMT) and collagen biosynthesis and modifying enzymes, were significantly upregulated both in the non-regenerative adult mouse hearts and *il11ra* mutants, but not in the regenerative neonatal hearts (**Fig. 4.26**).

Altogether, these data strongly indicate that Il-11/Stat3 signaling limits mammalian-like scarring program during regeneration in zebrafish.

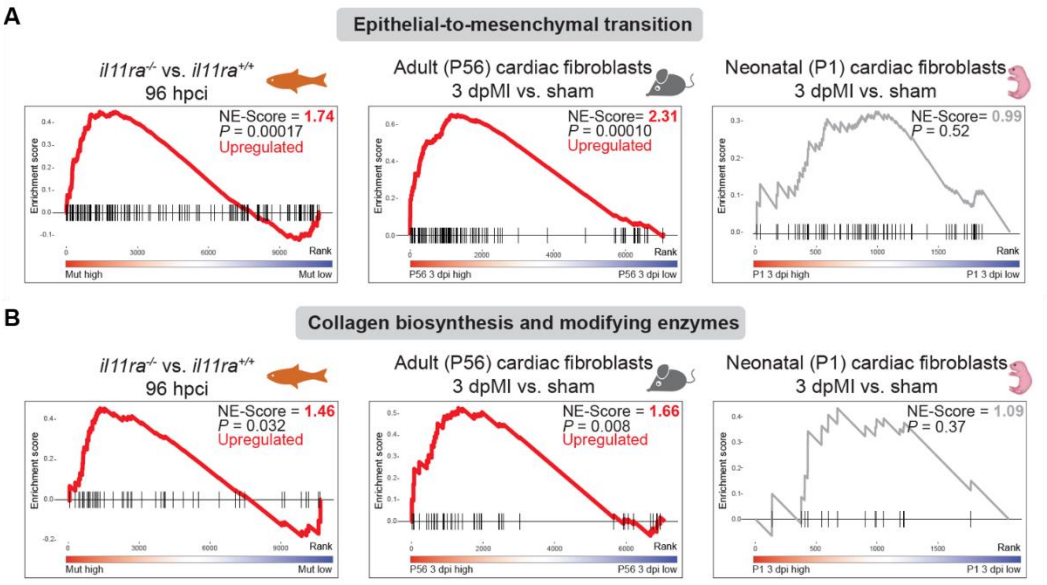

Figure 4.26. *il11ra* mutants display mammalian-like fibrosis. (**A and B**) GSE analysis plots comparing fibrosis-associated ontology terms between *il11ra*$^{-/-}$ vs. wild-type sibling ventricle transcriptomic profiles (96 hpci) and myocardial infarction (MI) vs. sham from adult (P56) and neonatal (P1) cardiac fibroblast transcriptomic profiles, 3 days post MI (dpMI) (reanalyzed from (Quaife-Ryan Gregory A. et al., 2017)). Adapted from (Allanki et al., 2021). License: CC BY 4.0.

4.6. Cellular mechanisms of the *il11ra* mutant fibrosis

To identify the cellular mechanisms downstream of Il-11 signaling, I asked – what are the effector cell types of Il-11 signaling during cardiac regeneration?

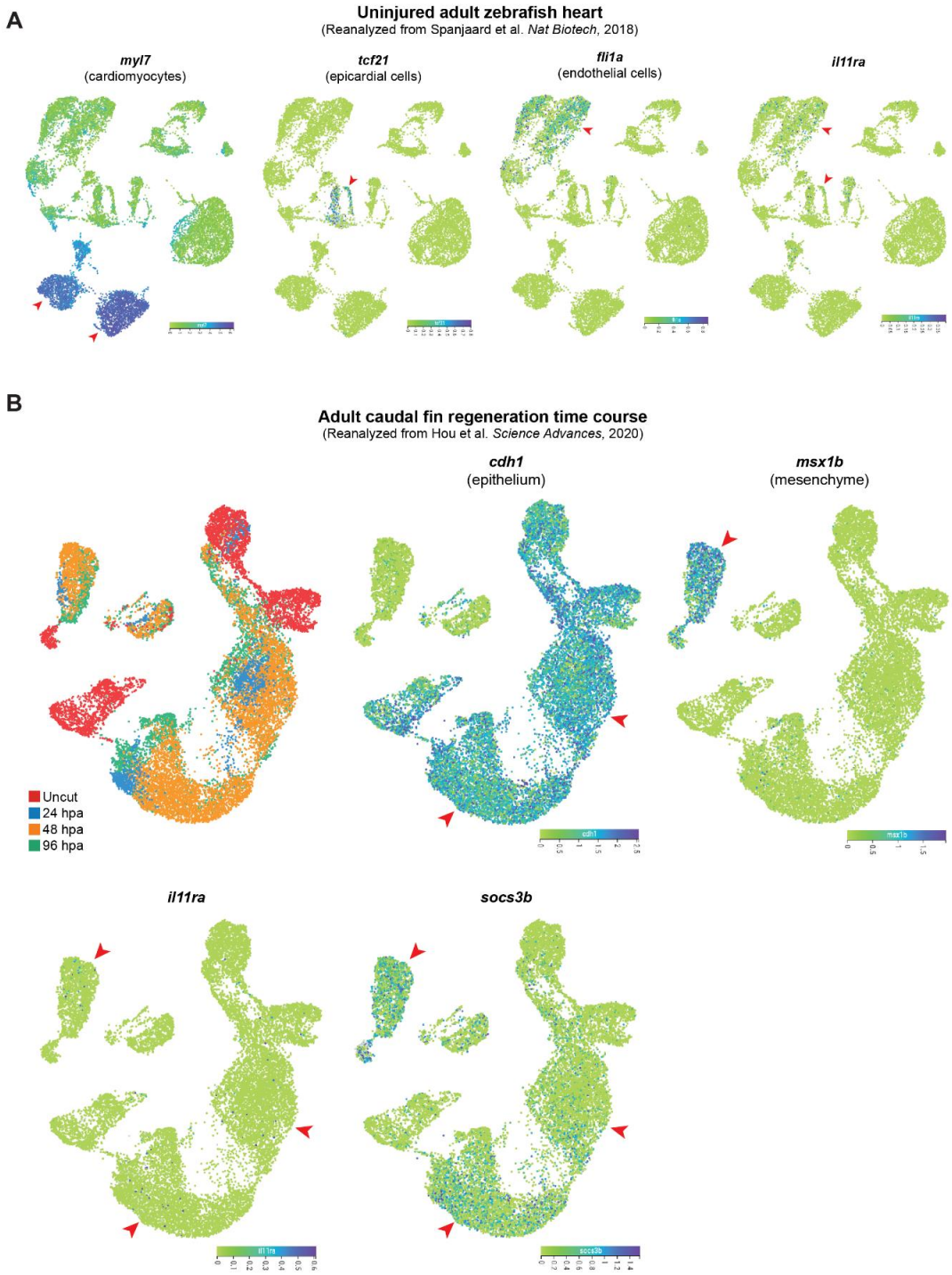

Figure 4.27. Il-11/Stat3 pathway gene expression patterns at the single-cell level in the uninjured heart and during caudal fin regeneration in adult zebrafish. (**A**) Expression patterns of selected cell population marker genes and *il11ra* in single-cell RNA-seq data from uninjured adult zebrafish hearts (reanalyzed from (Spanjaard et al., 2018)). (**B**) Expression patterns of selected cell population marker genes, *il11ra*, and *socs3b* in single-cell RNA-seq data from regenerating adult zebrafish caudal fins (reanalyzed from (Hou et al.,

2020)). Red arrowheads point to respective cell clusters (A, B). Adapted from (Allanki et al., 2021). License: CC BY 4.0.

4.6.1. *il11ra* is expressed in endothelial and epicardial lineages

I reasoned that the cells that express *il11ra* are likely responding to injury-induced Il-11 molecules. Hence, I investigated the expression patterns of *il11ra* by using the previously published single-cell RNA-seq datasets of the adult zebrafish heart and the regenerating zebrafish caudal fins (Hou et al., 2020; Spanjaard et al., 2018). Similar to its mammalian orthologue, *il11ra* is mainly expressed in mesenchymal and epithelial lineages, including the cardiac endothelium and epicardium/fibroblasts (**Fig. 4.27**). To confirm this experimentally, I performed RT-qPCRs for *il11ra* expression in sorted cardiac endothelial cells. In line with the single-cell RNA-seq data (**Fig. 4.27A**), I observed that *il11ra* is highly expressed in cardiac endothelial cells when compared to non-endothelial cells in the uninjured ventricles (**Fig. 4.28A**). In addition, *socs3b*, a Stat3 downstream signaling molecule, is also enriched in cardiac endothelial cells when compared with non-endothelial cells at 96 hpci, indicating that Stat3 signaling is activated in the cardiac endothelium during regeneration (**Fig. 4.28A**). To further analyse Il-11 dependent Stat3 activation in endocardial cells, I performed immunostaining for p-Stat3 on *il11ra* mutants after injury. I observed a robust activation of p-Stat3 in endocardial cells inside the injured area in wild types, at 96 hpci. Notably, the mutant endocardial cells displayed a severe reduction in p-Stat3 staining, showing that Il-11 signaling is required for endocardial Stat3 activation during regeneration (**Fig. 4.28B**).

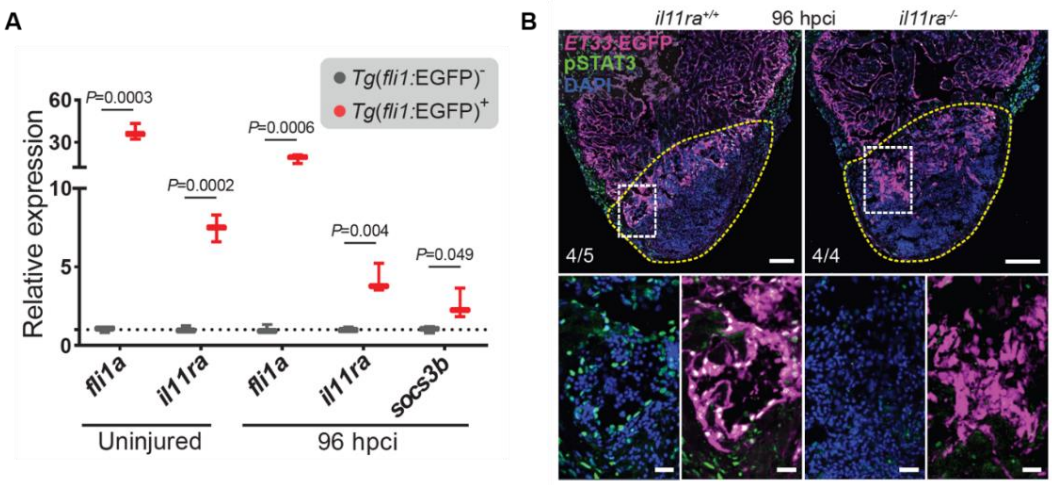

Figure 4.28. Endothelial cells respond to Il-11/Stat3 signaling after injury. (**A**) RT-qPCR analysis on sorted *Tg(fli1:*EGFP)$^{+}$ vs. *Tg(fli1:*EGFP)$^{-}$ cardiac ventricular cells (uninjured siblings, n = 3; 96 hpci, n = 3). (**B**) Immunostaining (GFP – magenta, pStat3 Y705 – green) on cryosections from *Tg(ET33:GFP) il11ra*$^{-/-}$ (n=4) vs. wild-type (n=5) siblings, 96 hpci. Box plots (A) show median, IQR (box margins), and 5th and 95th percentiles (whiskers). Student's t tests (A). n, pools of two ventricles (A); n, ventricles (B). Yellow dashed lines demarcate the injured area (B). Scale bars, 100 μm (A), and 10 μm (A insets). Adapted from (Allanki et al., 2021). License: CC BY 4.0.

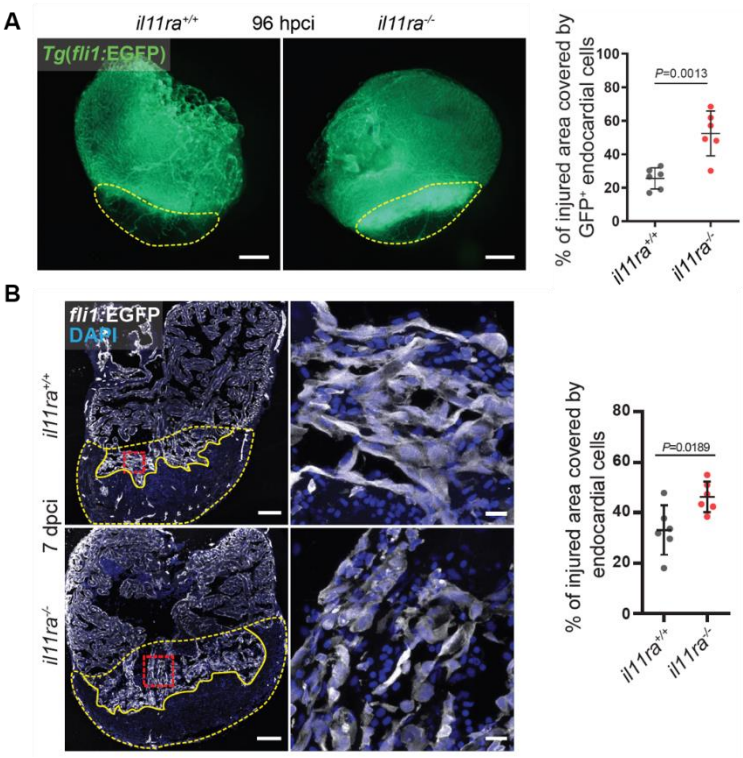

Figure 4.29. Endocardial behaviour in *il11ra* mutants after cardiac injury. (**A**) Wholemount fluorescence images of (wt siblings, n = 6; mut, n = 6; 96 hpci) *Tg(fli1:*EGFP*)* expression in ventricles and quantification of percentage of injured area covered by GFP+ endocardial cells. (**B**) Immunostaining (GFP – white) on ventricle cryosections from *Tg(fli1:EGFP) il11ra*$^{-/-}$ vs. wild-type siblings, and quantification of percentage of injured area covered by *Tg(fli1:*EGFP)$^{+}$ endocardial cells (wt siblings, n=6; mut, n=6) from 50 μm thick ventricle cryosections, 7 dpci. Data represent means ± SD. Student's t tests. n, ventricles. Yellow dashed lines demarcate the injured area; yellow lines demarcate endocardial invasion of the injured area (B). Scale bars, 200 μm (A), 100 μm (B), and 10 μm (B insets). Adapted from (Allanki et al., 2021). License: CC BY 4.0.

4.6.2. Endocardial behaviour in *il11ra* mutants

I then analysed for endothelial phenotypes in *il11ra* mutants. Previous reports show that endocardial cells invade the injury and form a cohesive network by 7-9 dpci (Münch et al., 2017). I observed that the mutant endocardial cells invaded nearly 55% if the injured area already by 96 hpci, while the wild type invasion stood at 25% (**Fig. 4.29A**). This hyper-invasive endocardial phenotype was consistent even at 7 dpci (**Fig. 4.29B**). In addition, I observed that the mutant endocardial cells were disorganized when compared to the cohesive networks formed in wild types at 7 dpci (**Fig. 4.29B**). These data show that the injury-activated endocardial cells are hyper-invasive and disorganized in *il11ra* mutants.

4.6.3. Il-11 signaling limits Endothelial-to-mesenchymal transition (EndoMT) after cardiac injury

The hyper-invasive, disorganized endocardial behaviour, endocardial-specific downregulation of RA activation, and endocardial Elastin1 deposition patterns, as well as the increased myofibroblast differentiation in the mutants suggested an endothelial-to-mesenchymal transition (EndoMT) phenotype. To investigate EndoMT, I first performed RT-qPCRs for EndoMT-associated genes (Chen et al., 2020). I observed that both *il11ra* mutants and *stat3* heterozygotes displayed a similar induction of EndoMT gene program, strengthening the EndoMT hypothesis (**Fig. 4.30**).

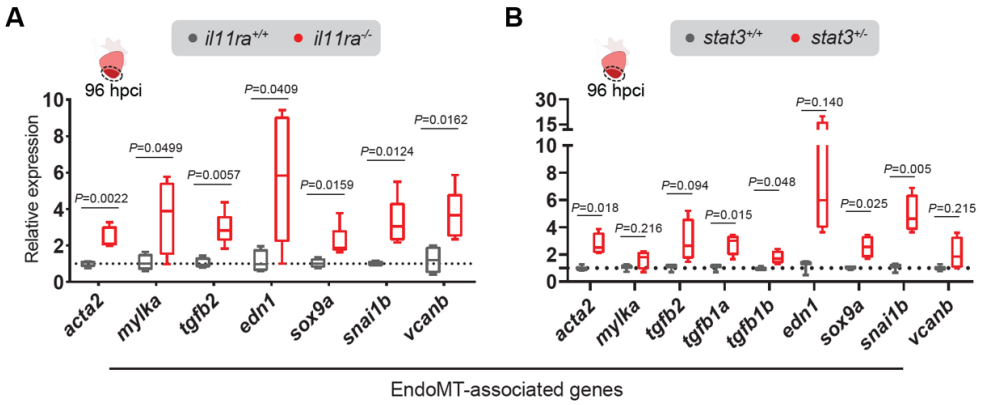

Figure 4.30. EndoMT-related gene expression is induced in *il11ra* mutants and *stat3* heterozygotes after cardiac injury. (**A and B**) RT-qPCR analysis on dissected injured areas of mutant *il11ra*^{bns251} (D, n=5) or heterozygous *stat3*^{stl27} (E, n=4) vs. wild-type siblings (n=4 and 3, respectively) ventricles, 96 hpci, for EndoMT-associated gene expression levels. *acta2*,

mylka, *tgfb2* and *vcanb* mRNA levels in panel A are taken from Fig. 4.24B for comparison. Box plots show median, interquartile range (IQR, box margins) and 5th and 95th percentiles (whiskers). Student's t-tests. n= ventricles. Adapted from (Allanki et al., 2021). License: CC BY 4.0.

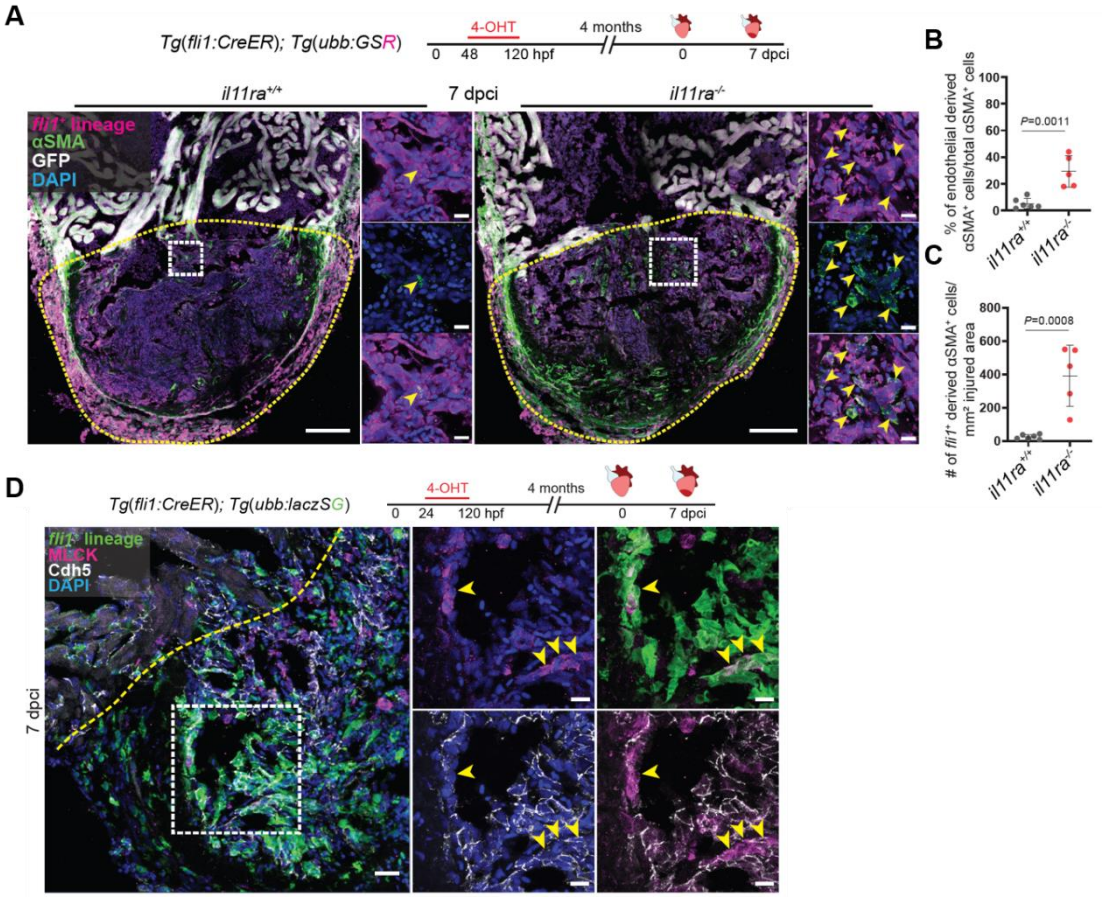

Figure 4.31. Increased EndoMT in *il11ra* mutants after cardiac injury. (**A**) Experimental design and confocal images of immunostaining (mCherry, magenta; αSMA, green) on cryosections from (wt siblings, n = 6; mut, n = 5; 7 dpci) *Tg(fli1:CreER); Tg(ubb:GSR)* ventricles. (**B and C**) Quantification of percentage (B) and density (C) of *fli1*$^{+}$-derived αSMA^{+} cells in the injured area, 7 dpci. (**D**) Experimental design and confocal images of immunostaining (GFP – green, Cdh5 – white, and Myosin light chain kinase, MLCK – magenta) on cryosections from *Tg(fli1:CreER); Tg(ubb:laczSG) il11ra*$^{-/-}$ ventricle, 7 dpci. Data represent means ± SD (B, C). Student's t tests (B, C). n, ventricles (A to C). Yellow dashed lines demarcate the injured area (A and D); yellow arrowheads point to *fli1*$^{+}$-derived αSMA^{+} or MLCK^{+} cells (A insets, D). Scale bars, 100 μm (A), 20 μm (D) and 10 μm (A insets, and D insets). Adapted from (Allanki et al., 2021). License: CC BY 4.0. Certain legends are quoted *verbatim* from Allanki et al., *Sci. Adv*. 7, eabg6497 (2021) for precise explanation.

To confirm EndoMT, I lineage traced *fli1*$^{+}$ endothelial cells after cardiac injury. I observed that, in line with the previous experiments (**Fig. 4.1B**), the wild types displayed minimal EndoMT (~5%), while the mutants displayed a drastic increased in EndoMT (~35%) (**Fig. 4.31A to C**). Furthermore, it was reported that endothelial cells undergoing EndoMT lose their Cdh5^{+} cell-cell adhesions and activate mesenchymal markers (Chen et al., 2020). To test this phenotype, I performed immunostaining for Cdh5 and MLCK in the lineage traced mutant cardiac sections. I observed that, indeed, endocardial cells in the injured area that activated MLCK, displayed lower Cdh5 expression on their cell membranes (**Fig. 4.31D**). These data confirm that the increased myofibroblast differentiation in the mutants after cardiac injury, at least in part is due to increased EndoMT.

In addition, to test whether the mutant endocardial cells contribute to excessive secretion of fibrotic ECM, I performed RT-qPCRs on sorted endothelial cells. In line with our lineage tracing data, I have observed that the mutant endothelial cells displayed an upregulation of mesenchymal genes, downregulation of endothelial marker genes, as well as an increased expression of pro-fibrotic ECM-associated genes. Altogether, these data show that Il-11/Stat3 signaling limits injury-induced EndoMT and pro-fibrotic remodeling during regeneration in the zebrafish heart.

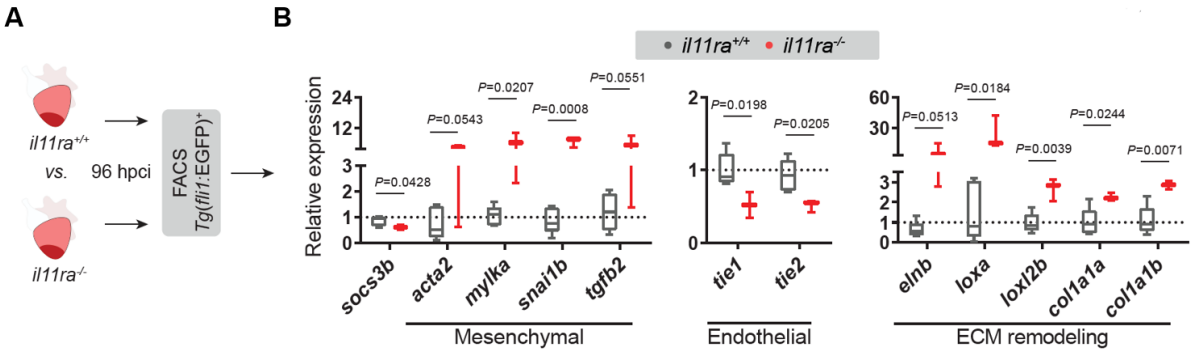

Figure 4.32. Increased fibrotic gene expression in *il11ra* mutant endothelial cells after cardiac injury. (**A and B**) Schematic (A) and RT-qPCR analysis (B) on sorted *Tg(fli1:*EGFP)$^{+}$ cells from (wt siblings, n = 5; mut, n = 3; 96 hpci) ventricles for EndoMT-associated gene mRNA levels. Box plots (B) show median, IQR (box margins), and 5th and 95th percentiles (whiskers). Student's t tests (B). n, pools of two ventricles (B). Adapted from (Allanki et al., 2021). License: CC BY 4.0.

4.6.4. Il-11 signaling limits myofibroblast differentiation in the epicardial lineage

Since *il11ra* is also expressed in the epicardial lineage (**Fig. 4.27A**), I tested whether Il-11 signaling limits myofibroblast differentiation in these cells as well. To investigate this phenotype, I lineage traced epicardial and epicardial-derived cells after cryoinjury. In line with our initial lineage tracing (**Fig. 4.1B**), we observed that ~10% of the wild type EPDCs activated the myofibroblast marker (**Fig. 4.33A and C**). In addition, we observed a significant increase in epicardial-derived myofibroblasts in the mutants (~35%) when compared with wild types (**Fig. 4.33A and C**). Notably, the total density of EPDCs in the injured area was not affected, suggesting that myofibroblast differentiation, but not proliferation of EPDCs is affected in an Il-11 dependent manner.

Altogether, these data show that Il-11 limits injury-induced myofibroblast differentiation from both the epicardial and endothelial lineages, and pro-fibrotic remodeling after cardiac injury in adult zebrafish.

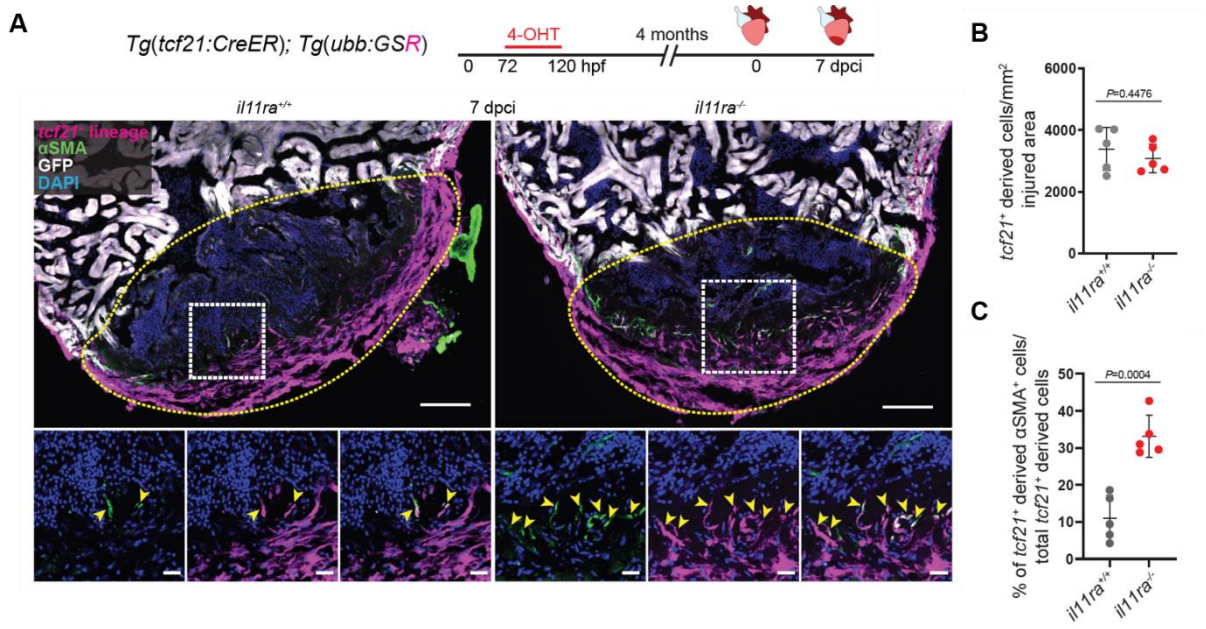

Figure 4.33. Epicardial contribution to myofibroblast differentiation in *il11ra* mutants after cardiac injury. (**A**) Experimental design and confocal images of immunostaining (mCherry – magenta, αSMA – green) on cryosections from *Tg(tcf21:CreER); Tg(ubb:GSR)* ventricles (wt siblings, n=5; mut, n=5; 7 dpci). (**B and C**) Quantification of density of *tcf21*$^{+}$ derived cells in the injured area (B) and percentage of *tcf21*$^{+}$ derived αSMA^{+} cells in the injured area (C). Data represent mean ± S.D. (B, C). Student's t-tests (B, C). n= ventricles (A).

Yellow dashed lines demarcate the injured area (A); yellow arrowheads point to *tcf21*$^{+}$ derived αSMA^{+} cells (A insets). Scale bars, 100 μm (A), 20 μm (A insets). Adapted from (Allanki et al., 2021). License: CC BY 4.0.

4.7. Il-11 signaling orchestrates endothelial-to-cardiomyocyte crosstalk during regeneration

In view of both endothelial and cardiomyocyte defects in *il11ra* mutants in similar time windows, I asked if there is any possible Il-11-mediated endothelial-to-cardiomyocyte crosstalk during cardiac regeneration.

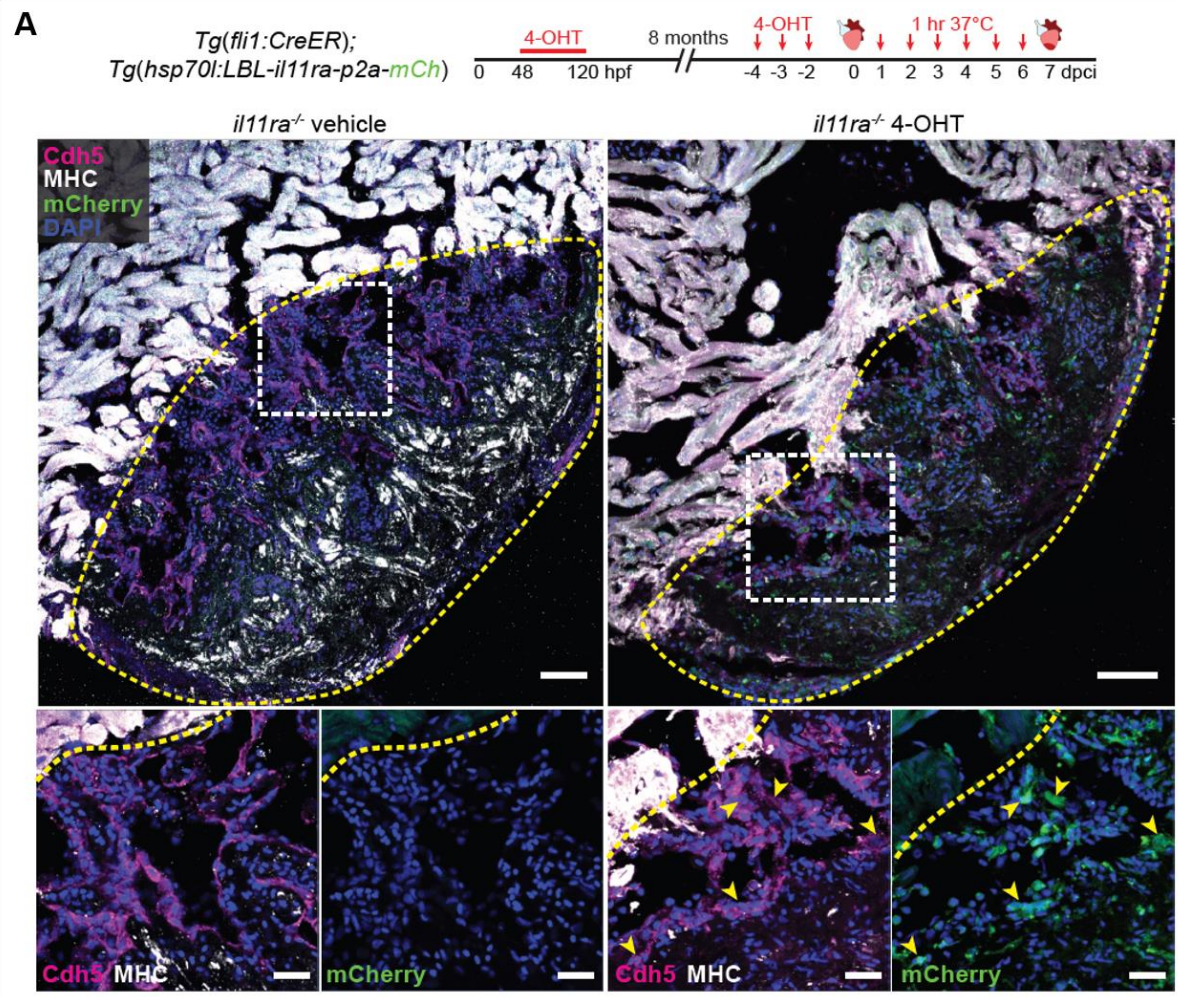

Figure 4.34. Validation of HOTCre *il11ra* overexpression line. (**A**) Experimental design and confocal images of immunostaining (Cdh5 – magenta, MHC – white, and mCherry – green) on cryosections from vehicle or 4-OHT treated *il11ra*$^{-/-}$ *Tg(fli1:CreER); Tg(hsp70l:LBL-il11ra-p2a-mCh)* sibling ventricles at 7 dpci. Yellow dashed lines demarcate the injured area (A).

Scale bars, 50 μm (A), 20 μm (A insets). Adapted from (Allanki et al., 2021). License: CC BY 4.0.

4.7.1. Endothelial-specific re-expression of *il11ra* in *il11ra* mutants

To address this question, I generated a new HOTCre (Hesselson et al., 2009) transgenic line that expresses *il11ra* in a spatially and temporally controlled manner. I then crossed it with endothelial-specific CreERT2 driver line in *il11ra* mutant background. Tamoxifen treatments in the embryonic stages and adult stages before injury resulted in floxing out of the *tagBFP* cassette, allowing the re-expression of *il11ra-p2a-mCherry* upon heat shocks. I validated the *il11ra-p2a-mCherry* re-expression by immunostaining for mCherry (**Fig. 4.34**). I observed that *il11ra* is re-expressed specifically in the endothelial lineage, but not in cardiomyocytes (**Fig. 4.34**).

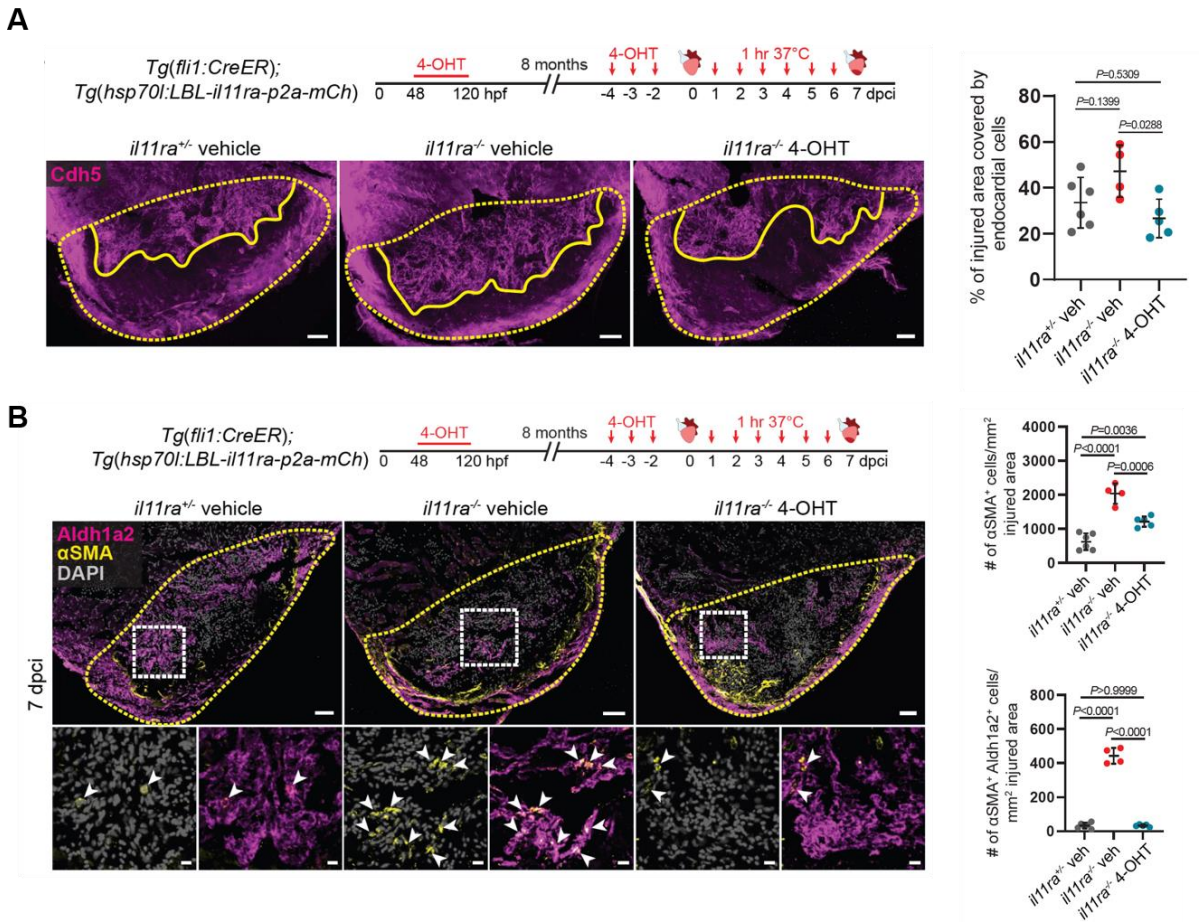

Figure 4.35. Cell autonomous regulation of EndoMT by Il-11 signaling. (**A**) Experimental design and confocal images of immunostaining for Cdh5 expression on 50 μm thick cryosections from vehicle treated *il11ra*$^{+/-}$ siblings, and vehicle or 4-OHT treated *il11ra*$^{-/-}$

Tg(fli1:CreER); Tg(hsp70l:LBL-il11ra-p2a-mCh) ventricles. Quantification of percentage of the injured area covered by Cdh5^{+} endocardial cells (*il11ra*$^{+/-}$ veh, n=6; *il11ra*$^{-/-}$ veh, n=4; *il11ra*$^{-/-}$ 4-OHT, n=5; 7 dpci). (**B**) Experimental design and confocal images of immunostaining (Aldh1a2, magenta; αSMA, yellow) on cryosections from vehicle-treated *il11ra*$^{+/-}$ siblings (n = 6) and vehicle- or 4-OHT–treated *il11ra*$^{-/-}$ (n = 4 and 5, respectively) *Tg(fli1:CreER); Tg(hsp70l:LBL-il11ra-p2a-mCh)* ventricles at 7 dpci. Quantification of total αSMA^{+} cell density and αSMA^{+} Aldh1a2^{+} cell density in the injured area, 7 dpci. Data represent mean ± S.D. One-way ANOVA. n= ventricles. Yellow dashed lines demarcate the injured area; yellow lines demarcate the endocardial invasion in the injured area (A). Scale bars, 50 μm (A, B), 10 μm (B insets). Adapted from (Allanki et al., 2021). License: CC BY 4.0. Certain legends are quoted *verbatim* from Allanki et al., *Sci. Adv*. 7, eabg6497 (2021) for precise explanation.

4.7.2. Rescue of endothelial hyper-invasion and EndoMT upon re-expression of *il11ra* in *il11ra* mutant endothelial cells

Next, I tested whether this endothelial-specific re-expression of *il11ra* in *il11ra* mutants can rescue endothelial phenotypes, including hyper-invasion and EndoMT. In line with my previous data, the *il11ra* mutant endocardial cells displayed a hyper-invasive phenotype and increased EndoMT when compared with the heterozygous controls (**Fig. 4.35**). Notably, the mutants with endothelial-specific re-expression of *il11ra* displayed near-control levels of endocardial invasion, as well as completely rescued EndoMT back to control levels (**Fig. 4.35**). These data show that Il-11 signaling limits EndoMT in a cell-autonomous manner.

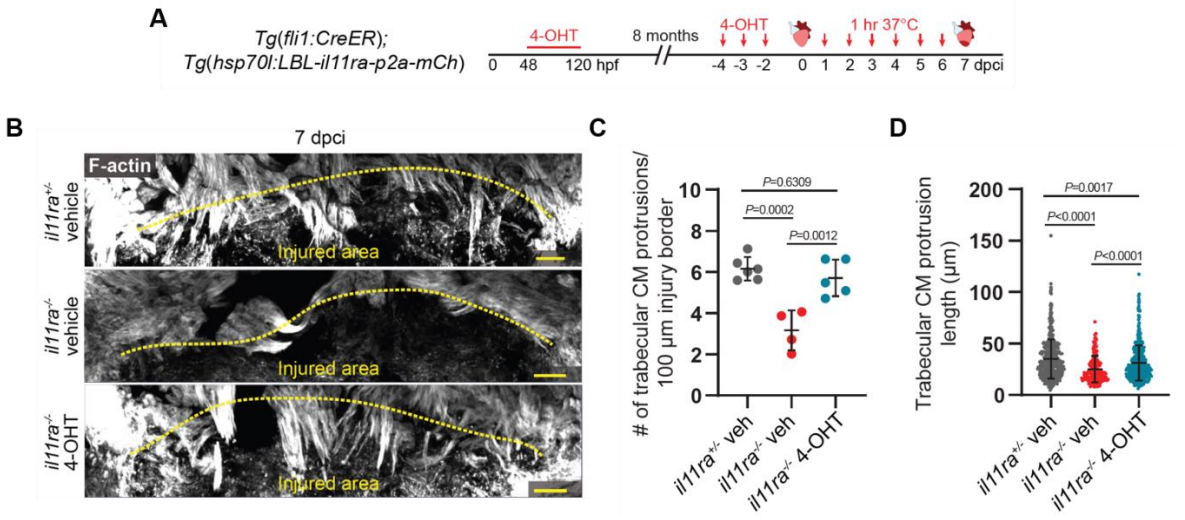

Figure 4.36. Il-11 signaling in endothelial cell allows cardiomyocyte repopulation of the injured area. (**A and B**) Experimental design (A) and F-actin staining (B) on 50-µm-thick cryosections from vehicle-treated *il11ra*$^{+/-}$ siblings and vehicle- or 4-OHT–treated *il11ra*$^{-/-}$ *Tg(fli1:CreER); Tg(hsp70l:LBL-il11ra-p2a-mCh)* ventricles at 7 dpci. (**C and D**) Quantification of the number per ventricle (C) (*il11ra*$^{+/-}$ veh, n = 6; *il11ra*$^{-/-}$ veh, n = 4; *il11ra*$^{-/-}$ 4-OHT, n = 5) and length (D) (*il11ra*$^{+/-}$ veh, n = 481; *il11ra*$^{-/-}$ veh, n = 185; *il11ra*$^{-/-}$ 4-OHT, n = 437) of CM protrusions at 7 dpci. Data represent means ± SD (C, D). One-way ANOVA (C); Kruskal-Wallis test (D). n, ventricles (C); n, CM protrusions (D). Yellow dashed lines demarcate the injured area (A). Scale bars, 50 µm (A). Adapted from (Allanki et al., 2021). License: CC BY 4.0. Certain legends are quoted *verbatim* from Allanki et al., *Sci. Adv*. 7, eabg6497 (2021) for precise explanation.

4.7.3. Il-11 signaling in endothelial cells allows cardiomyocyte repopulation after cardiac injury

Finally, I analysed cardiomyocyte protrusive behaviour in these ventricles. In line with my previous data, *il11ra* mutants displayed reduced number and length of cardiomyocyte protrusions when compared to heterozygous siblings (**Fig. 4.36**). In addition, the mutants with endothelial-specific re-expression of *il11ra* displayed a complete rescue of cardiomyocyte protrusion back to control levels (**Fig. 4.36**). These data indicate that Il-11 signaling in endothelial cells allows cardiomyocyte repopulation of the injured area. Further re-expression studies in other cell types are needed to uncover any other possible intercellular crosstalk mediated by Il-11 signaling during regeneration.

4.8. Interactions between IL-11 and TGF-β signaling pathways

Previous studies show that TGF-β signaling transcriptionally regulates IL-11 levels in fibroblasts (Schafer et al., 2017). Notably, from my previous data (**Fig. 4.32B**), I have observed that TGF-β ligand expression is induced in *il11ra* mutants endothelial cells after cardiac injury. These data suggest a potential feedback regulation in between TGF-β and IL-11 pathways in endothelial cells.

4.8.1. *In vivo* analysis of TGF-β activity in *il11ra* mutants

First, to confirm TGF-β activation in the mutant endothelial cells, I performed immunostaining for the downstream effector pSmad3. I observed a significant increase in the proportion of pSmad3^{+} endocardial cells in the mutant injured areas when compared with the wild types (**Fig. 4.37**), indicating increased TGF-β activity in the mutant endocardial cells in response to cardiac injury.

4.8.2. Analysis of the feedback interactions in between TGF-β and IL-11 signaling in human endothelial cells in culture

Next, to investigate the potential feedback interactions between TGF-β and IL-11 signaling pathways, I used human endothelial cells in culture – Human umbilical vein endothelial cells (HUVECs) (**Fig. 4.38A**). First, I tested if TGFB treatment can induced *IL-11* expression in these endothelial cells. I treated HUVECs with recombinant human TGFB2 protein (rhTGFB2) and performed RT-qPCRs for *IL-11* expression. I observed a sharp increase in *IL-11* mRNA levels upon TGFB2 treatment (**Fig. 4.38D**). I then manipulated IL-11 signaling either by treating HUVECs with rhIL-11 or by knocking down *IL11RA* using siRNA. In line with my *in vivo il11ra* mutant data, knocking down *IL11RA* in HUVECs resulted in an increased expression of TGFB ligands and the downstream effector *SNAI1* (**Fig. 4.38B**). On the other hand, stimulating HUVECs with rhIL-11 diminished the expression levels of the same genes (**Fig. 4.38C**). These data indicate a feedback inhibition of TGFB signaling by IL-11. To confirm these findings, I performed rhTGFB and rhIL-11 co-treatments. The aim was to observe if self-induced TGFB levels can be rescued by IL-11 treatment. As shown previously, TGFB treatment induces both TGFB ligands and *SNAI1* levels, which is rescued completely by stimulating the TGFB treated cells with rhIL-11 (**Fig. 4.38D**). These data confirm the feedback interaction between TGFB and IL-11 pathways.

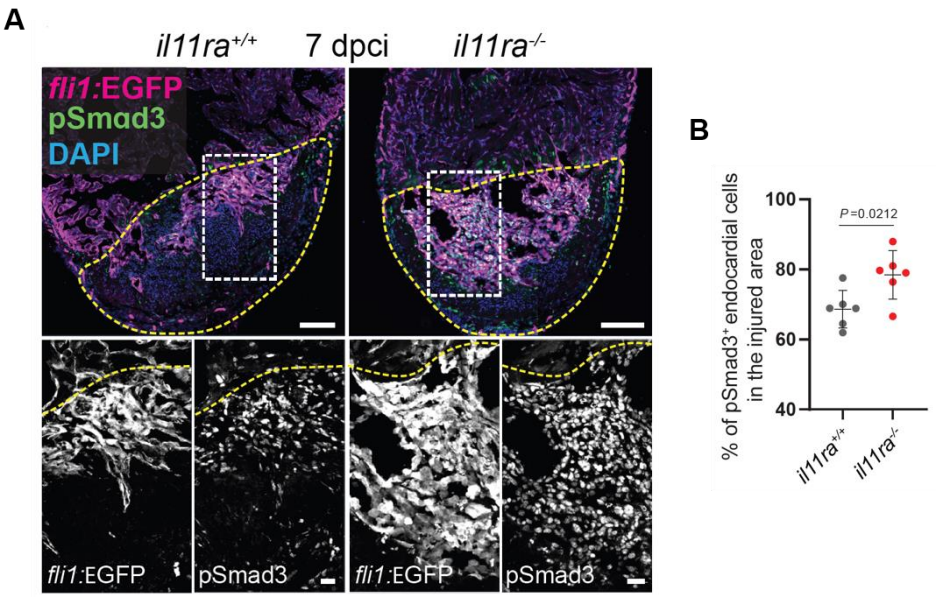

Figure 4.37. *il11ra* mutant endocardial cells display increased TGF-β activity after cardiac injury. (**A and B**) Confocal images of immunostaining (A) (GFP, magenta; pSmad3, green; 7 dpci) on cryosections from *il11ra*$^{-/-}$ vs. wild-type *Tg(fli1:EGFP)* ventricles and quantification of percentage of pSmad3^{+} endocardial cells in the injured area (B) (wt siblings, n = 6; mut, n = 6). Data represent means ± SD (B). Student's t tests (B). n, ventricles (B). Yellow dashed lines demarcate the injured area (A). Scale bars, 100 μm (A) and 20 μm (A, insets). Adapted from (Allanki et al., 2021). License: CC BY 4.0. Certain legends are quoted *verbatim* from Allanki et al., *Sci. Adv*. 7, eabg6497 (2021) for precise explanation.

I then asked a question if inhibiting TGF-β can rescue the fibrotic gene expression induced by knocking down *IL11RA*. In line with our *in vivo* data, knocking down *IL11RA* induced myofibroblast differentiation and pro-fibrotic remodeling associated gene expression (**Fig. 4.38E**). In addition, treating these *IL11RA* knocked down cells with TGF-β inhibitor completely rescued the fibrotic gene expression (**Fig. 4.38E**). These data suggest that the pro-fibrotic effects observed in *il11ra* mutants are due to increased TGF-β activity in endothelial cells.

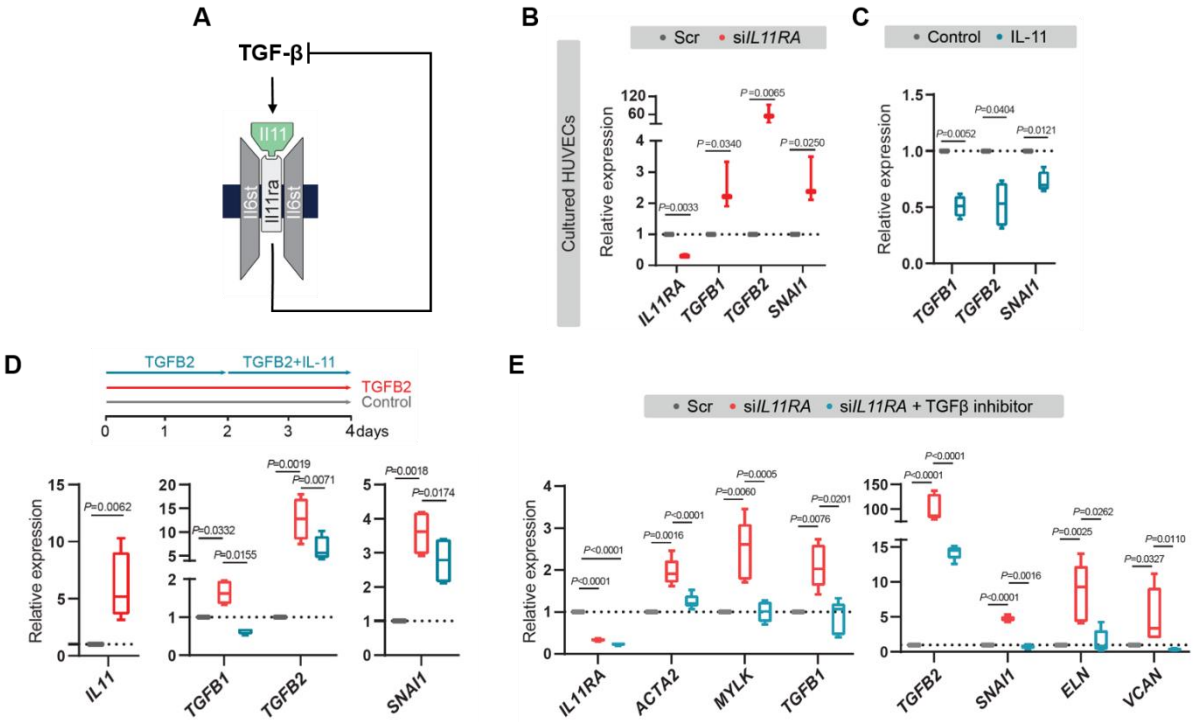

Figure. 4.38. Feedback interaction in between TGF-β and IL-11 signaling. (**A**) Schematic showing the feedback interactions. (**B**) RT-qPCR analysis for *IL11RA*, genes encoding TGF-β ligands, and TGF-β downstream target *SNAI1* mRNA levels on HUVECs transfected with scrambled (n = 3) or *IL11RA* siRNAs (n = 3). (**C**) RT-qPCR analysis for genes encoding TGF-β ligands and for TGF-β downstream target *SNAI1* mRNA levels on HUVECs treated with control (n = 4) or rhIL-11 (10 ng/ml; n = 4). (**D**) Experimental design and RT-qPCR analysis for *IL11*, genes encoding TGF-β ligands, and for TGF-β downstream target *SNAI1* mRNA levels on HUVECs treated with control (n = 4) or rhTGFB2 (10 ng/ml; n = 4) or rhTGFB2 + rhIL-11 (10 ng/ml) (n = 4). (**E**) RT-qPCR analysis for genes encoding myofibroblast markers, TGF-β ligands, TGF-β downstream target *SNAI1*, and for fibrogenic ECM component mRNA levels on HUVECs transfected with scrambled (n = 4) or si*IL11RA* (n = 4) or si*IL11RA* + 10 μM TGFBR1 inhibitor (SB431542; n = 4). Box plots (B to E) show median, IQR (box margins), and 5th and 95th percentiles (whiskers). Student's t tests [B, C, E - IL11]; one-way ANOVA (D and E). n, biological replicates (B to E). Adapted from (Allanki et al., 2021). License: CC BY 4.0. Certain legends are quoted *verbatim* from Allanki et al., *Sci. Adv*. 7, eabg6497 (2021) for precise explanation.

4.9. Proposed model

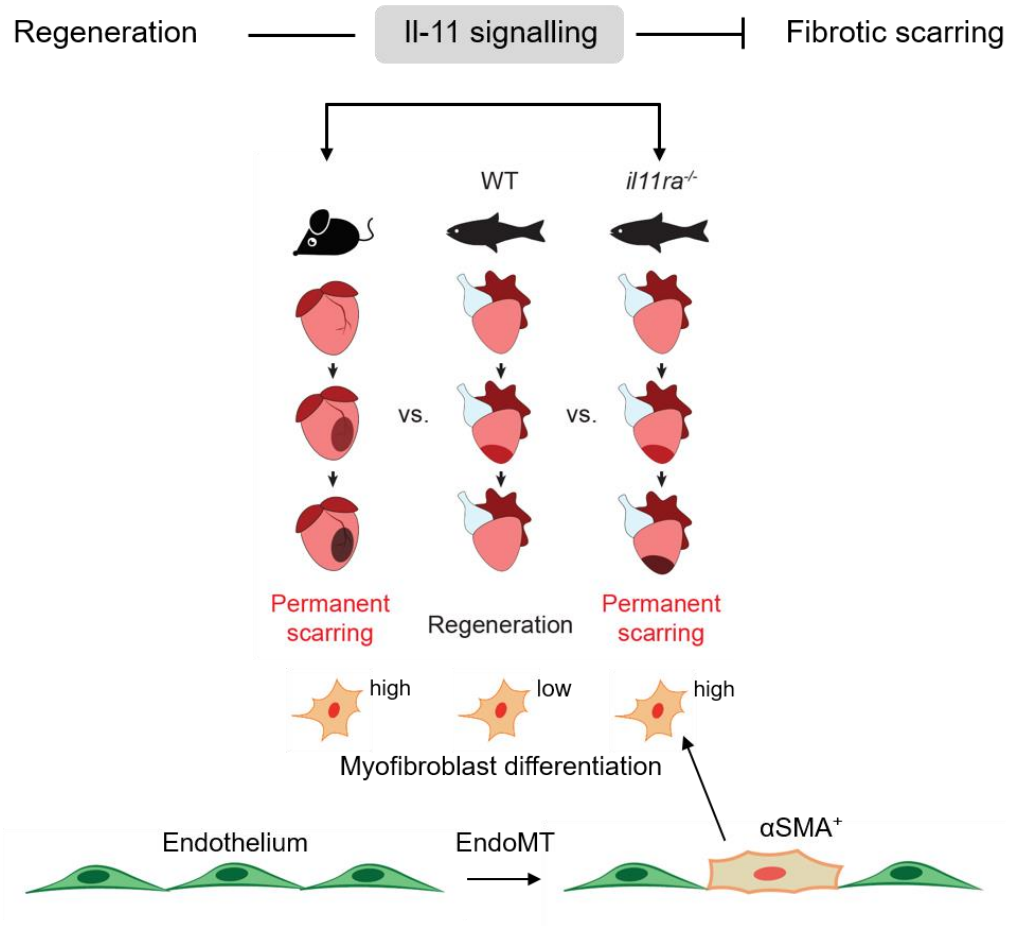

Figure. 4.39. Model describing the role of Il-11 signaling during regeneration and scarring. Il-11/Stat3 signaling promotes regeneration by orchestrating regenerative reprogramming and limits mammalian-like scarring by inhibiting myofibroblast differentiation and TGF-β signaling. Specifically, Il-11 signaling in endothelial cells limits EndoMT and fibrosis, allowing cardiomyocyte migration into the injured area.

5. Discussion

5.1. Regeneration and fibrotic scarring

Tissue damage, most often, results in either permanent scarring or functional regeneration. Upon injury, some species undergo regenerative reprogramming to facilitate flawless regeneration of the lost tissue and functional recovery. In these species, cells adjacent to the damaged area change their homeostatic transcriptional profiles to establish a regenerative microenvironment. Thousands of genes that are required for successful regeneration are activated, while the genes that are detrimental for regeneration are silenced. This phenomenon is characterized well during regeneration in the axolotl limb, the zebrafish fin and heart (Gerber et al., 2018; González- Rosa et al., 2017; Lin et al., 2021; Pfefferli and Jaźwińska, 2015). Instead of activating regenerative reprogramming, most mammalian species, including rodents and humans, mount a scarring response by mainly activating a fibrogenic gene program (Davis and Molkentin, 2014; Murawala et al., 2012). Consequently, myofibroblast differentiation is induced from various lineages, including tissue resident fibroblasts, endothelial cells and circulating blood cells (Falke et al., 2015). Some of the primary functions of myofibroblasts is to repair the damaged tissue by secreting excessive amounts of ECM and provide contractile support to organs like the heart. Upon injury, fibrotic scarring prevents the tissue from rupturing. The excessive amount of ECM deposited then is remodeled and matured by matrifibrocytes, forming a permanent scar that leads to sub-optimal tissue function, which sometimes results in lethality. To understand these processes and develop anti-fibrotic and pro-regenerative therapies, plenty of human and financial resources are employed year after year. Thus, decades of research on regenerative and non-regenerative organisms led to the discovery of important mechanisms, including several components of the global and tissue-specific regeneration program. Albeit, most of these mechanisms are non-specific, i.e., have pleiotropic effects on other essential biological processes, including tissue homeostasis and organogenesis. Hence, the identity of regeneration-specific global regulators remains unknown.

In this study, using the zebrafish heart as a model system, we aimed to identify such mechanisms by comparing the tissue response to physical exercise and to injury-induced regeneration. I have identified the Il-6 cytokine family-mediated Stat3 signaling as a promising candidate for further analysis. Using genetic loss-of-function analyses, I have narrowed down to Interleukin-11 signaling as the prime candidate. I show that Il-11 is transcriptionally activated in an evolutionarily conserved manner during regeneration. By deep-phenotyping regeneration in multiple zebrafish tissues and using tissue-specific genetic manipulations, I identified a dual role for Il-11 signaling during regeneration and scarring – 1) it promotes both global and tissue-specific regenerative reprogramming and 2) it blocks mammalian-like scarring response. Mechanistically, I also highlight the anti-fibrotic effects of Il-11 signaling both in the endothelial and epicardial lineages. Finally, I uncover a novel feedback mechanism by which IL-11 signaling inhibits TGF-β mediated fibrotic scarring.

5.2. A global role for Interleukin-6 cytokine family-mediated Stat3 signaling in tissue regeneration

First, by performing comparative expression profiling and genetic loss-of-function studies to block Il-6 family mediated Stat3 signaling broadly, I highlight the pro-regenerative role of this pathway. In line with these findings, previous studies in various model systems have also reported pro-regenerative roles for the Il-6 family members. For instance, Yandong and colleagues report that Osmr/Gp130 signaling in cardiomyocytes is pro-regenerative by inducing cardiomyocyte proliferation (Li Yandong et al., 2020). A study conducted by Kubin and colleagues showed that Osm induces cardiomyocyte dedifferentiation to support cardiac regeneration (Kubin et al., 2011). In addition, Zou and colleagues showed that intramuscular injections of LIF cDNA promoted cardiomyocyte proliferation, neovascularization, and functional recovery after myocardial infarction in adult mouse (Zou et al., 2003). In the zebrafish heart, using cardiomyocyte specific manipulations, a study by Fang and colleagues reports that Jak/Stat3 signaling is an early response to ventricular resection, and that it is required for cardiac regeneration via inducing cardiomyocyte proliferation (Fang et al., 2013). Another recent study in the zebrafish heart showed that Cntf-mediated Lifr/Gp130 stimulates cardioprotection and regeneration (Bise et al., 2019). In tissues

other than the heart, including spinal cord, optic nerve, and retina, Il-6 family-mediated Stat3 signaling has been shown to be required for regeneration (Cressman et al., 1996; Leibinger et al., 2021; Mehta et al., 2016; Paris et al., 2020; Taniguchi et al., 2015). All these reports, together with our findings in zebrafish highlight the importance of further investigating this pathway for novel therapeutic avenues to induce regeneration in humans.

5.3. Evolutionarily conserved transcriptional activation of IL-11 during regeneration

Next, I have identified that Il-11 transcripts are induced within minutes after cardiac or fin injuries in the regenerative zebrafish. By literature survey, I have also identified that Il-11 induction is not just restricted to different tissues in zebrafish, but is evolutionarily conserved at least in most of the known regenerative species. However, it was also reported that Il-11 is induced after myocardial infarction in the non-regenerative adult mouse (Obana Masanori et al., 2010). Furthermore, Il-11 is reported to be induced in various cancers and inflammatory diseases (Cook and Schafer, 2020). These correlative observations demand a deeper investigation of the downstream effects of IL-11 induction in regenerative vs. non-regenerative species. In addition, evolution of the IL-11 molecule itself should not be ignored. Future studies to directly compare the effects of IL-11 from different species can shed light upon these potential differences.

5.4. Il-11 signaling is required for blastema formation

After amputation, cells adjacent the injury plane dedifferentiate and migrate to seed a layer of undifferentiated cells called as a blastema. This phenomenon is a hallmark feature of epimorphic regeneration, including in the zebrafish, axolotl, *Xenopus*, mouse digit tips, and spiny mouse ears (Murawala et al., 2012). Signals from the wound epidermis induce blastema formation. Cells in the blastema secrete ECM and signaling molecules, and contribute to the formation of a regenerative niche. In the axolotl limb after amputation, combining scRNA-seq and lineage tracing, it has been shown that connective tissue cells majorly contribute to blastema formation by dedifferentiating and acquiring a similar transcriptional identity (Gerber et al., 2018). Furthermore, a similar analysis on the partially regenerative *Xenopus* limb shows that

connective tissue dedifferentiation is impaired, suggesting a functional role for cell dedifferentiation (Lin et al., 2021). Likewise, during zebrafish caudal fin blastema formation, osteoblasts dedifferentiate and migrate (Knopf et al., 2011; Sousa et al., 2011). Furthermore, both in axolotl limb and *Xenopus* tadpole tail, expression profiles show a transient induction of Il-11 after injury (Gerber et al., 2018; Tsujioka et al., 2017). These data suggest a potential role for Il-11 signaling in regenerative reprogramming leading to blastema formation. Indeed, gene knockdown studies in the *Xenopus* tadpole tail during regeneration suggest the importance of Il-11 signaling in maintaining the progenitor state in the blastema (Tsujioka et al., 2017). Now, using state-of-the-art genetic mutants, my findings in the adult zebrafish caudal fin provide conclusive evidence that Il-11 signaling is indispensable for blastema formation and the upstream regenerative response. In addition, I show that Il-11 is required for the induction of a blastema-specific and evolutionarily conserved regenerative gene program. Similarly, in the zebrafish heart, we show a role for Il-11 signaling in inducing regenerative reprogramming after injury. However, the existence of blastema-like features in the regenerating heart has only been discussed once thus far and will need further investigation (Sallin et al., 2015). In line with this hypothesis, increasing evidence shows that cardiomyocytes dedifferentiate during regeneration (Honkoop et al., 2019; Kubin et al., 2011; Ogawa et al., 2021; Sallin et al., 2015). Furthermore, it would be very interesting to see how/if the fibroblast and endothelial lineages dedifferentiate, and whether it is required for regeneration.

5.5. Il-11 signaling is required for cell repopulation of the injured area

Impaired regenerative reprogramming at the transcriptional levels affects downstream cellular processes, including proliferation, migration and dedifferentiation. Supporting this statement, I found impaired cell repopulation in the *il11ra* mutant hearts and fins. In the mutant hearts, permanent scarring at 90 dpci indicates a failure of cardiomyocytes to repopulate the injured area. Deeper analysis of cardiomyocyte behaviour at early stages showed that cardiomyocytes fail to extend protrusions into the injured area starting from 72 hpci. Similarly, in the mutant fins, osteoblasts fail to migrate past the amputation plane. However, similar to mammals, the zebrafish *il11ra* is not highly expressed in cardiomyocytes when compared with the non-myocardial

lineages, including the endothelium and fibroblasts. Supporting these data, I show that the mutant cardiac endothelial cells fail to activate p-Stat3 when compared with the wild types at 96 hpci. Furthermore, I was able to rescue the mutant cardiomyocyte repopulation defects by re-expressing *il11ra* specifically in endothelial cells. Together, these data strongly support the cell non-autonomous effects of endothelial and fibroblast Il-11 signaling on cardiomyocyte protrusion. Two major reasons explain how endothelial Il-11 signaling controls cardiomyocyte migration, including – 1) the lack of pro-migratory matrix deposition (Fibronectin), and on the other hand 2) excessive fibrotic matrix deposition mediated by myofibroblasts derived from endothelial and epicardial lineages in the mutants. Notably, previous work on ventricular resection in zebrafish showed that blocking Fn1 function did not affect cardiomyocyte proliferation at 7 dpa, but resulted in impaired cardiomyocyte repopulation at 30 dpa (Wang et al., 2013). Other work in mice shows that reducing matrix stiffness or altering the matrix composition results improved cardiomyocyte regeneration (Notari et al., 2018). Furthermore, the mutant cardiomyocyte proliferation was not affected at 7 dpci, but only mildly reduced at 14 dpci. I speculate that the mutant cardiomyocyte proliferation defects at 14 dpci are secondary to the lack of a permissive microenvironment. However, further cell type–specific rescue analyses or cell-type specific mutants will be needed to comprehensively analyze roles of Il-11 signaling in individual cell types during regeneration.

Together with the previous reports, my findings in the zebrafish strongly highlight an indispensable and evolutionarily conserved role for Il-11 signaling in regulating regenerative reprogramming and cell repopulation during general tissue regeneration.

5.6. Il-11 signaling limits mammalian-like scarring during regeneration

Fibrotic scarring limits regeneration (Gurtner et al., 2008). Indeed, using lineage tracing, I show that zebrafish exhibit limited myofibroblast differentiation from epicardial and endothelial lineages when compared to adult mouse after cardiac injury. In line with these data, a recent report showed that the injury-activated fibroblasts return to their ground transcriptional state at late time points after cardiac cryoinjury in zebrafish

(Sánchez-Iranzo et al., 2018). In contrast, the adult mammals induce extensive myofibroblast differentiation, which at late time points then are terminally differentiated into matrifibrocytes to maintain the mature scar (Fu et al., 2018). Furthermore, I show that nullifying Il-11 function fundamentally changes these myofibroblast differentiation and scarring dynamics in *il11ra* mutant heart and fins. In the heart, using lineage-tracing strategies after injury, I show that both the epicardial and endothelial lineages display a significantly increased tendency towards myofibroblast fate in *il11ra* mutants. In line with these data, I observed increased mammalian-like fibrotic remodeling of the injured area in the mutants. A recently reported marker for activated fibroblasts - FAP (fibroblast activation protein), along with majority of the top 15 matrifibrocyte marker genes, are upregulated in *il11ra* mutant hearts after injury (Aghajanian et al., 2019; Fu et al., 2018). Furthermore, key regulators of mammalian tissue fibrosis, including *egr1*, *egr2b*, and *meox1*, as well as other fibrotic ECM components (Elastin1) and cross-linking enzymes (*loxa* and *loxl2b*) display increased expression levels in the mutants when compared to wild types, after injury (Fang et al., 2011). Of note, *MEOX1*, the mammalian orthologue of zebrafish *meox1*, acts as a key transcriptional factor for fibroblast activation during mammalian cardiac fibrosis (Alexanian et al., 2021). Finally, an unbiased transcriptome-wide comparison shows that *il11ra* mutant heart fibrosis is similar to the adult mammalian fibrotic response, but not with the regenerative neonates', after injury. Together, these data strongly indicate that Il-11/Stat3 signaling limits hallmarks of the mammalian fibrogenic program in zebrafish during tissue regeneration.

5.7. Controversial role of IL-11 signaling in tissue fibrosis

In light of the recent controversial data, the role of IL-11 signaling in tissue fibrosis and regeneration is highly debated (Cook and Schafer, 2020). IL-11 biology was of high interest in the early 1990s. IL-11 was first discovered as a hematopoietic cytokine that supports the growth of platelets. These findings led to the therapeutic usage of recombinant human (rh) IL-11, an FDA approved drug, to treat thrombocytopenia in chemotherapy patients. However, genetic loss-of-function mutants in mice showed no severe defects in hematopoiesis. Later, it was reported that IL-11 is a cardioprotective and anti-fibrotic cytokine that acts mainly via STAT3 in mouse MI and kidney injury

models (Obana Masanori et al., 2010). These reports proposed to use rhIL-11 to ameliorate cardiac fibrosis. Follow-up studies showed that injecting human MI patients with rhIL-11 did not lead to any adverse reactions (Nakagawa et al., 2016). Reports on other IL-6 family cytokines, including hyper-IL-6, and CNTF, which majorly signal through IL6ST/STAT3, were recently used successfully to promote central nervous system and cardiac regeneration in adult mice, respectively (Fazel Modares et al., 2019; Leibinger et al., 2021).

In contrast, chronic heart failure patients displayed increased IL-11 levels that correlated with cardiac damage. Furthermore, other recent studies have reported that IL-11 is pro-fibrotic in various mammalian tissues. These studies portrayed IL-11 as a regeneration-limiting and fibrogenic molecule. Schaefer and colleagues identified that IL-11 is a major transcriptional response to TGFB treatments in human cardiac fibroblast cultures (Schafer et al., 2017). Moreover, they showed that IL-11, instead of acting through canonical STAT3, acts through non-canonical ERK to induce fibrogenic ECM production and myofibroblast differentiation. Follow-up studies on systemic sclerosis, rheumatoid arthritis, pulmonary fibrosis, kidney disease, liver damage, inflammatory bowel disease and cancer showed that IL-11 drives tissue fibrosis via non-canonical ERK pathway (Cook and Schafer, 2020). Furthermore, it was also shown that IL-11-neutralizing antibodies or genetic loss-of-function mutations can protect the mice from tissue fibrosis and maladaptive remodeling. Hence, they proposed that blocking IL-11/ERK activity can induce regeneration and limit fibrosis in human pathologies, to restore organ function.

In addition to these mammalian data, it was reported that bony fish constitutively activate Il-11 expression in their intestines and gills, which are constantly under pathogenic threat. Teleosts, including zebrafish, also possess miraculous regenerative capabilities. Hence, we aimed to understand the role of IL-11 signaling in a regenerative context. My findings in zebrafish provide unequivocal evidence that Il-11/Stat3 signaling is anti-fibrotic and pro-regenerative upon tissue damage. Although my findings add more evidence to the anti-fibrotic side of the debate, some important aspects and perspectives need to be considered for further studies. First, the evolutionary modifications that the components of IL-11 signaling have underwent.

My phylogenetic and synteny analyses indeed confirm that the zebrafish genes encoding Il11ra and Il-11 investigated in this study are direct orthologs of their human counterparts. However, careful analysis of specific domains need to be carried out to identify their functional relevance. Of note, while zebrafish and humans have a single IL-11 receptor encoding gene, mice carry a duplication of *Il11ra* (*Il11ra1* and *Il11ra2*). This gene duplication potentially complicates mechanistic studies. Another important aspect to consider is the difference in the downstream signaling in between mammals and zebrafish. In line with the earlier mammalian studies, we show that zebrafish Il-11 is pro-regenerative through the canonical Stat3 pathway, while the recent mammalian studies show that its pro-fibrotic effects are driven by non-canonical ERK signaling. One can assume that, during evolution, IL-11 signaling drifted from regulating the regenerative program via STAT3 to driving a fibrogenic program via ERK. Additionally, we show the anti-fibrotic effects of IL-11 in endothelial cells, while its pro-fibrotic role was characterized in fibroblasts. Hence, Il-11 signaling in various cell types could also be different. However, this hypothesis needs to be tested using thorough cell-type specific molecular and mechanistic investigation by directly cross comparing the IL-11 molecule from different species and observing the differences in their downstream effects in various cell types. Despite of these potential evolutionary differences, my analyses in human endothelial cultures show a conserved feedback mechanism in between IL-11 and TGF-β signaling pathways.

6. Conclusion

Following are the conclusions drawn from my results for each of the specific aims:

Aim 1: Identify a regenerative mechanism that limits fibrotic scarring.

Interleukin-6 family mediated Stat3 signaling is a pro-regenerative pathway in zebrafish. Specifically, Il-11, an Il-6 family cytokine, is upregulated in an evolutionarily conserved manner during regeneration. Using an in-depth genetic loss-of-function analysis from the ligands (*il11a* and *il11b*), to the receptors (*il11ra* and *il6st*), through the transcription factor (*stat3*), as well as analyzing regeneration in multiple zebrafish tissues throughout life, I establish Il-11 signaling as a global regulator of regeneration in zebrafish.

Aim 2: Investigate the cellular mechanisms downstream of this pathway during regeneration and scarring.

By deep phenotyping regeneration in at least two fundamentally different adult zebrafish tissues, I identify that Il-11 signaling plays a dual role during regeneration:

1. It promotes regenerative reprogramming and cell repopulation
2. It limits mammalian-like scarring response

Aim 3: Uncover the downstream molecular mechanisms that this pathway during regeneration and scarring.

Using both *in vivo* analysis in zebrafish and *in vitro* analysis in primary human endothelial cells, I identify a conserved novel feedback relationship between IL-11 and TGFB signaling pathways.

Altogether, I propose that understanding the cell-type specific downstream differences of IL-11 signaling in regenerative vs. non-regenerative species will uncover novel regenerative and anti-fibrotic therapies.

7. Zusammenfassung

7.1. Einleitung

Die beiden diametral entgegengesetzten Ergebnisse nach einer Gewebeschädigung sind Regeneration und fibrotische Vernarbung (Gurtner et al., 2008). Nach einer Verletzung kommt es bei erwachsenen Säugetieren überwiegend zu einer fibrotischen Narbenbildung, die in den meisten Fällen zur Letalität des Patienten führt. Fibrotische Narbenbildung ist die Ablagerung von übermäßiger extrazellulärer Matrix, die ausdifferenziert und die Gewebefunktion behindert. Die Vernarbungsreaktion wird hauptsächlich von Myofibroblasten orchestriert, die nur bei einer Gewebeschädigung aus verschiedenen zellulären Ursprüngen entstehen, darunter gewebeansässige Fibroblasten, Endothelzellen und zirkulierende Blutzellen (Davis and Molkentin, 2014). Neben den narbenbildenden extrazellulären Matrixgenen exprimieren Myofibroblasten Komponenten die für die kontraktile Funktion der Muskeln benötigt werden, einschließlich α-Smooth muscle actin (αSMA/Acta2), um dem geschädigten Gewebe kontraktile Eigenschaften zu verleihen. Es hat sich auch gezeigt, dass sich die Myofibroblasten weiter zu Matrifibrozyten differenzieren, die zur Differenzierung und Erhaltung der Narbe beitragen (Fu et al., 2018).

Im Gegensatz dazu besitzen Arten wie Zebrafisch, Axolotl und Hydra die bemerkenswerte Fähigkeit, ihr beschädigtes Gewebe zu regenerieren (Joven et al., 2019; Murawala et al., 2012; Poss et al., 2002; Vogg et al., 2019). Nach einer Verletzung induzieren diese Arten kein myofibroblastenvermitteltes fibrogenes Genprogramm, sondern eine regenerative Reprogrammierung auf Transkriptionsebene. Die regenerative Reprogrammierung einer Zelle ist der Übergang von einer homöostatischen Transkriptionslandschaft zu einem regenerativen Genprogramm. Bei dieser Reprogrammierung werden Tausende von pro-regenerativen Genen induziert und gleichzeitig die Expression mehrerer anti-regenerativer Gene herunterreguliert. Infolge dieser Transkriptionsveränderungen werden lebenswichtige zelluläre Prozesse, die für die Regeneration erforderlich sind, wie Proliferation, Dedifferenzierung, Redifferenzierung und Migration, aktiviert. Dieses Phänomen ist bei den vollständig regenerativen Axolotl- und den teilweise

regenerativen Xenopus-Gliedmaßen in den aus dem Bindegewebe stammenden Zellen gut dokumentiert (Gerber et al., 2018; Lin et al., 2021). Eine gestörte regenerative Reprogrammierung führt meist zu fibrotischer Narbenbildung.

Bei der Reparatur von menschlichem Gewebe besteht die Idee darin, die fibrotische Vernarbung zu begrenzen und so eine optimale Gewebefunktion zu unterstützen. Gleichzeitig wird versucht, die Regeneration zu fördern, indem die regenerationsfördernden Signale verstärkt werden, die die regenerativen Spezies nach einer Gewebeschädigung einsetzen. Mehrere Jahrzehnte der Forschung haben zur Entdeckung von mehr als ein paar solcher pro-regenerativen und anti-fibrotischen Moleküle geführt. Die meisten, wenn nicht alle dieser Signalmoleküle beeinflussen jedoch auch andere lebenswichtige zelluläre Prozesse, die für die Homöostase erforderlich sind. Daher besteht eines der Hauptziele dieser Studie darin, verletzungsspezifische Mechanismen zu identifizieren, die nicht nur die Regeneration einleiten, sondern auch die fibrotische Narbenbildung begrenzen.

Zu diesem Zweck, habe ich den Interleukin-11/Stat3-Signalweg als den ersten globalen Regulator der Regeneration im Zebrafisch identifiziert. Kurz gesagt zeige ich, dass der Interleukin-11-Signalweg die Regeneration fördert, indem er zwei entscheidende zelluläre Aspekte der Reaktion auf eine Verletzung reguliert - (1) er fördert die regenerative Reprogrammierung und ermöglicht dadurch die Wiederbesiedlung des verletzten Bereichs mit Zellen und (2) er begrenzt die Säugetier-ähnliche fibrotische Narbenbildung, indem er die Myofibroblasten-Differenzierung und den TGF-β-Signalweg, den Hauptregulator der Gewebefibrose, hemmt.

7.2. Ergebnisse

7.2.1. Zebrafische zeigen eine begrenzte Narbenbildung als Reaktion auf Herzverletzungen

Fibrotische Narbenbildung begrenzt die Regeneration. Um diesen Gedanken zu überprüfen, verglich ich die fibrotische Reaktion in Bezug auf die Myofibroblasten-Differenzierung im regenerativen Zebrafischherz direkt mit dem, was im erwachsenen

Mausherz gezeigt wurde. Ich verfolgte die Abstammung der im Gewebe ansässigen Fibroblasten und Endothelzellen nach einer Kryoverletzung des Herzens im erwachsenen Zebrafisch. Ich beobachtete, dass sich nur ~12 % der gewebeansässigen Fibroblasten in Myofibroblasten differenzierten (**Fig. 4.1B und C**), im Vergleich zu ~95 % bei erwachsenen Mäusen (Fu et al., 2018). In ähnlicher Weise beobachtete ich, dass nur 4 % der aus dem Endothel stammenden Zellen ein Myofibroblasten-Schicksal erlangten (**Fig. 4.1B und D**), verglichen mit ~35 % in der erwachsenen Maus (Aisagbonhi et al., 2011). Diese Daten zeigen, dass Zebrafische nach einer Kryoverletzung des Herzens nur eine begrenzte fibrotische Vernarbungsreaktion zeigen. Daher stellten wir die Hypothese auf, dass Zebrafische Mechanismen einsetzen, um die verletzungsbedingte Fibrose zu begrenzen und die Regeneration zu fördern.

7.2.2. Die Interleukin-6-Familie der Zytokin-vermittelten Stat3-Signalgebung wirkt in Zebrafischen regenerationsfördernd

Um diese Mechanismen zu identifizieren, führte ich ein vergleichendes Expressionsprofil des adulten Zebrafischventrikels während der Regeneration und physiologischer Belastung durch, die beide als kardioprotektiv bekannt sind (Konhilas John P. et al., 2006; Shephard Roy J. und Balady Gary J., 1999). Das Experiment identifizierte ~180 Gene, die sowohl während der Regeneration als auch während des Trainings reguliert waren (**Appendix I**). Eine Analyse der kanonischen Signalwege und der vorgelagerten Regulatoren dieser Gene ergab, dass die Interleukin-6-Familie der Zytokin-vermittelten Stat3-Signalgebung ein vielversprechender Kandidat ist (**Fig. 4.2; Appendix II**).

Als nächstes stellten wir diese Hypothese in Frage, indem wir die Regenerationsfähigkeiten von *il6st* und *stat3* Zebrafischmutanten testeten, denen die Il-6-Familie/Stat3-Signalübertragung weitgehend fehlt (Liu et al., 2017). Il6st (Gp130) ist der gemeinsame Co-Rezeptor aller Zytokine der Il-6-Familie und ist allein für die nachgeschaltete Signalübertragung verantwortlich, während Stat3 der Effektor-Transkriptionsfaktor ist (Rose-John, 2018). Diese beiden Mutanten überleben nicht bis zum Erwachsenenalter, außer gelegentlich mit schweren Knochendeformationen,

was Studien zur Regeneration im Erwachsenenalter ausschließt. Daher untersuchten wir die Regeneration der larvalen Schwanzflosse nach einer Amputation. Beide Mutanten zeigten eine ähnliche und stark beeinträchtigte Schwanzflossenregeneration (**Fig. 4.3**) (Miskolci et al., 2019). Diese Daten zeigen, dass das durch die Il-6-Familie vermittelte Stat3 für die Regeneration im Zebrafisch erforderlich ist, zumindest im Larvenstadium.

7.2.3. Interleukin-11-Signalübertragung ist ein globaler Regulator der Regeneration im Zebrafisch

Um die spezifischen Zytokine der Il-6-Familie zu identifizieren, die für die Regeneration erforderlich sind, habe ich Genexpressionsanalysen nach Verletzungen im erwachsenen Herzen und in den Flossen durchgeführt. Dabei habe ich festgestellt, dass die beiden Paraloge der Interleukin-11-Zytokin-Gene *il11a* und *il11b* nicht nur am stärksten hochreguliert, sondern auch am stärksten exprimiert werden, und zwar nach einer Gewebeschädigung, unabhängig vom Organ/Körperanhängsel (**Fig. 4.4 und 4.5**). Bei der Literaturrecherche stellte ich außerdem fest, dass die Il-11-Induktion während der Regeneration evolutionär konserviert ist (Darnet et al., 2019; Fang et al., 2013; Gerber et al., 2018; Tsujioka et al., 2017; Wang et al., 2020). Daraufhin beschloss ich, die Rolle der Il-11-Signalübertragung während der Regeneration und Narbenbildung zu untersuchen. Zu diesem Zweck erzeugte ich mithilfe der CRISPR-Cas9-Mutagenese globale Knockouts für das Il-11-Rezeptor-Gen (*il11ra*) und die beiden Zytokin-Paralog-Gene (*il11a* und *il11b*) (**Fig. 4.7**). Anschließend habe ich diese mutierten Allele mit verschiedenen Verletzungsmodellen in unterschiedlichen Entwicklungsstadien getestet.

Ähnlich wie bei *il6st*- und *stat3*-Mutanten konnte ich beobachten, dass *il11ra*- und *il11a*-Mutanten nach einer Amputation eine stark beeinträchtigte larvale Schwanzflossenregeneration aufwiesen, während *il11b* Mutanten keinen solchen Phänotyp zeigten (**Fig. 4.8**). Diese Daten zeigen, dass der Il11a-Il11ra-Il6st-Stat3-Signalweg für die larvale Schwanzflossenregeneration erforderlich ist. Bei der Analyse der Regeneration der adulten Schwanzflosse habe ich festgestellt, dass *il11ra* und *il11a* Mutanten ein beeinträchtigtes Nachwachsen aufweisen. *il11ra* Mutanten wiesen

den schwersten Phänotyp auf, da sie nicht über die Amputationsebene hinauswuchsen (**Fig. 4.9**). Daher wählte ich das Allel *il11ra* für die weitere Analyse aus. Als Nächstes testete ich die Schuppenregeneration. *il11ra* Mutanten zeigten nach dem Zupfen ein beeinträchtigtes Nachwachsen der Schuppen (**Fig. 4.11**). Schließlich beobachtete ich nach einer Kryoverletzung des Herzens, dass *il11ra* Mutanten nach 90 dpci (days post cryo-injury/Tage nach der Kryoverletzung) eine permanente, kollagene Narbe aufwiesen, während die Wildtypen eine nahezu vollständige Regeneration zeigten (**Fig. 4.12**) (Chablais et al., 2011). Da ich globale Knockouts verwendet habe, habe ich außerdem eine transgene *il11ra* Re-Expressionslinie in *il11ra* Mutanten erzeugt, um die verletzungsspezifischen Anforderungen an die Il-11-Signalübertragung zu testen. Bemerkenswert ist, dass die Re-Expression von *il11ra* in *il11ra* Mutanten nach einer Verletzung den Phänotyp der Flossenregeneration rettete (**Fig. 4.13**). Zusammengenommen zeigen diese Daten, dass die verletzungsinduzierte Il-11-Signalübertragung ein globaler Regulator der Regeneration im Zebrafisch ist.

7.2.4. Il-11 fördert die regenerative Neuprogrammierung und Zellrepopulation

Als nächstes versuchte ich, die zellulären und molekularen Mechanismen aufzudecken, die der Il-11-Signalweg zur Förderung der Regeneration einsetzt. Zu diesem Zweck erstellte ich Expressionsprofile von Wildtyp- und *il11ra*-Mutantenflossen und Herzen nach Verletzungen durch. In den mutierten Flossenstümpfen beobachtete ich eine beeinträchtigte Induktion von Flossenregenerationsgenen, darunter *fgf20a* (Whitehead et al., 2005), *hspd1* (Makino et al., 2005) und die evolutionär konservierten Flossenregenerationsgene, die kürzlich identifiziert wurden (Wang et al., 2020) (**Fig. 4.14 und 4.15A; Appendix III**). Neben der fehlenden Induktion von pro-regenerativen Genen zeigten die Mutanten auch eine gestörte Herunterregulierung von Genen, die normalerweise während der Regeneration stillgelegt werden, darunter *bglap* (*osteocalcin*). Osteocalcin ist ein Marker für reife Osteoblasten, der normalerweise speziell an der Amputationsebene herunterreguliert wird, was auf eine Dedifferenzierung der Osteoblasten hinweist (Knopf et al., 2011; Sousa et al., 2011). Unter Verwendung einer *bglap*-Reporterlinie konnte ich beobachten, dass die Mutanten eine stark beeinträchtigte Reprogrammierung und Migration der Osteoblasten aufweisen (**Fig. 4.15C bis E**). Ähnlich wie bei den Defekten in den

Flossen der erwachsenen Mutanten beobachtete ich auch eine gestörte Induktion der Gene für das Regenerationsprogramm der Larvenflosse (**Fig. 4.16**) (Yoshinari et al., 2009). Eine ähnliche Analyse des Transkriptoms des Herzens erwachsener Mutanten ergab eine beeinträchtigte Induktion bekannter regenerativer Gene, während die anti-regenerativen Gene nicht herunterreguliert wurden (Aghajanian et al., 2019; Dogra et al., 2017; González-Rosa et al., 2017). Weitere Analysen zeigten einen beeinträchtigten Retinsäure-Signalweg speziell im Endokard und eine verminderte Ablagerung von regenerativer Matrix, einschließlich Fibronectin (**Fig. 4.17, 4.18 und 4.19**). Darüber hinaus beobachtete ich auch eine beeinträchtigte Fibronectin-Induktion in den larvalen Schwanzflossen sowie in den erwachsenen Flossen. Fibronectin ist eine evolutionär konservierte, migrationsfördernde ECM-Komponente, die nachweislich eine wichtige Rolle bei der Wiederbesiedlung des verletzten Bereichs im Zebrafischherz durch Kardiomyozyten spielt (Calve et al., 2010; Govindan und Iovine, 2015; Li et al., 2020; Wang et al., 2013). Daher beschloss ich, das Verhalten der Kardiomyozyten in den *il11ra* Mutanten zu untersuchen. Überraschenderweise konnte ich keine Verringerung der Proliferation der Kardiomyozyten bei 7 dpci beobachten, aber einen geringfügig abnehmenden Trend bei 14 dpci (**Fig. 4.20**). Die migrationsunterstützende Protrusionsaktivität der Kardiomyozyten ist jedoch ab 72 hpci bis 14 dpci stark beeinträchtigt, was mit einer permanenten Vernarbung bei 90 dpci übereinstimmt (**Fig. 4.21**). In Übereinstimmung mit diesen Daten beobachtete ich, dass die regenerierenden Kardiomyozyten, die von der *Tg(gata4:EGFP)*-Linie markiert wurden, nur bei 14 dpci, nicht aber bei 7 dpci, eine stark beeinträchtigte Abdeckung des verletzten Bereichs zeigten (**Fig. 4.22**).

Zusammengenommen zeigen diese Daten, dass der Il-11-Signalweg globale und gewebespezifische Aspekte der regenerativen Reprogrammierung reguliert und die Zellneubesiedlung des verletzten Bereichs fördert.

7.2.5. Il-11 begrenzt die säugetierähnliche Narbenbildung nach Verletzungen

Jüngste Studien an Säugetieren zeigen, dass die IL-11-Signalübertragung pro-fibrotisch ist (Ng et al., 2019; Schafer et al., 2017), während meine und andere Daten (Fang et al., 2013; Tsujioka et al., 2017) auf eine pro-regenerative Rolle in

regenerativen Organismen hinweisen. Daher beschloss ich, die Fibrose in *il11ra* Mutanten zu untersuchen, um die Hauptunterschiede zwischen der Il-11-Signalübertragung bei Maus und Zebrafisch zu ermitteln. In Übereinstimmung mit dem Phänotyp der permanenten Narbenbildung im Herzen und in der Flosse zeigten die Mutanten eine stark erhöhte Myofibroblasten-Differenzierung und Persistenz in beiden Geweben nach einer Verletzung (**Fig. 4.23**). Die verstärkte Myofibroblasten-Differenzierung geht einher mit einer gleichzeitigen Abnahme der Stat3-Signalgebung und einer Hochregulierung von pro-fibrotischen ECM-Umbau- und Säugetierfibrose-assoziierten Signalwegen, einschließlich des TGF-β-Signalweges (**Fig. 4.24**). Eine unvoreingenommene funktionelle Gensatz-Anreicherungsanalyse zeigte, dass die *il11ra*-Mutantenfibrose der Herzfibrose erwachsener Säugetiere nach Myokardinfarkt ähnelt, im Gegensatz zur Regeneration im neonatalen Mausherz (**Fig. 4.26**). Zusammengenommen zeigen meine Daten, dass der Il-11-Signalweg das Säugetier-ähnliche Vernarbungsprogramm nach Gewebeschäden im Zebrafisch begrenzt.

7.2.6. Il-11 begrenzt die Endothelial-Mesenchymale Transition (EndoMT)

Um die zellulären Mechanismen der mutierten *il11ra*-Herzfibrose zu verstehen, analysierte ich die Expressionsmuster von *il11ra* anhand veröffentlichter Einzelzell-RNA-seq-Datensätze (Hou et al., 2020; Spanjaard et al., 2018). Ähnlich wie sein Ortholog bei Säugetieren wird *il11ra* hauptsächlich in den Bindegewebs- und Endothelzellen exprimiert (**Fig. 4.27**). In Übereinstimmung mit diesen Ergebnissen zeigten sortierte Endothelzellen eine höhere Expression von *il11ra* im Vergleich zu nicht endothelialen Zellen im adulten Zebrafischherz. Zur Unterstützung dieser Daten beobachtete ich eine stark beeinträchtigte p-Stat3-Aktivierung in den mutierten Endokardzellen im verletzten Bereich (**Fig. 4.28**). Außerdem waren die Endothelzellen der *il11ra*-Mutanten als Reaktion auf die Kryoverletzung hyperinvasiv und desorganisiert (**Fig. 4.29**). Die *il11ra*-Expressionsmuster, die endothelspezifischen Defekte in il11ra-Mutanten und die verstärkte Myofibroblasten-Differenzierung veranlassten mich zu der Hypothese, dass der Il-11-Signalweg die EndoMT begrenzt. EndoMT ist ein Phänomen, bei dem Endothelzellen ihre Eigenschaften verlieren und ein Fibroblasten-ähnliches Verhalten annehmen. RT-qPCR-Analysen für EndoMT-assoziierte Gene (Chen et al., 2020) und Lineage-Tracing von Endothelzellen

bestätigten eine dramatische Zunahme der EndoMT in den Mutanten im Vergleich zum Wildtyp (**Fig. 4.30 und 4.31**). Kurz gesagt, einige der von der Mutante stammenden Endothelzellen im verletzten Bereich verloren die endothelialen Membranmarker und gewannen mesenchymale (Myofibroblastenmarker) hinzu, was zur Zunahme der Myofibroblastendifferenzierung beitrug (**Fig. 4.31**). Darüber hinaus zeigten RT-qPCRs an sortierten Endothelzellen eine Zunahme mesenchymaler Marker und pro-fibrotischer ECM-Gene und eine Abnahme endothelialer Marker in den Mutanten im Vergleich zu den Wildtypen (**Fig. 4.32**). Darüber hinaus zeigte sich beim Lineage-Tracing epikardialer Zellen eine Zunahme des epikardialen Beitrags zur Myofibroblasten-Differenzierung in den Mutanten (**Fig. 4.33**).

Zusammengenommen zeigen diese Daten, dass der Il-11/Stat3-Signalweg die verletzungsinduzierte Myofibroblasten-Differenzierung und den pro-fibrotischen ECM-Umbau sowohl in den endothelialen als auch in den epikardialen Abstammungslinien begrenzt.

7.2.7. Il-11-Signalgebung vermittelt den Crosstalk zwischen Endothel und Kardiomyozyten

Um zu testen, ob die verstärkte Fibrose in Endothelzellen bei *il11ra*-Mutanten zu Defekten bei der Kardiomyozytenmigration führt, habe ich eine transgene Linie erzeugt, die il11ra bedingt re-exprimiert. Zu diesem Zweck rettete die endothelspezifische Re-Expression von *il11ra* in *il11ra*-Mutanten nicht nur endotheliale Defekte, einschließlich EndoMT und Hyperinvasion, sondern auch die Kardiomyozytenmigration auf Wildtypniveau (**Fig. 4.35 und 4.36**). Diese Daten zeigen, dass die Il-11-Signalisierung in Endothelzellen die Kardiomyozytenmigration nach kardialer Kryoverletzung in *il11ra*-Mutanten ermöglicht.

7.2.8. Rückkopplungsinteraktionen zwischen den IL-11 und TGF-β-Signalwegen

Die IL-11-Studien an Säugetieren zeigten, dass IL-11 dominant von TGF-β-reguliert wird und die Fibrose in Fibroblasten fördert (Schafer et al., 2017). Bemerkenswerterweise beobachtete ich eine konsistente Induktion von TGF-β-Signalen in *il11ra*-mutierten Herzen und Flossen nach Verletzungen. Diese Daten

deuten auf eine mögliche Rückkopplungshemmung der TGF-β-Signalgebung durch die Il-11-Signalgebung hin. In Übereinstimmung mit dieser Hypothese beobachtete ich in den mutierten Herzen nach der Verletzung einen Anstieg der endothelspezifischen p-Smad3-Aktivität (**Fig. 4.37**). Um diese Rückkopplungen zu entschlüsseln, habe ich auf kultivierte menschliche Endothelzellen zurückgegriffen. Zunächst beobachtete ich, ähnlich wie bei Fibroblasten (Schafer et al., 2017), dass IL-11 ein transkriptionelles Ziel von TGF-β-Signalen ist (**Fig. 4.38D**). Mit TGFB- und IL-11-Behandlungen sowie *IL11RA*-Knockdown-Experimenten bestätigte ich, dass TGF-β IL-11 induziert, das wiederum seinen übergeordneten Aktivator, das TGF-β-Signal, hemmt (**Fig. 4.38**). Um schließlich zu testen, ob die pro-fibrotischen Effekte der Blockierung des IL-11-Signals über den TGF-β-Signalweg laufen, verwendete ich einen TGF-β-Inhibitor auf *IL11RA*-knockdown-HUVECs. In Übereinstimmung mit meinen *In vivo*-Daten führte das Ausschalten von *IL11RA* zu einem Anstieg der fibrotischen Genexpression, die durch die Blockierung der TGF-β-Funktion vollständig gerettet wurde (**Fig. 4.38E**). Diese Daten zeigen eine neuartige Rückkopplung zwischen IL-11 und TGF-β-Signalwegen, die die Gewebefibrose und -regeneration reguliert.

7.3. Diskussion und Schlussfolgerung

In dieser Studie identifiziere ich durch tiefgreifende Phänotypisierung und umfangreiche genetische Funktionsverlust-Analysen, angefangen bei den Liganden (*il11a* und *il11b*) über die Rezeptoren (*il11ra* und *il6st*) bis hin zum Transkriptionsfaktor (*stat3*), den ersten globalen Regulator der Regeneration im Zebrafisch - die Il-11/Stat3-Signalübertragung - und tauche tiefer in die nachgeschalteten zellulären und molekularen Mechanismen ein. Auf mechanistischer Ebene zeige ich, dass der verletzungsbedingte Il-11-Signalweg die regenerative Neuprogrammierung fördert und eine Fibrose, wie sie bei Säugetieren auftritt, begrenzt, was die Regeneration im Zebrafisch unterstützt. Insbesondere zeige ich, dass die Il-11-Signalisierung die EndoMT und die TGF-β-Signalisierung begrenzt und so die verletzungsbedingte Fibrose unter Kontrolle hält.

Il-11-Signalisierung wurde in mehreren Säugetier- und Xenopus-Studien als pro-regenerativ und kardioprotektiv vorgeschlagen (Obana Masanori et al., 2010; Tamura et al., 2018; Tsujioka et al., 2017). In krassem Gegensatz dazu zeigen neuere Studien an Säugetieren, dass IL-11 pro-fibrotisch wirkt, und deuten darauf hin, dass IL-11-Blocker eingesetzt werden können, um die Gewebefibrose zu mildern (Lim et al., 2020; Ng et al., 2019; Schafer et al., 2017). Meine Daten unterstützen eindeutig die pro-regenerative und anti-fibrotische Seite der Debatte. Weitere artenübergreifende vergleichende Analysen werden von großer Bedeutung sein, um diese Diskrepanz zu entschlüsseln - seien es die Unterschiede, die im Laufe der Evolution entstanden sind (regenerative vs. nicht-regenerative Arten) oder nachgeschaltete Signalmechanismen (Stat3 vs. Erk). Insgesamt deuten meine Daten zusammen mit den widersprüchlichen Daten von Säugetieren stark darauf hin, dass die Geheimnisse der Geweberegeneration in den Unterschieden zwischen regenerativen und nicht-regenerativen Arten der IL-11-Signalübertragung nachgeschaltet sind. Darüber hinaus habe ich die nicht-regenerative *il11ra*-Mutante als wertvolles Zebrafischmodell zur Untersuchung der Fibrose bei Säugetieren etabliert.

8. English summary

8.1. Introduction

The two diametrically opposing outcomes after tissue damage are regeneration and fibrotic scarring (Gurtner et al., 2008). After injury, adult mammals predominantly induce fibrotic scarring, which most often leads to patient lethality. Fibrotic scarring is the deposition of excessive extracellular matrix that matures and hinders tissue function. The scarring response is mainly orchestrated by myofibroblasts, which arise only upon tissue damage, from various cellular origins, including tissue resident fibroblasts, endothelial cells and circulating blood cells (Davis and Molkentin, 2014). Other than the scar-forming extracellular matrix genes, myofibroblasts express contractile machinery, including α-Smooth muscle actin (αSMA/Acta2), in order to confer contractile properties to the damaged tissue. It has also been shown that the myofibroblasts differentiate further to become matrifibrocytes, which help in scar maturation and maintenance (Fu et al., 2018).

On the contrary, species like zebrafish, axolotl and hydra, possess the remarkable capacity to regenerate their damaged tissues (Joven et al., 2019; Murawala et al., 2012; Poss et al., 2002; Vogg et al., 2019). After injury, instead of inducing a myofibroblast-mediated fibrogenic gene program, these species induce regenerative reprogramming at the transcriptional level. Regenerative reprogramming of a cell is the shift from a homeostatic transcriptional landscape to a regenerative gene program. This reprogramming includes inducing thousands of pro-regenerative genes, and a simultaneous silencing of several anti-regenerative genes. As a result of these transcriptional changes, vital cellular processes needed for regeneration, including proliferation, dedifferentiation, re-differentiation and migration, are activated. This phenomenon is well documented in the fully regenerative axolotl and the partial regenerative *Xenopus* limbs in the connective tissue-derived cells (Gerber et al., 2018; Lin et al., 2021). Impaired regenerative reprogramming most often leads to fibrotic scarring.

In human tissue repair, the idea has been to limit fibrotic scarring, thereby aiding optimal tissue function. Another side of the same coin is to induce regeneration by

boosting the pro-regenerative signals that the regenerative species employ after tissue damage. Several decades of research has led to the discovery of more than a few such pro-regenerative and anti-fibrotic molecules. However, most, if not all of these signaling molecules also affect other vital cellular processes that are required for day-to-day survival. Hence, one of the main aims of this study is to identify injury-specific mechanisms that not only induce regeneration, but also limit fibrotic scarring.

To this end, I identified Interleukin-11/Stat3 signaling as the first global regulator of regeneration in zebrafish. Briefly, I show that Interleukin-11 signaling promotes regeneration by regulating two crucial cellular aspects in response to injury – (1) it promotes regenerative reprogramming thereby allowing cell repopulation of the injured area and (2) it limits mammalian-like fibrotic scarring by inhibiting myofibroblast differentiation and TGF-β signaling, the master regulator of tissue fibrosis.

8.2. Results

8.2.1. Zebrafish display limited scarring in response to cardiac injury

Fibrotic scarring limits regeneration. To test this notion, I directly compared the fibrotic response in terms of myofibroblast differentiation in the regenerative zebrafish heart with that of what was shown in the adult mouse heart. I lineage traced the tissue resident fibroblasts and endothelial cells after a cardiac cryoinjury in adult zebrafish. I observed that only ~12% of the tissue resident fibroblasts differentiated into myofibroblasts (**Fig. 4.1B and C**) when compared to ~95% in adult mouse (Fu et al., 2018). Similarly, I observed that only 4% of the endothelial-derived cells acquired a myofibroblast fate (**Fig. 4.1B and D**) when compared to ~35% in the adult mouse (Aisagbonhi et al., 2011). These data show that zebrafish display limited fibrotic scarring response after cardiac cryoinjury. Hence, we hypothesized that zebrafish employ mechanisms to limit injury-induced fibrosis and promote regeneration.

8.2.2. Interleukin-6 family of cytokine-mediated Stat3 signaling is pro-regenerative in zebrafish

To identify these mechanisms, I performed a comparative expression profiling of the adult zebrafish ventricle during regeneration and physiological exercise, both of which

are known to be cardioprotective (Konhilas John P. et al., 2006; Shephard Roy J. and Balady Gary J., 1999). The experiment resulted in ~180 co-regulated genes during both regeneration and exercise. Canonical pathway and upstream regulator analysis on these genes showed that Interleukin-6 family of cytokine-mediated Stat3 signaling as a promising candidate pathway (**Fig. 4.2**).

Next, we challenged this hypothesis by testing the regenerative capabilities of zebrafish that broadly lack Il-6 family/Stat3 signaling – *il6st* and *stat3* mutants (Liu et al., 2017). Il6st (Gp130) is the common co-receptor of all the Il-6 family of cytokines and is solely responsible for the downstream signaling, while Stat3 is the effector transcription factor (Rose-John, 2018). Both these mutants do not survive to adulthood, except occasionally with similar bone deformities, precluding adult regeneration studies. Hence, we tested for their larval fin fold regeneration after amputation. Both the mutants displayed a similar and severely impaired fin fold regeneration (**Fig. 4.3**) (Miskolci et al., 2019). These data show that Il-6 family-mediated Stat3 is required for regeneration in zebrafish, at least at the larval stages.

8.2.3. Interleukin-11 signaling is a global regulator of regeneration in zebrafish

To identify the specific Il-6 family of cytokine that is required for regeneration, I have performed gene expression analysis after injury in the adult heart and fins. I have identified that both the paralogues of Interleukin-11 cytokine genes – *il11a* and *il11b* – are not only the highest upregulated, but also the highest expressed after tissue damage, irrespective of the organ/appendage (**Fig. 4.4 and 4.5**). By literature survey, I also noticed that Il-11 induction during regeneration is evolutionarily conserved (Darnet et al., 2019; Fang et al., 2013; Gerber et al., 2018; Tsujioka et al., 2017; Wang et al., 2020). I then decided to follow up on the role of Il-11 signaling during regeneration and scarring. To this end, using CRISPR-Cas9 mutagenesis, I generated zebrafish global knockouts for the Il-11 receptor gene (*il11ra*) and both the cytokine paralogue genes (*il11a* and *il11b*) (**Fig. 4.7**). I then challenged these mutant alleles with various injury models at different developmental stages.

Similar to *il6st* and *stat3* mutants, I have observed that *il11ra* and *il11a* mutants displayed a severely impaired larval fin fold regeneration after amputation, while *il11b*

did not (**Fig. 4.8**). These data show that Il11a-Il11ra-Il6st-Stat3 signaling is required for larval fin fold regeneration. By analyzing regeneration in the adult caudal fin, I have observed that *il11ra* and *il11a* mutants displayed impaired regrowth. Notably, *il11ra* mutants displayed the most severe phenotype with no outgrowth past the amputation plane (**Fig. 4.9**). Hence, I chose the *il11ra* allele for further analysis. Next, I tested for scale regeneration. *il11ra* mutants displayed impaired scale outgrowth after plucking (**Fig. 4.11**). Finally, after cardiac cryoinjury, I observed that *il11ra* mutants displayed a permanent, collagenous scar at 90 dpci (days post cryoinjury) when the wild types displayed near-complete regeneration (**Fig. 4.12**) (Chablais et al., 2011). In addition, since I used global knockouts, to test the injury-specific requirement for Il-11 signaling, I generated an *il11ra* re-expression transgenic line in *il11ra* mutant background. Notably, re-expression of *il11ra* in *il11ra* mutants after injury, rescued the fin regeneration phenotype (**Fig. 4.13**). Taken together, these data show that injury-induced Il-11 signaling is a global regulator of regeneration in zebrafish.

8.2.4. Il-11 promotes regenerative reprogramming and cell repopulation

Next, I sought out to uncover the cellular and molecular mechanisms that Il-11 signaling employs to promote regeneration. To this end, I performed RNA-seq on wild-type vs. *il11ra* mutant fins and hearts after injury. In the mutant fin stumps, I observed an impaired induction of fin regeneration genes, including *fgf20a* (Whitehead et al., 2005)*, hspd1* (Makino et al., 2005), and the evolutionarily conserved fin regeneration genes identified recently (Wang et al., 2020) (**Fig. 4.14 and 4.15A**). Along with this failure to induce pro-regenerative genes, the mutants also displayed impaired silencing of genes that are normally silenced during regeneration, including *bglap* (*osteocalcin*). *Osteocalcin* is a mature osteoblast marker that is normally downregulated specifically at the amputation plane, indicating osteoblast dedifferentiation (Knopf et al., 2011; Sousa et al., 2011). Using a *bglap* reporter line, I observed that the mutants displayed severely impaired osteoblast reprogramming and migration (**Fig. 4.15C to E**). Similar to the defects in adult mutant fins, I observed an impaired induction of the larval fin fold regenerative program genes as well (**Fig. 4.16**) (Yoshinari et al., 2009). A similar analysis on the adult mutant heart transcriptome identified an impaired induction of known regenerative genes, while the anti-regenerative genes failed to be

downregulated (Aghajanian et al., 2019; Dogra et al., 2017; González- Rosa et al., 2017). Further analysis showed an impaired retinoic acid signaling specifically in the endocardium and a reduced deposition of regenerative matrix, including Fibronectin (**Figs. 4.17, 4.18 and 4.19**). In addition, I also observed an impaired Fibronectin induction in the larval fin folds as well as the adult fins. Fibronectin is an evolutionarily conserved pro-migratory ECM component that has been shown to be important in driving cardiomyocyte repopulation of the injured area in the zebrafish heart (Calve et al., 2010; Govindan and Iovine, 2015; Li et al., 2020; Wang et al., 2013). Hence, I decided to assess cardiomyocyte behaviour in the *il11ra* mutants. Surprisingly, I did not observe any reduction in cardiomyocyte proliferation at 7 dpci, but a marginal decreasing trend at 14 dpci (**Fig. 4.20)**. However, the migration-assisting protrusive activity of cardiomyocytes is severely impaired starting from 72 hpci to 14 dpci, which is consistent with permanent scarring at 90 dpci (**Fig. 4.21**). In line with these data, I observed that the regenerating cardiomyocytes as labelled by the *Tg(gata4:EGFP)* line, displayed severely impaired coverage of the injured area only at 14 dpci, but not at 7 dpci (**Fig. 4.22**).

Taken together, these data show that Il-11 signaling regulates global and tissue-specific aspects of regenerative reprogramming and promotes cell repopulation of the injured area.

8.2.5. Il-11 limits mammalian-like scarring after injury

Recent studies in mammals show that IL-11 signaling is pro-fibrotic (Ng et al., 2019; Schafer et al., 2017), while my data and others (Fang et al., 2013; Tsujioka et al., 2017) indicate a pro-regenerative role in regenerative organisms. Hence, I decided to investigate fibrosis in *il11ra* mutants to identify the major differences between mouse and zebrafish Il-11 signaling. In line with the permanent scarring phenotype in the heart and fin, the mutants displayed highly increased myofibroblast differentiation and persistence in both tissues after injury (**Fig. 4.23**). The increased myofibroblast differentiation is accompanied by a concomitant decrease in Stat3 signaling and an upregulation of pro-fibrotic ECM remodeling and mammalian fibrosis-related pathways, including TGF-β signaling (**Fig. 4.24**). An unbiased gene set enrichment analysis

showed that *il11ra* mutant fibrosis is similar to adult mammalian cardiac fibrosis after myocardial infarction, as opposed to regeneration in the neonatal mouse heart (**Fig. 4.26**). Together, my data show that Il-11 signaling limits mammalian-like scarring program after tissue damage in zebrafish.

8.2.6. Il-11 limits endothelial-to-mesenchymal transition (EndoMT)

To understand the cellular mechanisms of the *il11ra* mutant cardiac fibrosis, I analysed the expression patterns of *il11ra* using published single-cell RNA-seq datasets (Hou et al., 2020; Spanjaard et al., 2018). Similar to its mammalian orthologue, *il11ra* is mainly expressed in the connective tissue and endothelial lineages (**Fig. 4.27**). In line with these findings, sorted endothelial cells displayed higher expression of *il11ra* when compared with non-endothelial cells in the adult zebrafish heart. Supporting these data, I observed a severely impaired p-Stat3 activation in the mutant endocardial cells in the injured area (**Fig. 4.28**). Furthermore, *il11ra* mutant endothelial cells were hyper-invasive and disorganized in response to cryoinjury (**Fig. 4.29**). The *il11ra* expression patterns, endothelial-specific defects in *il11ra* mutants, and the increased myofibroblast differentiation led me to hypothesize that Il-11 signaling limits EndoMT. EndoMT is a phenomenon where endothelial cells lose their properties and gain fibroblast-like behaviour. RT-qPCR analysis for EndoMT-associated genes (Chen et al., 2020) and lineage tracing endothelial cells confirmed a dramatic increase in EndoMT in the mutants when compared with wild types (**Figs. 4.30 and 4.31**). Briefly, some of the mutant endothelial-derived cells in the injured area lost the endothelial membrane markers and gained mesenchymal (myofibroblast markers), thereby contributing to the increase in myofibroblast differentiation (**Fig. 4.31**). Furthermore, RT-qPCRs on sorted endothelial cells showed an increase in mesenchymal markers and pro-fibrotic ECM genes, and a decrease in endothelial markers in the mutants when compared with the wild types (**Fig. 4.32**). In addition, lineage tracing epicardial-derived cells also showed an increase in the epicardial contribution to myofibroblast differentiation in the mutants (**Fig. 4.33**).

Taken together, these data show that Il-11/Stat3 signaling limits injury-induced myofibroblast differentiation and pro-fibrotic ECM remodeling in both endothelial and epicardial lineages.

8.2.7. Il-11 signaling-mediated endothelial-to-cardiomyocyte crosstalk

In *il11ra* mutants, to test if the increased fibrosis in endothelial cells leads defects in cardiomyocyte migration, I generated a transgenic line that conditionally re-expresses *il11ra*. To this end, endothelial-specific re-expression of *il11ra* in *il11ra* mutants not only rescued endothelial defects, including EndoMT and hyper-invasion, but also rescued cardiomyocyte migration to wild-type levels (**Fig. 4.35 and 4.36**). These data show that Il-11 signaling in endothelial cells allows cardiomyocyte migration after cardiac cryoinjury in *il11ra* mutants.

8.2.8. Feedback interactions between IL-11 and TGF-β signaling pathways

The mammalian IL-11 studies showed that IL-11 is a dominant TGF-β downstream target that promotes fibrosis in fibroblasts (Schafer et al., 2017). Notably, I observed a consistent induction of TGF-β signaling in *il11ra* mutant hearts and fins after injury. These data suggested a potential feedback inhibition of TGF-β signaling by Il-11 signaling. In line with this hypothesis, I observed an increase in endothelial-specific p-Smad3 activity in the mutant hearts after injury (**Fig. 4.37**). To tease these feedback interactions apart, I resorted to cultured human endothelial cells. First, similar to what was shown in fibroblasts (Schafer et al., 2017), I observed that IL-11 is a transcriptional target of TGF-β signaling (**Fig. 4.38D**). Using TGFB, and IL-11 treatments, as well as *IL11RA* knockdown experiments, I confirmed that TGF-β induces IL-11, which in turn inhibits its parent activator, TGF-β signaling (**Fig. 4.38**). Finally, to test whether the pro-fibrotic effects of blocking IL-11 signaling go through the TGF-β pathway, I used a TGF-β inhibitor on *IL11RA* knocked down HUVECs. Consistent with my *in vivo* data, knocking down *IL11RA* led to an increase in fibrotic gene expression, which was completely rescued by blocking TGF-β function (**Fig. 4.38E**). These data show a novel feedback interaction between IL-11 and TGF-β signaling pathways that regulates tissue fibrosis and regeneration.

8.3. Discussion and conclusion

In this study, using deep phenotyping and extensive genetic loss-of-function analysis starting from the ligands (*il11a* and *il11b*), through the receptors (*il11ra* and *il6st*), to the transcription factor (*stat3*), I identify the first global regulator of regeneration in zebrafish – Il-11/Stat3 signaling – and dive deeper into the downstream cellular and molecular mechanisms. Mechanistically, I show that injury-induced Il-11 signaling promotes regenerative reprogramming and limits mammalian-like fibrosis, supporting regeneration in zebrafish. Specifically, I show that Il-11 signaling limits EndoMT and TGF-β signaling, keeping injury-induced fibrosis under check.

Il-11 signaling was suggested to be pro-regenerative and cardioprotective in several mammalian and *Xenopus* studies (Obana Masanori et al., 2010; Tamura et al., 2018; Tsujioka et al., 2017). In stark contrast, recent mammalian studies show that IL-11 is pro-fibrotic and point at using IL-11 blockers to mitigate tissue fibrosis (Lim et al., 2020; Ng et al., 2019; Schafer et al., 2017). My data clearly support the pro-regenerative and anti-fibrotic side of the debate. Further cross-species comparative analyses will be of great importance to disentangle this discrepancy – be it the differences that arose during evolution (regenerative vs. non-regenerative species) or downstream signaling mechanisms (Stat3 vs. Erk). Overall, my data, together with the contradicting mammalian data strongly indicate that the secrets of tissue regeneration lie downstream of IL-11 signaling, in the differences between regenerative and non-regenerative species. Furthermore, I also establish the non-regenerative *il11ra* mutant as an invaluable zebrafish model to study mammalian fibrosis.

9. References

Aghajanian, H., Kimura, T., Rurik, J.G., Hancock, A.S., Leibowitz, M.S., Li, L., Scholler, J., Monslow, J., Lo, A., Han, W., Wang, T., Bedi, K., Morley, M.P., Linares Saldana, R.A., Bolar, N.A., McDaid, K., Assenmacher, C.-A., Smith, C.L., Wirth, D., June, C.H., Margulies, K.B., Jain, R., Puré, E., Albelda, S.M., Epstein, J.A., 2019. Targeting cardiac fibrosis with engineered T cells. Nature 573, 430–433. https://doi.org/10.1038/s41586-019-1546-z

Aisagbonhi, O., Rai, M., Ryzhov, S., Atria, N., Feoktistov, I., Hatzopoulos, A.K., 2011. Experimental myocardial infarction triggers canonical Wnt signaling and endothelial-to-mesenchymal transition. Dis Model Mech 4, 469–483. https://doi.org/10.1242/dmm.006510

Alexanian, M., Przytycki, P.F., Micheletti, R., Padmanabhan, A., Ye, L., Travers, J.G., Gonzalez-Teran, B., Silva, A.C., Duan, Q., Ranade, S.S., Felix, F., Linares-Saldana, R., Li, L., Lee, C.Y., Sadagopan, N., Pelonero, A., Huang, Y., Andreoletti, G., Jain, R., McKinsey, T.A., Rosenfeld, M.G., Gifford, C.A., Pollard, K.S., Haldar, S.M., Srivastava, D., 2021. A transcriptional switch governs fibroblast activation in heart disease. Nature 1–6. https://doi.org/10.1038/s41586-021-03674-1

Allanki, S., Strilic, B., Scheinberger, L., Onderwater, Y.L., Marks, A., Günther, S., Preussner, J., Kikhi, K., Looso, M., Stainier, D.Y.R., Reischauer, S., 2021. Interleukin-11 signaling promotes cellular reprogramming and limits fibrotic scarring during tissue regeneration. Science Advances. https://doi.org/10.1126/sciadv.abg6497

Anderson, J.L., Morrow, D.A., 2017. Acute Myocardial Infarction. New England Journal of Medicine 376, 2053–2064. https://doi.org/10.1056/NEJMra1606915

Awada, H.K., Hwang, M.P., Wang, Y., 2016. Towards comprehensive cardiac repair and regeneration after myocardial infarction: Aspects to consider and proteins to deliver. Biomaterials 82, 94–112. https://doi.org/10.1016/j.biomaterials.2015.12.025

Beisaw, A., Kuenne, C., Guenther, S., Dallmann, J., Wu, C.-C., Bentsen, M., Looso, M., Stainier, D.Y.R., 2020. AP-1 Contributes to Chromatin Accessibility to

Promote Sarcomere Disassembly and Cardiomyocyte Protrusion During Zebrafish Heart Regeneration. Circulation Research 126, 1760–1778. https://doi.org/10.1161/CIRCRESAHA.119.316167

Bensimon-Brito, A., Ramkumar, S., Boezio, G.L.M., Guenther, S., Kuenne, C., Helker, C.S.M., Sánchez-Iranzo, H., Iloska, D., Piesker, J., Pullamsetti, S., Mercader, N., Beis, D., Stainier, D.Y.R., 2020. TGF-β Signaling Promotes Tissue Formation during Cardiac Valve Regeneration in Adult Zebrafish. Developmental Cell 52, 9-20.e7. https://doi.org/10.1016/j.devcel.2019.10.027

Bertozzi, A., Wu, C.-C., Nguyen, P.D., Vasudevarao, M.D., Mulaw, M.A., Koopman, C.D., de Boer, T.P., Bakkers, J., Weidinger, G., 2021. Is zebrafish heart regeneration “complete”? Lineage-restricted cardiomyocytes proliferate to pre-injury numbers but some fail to differentiate in fibrotic hearts. Developmental Biology 471, 106–118. https://doi.org/10.1016/j.ydbio.2020.12.004

Bertrand, J.Y., Chi, N.C., Santoso, B., Teng, S., Stainier, D.Y.R., Traver, D., 2010. Haematopoietic stem cells derive directly from aortic endothelium during development. Nature 464, 108–111. https://doi.org/10.1038/nature08738

Bise, T., de Preux Charles, A.-S., Jaźwińska, A., 2019. Ciliary neurotrophic factor stimulates cardioprotection and the proliferative activity in the adult zebrafish heart. npj Regen Med 4, 1–14. https://doi.org/10.1038/s41536-019-0064-9

Bise, T., Sallin, P., Pfefferli, C., Jaźwińska, A., 2020. Multiple cryoinjuries modulate the efficiency of zebrafish heart regeneration. Sci Rep 10, 11551. https://doi.org/10.1038/s41598-020-68200-1

Bolger, A.M., Lohse, M., Usadel, B., 2014. Trimmomatic: a flexible trimmer for Illumina sequence data. Bioinformatics 30, 2114–2120. https://doi.org/10.1093/bioinformatics/btu170

Boskovic, S., Marín-Juez, R., Jasnic, J., Reischauer, S., Sammak, H.E., Kojic, A., Faulkner, G., Radojkovic, D., Stainier, D.Y.R., Kojic, S., 2018. Characterization of zebrafish (Danio rerio) muscle ankyrin repeat proteins reveals their conserved response to endurance exercise. PLOS ONE 13, e0204312. https://doi.org/10.1371/journal.pone.0204312

Calve, S., Odelberg, S.J., Simon, H.-G., 2010. A Transitional Extracellular Matrix Instructs Cell Behavior During Muscle Regeneration. Dev Biol 344, 259–271. https://doi.org/10.1016/j.ydbio.2010.05.007

Cao, J., Navis, A., Cox, B.D., Dickson, A.L., Gemberling, M., Karra, R., Bagnat, M., Poss, K.D., 2016. Single epicardial cell transcriptome sequencing identifies Caveolin 1 as an essential factor in zebrafish heart regeneration. Development 143, 232–243. https://doi.org/10.1242/dev.130534

Cao, J., Poss, K.D., 2018. The epicardium as a hub for heart regeneration. Nat Rev Cardiol 15, 631–647. https://doi.org/10.1038/s41569-018-0046-4

Cao, J., Wang, J., Jackman, C.P., Cox, A.H., Trembley, M.A., Balowski, J.J., Cox, B.D., De Simone, A., Dickson, A.L., Di Talia, S., Small, E.M., Kiehart, D.P., Bursac, N., Poss, K.D., 2017. Tension Creates an Endoreplication Wavefront that Leads Regeneration of Epicardial Tissue. Developmental Cell 42, 600-615.e4. https://doi.org/10.1016/j.devcel.2017.08.024

Chablais, F., Veit, J., Rainer, G., Jaźwińska, A., 2011. The zebrafish heart regenerates after cryoinjury-induced myocardial infarction. BMC Developmental Biology 11, 21. https://doi.org/10.1186/1471-213X-11-21

chanzuckerberg/cellxgene, 2020. . Chan Zuckerberg Initiative.

Chassot, B., Pury, D., Jaźwińska, A., 2016. Zebrafish fin regeneration after cryoinjury-induced tissue damage. Biology Open 5, 819–828. https://doi.org/10.1242/bio.016865

Chen, C.-H., Puliafito, A., Cox, B.D., Primo, L., Fang, Y., Di Talia, S., Poss, K.D., 2016. Multicolor Cell Barcoding Technology for Long-Term Surveillance of Epithelial Regeneration in Zebrafish. Developmental Cell 36, 668–680. https://doi.org/10.1016/j.devcel.2016.02.017

Chen, W., Li, X., Liu, D., Cui, C., Wang, X., 2020. Endothelial-to-Mesenchymal Transition: Role in Cardiac Fibrosis: Journal of Cardiovascular Pharmacology and Therapeutics. https://doi.org/10.1177/1074248420952233

Choi, W.-Y., Gemberling, M., Wang, J., Holdway, J.E., Shen, M.-C., Karlstrom, R.O., Poss, K.D., 2013. In vivo monitoring of cardiomyocyte proliferation to identify chemical modifiers of heart regeneration. Development 140, 660–666. https://doi.org/10.1242/dev.088526

Choi, W.-Y., Poss, K.D., 2012. Cardiac regeneration. Curr Top Dev Biol 100, 319–344. https://doi.org/10.1016/B978-0-12-387786-4.00010-5

Cook, S.A., Schafer, S., 2020. Hiding in Plain Sight: Interleukin-11 Emerges as a Master Regulator of Fibrosis, Tissue Integrity, and Stromal Inflammation. Annual Review of Medicine 71, 263–276. https://doi.org/10.1146/annurev-med-041818-011649

Corden, B., Lim, W.-W., Song, W., Chen, X., Ko, N.S.J., Su, L., Tee, N.G.Z., Adami, E., Schafer, S., Cook, S.A., 2020. Therapeutic Targeting of Interleukin-11 Signalling Reduces Pressure Overload–Induced Cardiac Fibrosis in Mice. J. of Cardiovasc. Trans. Res. https://doi.org/10.1007/s12265-020-10054-z

Cox, B.D., De Simone, A., Tornini, V.A., Singh, S.P., Di Talia, S., Poss, K.D., 2018. In Toto Imaging of Dynamic Osteoblast Behaviors in Regenerating Skeletal Bone. Current Biology 28, 3937-3947.e4. https://doi.org/10.1016/j.cub.2018.10.052

Cressman, D.E., Greenbaum, L.E., DeAngelis, R.A., Ciliberto, G., Furth, E.E., Poli, V., Taub, R., 1996. Liver Failure and Defective Hepatocyte Regeneration in Interleukin-6-Deficient Mice. Science 274, 1379–1383. https://doi.org/10.1126/science.274.5291.1379

Darnet, S., Dragalzew, A.C., Amaral, D.B., Sousa, J.F., Thompson, A.W., Cass, A.N., Lorena, J., Pires, E.S., Costa, C.M., Sousa, M.P., Fröbisch, N.B., Oliveira, G., Schneider, P.N., Davis, M.C., Braasch, I., Schneider, I., 2019. Deep evolutionary origin of limb and fin regeneration. PNAS 116, 15106–15115. https://doi.org/10.1073/pnas.1900475116

Davis, J., Molkentin, J.D., 2014. Myofibroblasts: Trust your heart and let fate decide. Journal of Molecular and Cellular Cardiology, Myocyte - Fibroblast Signalling in Myocardium 70, 9–18. https://doi.org/10.1016/j.yjmcc.2013.10.019

de Bakker, D.E.M., Bouwman, M., Dronkers, E., Simões, F.C., Riley, P.R., Goumans, M.-J., Smits, A.M., Bakkers, J., 2021. Prrx1b restricts fibrosis and promotes Nrg1-dependent cardiomyocyte proliferation during zebrafish heart regeneration. Development 148, dev198937. https://doi.org/10.1242/dev.198937

De Simone, A., Evanitsky, M.N., Hayden, L., Cox, B.D., Wang, J., Tornini, V.A., Ou, J., Chao, A., Poss, K.D., Di Talia, S., 2021. Control of osteoblast regeneration by

a train of Erk activity waves. Nature 590, 129–133. https://doi.org/10.1038/s41586-020-03085-8

Dereeper, A., Guignon, V., Blanc, G., Audic, S., Buffet, S., Chevenet, F., Dufayard, J.-F., Guindon, S., Lefort, V., Lescot, M., Claverie, J.-M., Gascuel, O., 2008. Phylogeny.fr: robust phylogenetic analysis for the non-specialist. Nucleic Acids Res 36, W465–W469. https://doi.org/10.1093/nar/gkn180

Distler, J.H.W., Györfi, A.-H., Ramanujam, M., Whitfield, M.L., Königshoff, M., Lafyatis, R., 2019. Shared and distinct mechanisms of fibrosis. Nat Rev Rheumatol 15, 705–730. https://doi.org/10.1038/s41584-019-0322-7

Dobin, A., Davis, C.A., Schlesinger, F., Drenkow, J., Zaleski, C., Jha, S., Batut, P., Chaisson, M., Gingeras, T.R., 2013. STAR: ultrafast universal RNA-seq aligner. Bioinformatics 29, 15–21. https://doi.org/10.1093/bioinformatics/bts635

Dogra, D., Ahuja, S., Kim, H.-T., Rasouli, S.J., Stainier, D.Y.R., Reischauer, S., 2017. Opposite effects of Activin type 2 receptor ligands on cardiomyocyte proliferation during development and repair. Nature Communications 8, 1902. https://doi.org/10.1038/s41467-017-01950-1

Donato, V.D., Santis, F.D., Auer, T.O., Testa, N., Sánchez-Iranzo, H., Mercader, N., Concordet, J.-P., Bene, F.D., 2016. 2C-Cas9: a versatile tool for clonal analysis of gene function. Genome Res. 26, 681–692. https://doi.org/10.1101/gr.196170.115

Dyck, P.K.V., Hockaden, N., Nelson, E.C., Koch, A.R., Hester, K.L., Pillai, N., Coffing, G.C., Burns, A.R., Lafontant, P.J., 2020. Cauterization as a Simple Method for Regeneration Studies in the Zebrafish Heart. Journal of Cardiovascular Development and Disease 7, 41. https://doi.org/10.3390/jcdd7040041

Falke, L.L., Gholizadeh, S., Goldschmeding, R., Kok, R.J., Nguyen, T.Q., 2015. Diverse origins of the myofibroblast—implications for kidney fibrosis. Nat Rev Nephrol 11, 233–244. https://doi.org/10.1038/nrneph.2014.246

Fang, F., Ooka, K., Bhattacharyya, S., Bhattachyya, S., Wei, J., Wu, M., Du, P., Lin, S., Del Galdo, F., Feghali-Bostwick, C.A., Varga, J., 2011. The early growth response gene Egr2 (Alias Krox20) is a novel transcriptional target of transforming growth factor-β that is up-regulated in systemic sclerosis and

mediates profibrotic responses. The American Journal of Pathology 178, 2077–2090. https://doi.org/10.1016/j.ajpath.2011.01.035

Fang, Y., Gupta, V., Karra, R., Holdway, J.E., Kikuchi, K., Poss, K.D., 2013. Translational profiling of cardiomyocytes identifies an early Jak1/Stat3 injury response required for zebrafish heart regeneration. PNAS 110, 13416–13421. https://doi.org/10.1073/pnas.1309810110

Fazel Modares, N., Polz, R., Haghighi, F., Lamertz, L., Behnke, K., Zhuang, Y., Kordes, C., Häussinger, D., Sorg, U.R., Pfeffer, K., Floss, D.M., Moll, J.M., Piekorz, R.P., Ahmadian, M.R., Lang, P.A., Scheller, J., 2019. IL-6 Trans-signaling Controls Liver Regeneration After Partial Hepatectomy. Hepatology 70, 2075–2091. https://doi.org/10.1002/hep.30774

Feeback, D.L., 1987. Organs and Systems, in: Feeback, D.L. (Ed.), Histology, Oklahoma Notes. Springer, New York, NY, pp. 89–190. https://doi.org/10.1007/978-1-4612-4630-5_3

Frangogiannis, N.G., 2020. Transforming growth factor–β in tissue fibrosis. J Exp Med 217. https://doi.org/10.1084/jem.20190103

Fu, X., Khalil, H., Kanisicak, O., Boyer, J.G., Vagnozzi, R.J., Maliken, B.D., Sargent, M.A., Prasad, V., Valiente-Alandi, I., Blaxall, B.C., Molkentin, J.D., 2018. Specialized fibroblast differentiated states underlie scar formation in the infarcted mouse heart. J Clin Invest 128, 2127–2143. https://doi.org/10.1172/JCI98215

Fukuda, R., 2020. Stimulation of glycolysis promotes cardiomyocyte proliferation after injury in adult zebrafish. EMBO reports 21, e49752. https://doi.org/10.15252/embr.201949752

Gagnon, J.A., Valen, E., Thyme, S.B., Huang, P., Ahkmetova, L., Pauli, A., Montague, T.G., Zimmerman, S., Richter, C., Schier, A.F., 2014. Efficient Mutagenesis by Cas9 Protein-Mediated Oligonucleotide Insertion and Large-Scale Assessment of Single-Guide RNAs. PLOS ONE 9, e98186. https://doi.org/10.1371/journal.pone.0098186

Gancz, D., Raftrey, B.C., Perlmoter, G., Marín-Juez, R., Semo, J., Matsuoka, R.L., Karra, R., Raviv, H., Moshe, N., Addadi, Y., Golani, O., Poss, K.D., Red-Horse, K., Stainier, D.Y., Yaniv, K., 2019. Distinct origins and molecular mechanisms

contribute to lymphatic formation during cardiac growth and regeneration. eLife 8, e44153. https://doi.org/10.7554/eLife.44153

Gerber, T., Murawala, P., Knapp, D., Masselink, W., Schuez, M., Hermann, S., Gac-Santel, M., Nowoshilow, S., Kageyama, J., Khattak, S., Currie, J.D., Camp, J.G., Tanaka, E.M., Treutlein, B., 2018. Single-cell analysis uncovers convergence of cell identities during axolotl limb regeneration. Science 362. https://doi.org/10.1126/science.aaq0681

Godwin, J.W., Debuque, R., Salimova, E., Rosenthal, N.A., 2017. Heart regeneration in the salamander relies on macrophage-mediated control of fibroblast activation and the extracellular landscape. npj Regen Med 2, 1–11. https://doi.org/10.1038/s41536-017-0027-y

Godwin, J.W., Pinto, A.R., Rosenthal, N.A., 2013. Macrophages are required for adult salamander limb regeneration. PNAS 110, 9415–9420. https://doi.org/10.1073/pnas.1300290110

Goldman, J.A., Poss, K.D., 2020. Gene regulatory programmes of tissue regeneration. Nat Rev Genet 21, 511–525. https://doi.org/10.1038/s41576-020-0239-7

González-Rosa, J.M., Burns, C.E., Burns, C.G., 2017. Zebrafish heart regeneration: 15 years of discoveries. Regeneration (Oxf) 4, 105–123. https://doi.org/10.1002/reg2.83

González-Rosa, J.M., Peralta, M., Mercader, N., 2012. Pan-epicardial lineage tracing reveals that epicardium derived cells give rise to myofibroblasts and perivascular cells during zebrafish heart regeneration. Developmental Biology 370, 173–186. https://doi.org/10.1016/j.ydbio.2012.07.007

Govindan, J., Iovine, M.K., 2015. Dynamic remodeling of the extra cellular matrix during zebrafish fin regeneration. Gene expression patterns: GEP 19, 21–29. https://doi.org/10.1016/j.gep.2015.06.001

Gunawan, F., Priya, R., Stainier, D.Y.R., 2021. Sculpting the heart: Cellular mechanisms shaping valves and trabeculae. Current Opinion in Cell Biology, Differentiation and development 73, 26–34. https://doi.org/10.1016/j.ceb.2021.04.009

Gupta, V., Poss, K.D., 2012. Clonally dominant cardiomyocytes direct heart morphogenesis. Nature 484, 479–484. https://doi.org/10.1038/nature11045

Gurtner, G.C., Werner, S., Barrandon, Y., Longaker, M.T., 2008. Wound repair and regeneration. Nature 453, 314–321. https://doi.org/10.1038/nature07039

Gut, P., Reischauer, S., Stainier, D.Y.R., Arnaout, R., 2017. Little Fish, Big Data: Zebrafish as a Model for Cardiovascular and Metabolic Disease. Physiological Reviews 97, 889–938. https://doi.org/10.1152/physrev.00038.2016

Gutierrez-Miranda, L., Yaniv, K., 2020. Cellular Origins of the Lymphatic Endothelium: Implications for Cancer Lymphangiogenesis. Frontiers in Physiology 11.

Harrison, M.R., Feng, X., Mo, G., Aguayo, A., Villafuerte, J., Yoshida, T., Pearson, C.A., Schulte-Merker, S., Lien, C.-L., 2019. Late developing cardiac lymphatic vasculature supports adult zebrafish heart function and regeneration. eLife 8, e42762. https://doi.org/10.7554/eLife.42762

Hasegawa, T., Hall, C.J., Crosier, P.S., Abe, G., Kawakami, K., Kudo, A., Kawakami, A., 2017. Transient inflammatory response mediated by interleukin-1β is required for proper regeneration in zebrafish fin fold. eLife 6, e22716. https://doi.org/10.7554/eLife.22716

Hayden, L.D., Poss, K.D., De Simone, A., Di Talia, S., 2021. Mathematical modeling of Erk activity waves in regenerating zebrafish scales. Biophysical Journal 120, 4287–4297. https://doi.org/10.1016/j.bpj.2021.05.004

Heicklen-Klein, A., Evans, T., 2004. T-box binding sites are required for activity of a cardiac GATA-4 enhancer. Developmental Biology 267, 490–504. https://doi.org/10.1016/j.ydbio.2003.09.042

Hesselson, D., Anderson, R.M., Beinat, M., Stainier, D.Y.R., 2009. Distinct populations of quiescent and proliferative pancreatic β-cells identified by HOTcre mediated labeling. PNAS 106, 14896–14901. https://doi.org/10.1073/pnas.0906348106

Hoang, T., Wang, J., Boyd, P., Wang, F., Santiago, C., Jiang, L., Yoo, S., Lahne, M., Todd, L.J., Jia, M., Saez, C., Keuthan, C., Palazzo, I., Squires, N., Campbell, W.A., Rajaii, F., Parayil, T., Trinh, V., Kim, D.W., Wang, G., Campbell, L.J., Ash, J., Fischer, A.J., Hyde, D.R., Qian, J., Blackshaw, S., 2020. Gene regulatory networks controlling vertebrate retinal regeneration. Science 370. https://doi.org/10.1126/science.abb8598

Honkoop, H., de Bakker, D.E., Aharonov, A., Kruse, F., Shakked, A., Nguyen, P.D., de Heus, C., Garric, L., Muraro, M.J., Shoffner, A., Tessadori, F., Peterson, J.C.,

Noort, W., Bertozzi, A., Weidinger, G., Posthuma, G., Grün, D., van der Laarse, W.J., Klumperman, J., Jaspers, R.T., Poss, K.D., van Oudenaarden, A., Tzahor, E., Bakkers, J., 2019. Single-cell analysis uncovers that metabolic reprogramming by ErbB2 signaling is essential for cardiomyocyte proliferation in the regenerating heart. eLife 8, e50163. https://doi.org/10.7554/eLife.50163

Hou, Y., Lee, H.J., Chen, Y., Ge, J., Osman, F.O.I., McAdow, A.R., Mokalled, M.H., Johnson, S.L., Zhao, G., Wang, T., 2020. Cellular diversity of the regenerating caudal fin. Science Advances 6, eaba2084. https://doi.org/10.1126/sciadv.aba2084

Itou, J., Oishi, I., Kawakami, H., Glass, T.J., Richter, J., Johnson, A., Lund, T.C., Kawakami, Y., 2012. Migration of cardiomyocytes is essential for heart regeneration in zebrafish. Development 139, 4133–4142. https://doi.org/10.1242/dev.079756

Joven, A., Elewa, A., Simon, A., 2019. Model systems for regeneration: salamanders. Development 146, dev167700. https://doi.org/10.1242/dev.167700

Kanisicak, O., Khalil, H., Ivey, M.J., Karch, J., Maliken, B.D., Correll, R.N., Brody, M.J., J. Lin, S.-C., Aronow, B.J., Tallquist, M.D., Molkentin, J.D., 2016. Genetic lineage tracing defines myofibroblast origin and function in the injured heart. Nat Commun 7, 12260. https://doi.org/10.1038/ncomms12260

Kaur Harmandeep, Takefuji Mikito, Ngai C.Y., Carvalho Jorge, Bayer Julia, Wietelmann Astrid, Poetsch Ansgar, Hoelper Soraya, Conway Simon J., Möllmann Helge, Looso Mario, Troidl Christian, Offermanns Stefan, Wettschureck Nina, 2016. Targeted Ablation of Periostin-Expressing Activated Fibroblasts Prevents Adverse Cardiac Remodeling in Mice. Circulation Research 118, 1906–1917. https://doi.org/10.1161/CIRCRESAHA.116.308643

Kettleborough, R.N.W., Busch-Nentwich, E.M., Harvey, S.A., Dooley, C.M., de Bruijn, E., van Eeden, F., Sealy, I., White, R.J., Herd, C., Nijman, I.J., Fényes, F., Mehroke, S., Scahill, C., Gibbons, R., Wali, N., Carruthers, S., Hall, A., Yen, J., Cuppen, E., Stemple, D.L., 2013. A systematic genome-wide analysis of zebrafish protein-coding gene function. Nature 496, 494–497. https://doi.org/10.1038/nature11992

Kikuchi, K., Gupta, V., Wang, J., Holdway, J.E., Wills, A.A., Fang, Y., Poss, K.D., 2011a. tcf21+ epicardial cells adopt non-myocardial fates during zebrafish heart development and regeneration. Development 138, 2895–2902. https://doi.org/10.1242/dev.067041

Kikuchi, K., Holdway, J.E., Major, R.J., Blum, N., Dahn, R.D., Begemann, G., Poss, K.D., 2011b. Retinoic acid production by endocardium and epicardium is an injury response essential for zebrafish heart regeneration. Developmental Cell 20, 397–404. https://doi.org/10.1016/j.devcel.2011.01.010

Kikuchi, K., Holdway, J.E., Werdich, A.A., Anderson, R.M., Fang, Y., Egnaczyk, G.F., Evans, T., MacRae, C.A., Stainier, D.Y.R., Poss, K.D., 2010. Primary contribution to zebrafish heart regeneration by gata4 + cardiomyocytes. Nature 464, 601–605. https://doi.org/10.1038/nature08804

Knopf, F., Hammond, C., Chekuru, A., Kurth, T., Hans, S., Weber, C.W., Mahatma, G., Fisher, S., Brand, M., Schulte-Merker, S., Weidinger, G., 2011. Bone Regenerates via Dedifferentiation of Osteoblasts in the Zebrafish Fin. Developmental Cell 20, 713–724. https://doi.org/10.1016/j.devcel.2011.04.014

Konhilas John P., Watson Peter A., Maass Alexander, Boucek Dana M., Horn Todd, Stauffer Brian L., Luckey Stephen W., Rosenberg Paul, Leinwand Leslie A., 2006. Exercise Can Prevent and Reverse the Severity of Hypertrophic Cardiomyopathy. Circulation Research 98, 540–548. https://doi.org/10.1161/01.RES.0000205766.97556.00

König, D., Dagenais, P., Senk, A., Djonov, V., Aegerter, C.M., Jaźwińska, A., 2019. Distribution and Restoration of Serotonin-Immunoreactive Paraneuronal Cells During Caudal Fin Regeneration in Zebrafish. Front. Mol. Neurosci. 0. https://doi.org/10.3389/fnmol.2019.00227

Korotkevich, G., Sukhov, V., Sergushichev, A., 2019. Fast gene set enrichment analysis. bioRxiv 060012. https://doi.org/10.1101/060012

Kubin, T., Pöling, J., Kostin, S., Gajawada, P., Hein, S., Rees, W., Wietelmann, A., Tanaka, M., Lörchner, H., Schimanski, S., Szibor, M., Warnecke, H., Braun, T., 2011. Oncostatin M is a major mediator of cardiomyocyte dedifferentiation and remodeling. Cell Stem Cell 9, 420–432. https://doi.org/10.1016/j.stem.2011.08.013

Lai, S.-L., Marín-Juez, R., Moura, P.L., Kuenne, C., Lai, J.K.H., Tsedeke, A.T., Guenther, S., Looso, M., Stainier, D.Y., 2017. Reciprocal analyses in zebrafish and medaka reveal that harnessing the immune response promotes cardiac regeneration. eLife 6, e25605. https://doi.org/10.7554/eLife.25605

Lai, S.-L., Marín-Juez, R., Stainier, D.Y.R., 2019. Immune responses in cardiac repair and regeneration: a comparative point of view. Cell. Mol. Life Sci. 76, 1365–1380. https://doi.org/10.1007/s00018-018-2995-5

Lawson, N.D., Weinstein, B.M., 2002. In Vivo Imaging of Embryonic Vascular Development Using Transgenic Zebrafish. Developmental Biology 248, 307–318. https://doi.org/10.1006/dbio.2002.0711

Leibinger, M., Zeitler, C., Gobrecht, P., Andreadaki, A., Gisselmann, G., Fischer, D., 2021. Transneuronal delivery of hyper-interleukin-6 enables functional recovery after severe spinal cord injury in mice. Nature Communications 12, 391. https://doi.org/10.1038/s41467-020-20112-4

Lepilina, A., Coon, A.N., Kikuchi, K., Holdway, J.E., Roberts, R.W., Burns, C.G., Poss, K.D., 2006. A Dynamic Epicardial Injury Response Supports Progenitor Cell Activity during Zebrafish Heart Regeneration. Cell 127, 607–619. https://doi.org/10.1016/j.cell.2006.08.052

Li, Y., He, X., Kawaguchi, R., Zhang, Y., Wang, Q., Monavarfeshani, A., Yang, Z., Chen, B., Shi, Z., Meng, H., Zhou, S., Zhu, J., Jacobi, A., Swarup, V., Popovich, P.G., Geschwind, D.H., He, Z., 2020. Microglia-organized scar-free spinal cord repair in neonatal mice. Nature 1–6. https://doi.org/10.1038/s41586-020-2795-6

Li Yandong, Feng Jie, Song Shen, Li Haotong, Yang Huijun, Zhou Bin, Li Yan, Yue Zhang, Lian Hong, Liu Lihui, Hu Shengshou, Nie Yu, 2020. gp130 Controls Cardiomyocyte Proliferation and Heart Regeneration. Circulation 142, 967–982. https://doi.org/10.1161/CIRCULATIONAHA.119.044484

Liao, Y., Smyth, G.K., Shi, W., 2014. featureCounts: an efficient general purpose program for assigning sequence reads to genomic features. Bioinformatics 30, 923–930. https://doi.org/10.1093/bioinformatics/btt656

Lim, W.-W., Ng, B., Widjaja, A., Xie, C., Su, L., Ko, N., Lim, S.-Y., Kwek, X.-Y., Lim, S., Cook, S.A., Schafer, S., 2020. Transgenic interleukin 11 expression causes

cross-tissue fibro-inflammation and an inflammatory bowel phenotype in mice. PLoS ONE 15, e0227505. https://doi.org/10.1371/journal.pone.0227505

Lin, T.-Y., Gerber, T., Taniguchi-Sugiura, Y., Murawala, P., Hermann, S., Grosser, L., Shibata, E., Treutlein, B., Tanaka, E.M., 2021. Fibroblast dedifferentiation as a determinant of successful regeneration. Developmental Cell 56, 1541-1551.e6. https://doi.org/10.1016/j.devcel.2021.04.016

Liu, X., De la Cruz, E., Gu, X., Balint, L., Oxendine-Burns, M., Terrones, T., Ma, W., Kuo, H.-H., Lantz, C., Bansal, T., Thorp, E., Burridge, P., Jakus, Z., Herz, J., Cleaver, O., Torres, M., Oliver, G., 2020. Lymphoangiocrine signals promote cardiac growth and repair. Nature 588, 705–711. https://doi.org/10.1038/s41586-020-2998-x

Liu, Y., Sepich, D.S., Solnica-Krezel, L., 2017. Stat3/Cdc25a-dependent cell proliferation promotes embryonic axis extension during zebrafish gastrulation. PLOS Genetics 13, e1006564. https://doi.org/10.1371/journal.pgen.1006564

Love, M.I., Huber, W., Anders, S., 2014. Moderated estimation of fold change and dispersion for RNA-seq data with DESeq2. Genome Biology 15, 550. https://doi.org/10.1186/s13059-014-0550-8

Lowe, V., Wisniewski, L., Pellet-Many, C., 2021. The Zebrafish Cardiac Endothelial Cell—Roles in Development and Regeneration. Journal of Cardiovascular Development and Disease 8, 49. https://doi.org/10.3390/jcdd8050049

Makino, S., Whitehead, G.G., Lien, C.-L., Kim, S., Jhawar, P., Kono, A., Kawata, Y., Keating, M.T., 2005. Heat-shock protein 60 is required for blastema formation and maintenance during regeneration. PNAS 102, 14599–14604. https://doi.org/10.1073/pnas.0507408102

Marín-Juez, R., El-Sammak, H., Helker, C.S.M., Kamezaki, A., Mullapuli, S.T., Bibli, S.-I., Foglia, M.J., Fleming, I., Poss, K.D., Stainier, D.Y.R., 2019. Coronary Revascularization During Heart Regeneration Is Regulated by Epicardial and Endocardial Cues and Forms a Scaffold for Cardiomyocyte Repopulation. Developmental Cell 51, 503-515.e4. https://doi.org/10.1016/j.devcel.2019.10.019

Marín-Juez, R., Marass, M., Gauvrit, S., Rossi, A., Lai, S.-L., Materna, S.C., Black, B.L., Stainier, D.Y.R., 2016. Fast revascularization of the injured area is

essential to support zebrafish heart regeneration. PNAS 113, 11237–11242. https://doi.org/10.1073/pnas.1605431113

Marques, I.J., Lupi, E., Mercader, N., 2019. Model systems for regeneration: zebrafish. Development 146. https://doi.org/10.1242/dev.167692

Mascharak, S., desJardins-Park, H.E., Davitt, M.F., Griffin, M., Borrelli, M.R., Moore, A.L., Chen, K., Duoto, B., Chinta, M., Foster, D.S., Shen, A.H., Januszyk, M., Kwon, S.H., Wernig, G., Wan, D.C., Lorenz, H.P., Gurtner, G.C., Longaker, M.T., 2021. Preventing Engrailed-1 activation in fibroblasts yields wound regeneration without scarring. Science. https://doi.org/10.1126/science.aba2374

McInnes, L., Healy, J., Melville, J., 2020. UMAP: Uniform Manifold Approximation and Projection for Dimension Reduction. arXiv:1802.03426 [cs, stat].

Mehta, A.S., Singh, A., 2019. Insights into regeneration tool box: An animal model approach. Developmental Biology 453, 111–129. https://doi.org/10.1016/j.ydbio.2019.04.006

Mehta, S.T., Luo, X., Park, K.K., Bixby, J.L., Lemmon, V.P., 2016. Hyperactivated Stat3 boosts axon regeneration in the CNS. Exp Neurol 280, 115–120. https://doi.org/10.1016/j.expneurol.2016.03.004

Miao, M., Bruce, A.E.E., Bhanji, T., Davis, E.C., Keeley, F.W., 2007. Differential expression of two tropoelastin genes in zebrafish. Matrix Biology 26, 115–124. https://doi.org/10.1016/j.matbio.2006.09.011

Michalak, M., Agellon, L.B., 2018. Stress Coping Strategies in the Heart: An Integrated View. Frontiers in Cardiovascular Medicine 5.

Miskolci, V., Squirrell, J., Rindy, J., Vincent, W., Sauer, J.D., Gibson, A., Eliceiri, K.W., Huttenlocher, A., 2019. Distinct inflammatory and wound healing responses to complex caudal fin injuries of larval zebrafish. eLife 8, e45976. https://doi.org/10.7554/eLife.45976

Mosimann, C., Kaufman, C.K., Li, P., Pugach, E.K., Tamplin, O.J., Zon, L.I., 2011. Ubiquitous transgene expression and Cre-based recombination driven by the ubiquitin promoter in zebrafish. Development 138, 169–177. https://doi.org/10.1242/dev.059345

Mullins, M.C., Acedo, J.N., Priya, R., Solnica-Krezel, L., Wilson, S.W., 2021. The zebrafish issue: 25 years on. Development 148, dev200343. https://doi.org/10.1242/dev.200343

Münch, J., Grivas, D., González-Rajal, Á., Torregrosa-Carrión, R., Pompa, J.L. de la, 2017. Notch signalling restricts inflammation and serpine1 expression in the dynamic endocardium of the regenerating zebrafish heart. Development 144, 1425–1440. https://doi.org/10.1242/dev.143362

Murawala, P., Tanaka, E.M., Currie, J.D., 2012. Regeneration: The ultimate example of wound healing. Seminars in Cell & Developmental Biology, Wound Repair 23, 954–962. https://doi.org/10.1016/j.semcdb.2012.09.013

Nakagawa, M., Owada, Y., Izumi, Y., Nonin, S., Sugioka, K., Nakatani, D., Iwata, S., Mizutani, K., Nishimura, S., Ito, A., Fujita, S., Daimon, T., Sawa, Y., Asakura, M., Maeda, M., Fujio, Y., Yoshiyama, M., 2016. Four cases of investigational therapy with interleukin-11 against acute myocardial infarction. Heart Vessels 31, 1574–1578. https://doi.org/10.1007/s00380-015-0788-4

Nandurkar, H.H., Robb, L., Tarlinton, D., Barnett, L., Köntgen, F., Begley, C.G., 1997. Adult Mice With Targeted Mutation of the Interleukin-11 Receptor (IL11Ra) Display Normal Hematopoiesis. Blood 90, 2148–2159. https://doi.org/10.1182/blood.V90.6.2148

Natarajan, N., Abbas, Y., Bryant, D.M., Gonzalez-Rosa, J.M., Sharpe, M., Uygur, A., Cocco-Delgado, L.H., Ho, N.N., Gerard, N.P., Gerard, C.J., MacRae, C.A., Burns, C.E., Burns, C.G., Whited, J.L., Lee, R.T., 2018. Complement Receptor C5aR1 Plays an Evolutionarily Conserved Role in Successful Cardiac Regeneration. Circulation 137, 2152–2165. https://doi.org/10.1161/CIRCULATIONAHA.117.030801

Ng, B., Dong, J., D'Agostino, G., Viswanathan, S., Widjaja, A.A., Lim, W.-W., Ko, N.S.J., Tan, J., Chothani, S.P., Huang, B., Xie, C., Pua, C.J., Chacko, A.-M., Guimarães-Camboa, N., Evans, S.M., Byrne, A.J., Maher, T.M., Liang, J., Jiang, D., Noble, P.W., Schafer, S., Cook, S.A., 2019. Interleukin-11 is a therapeutic target in idiopathic pulmonary fibrosis. Science Translational Medicine 11. https://doi.org/10.1126/scitranslmed.aaw1237

Ng, B., Dong, J., Viswanathan, S., Widjaja, A.A., Paleja, B.S., Adami, E., Ko, N.S.J., Wang, M., Lim, S., Tan, J., Chothani, S.P., Albani, S., Schafer, S., Cook, S.A., 2020. Fibroblast-specific IL11 signaling drives chronic inflammation in murine fibrotic lung disease. FASEB j. 34, 11802–11815. https://doi.org/10.1096/fj.202001045RR

Notari, M., Ventura-Rubio, A., Bedford-Guaus, S.J., Jorba, I., Mulero, L., Navajas, D., Martí, M., Raya, Á., 2018. The local microenvironment limits the regenerative potential of the mouse neonatal heart. Science Advances 4, eaao5553. https://doi.org/10.1126/sciadv.aao5553

Obana Masanori, Maeda Makiko, Takeda Koji, Hayama Akiko, Mohri Tomomi, Yamashita Tomomi, Nakaoka Yoshikazu, Komuro Issei, Takeda Kiyoshi, Matsumiya Goro, Azuma Junichi, Fujio Yasushi, 2010. Therapeutic Activation of Signal Transducer and Activator of Transcription 3 by Interleukin-11 Ameliorates Cardiac Fibrosis After Myocardial Infarction. Circulation 121, 684–691. https://doi.org/10.1161/CIRCULATIONAHA.109.893677

Ogawa, M., Geng, F.-S., Humphreys, D.T., Kristianto, E., Sheng, D.Z., Hui, S.P., Zhang, Y., Sugimoto, K., Nakayama, M., Zheng, D., Hesselson, D., Hodson, M.P., Bogdanovic, O., Kikuchi, K., 2021. Krüppel-like factor 1 is a core cardiomyogenic trigger in zebrafish. Science. https://doi.org/10.1126/science.abe2762

Owlarn, S., Klenner, F., Schmidt, D., Rabert, F., Tomasso, A., Reuter, H., Mulaw, M.A., Moritz, S., Gentile, L., Weidinger, G., Bartscherer, K., 2017. Generic wound signals initiate regeneration in missing-tissue contexts. Nat Commun 8, 2282. https://doi.org/10.1038/s41467-017-02338-x

Paris, A.J., Hayer, K.E., Oved, J.H., Avgousti, D.C., Toulmin, S.A., Zepp, J.A., Zacharias, W.J., Katzen, J.B., Basil, M.C., Kremp, M.M., Slamowitz, A.R., Jayachandran, S., Sivakumar, A., Dai, N., Wang, P., Frank, D.B., Eisenlohr, L.C., Cantu, E., Beers, M.F., Weitzman, M.D., Morrisey, E.E., Worthen, G.S., 2020. STAT3–BDNF–TrkB signalling promotes alveolar epithelial regeneration after lung injury. Nature Cell Biology 22, 1197–1210. https://doi.org/10.1038/s41556-020-0569-x

Pfefferli, C., Jaźwińska, A., 2015. The art of fin regeneration in zebrafish. Regeneration 2, 72–83. https://doi.org/10.1002/reg2.33

Phipps, L.S., Marshall, L., Dorey, K., Amaya, E., 2020. Model systems for regeneration: Xenopus. Development 147, dev180844. https://doi.org/10.1242/dev.180844

Polański, K., Young, M.D., Miao, Z., Meyer, K.B., Teichmann, S.A., Park, J.-E., 2020. BBKNN: fast batch alignment of single cell transcriptomes. Bioinformatics 36, 964–965. https://doi.org/10.1093/bioinformatics/btz625

Poon, K.-L., Liebling, M., Kondrychyn, I., Garcia-Lecea, M., Korzh, V., 2010. Zebrafish cardiac enhancer trap lines: New tools for in vivo studies of cardiovascular development and disease. Developmental Dynamics 239, 914–926. https://doi.org/10.1002/dvdy.22203

Porrello, E.R., Mahmoud, A.I., Simpson, E., Hill, J.A., Richardson, J.A., Olson, E.N., Sadek, H.A., 2011. Transient Regenerative Potential of the Neonatal Mouse Heart. Science. https://doi.org/10.1126/science.1200708

Poss, K.D., Wilson, L.G., Keating, M.T., 2002. Heart Regeneration in Zebrafish. Science 298, 2188–2190. https://doi.org/10.1126/science.1077857

Pronobis, M.I., Poss, K.D., 2020. Signals for cardiomyocyte proliferation during zebrafish heart regeneration. Current Opinion in Physiology, Regeneration 14, 78–85. https://doi.org/10.1016/j.cophys.2020.02.002

Quaife-Ryan Gregory A., Sim Choon Boon, Ziemann Mark, Kaspi Antony, Rafehi Haloom, Ramialison Mirana, El-Osta Assam, Hudson James E., Porrello Enzo R., 2017. Multicellular Transcriptional Analysis of Mammalian Heart Regeneration. Circulation 136, 1123–1139. https://doi.org/10.1161/CIRCULATIONAHA.117.028252

Rinkevich, Y., Walmsley, G.G., Hu, M.S., Maan, Z.N., Newman, A.M., Drukker, M., Januszyk, M., Krampitz, G.W., Gurtner, G.C., Lorenz, H.P., Weissman, I.L., Longaker, M.T., 2015. Identification and isolation of a dermal lineage with intrinsic fibrogenic potential. Science 348. https://doi.org/10.1126/science.aaa2151

Rose-John, S., 2018. Interleukin-6 Family Cytokines. Cold Spring Harb Perspect Biol 10, a028415. https://doi.org/10.1101/cshperspect.a028415

Rurik, J.G., Tombácz, I., Yadegari, A., Fernández, P.O.M., Shewale, S.V., Li, L., Kimura, T., Soliman, O.Y., Papp, T.E., Tam, Y.K., Mui, B.L., Albelda, S.M., Puré, E., June, C.H., Aghajanian, H., Weissman, D., Parhiz, H., Epstein, J.A., 2022. CAR T cells produced in vivo to treat cardiac injury. Science. https://doi.org/10.1126/science.abm0594

Sagaradze, G.D., Basalova, N.A., Efimenko, A.Yu., Tkachuk, V.A., 2020. Mesenchymal Stromal Cells as Critical Contributors to Tissue Regeneration. Frontiers in Cell and Developmental Biology 8.

Sallin, P., de Preux Charles, A.-S., Duruz, V., Pfefferli, C., Jaźwińska, A., 2015. A dual epimorphic and compensatory mode of heart regeneration in zebrafish. Developmental Biology 399, 27–40. https://doi.org/10.1016/j.ydbio.2014.12.002

Sánchez-Iranzo, H., Galardi-Castilla, M., Sanz-Morejón, A., González-Rosa, J.M., Costa, R., Ernst, A., Aja, J.S. de, Langa, X., Mercader, N., 2018. Transient fibrosis resolves via fibroblast inactivation in the regenerating zebrafish heart. PNAS 115, 4188–4193. https://doi.org/10.1073/pnas.1716713115

Sanz-Morejón, A., García-Redondo, A.B., Reuter, H., Marques, I.J., Bates, T., Galardi-Castilla, M., Große, A., Manig, S., Langa, X., Ernst, A., Piragyte, I., Botos, M.-A., González-Rosa, J.M., Ruiz-Ortega, M., Briones, A.M., Salaices, M., Englert, C., Mercader, N., 2019. Wilms Tumor 1b Expression Defines a Pro-regenerative Macrophage Subtype and Is Required for Organ Regeneration in the Zebrafish. Cell Reports 28, 1296-1306.e6. https://doi.org/10.1016/j.celrep.2019.06.091

Sawamiphak, S., Kontarakis, Z., Filosa, A., Reischauer, S., Stainier, D.Y.R., 2017. Transient cardiomyocyte fusion regulates cardiac development in zebrafish. Nature Communications 8, 1525. https://doi.org/10.1038/s41467-017-01555-8

Schafer, S., Viswanathan, S., Widjaja, A.A., Lim, W.-W., Moreno-Moral, A., DeLaughter, D.M., Ng, B., Patone, G., Chow, K., Khin, E., Tan, J., Chothani, S.P., Ye, L., Rackham, O.J.L., Ko, N.S.J., Sahib, N.E., Pua, C.J., Zhen, N.T.G., Xie, C., Wang, M., Maatz, H., Lim, S., Saar, K., Blachut, S., Petretto, E., Schmidt, S., Putoczki, T., Guimarães-Camboa, N., Wakimoto, H., van Heesch, S., Sigmundsson, K., Lim, S.L., Soon, J.L., Chao, V.T.T., Chua, Y.L., Tan, T.E., Evans, S.M., Loh, Y.J., Jamal, M.H., Ong, K.K., Chua, K.C., Ong, B.-H., Chakaramakkil, M.J., Seidman, J.G., Seidman, C.E., Hubner, N., Sin, K.Y.K.,

Cook, S.A., 2017. IL-11 is a crucial determinant of cardiovascular fibrosis. Nature 552, 110–115. https://doi.org/10.1038/nature24676

Schaum, N., Karkanias, J., Neff, N.F., May, A.P., Quake, S.R., Wyss-Coray, T., Darmanis, S., Batson, J., Botvinnik, O., Chen, M.B., Chen, S., Green, F., Jones, R.C., Maynard, A., Penland, L., Pisco, A.O., Sit, R.V., Stanley, G.M., Webber, J.T., Zanini, F., Baghel, A.S., Bakerman, I., Bansal, I., Berdnik, D., Bilen, B., Brownfield, D., Cain, C., Chen, M.B., Chen, S., Cho, M., Cirolia, G., Conley, S.D., Darmanis, S., Demers, A., Demir, K., de Morree, A., Divita, T., du Bois, H., Dulgeroff, L.B.T., Ebadi, H., Espinoza, F.H., Fish, M., Gan, Q., George, B.M., Gillich, A., Green, F., Genetiano, G., Gu, X., Gulati, G.S., Hang, Y., Hosseinzadeh, S., Huang, A., Iram, T., Isobe, T., Ives, F., Jones, R.C., Kao, K.S., Karnam, G., Kershner, A.M., Kiss, B.M., Kong, W., Kumar, M.E., Lam, J.Y., Lee, D.P., Lee, S.E., Li, G., Li, Q., Liu, L., Lo, A., Lu, W.-J., Manjunath, A., May, A.P., May, K.L., May, O.L., Maynard, A., McKay, M., Metzger, R.J., Mignardi, M., Min, D., Nabhan, A.N., Neff, N.F., Ng, K.M., Noh, J., Patkar, R., Peng, W.C., Penland, L., Puccinelli, R., Rulifson, E.J., Schaum, N., Sikandar, S.S., Sinha, R., Sit, R.V., Szade, K., Tan, W., Tato, C., Tellez, K., Travaglini, K.J., Tropini, C., Waldburger, L., van Weele, L.J., Wosczyna, M.N., Xiang, J., Xue, S., Youngyunpipatkul, J., Zanini, F., Zardeneta, M.E., Zhang, F., Zhou, L., Bansal, I., Chen, S., Cho, M., Cirolia, G., Darmanis, S., Demers, A., Divita, T., Ebadi, H., Genetiano, G., Green, F., Hosseinzadeh, S., Ives, F., Lo, A., May, A.P., Maynard, A., McKay, M., Neff, N.F., Penland, L., Sit, R.V., Tan, W., Waldburger, L., Youngyunpipatkul, J., Batson, J., Botvinnik, O., Castro, P., Croote, D., Darmanis, S., DeRisi, J.L., Karkanias, J., Pisco, A.O., Stanley, G.M., Webber, J.T., Zanini, F., Baghel, A.S., Bakerman, I., Batson, J., Bilen, B., Botvinnik, O., Brownfield, D., Chen, M.B., Darmanis, S., Demir, K., de Morree, A., Ebadi, H., Espinoza, F.H., Fish, M., Gan, Q., George, B.M., Gillich, A., Gu, X., Gulati, G.S., Hang, Y., Huang, A., Iram, T., Isobe, T., Karnam, G., Kershner, A.M., Kiss, B.M., Kong, W., Kuo, C.S., Lam, J.Y., Lehallier, B., Li, G., Li, Q., Liu, L., Lu, W.-J., Min, D., Nabhan, A.N., Ng, K.M., Nguyen, P.K., Patkar, R., Peng, W.C., Penland, L., Rulifson, E.J., Schaum, N., Sikandar, S.S., Sinha, R., Szade, K., Tan, S.Y., Tellez, K., Travaglini, K.J., Tropini, C., van Weele, L.J., Wang,

B.M., Wosczyna, M.N., Xiang, J., Yousef, H., Zhou, L., Batson, J., Botvinnik, O., Chen, S., Darmanis, S., Green, F., May, A.P., Maynard, A., Pisco, A.O., Quake, S.R., Schaum, N., Stanley, G.M., Webber, J.T., Wyss-Coray, T., Zanini, F., Beachy, P.A., Chan, C.K.F., de Morree, A., George, B.M., Gulati, G.S., Hang, Y., Huang, K.C., Iram, T., Isobe, T., Kershner, A.M., Kiss, B.M., Kong, W., Li, G., Li, Q., Liu, L., Lu, W.-J., Nabhan, A.N., Ng, K.M., Nguyen, P.K., Peng, W.C., Rulifson, E.J., Schaum, N., Sikandar, S.S., Sinha, R., Szade, K., Travaglini, K.J., Tropini, C., Wang, B.M., Weinberg, K., Wosczyna, M.N., Wu, S.M., Yousef, H., Barres, B.A., Beachy, P.A., Chan, C.K.F., Clarke, M.F., Darmanis, S., Huang, K.C., Karkanias, J., Kim, S.K., Krasnow, M.A., Kumar, M.E., Kuo, C.S., May, A.P., Metzger, R.J., Neff, N.F., Nusse, R., Nguyen, P.K., Rando, T.A., Sonnenburg, J., Wang, B.M., Weinberg, K., Weissman, I.L., Wu, S.M., Quake, S.R., Wyss-Coray, T., The Tabula Muris Consortium, Overall coordination, Logistical coordination, Organ collection and processing, Library preparation and sequencing, Computational data analysis, Cell type annotation, Writing group, Supplemental text writing group, Principal investigators, 2018. Single-cell transcriptomics of 20 mouse organs creates a Tabula Muris. Nature 562, 367–372. https://doi.org/10.1038/s41586-018-0590-4

Seifert, A.W., Muneoka, K., 2018. The blastema and epimorphic regeneration in mammals. Developmental Biology, Regeneration: from cells to tissues to organisms 433, 190–199. https://doi.org/10.1016/j.ydbio.2017.08.007

Shephard Roy J., Balady Gary J., 1999. Exercise as Cardiovascular Therapy. Circulation 99, 963–972. https://doi.org/10.1161/01.CIR.99.7.963

Sousa, S., Afonso, N., Bensimon-Brito, A., Fonseca, M., Simões, M., Leon, J., Roehl, H., Cancela, M.L., Jacinto, A., 2011. Differentiated skeletal cells contribute to blastema formation during zebrafish fin regeneration. Development 138, 3897–3905. https://doi.org/10.1242/dev.064717

Sousa, S., Valerio, F., Jacinto, A., 2012. A new zebrafish bone crush injury model. Biology Open 1, 915–921. https://doi.org/10.1242/bio.2012877

Spanjaard, B., Hu, B., Mitic, N., Olivares-Chauvet, P., Janjuha, S., Ninov, N., Junker, J.P., 2018. Simultaneous lineage tracing and cell-type identification using

CRISPR–Cas9-induced genetic scars. Nature Biotechnology 36, 469–473. https://doi.org/10.1038/nbt.4124

Subramanian, A., Tamayo, P., Mootha, V.K., Mukherjee, S., Ebert, B.L., Gillette, M.A., Paulovich, A., Pomeroy, S.L., Golub, T.R., Lander, E.S., Mesirov, J.P., 2005. Gene set enrichment analysis: A knowledge-based approach for interpreting genome-wide expression profiles. PNAS 102, 15545–15550. https://doi.org/10.1073/pnas.0506580102

Tahara, N., Brush, M., Kawakami, Y., 2016. Cell Migration During Heart Regeneration in Zebrafish. Dev Dyn 245, 774–787. https://doi.org/10.1002/dvdy.24411

Talman, V., Ruskoaho, H., 2016. Cardiac fibrosis in myocardial infarction—from repair and remodeling to regeneration. Cell Tissue Res 365, 563–581. https://doi.org/10.1007/s00441-016-2431-9

Tamura, Y., Kohno, H., Mohri, T., Fujio, Y., Matsumiya, G., 2018. The cardioprotective effect of interleukin-11 against ischemia-reperfusion injury in a heart donor model. Ann Cardiothorac Surg 7, 99–105. https://doi.org/10.21037/acs.2017.09.11

Taniguchi, K., Wu, L.-W., Grivennikov, S.I., de Jong, P.R., Lian, I., Yu, F.-X., Wang, K., Ho, S.B., Boland, B.S., Chang, J.T., Sandborn, W.J., Hardiman, G., Raz, E., Maehara, Y., Yoshimura, A., Zucman-Rossi, J., Guan, K.-L., Karin, M., 2015. A gp130–Src–YAP module links inflammation to epithelial regeneration. Nature 519, 57–62. https://doi.org/10.1038/nature14228

Traag, V.A., Waltman, L., van Eck, N.J., 2019. From Louvain to Leiden: guaranteeing well-connected communities. Sci Rep 9, 5233. https://doi.org/10.1038/s41598-019-41695-z

Tsedeke, A.T., Allanki, S., Gentile, A., Jimenez-Amilburu, V., Rasouli, S.J., Guenther, S., Lai, S.-L., Stainier, D.Y.R., Marín-Juez, R., 2021. Cardiomyocyte heterogeneity during zebrafish development and regeneration. Developmental Biology 476, 259–271. https://doi.org/10.1016/j.ydbio.2021.03.014

Tsujioka, H., Kunieda, T., Katou, Y., Shirahige, K., Fukazawa, T., Kubo, T., 2017. interleukin-11 induces and maintains progenitors of different cell lineages during Xenopus tadpole tail regeneration. Nature Communications 8, 495. https://doi.org/10.1038/s41467-017-00594-5

Vanoevelen, J., Janssens, A., Huitema, L.F.A., Hammond, C.L., Metz, J.R., Flik, G., Voets, T., Schulte-Merker, S., 2011. Trpv5/6 is vital for epithelial calcium uptake and bone formation. The FASEB Journal 25, 3197–3207. https://doi.org/10.1096/fj.11-183145

Vogg, M.C., Galliot, B., Tsiairis, C.D., 2019. Model systems for regeneration: Hydra. Development 146, dev177212. https://doi.org/10.1242/dev.177212

Wang, J., Cao, J., Dickson, A.L., Poss, K.D., 2015. Epicardial regeneration is guided by cardiac outflow tract and Hedgehog signalling. Nature 522, 226–230. https://doi.org/10.1038/nature14325

Wang, J., Karra, R., Dickson, A.L., Poss, K.D., 2013. Fibronectin is deposited by injury-activated epicardial cells and is necessary for zebrafish heart regeneration. Developmental Biology 382, 427–435. https://doi.org/10.1016/j.ydbio.2013.08.012

Wang, W., Hu, C.-K., Zeng, A., Alegre, Dana, Hu, D., Gotting, K., Granillo, A.O., Wang, Y., Robb, S., Schnittker, R., Zhang, S., Alegre, Dillon, Li, H., Ross, E., Zhang, N., Brunet, A., Alvarado, A.S., 2020. Changes in regeneration-responsive enhancers shape regenerative capacities in vertebrates. Science 369. https://doi.org/10.1126/science.aaz3090

Wehner, D., Cizelsky, W., Vasudevaro, M.D., Özhan, G., Haase, C., Kagermeier-Schenk, B., Röder, A., Dorsky, R.I., Moro, E., Argenton, F., Kühl, M., Weidinger, G., 2014. Wnt/β-Catenin Signaling Defines Organizing Centers that Orchestrate Growth and Differentiation of the Regenerating Zebrafish Caudal Fin. Cell Reports 6, 467–481. https://doi.org/10.1016/j.celrep.2013.12.036

Whitehead, G.G., Makino, S., Lien, C.-L., Keating, M.T., 2005. fgf20 Is Essential for Initiating Zebrafish Fin Regeneration. Science 310, 1957–1960. https://doi.org/10.1126/science.1117637

Wolf, F.A., Angerer, P., Theis, F.J., 2018. SCANPY: large-scale single-cell gene expression data analysis. Genome Biology 19, 15. https://doi.org/10.1186/s13059-017-1382-0

Yoshinari, N., Ishida, T., Kudo, A., Kawakami, A., 2009. Gene expression and functional analysis of zebrafish larval fin fold regeneration. Developmental Biology 325, 71–81. https://doi.org/10.1016/j.ydbio.2008.09.028

Yoshinari, N., Kawakami, A., 2011. Mature and Juvenile Tissue Models of Regeneration in Small Fish Species. The Biological Bulletin 221, 62–78. https://doi.org/10.1086/BBLv221n1p62

Zou, Y., Takano, H., Mizukami, M., Akazawa, H., Qin, Y., Toko, H., Sakamoto, M., Minamino, T., Nagai, T., Komuro, I., 2003. Leukemia Inhibitory Factor Enhances Survival of Cardiomyocytes and Induces Regeneration of Myocardium After Myocardial Infarction. Circulation 108, 748–753. https://doi.org/10.1161/01.CIR.0000081773.76337.44

11. Appendix

11.1. Genes co-regulated in the heart during moderate physical exercise and after cryoinjury.

Table 11.1. List of co-regulated genes in moderate physical exercise and cardiac regeneration.

Probe ID	Fold change (Exercise/Control)	Fold change (96 hpci/Control)	Human gene symbol
A_15_P545132	9.31	11.61	IFI27
A_15_P657581	6.60	7.84	IFI6
A_15_P633181	4.78	6.92	CD9
A_15_P552552	4.26	20.68	STAT1
A_15_P100671	3.81	8.43	CD9
A_15_P154771	3.68	5.33	CD9
A_15_P462275	3.43	2.40	KLHL29
A_15_P401765	3.37	2.28	LRRC3B
A_15_P508093	3.04	8.87	TOP2A
A_15_P627971	2.02	10.70	CYP27C1
A_15_P595557	2.99	2.69	GIRK1
A_15_P151331	2.98	4.97	MXE
A_15_P675493	2.90	6.15	-
A_15_P310796	2.89	12.81	GIMAP7
A_15_P217296	2.85	2.24	COMP
A_15_P149586	2.82	4.87	STMN1
A_15_P110417	2.79	2.55	APOEB
A_15_P620146	2.78	3.18	H1F0
A_15_P631911	2.74	12.01	ANLN
A_15_P403565	2.72	6.18	CKAP2
A_15_P156241	2.64	2.70	SLC2A13
A_15_P306636	2.54	9.54	CDK1
A_15_P120756	2.45	2.58	GPR173
A_15_P754826	2.36	2.72	ACTA1
A_15_P678986	2.35	2.92	IFI27L2
A_15_P135361	2.34	2.55	SRL
A_15_P596307	2.32	9.29	MFAP2
A_15_P108587	2.22	2.50	MIDN
A_15_P700321	2.18	3.23	HNRNPAB
A_15_P174606	2.17	3.91	MUS81
A_15_P185791	2.17	3.95	STAT2
A_15_P627411	2.16	6.20	HIST1H1E
A_15_P156331	2.15	11.92	F13A1
A_15_P145996	2.14	10.25	ISG15
A_15_P630791	2.13	3.72	MXC
A_15_P195781	2.12	2.09	KIFBP

A_15_P635461	2.11	6.19	HIST1H1B
A_15_P237981	2.11	2.02	KIAA1432
A_15_P582052	2.11	2.27	CD84
A_15_P624076	2.11	6.98	CCNA2
A_15_P705451	2.07	2.50	MIDN
A_15_P660556	2.05	2.41	HIST1H4
A_15_P370340	2.02	3.38	KCTD3
A_15_P625206	2.01	3.11	TLR5
A_15_P162231	2.01	2.77	TMEM88
A_15_P106239	1.81	8.24	CCNB1
A_15_P630301	-2.08	-2.05	EIF4EBP2
A_15_P101922	-2.02	-2.40	HES1
A_15_P673521	-2.59	-3.13	NDNF
A_15_P113561	-2.71	-2.14	FTH1
A_15_P304426	-2.65	-3.21	NDNF
A_15_P683191	-3.19	-8.57	D2R
A_15_P621916	-4.25	-4.26	LECT2
A_15_P187701	-2.44	-3.76	G6PC
A_15_P754146	-2.55	-2.74	LPL
A_15_P758096	-3.42	-10.57	-
A_15_P117042	-2.04	-2.01	ST13
A_15_P496122	-2.35	-2.72	BTG2
A_15_P749991	-2.52	-18.01	IGFBP1
A_15_P625946	-6.82	-2.27	HSPB8
A_15_P666131	-3.34	-3.69	NPSN
A_15_P658811	-2.10	-2.45	BTG2
A_15_P205321	-2.41	-466.84	PSMB9
A_15_P631996	-2.02	-4.74	LYZ
A_15_P269846	-4.02	-3.84	LECT2
A_15_P102590	-3.24	-2.07	HSP90
A_15_P397325	-2.59	-4.03	IGFBP6
A_15_P175816	-2.19	-430.11	PSMB8
A_15_P656751	-2.30	-396.21	PSMB8
A_15_P204426	-2.31	-3.60	KLHL38
A_15_P654616	-2.26	-2.18	FABP7
A_15_P103679	-2.14	-4.83	FUOM
A_15_P620061	-20.58	-20.56	NTAN1
A_15_P299476	-2.37	-3.57	-
A_15_P120089	-2.50	-22.87	SGCG
A_15_P189366	-5.43	-21.22	TNFRSF14
A_15_P399525	-2.50	-3.91	CSTB
A_15_P669726	-3.35	-3.05	NPSN
A_15_P637146	-2.11	-3.24	CD276
A_15_P103119	-2.25	-2.37	BTG2
A_15_P162361	-2.21	-3.45	GADD45G
A_15_P399845	-3.15	-18.48	-

A_15_P658461	-2.37	-2.42	FZD3
A_15_P206281	-4.37	-5.34	CUEDC1
A_15_P103427	-3.00	-2.20	F5
A_15_P209266	-20.54	-2.81	MMP13
A_15_P689856	-2.38	-3.71	HDAC11
A_15_P670166	-5.19	-2.25	FCER2
A_15_P631546	-7.07	-18.77	THRSP
A_15_P378065	-8.83	-2.51	-
A_15_P113807	-3.09	-8.84	PPP1R14A
A_15_P188701	-3.15	-2.85	MFAP4
A_15_P102880	-2.12	-2.34	FABP7
A_15_P681476	-2.23	-10.31	NR1D2
A_15_P111404	-2.14	-3.59	VPS53
A_15_P663691	-5.94	-3.95	NPSN
A_15_P176801	-4.10	-6.31	OCIAD2
A_15_P119600	-2.46	-2.61	IGFBP6
A_15_P113448	-4.06	-2.46	CRYBA1
A_15_P628801	-2.46	-2.37	FABP7
A_15_P665681	-2.80	-3.99	CIZ1
A_15_P137696	-2.06	-2.92	-
A_15_P537847	-2.23	-34.93	-
A_15_P669096	-2.51	-6.57	-
A_15_P118830	-2.31	-3.16	NPSN
A_15_P365000	-2.95	-11.17	GPC1
A_15_P307356	-6.71	-3.27	-
A_15_P405435	-2.58	-6.36	ULK1
A_15_P366710	-2.37	-2.04	MIF4
A_15_P187296	-5.72	-21.45	-
A_15_P697181	-2.25	-2.01	LIMD2
A_15_P201771	-3.88	-2.27	-
A_15_P685886	-2.64	-4.34	ECE1
A_15_P726616	-2.05	-3.02	CUEDC1
A_15_P102638	-3.57	-2.46	F5
A_15_P323006	-2.35	-33.48	DYRK1A
A_15_P623981	-2.03	-3.34	MSTO1
A_15_P106002	-2.59	-58.94	XYLB
A_15_P628611	-2.32	-2.08	SLC19A3
A_15_P573652	-6.31	-2.65	PSG16
A_15_P449700	-2.86	-2.28	-
A_15_P637411	-4.43	-3.79	MPX
A_15_P412605	-2.39	-2.86	-
A_15_P493577	-2.37	-4.34	-
A_15_P182516	-11.32	-7.22	-
A_15_P695651	-6.57	-47.19	PPP1R3C
A_15_P620681	-26.45	-5.51	LGALS1L1
A_15_P695121	-2.18	-2.38	CISH

A_15_P106413	-2.52	-2.16	-
A_15_P248911	-2.13	-8.67	-
A_15_P486230	-5.52	-3.33	WNT5
A_15_P167891	-3.81	-2.04	-
A_15_P146386	-3.99	-3.56	CYB5D2
A_15_P706311	-3.23	-7.38	-
A_15_P165811	-2.13	-2.67	-
A_15_P161296	-2.82	-2.26	SP8
A_15_P629051	-2.94	-2.34	ITLN1
A_15_P558087	-2.18	-6.55	-
A_15_P392500	-2.96	-2.47	TFIIIB
A_15_P109012	-2.16	-2.10	LRP1B
A_15_P402655	-2.26	-2.05	CEBPD
A_15_P403185	-4.38	-3.58	-
A_15_P623292	-36.82	-18.59	SIGLEC1
A_15_P115293	-3.15	-2.24	ALDH8A1
A_15_P395570	-2.24	-5.50	SINUP
A_15_P751206	-4.08	-2.46	-
A_15_P164606	-2.38	-3.04	UTP3
A_15_P762721	-3.68	-2.90	-
A_15_P494842	-6.01	-12.35	PPP1R3G
A_15_P223311	-62.08	-158.65	IGK-V23
A_15_P498212	-3.80	-2.15	-
A_15_P758681	-2.14	-2.60	GVINP1
A_15_P499057	-23.63	-8.65	GVINP1
A_15_P192911	-2.02	-12.02	PRTG
A_15_P208311	-2.58	-37.74	CPA2
A_15_P138191	-3.59	-8.17	CFH
A_15_P621406	-2.27	-3.32	-
A_15_P656721	-2.82	-7.20	MYB
A_15_P159411	-2.18	-3.95	SOCS2
A_15_P449775	-2.30	-2.54	-
A_15_P172846	-4.38	-2.19	NME2
A_15_P117914	-13.49	-2.53	-
A_15_P723321	-6.43	-2.02	-
A_15_P146966	-3.31	-2.05	-
A_15_P627701	-2.71	-2.22	TNFB
A_15_P568152	-3.29	-4.09	-
A_15_P676121	-2.62	-5.20	MAPT
A_15_P107376	-3.00	-18.87	COLEC11
A_15_P246311	-10.61	-3.51	ILLR4
A_15_P142756	-2.24	-27.12	ALOX5
A_15_P113444	-18.76	-3.74	-
A_15_P116861	-2.01	-5.61	MYB
A_15_P666481	-8.90	-8.67	MED7
A_15_P141076	-8.22	-6.10	CYP24A1

A_15_P209581	-3.87	-6.39	BRP16
A_15_P141356	-2.76	-34.55	TRIM39
A_15_P202961	-2.40	-4.47	CUZD1
A_15_P168151	-3.76	-3.87	-
A_15_P178421	-14.39	-16.93	MOXD1
A_15_P161841	-3.41	-26.03	CYP46A1

11.2. Canonical pathway and upstream regulator prediction analyses.

Table 11.2. Canonical pathway analysis on the co-regulated genes.

Canonical pathway analysis	Z-score	P-value
Protein Kinase A signalling	2.236	4.42E-02
Jak/Stat signalling	2	6.18E-04
Interferon signalling	1.342	8.09E-07
Production of nitric oxide and reactive oxygen species in macrophages	1	1.32E-02
Systemic lupus erthematosus in B-cell signalling pathway	1	4.47E-02
Salvage pathways of pryramidine ribonucleotides	-1	1.27E-03
Osteoarthritis pathway	-2	1.94E-02

Table 11.3. Upstream regulator prediction analysis on the co-regulated genes.

Upstream regulator	Category	P-value
IL6	cytokine	1.32E-14
IGF1	growth factor	3.61E-10
lipopolysaccharide	chemical drug	3.72E-10
beta-estradiol	chemical drug	5.80E-10
SPI1	transcription regulator	9.86E-10
STAT3	transcription regulator	1.22E-09
TGFB1	growth factor	2.20E-08
PPARA	receptor	8.94E-08
NCOA2	transcription regulator	9.46E-08
LDLR	transporter	1.47E-07
IFNG	cytokine	1.78E-07
HRAS	enzyme	1.92E-07
MAPK1	kinase	2.48E-07
IL1B	cytokine	2.70E-07
NFYA	transcription regulator	2.92E-07
IFNA1/IFNA13	cytokine	3.84E-07
IRF1	transcription regulator	4.44E-07
CNOT7	transcription regulator	4.61E-07
CKS2	kinase	5.01E-07
tetradecanoylphorbol acetate	chemical drug	5.10E-07

MYC	transcription regulator	5.31E-07
STAT2	transcription regulator	5.83E-07
Ptprd	phosphatase	5.95E-07
poly rI:rC-RNA	biologic drug	6.03E-07
TP53	transcription regulator	8.38E-07
HSPB1	other	9.20E-07
calcitrol	chemical drug	1.14E-06
CSF2	cytokine	1.16E-06
CREB1	transcription regulator	1.19E-06
TRIM24	transcription regulator	1.44E-06
PML	transcription regulator	1.96E-06
IL31	cytokine	2.26E-06
Epinephrine	chemical drug	2.39E-06
Growth hormone	group	2.78E-06
ZMPSTE24	peptidase	3.13E-06
Interferon alpha	cytokine	3.35E-06
ZBTB17	transcription regulator	3.73E-06
CKS1B	kinase	4.33E-06
Thyroid hormone	chemical drug	4.59E-06
IFNL1	cytokine	4.92E-06
MAPK14	kinase	5.59E-06
HDAC4	transcription regulator	5.66E-06
RORA	receptor	6.51E-06
ERBB2	kinase	7.38E-06
L-methionine	chemical drug	7.83E-06
Oblimersen	chemical drug	8.57E-06
miR-336-3p	microRNA	9.32E-06
NFATC2	transcription regulator	1.05E-05
Dextran sulfate	chemical drug	1.07E-05
Fulvestrant	chemical drug	1.13E-05

11.3. Regeneration responsive gene program is downregulated in *il11ra* mutant fins.

Table 11.4. Fin regeneration program genes in *il11ra* mutant fin transcriptome.

Ensembl gene ID	Ensembl gene symbol	log_2(*il11ra* mut/wt) 24 hpa	*P*-value	*P*-adj
ENSDARG00000079327	*hmcn2*	-2.46	0	0
ENSDARG00000017901	*tln2a*	-2.25	0	0
ENSDARG00000011821	*plod2*	-1.98	0	0
ENSDARG00000070903	*met*	-1.55	0	0

ENSDARG00000042259	*tgfbr1b*	-1.53	0.03	0.09
ENSDARG00000043593	*rapgef1a*	-1.43	0	0
ENSDARG00000103056	*itga4*	-1.3	0	0
ENSDARG00000095339	*col23a1*	-1.28	0	0
ENSDARG00000054941	*ldlrad4b*	-1.2	0.09	0.2
ENSDARG00000089190	*tanc1b*	-1.17	0	0
ENSDARG00000090585	*gpc1b*	-1.13	0	0
ENSDARG00000074319	*sall1a*	-1.06	0	0
ENSDARG00000077002	*igsf3*	-1.05	0	0
ENSDARG00000079148	*nckap5l*	-1.04	0	0.01
ENSDARG00000009689	*daam1b*	-1.01	0	0
ENSDARG00000075608	*mical2a*	-0.97	0	0
ENSDARG00000103981	*bhlha9*	-0.92	0	0
ENSDARG00000075707	*nid2a*	-0.89	0	0
ENSDARG00000079144	*bcl2l11*	-0.82	0.11	0.24
ENSDARG00000017835	*brf1a*	-0.82	0	0
ENSDARG00000007356	*fgf20a*	-0.81	0	0.01
ENSDARG00000103026	*p3h2*	-0.79	0	0.01
ENSDARG00000023933	*skila*	-0.75	0.01	0.04
ENSDARG00000006353	*itga5*	-0.72	0	0
ENSDARG00000019815	*fn1a*	-0.72	0	0
ENSDARG00000024365	*crlf1a*	-0.68	0	0
ENSDARG00000006526	*fn1b*	-0.67	0	0
ENSDARG00000087780	*tiam2a*	-0.61	0	0
ENSDARG00000012450	*vmp1*	-0.59	0	0
ENSDARG00000076225	*tha1*	-0.57	0.05	0.14
ENSDARG00000040009	*palld*	-0.53	0	0
ENSDARG00000031783	*adcy8*	-0.53	0.19	0.35
ENSDARG00000002445	*prdm1a*	-0.41	0.02	0.06
ENSDARG00000034375	*chst11*	-0.38	0.01	0.03
ENSDARG00000061335	*galnt1*	-0.35	0	0.02
ENSDARG00000037859	*il11a*	-0.18	0.64	0.77
ENSDARG00000000212	*krt97*	-0.13	0.37	0.55
ENSDARG00000017624	*krt4*	-0.12	0.37	0.55
ENSDARG00000099312	*jpt1b*	-0.1	0.51	0.67
ENSDARG00000099730	*pkma*	0.02	0.85	0.92
ENSDARG00000025147	*cd63*	0.04	0.81	0.89
ENSDARG00000027933	*glis1b*	0.1	0.68	0.81
ENSDARG00000018787	*efna1b*	0.36	0.01	0.04
ENSDARG00000012671	*inhbaa*	0.39	0.04	0.11
ENSDARG00000104039	*errfi1a*	0.39	0.02	0.06
ENSDARG00000104773	*junbb*	0.43	0	0.01

ENSDARG00000075121	*hbegfa*	0.47	0	0
ENSDARG00000104571	*gadd45ab*	0.68	0	0
ENSDARG00000019307	*dusp5*	0.71	0	0.01